Genetically encoded conformational probes for small GTPase activity

Dissertation

Zur Erlangung des akademischen Grades
eines Doktors der Naturwissenschaften der
Fakultät für Chemie und Chemische Biologie an
der Technischen Universität Dortmund

angefertigt am

Max-Planck-Institut für Molekulare Physiologie

in Dortmund

Vorgelegt von

Simone Brand, M. Sc.

Januar 2018

„Wer aufhört besser zu werden, hat aufgehört gut zu sein.“

P. Rosenthal

Diese Arbeit wurde in der Zeit von Mai 2013 bis Januar 2018 am Max-Planck-Institut für Molekular Physiologie und am Chemical Genomics Center der Max-Planck-Gesellschaft in Dortmund unter Aufsicht von Dr. Yao-Wen Wu und Prof. Dr. Roger S. Goody angefertigt.

1. Gutachter: Prof. Dr. Roger S. Goody
2. Gutachter: Prof. Dr. Philippe I. Bastiaens

The following publications were prepared in the context of this thesis:

Brand, S. & Wu, Y.-W. Generation of intramolecular FRET probes via noncanonical amino acid mutagenesis. Methods in Molecular Biology 2018; 1728:327-335

Brand, S. & Wu, Y.-W. Semi-synthesis of proteins via oxime ligation. Methods in Molecular Biology, *Manuscript accepted*

Brand, S. & Wu, Y.-W. Development of genetically encoded conformational probes for small GTPase activity using amber suppression and intracellular labeling in live cells. *Manuscript in preparation*

Content

Zusammenfassung

Kleine GTPasen sind Guanosinnukleotidbindende und –hydrolysierende Enzyme die, in Abhängigkeit von dem gebundenen Nukleotid, Guanosintriphosphat (GTP) oder Guanosindiphosphat (GDP), in zwei Aktivitätszuständen existieren. Dadurch fungieren sie als binäre Schalter, die Signalprozesse ausschließlich in aktivem, GTP-gebundenem Zustand ermöglichen. Kleine GTPasen sind in zahlreichen intrazellulären Signalprozessen, wie der Organisation des Zytoskeletts, vesikulärem Transport, Zellkernimport und –export, sowie Zellwachstum und –überleben, involviert.

Aufgrund ihrer spezifischen Lokalisierung zu zellulären Membrankompartimenten, sowie der Abhängigkeit ihrer Aktivität von der Lokalisierung und dem Nukleotidstatus, sind kleine GTPasen attraktive Ziele für die Entwicklung von Biosensoren. Traditionelle Aktivitätssensoren für kleine GTPasen basieren auf Förster-Resonanz-Energietransfer zwischen zwei Fluoreszenzproteinen, die an die Ziel-GTPase und eine spezifische Bindedomäne fusioniert sind. Die Bindedomäne, ein natürlicher Bestandteil von Effektorproteinen, fungiert hier als Affinitätstag, der nur mit der GTP-gebundenen GTPase interagiert und somit die Differenzierung des Aktivitätsstatus ermöglicht. Obwohl dieses Sensordesign weitverbreitet ist, weist es einige Nachteile auf. Zum einen wird nicht die direkte Aktivierung der kleinen GTPase, sondern das nachfolgende Bindeereignis der Effektordomäne detektiert. Diese Interaktion konkurriert mit endogenen Interaktionspartnern wie Effektoren oder GAP. Desweiteren besteht die Annahme, dass Effektorbindung kleine GTPasen auf Membranen stabilisieren kann, wodurch traditionelle Sensoren möglicherweise nicht den tatsächlichen Regulationszustand reflektieren. Zum anderen sind diese FRET-basierte Sensoren vergleichbar groß, da neben der kleinen GTPase und der Effektordomäne noch zwei Fluoreszenzproteine und mehrere Verbindungssequenzen enthalten sind.

Kürzlich wurde eine neue Art von FRET-basierten Sensoren zur Visualisierung der Aktivität von kleinen GTPasen entwickelt. Diese Sensoren ermöglichen eine direkte Detektion von konformationellen Änderungen in der kleinen GTPase, oder der Interaktion mit Effektorproteinen, und bestehen lediglich aus einem Fluoreszenzprotein, der kleinen GTPase und einem synthetischen Fluorophor, welches durch Aminosäureseitenketten-markierung in die GTPase eingebracht wird. Dadurch sind diese Sensoren einerseits deutlich kleiner als herkömmliche Sonden und verwenden das ursprüngliche C-terminale Lokalisierungssignal der kleinen GTPase. Andererseits enthalten diese konformationellen Sensoren keinen Affinitätstag. Diese Unabhängigkeit von einer spezifischen Bindedomäne ermöglicht zum einen eine native Regulation des Sensors durch endogene

Regulationssysteme, während das Sensordesign andererseits auch für GTPasen ohne bekannte Effektorproteine anwendbar ist. Zunächst wurden die konformationellen Sensoren zur Visualisierung von Rab1b Aktivität entwickelt und wurden später auf eine weitere kleine GTPase, KRas, übertragen. Dadurch konnte die Universalität des Sensordesigns demonstriert werden. Nichts desto trotz weißt diese erste Generation der konformationellen Sensoren durch den sehr aufwendigen Herstellungsprozess, der Expertise in zahlreichen biochemischen und chemisch biologischen Methodiken benötigt, einen großen Nachteil auf. Daher ist das Ziel dieser Arbeit die Entwicklung einer zweiten Generation konformationeller Sensoren, bei der der Herstellungsprozess und die Anwendung in Zellstudien durch genetische Kodierung des Sensors massiv erleichtert werden. Um den benötigten FRET-Akzeptor, ein synthetisches Fluorophor, in die kleine GTPase einfügen zu können, wurde Stopkodonsuppressionsmutagenese und intrazelluläre orthogonale Fluoreszenzmarkierung verwendet. Der erste Teil dieser Arbeit fokussiert auf die Etablierung dieser beiden Schritte und verwendet Rab1b als Zielprotein, um eine Vergleichbarkeit mit der ersten Sensorgeneration zu gewährleisten. Der neu entwickelte, genetisch kodierte konformationelle Rab1b Sensor ermöglicht die raumzeitliche Visualisierung von Rab1b Aktivität in lebenden Zellen. Im Weiteren wurde der genetisch kodierte Rab1b Sensor mit dem neu entwickelten reversiblen Kryo-Arrest von lebenden Zellen kombiniert, um Rab1b Aktivität während vesikulärem Transport zu detektieren.

Der zweite Teil dieser Arbeit konzentriert sich auf die Übertragung des Sensordesigns auf eine weitere kleine GTPase, Rheb. Bislang ist kein spezifisches Effektorprotein für Rheb bekannt, wodurch die Entwicklung von traditionellen Aktivitätssensoren nicht möglich ist. Rheb ist ein außergewöhnlich interessantes Ziel für die Biosensorenentwicklung, da dieses Protein als Aktivator für mTOR-Komplex 1, einen Masterregulator von Zellmetabolismus und –wachstum, bekannt ist. Der in dieser Arbeit entwickelte genetisch kodierte Rhebsensor ermöglicht die raumzeitliche Visualisierung von Rhebaktivität in lebenden Zellen.

Abstract

Small GTPases are guanosine nucleotide binding enzymes that exist in two states, being active in the guanosine-triphosphate- (GTP) and inactive in the guanosine-diphosphate- (GDP) bound state. Thus, these proteins act as binary molecular switches, allowing signaling exclusively in the GTP-bound state and function in a variety of cellular signaling processes, including cytoskeleton organization, membrane trafficking, nuclear transport, cell survival and proliferation.

Due to their localization to different cellular compartments as well as their nucleotide- and localization-dependent activity, small GTPases are attractive targets for biosensor development. Traditional biosensors for small GTPase activity are FRET-based and utilize binding domains of effector proteins as affinity tags. Effector proteins interact specifically with the GTP-bound state of a small GTPase. Thus, the affinity tag allows for discrimination between the activity states. To generate a FRET-probe, both interaction partners are fused to a fluorescent protein, enabling sensor read-out by FRET.

Although widely used, this approach suffers a number of disadvantages. On the one hand, they report the activity indirectly, by binding of the affinity tag to the activated protein, instead of reporting the activation event directly. In fact, the interaction of the affinity tag with the small GTPase competes with endogenous effector proteins. As effector binding can stabilize small GTPases on membranes, these probes may not report the native regulation of the respective protein. On the other hand, such probes are comparatively large, containing the small GTPase, the affinity tag, two fluorescent proteins and several linkers.

Recently, a new type of FRET-based sensors for small GTPase activity was developed. These probes allow for direct detection of conformational changes within the target protein and hence report activation or binding of endogenous effector directly. Moreover, the conformational probes consist only of a fluorescent protein, the target small GTPase and a synthetic dye introduced to the protein fold. Thus, these probes are smaller than traditional sensors, do not utilize an affinity tag and contain the native C-terminal localization signal of the small GTPase. This design allows for native regulation by endogenous proteins and the sensor principle is also applicable to targets with unknown effector proteins. Initially, such conformational sensors were developed for Rab1b activity and were later on applied onto a second small GTPase, KRas, demonstrating the versatility of the sensor design. However, the first generation of conformational sensors for small GTPase activity suffers from a labor-intensive preparation process, which requires a high number of methods and expertise. The work presented in this thesis focused on the development of a second generation of the

conformational probes for small GTPases. In the first part, the sensor approach was genetically encoded, facilitating the preparation process and the application to cellular studies. The stop codon suppression technique and subsequent intracellular fluorescence labeling were used to introduce the FRET acceptor into the protein fold. To establish the protocols for stop codon mutagenesis and intracellular fluorescence labeling of small GTPases, the previously well characterized Rab1b conformational sensor was used. The obtained genetically encoded conformational Rab1b sensor allowed for spatiotemporal monitoring of Rab1b effector binding in live cells. Moreover, the genetically encoded Rab1b sensor was combined with the novel reversible cryo-arrest of living cells to analyze Rab1b vesicular transport in living cells.

The second part of this work focused on the application of the genetically encoded sensor design to another small GTPase, Rheb. At the present time, no effector protein has been reported for Rheb, hindering the development of conventional probes to monitor Rheb spatiotemporal activity. Rheb is a particularly interesting target due to its role as an activator of mTORC1, a master regulator for cell metabolism, growth and proliferation. This work demonstrates the establishment of a genetically encoded Rheb sensor using the previously described conformational sensor design. This Rheb sensor allows visualization of spatiotemporal Rheb activity in living cells.

List of Abbreviations

Abbreviation	Name
°C	Degree Celsius
µM	Micromolar
aGFP	Amber GFP mutant
APS	Ammonium persulfate
aRab1b	Amber Rab1b mutant
aRheb	Amber Rheb mutant
AzF	4-Azido-L-Phenylalanine
BcnK	endo-BCN-L-Lysine
BDP	Tetrazine - BDP-FL
BSA	Bovine Serum Albumine
ddH_2O	Double Destilled Water
DMEM	Dulbecco's Modified Eagle's Medium
DMSO	Dimethylsulfoxide
DNA	Deoxyribonucleic acid
EDTA	Ethylenediaminetetraacetic adic
eGFP	Enhanced green fluorescent protein
EtOH	Ethanol
FAM	Tetrazine - 5-Fluorescein
FBS	Fetal bovine serum
FD	FastDigest
FDAC	6-Methyl-Tetrazine-Fluorescein Diacetate
FLIM	Fluorescence Lifetime Imaging
FRET	Foerster Resonance Energy Transfer
GntC	$mKate2\_Giantin_{3131-3259}$
h	Hours
Kx	CAAX motif
MEM	Minimum Essential Medium Eagle
min	Minutes
mTORC1	Mammalian/mechanistic target of Rapamycin complex 1
mtz	6-Methyl-Tetrazine
NEAA	Non-Essential Amino Acids
nM	Nanomolar

nmol	Nanomole
PBS	Phosphate-Buffered Saline
PFA	Paraformaldehyde
pmol	Picomole
PMSF	Phenylmethylsulfonylfluoride
POI	Protein of Interest
ps	picosecond
Rab	Ras-like proteins from rat brain
Rheb	Ras homolog enriched in brain
RIPA buffer	Radioimmunoprecipitation assay buffer
RT	Room Temperature
SDS	Sodium dodecyl sulfate
sec	Seconds
TBS-T	Tris-Buffered Saline Tween-20
TcoK*	Trans-cyclooctene–L-Lysine
TEMED	Tetramethylethylenediamine
TMR	Tetrazine - 5-Carboxytetramethylrhodamine
TSC	Tuberous sclerosis complex
tz	H-Tetrazine
UAA	Unnatural Amino Acid

1. Introduction

1.1 Small GTPases

Small GTPases are guanosine nucleotide binding and hydrolyzing enzymes. The bound nucleotide, either guanosine triphosphate (GTP) or guanosine diphosphate (GDP), defines the enzyme's activity state, being active in the GTP-bound state and inactive in the GDP-bound form. Thereby small GTPases act as binary molecular switches, allowing for signal transduction only in the active state [1]. Members of the Ras superfamily of small GTPases function as monomeric G proteins and possess key roles in a variety of cellular signaling processes including cytoskeleton organization, cell movement, membrane trafficking, nuclear transport and proliferation [2]. Based on sequence and functional similarities, the Ras superfamily is divided into five major branches: Ras, Rho, Rab, Ran and Arf [3]. Nucleotide binding and hydrolysis are performed by a set of conserved sequence elements, the G domain, which is common to all G proteins [4]. The G domain comprises five G boxes (G1-G5) that are located over a stretch of approximately 20 kDa, conserved in structure and biochemistry. Small GTPases share two additional elements, the switch I and switch II regions [1]. These regions undergo conformational changes during nucleotide exchange and hydrolysis and report the nucleotide of a GTPase, enabling the interaction with effector proteins. Effector proteins bind specifically to the active, GTP-bound state and thereby mediate downstream signaling in dependency of the nucleotide state of the small GTPase.

Another hallmark shared by the majority of small GTPases is their post-translational modification, which, in combination with the sequence context directly upstream, dictates the specific subcellular localizations [5,6]. The majority of Ras and Rho GTPases contain a C-terminal CAAX motif, which serves as a recognition site for the farnesyltransferase and the geranylgeranyltransferase I [7,8]. Both enzymes catalyze a covalent addition of isoprenoid moieties to the cysteine residue of the tetrapeptide motif. In contrast, members of the Rab family do not share a consensus prenylation motif and terminate in a distinct set of cysteine-containing C-terminal motifs (CC, CXC, CCX, CCXX, or CCXXX) [9]. These motifs are recognized and modified by the geranylgeranyltransferase II, which covalently attaches (two) geranylgeranyl groups to the cysteine residues [9]. Together with the sequence context directly upstream, the hypervariable domain, these lipid modifications facilitate membrane targeting of the small GTPases to their specific cellular compartments, which is essential for their respective biological function [10].

The activity of small GTPases is regulated by a set of specific enzymes called Guanosine-nucleotide exchange factors (GEFs) and GTPase activating proteins (GAPs). GEFs bind to the

inactive, GDP-bound state of a small GTPase and activate the protein by promoting exchange of the nucleotide from GDP to GTP. In contrast, GAPs catalyze the hydrolysis of GTP to GDP, resulting in inactivation of the small GTPase [11]. Inactive Rho and Rab GTPases can further be regulated by guanine nucleotide dissociation inhibitors (GDIs) [12]. The Rab-GDI interaction involves the switch regions and allows for masking of the prenyl modification, promoting cytosolic sequestration of the GTPase [13]. As membrane localization is essential for the biological function, the GDI-mediated membrane extraction of small GTPases represents an additional regulatory mechanism.

1.1.1 The family of Rab GTPases

Ras-like proteins from rat brain (Rab) GTPases have been initially identified as key players for the secretory pathway in yeast [14,15]. Until now, 11 Ypt/Rabs were found in budding yeast and more than 60 different Rabs in mammals. At least 42 Rab proteins are expressed in all cells, while others are more tissue-specific [16,17].

Rab GTPases share five conserved sequences motifs in addition to the conserved G domain, distinguishing them from other members of the Ras superfamily [18]. These Rab family motifs (RabF1-F5) are located in or in close proximity to the switch and interswitch regions and were identified by sequence alignment. Moreover, based on four Rab subfamily conserved sequences (RabSF1-RabSF4) Rab GTPases can be divided into subfamilies. The RabSF motifs are believed to convey specificity towards the respective GEFs, GAPs and effector proteins, whereas the RabF motifs are thought to be responsible for the discrimination of the nucleotide state and/or involved in the interaction with universal regulators such as Rab escort protein (REP) and GDP dissociation inhibitor (GDI) [18].

REP binds to newly synthesized, unmodified Rab proteins and presents the protein to the RabGGTase, which then covalently attaches (two) geranylgeranyl groups at the C-terminal cysteines of Rab [9,19]. REP is believed to subsequently deliver the modified Rab to its specific target membrane [20,21]. In contrast to REP, which interacts with both modified and unmodified Rab with high affinity, the structurally and functionally closely related GDI binds only to prenylated Rabs with high affinity [22-24]. Two GDI were found in human, whereas only one GDI has been identified in yeast [25]. These GDI proteins have the capacity to bind and solubilize all Rabs. The affinity of GDI towards Rab is reduced by three orders of magnitude upon exchange of GDP to GTP, raising the idea that Rab activation stabilizes its membrane association by impeding the GDI-mediated membrane extraction [22]. In contrast, delivery of Rab proteins to membranes is believed to be mediated by a GDI-displacement factor (GDF). GDF can dissociate the Rab:GDI complex, facilitating the membrane attachment of Rab [26,27]. However, whether all Rab proteins require a GDF, as well as the

exact mechanism of GDF-mediated GDI displacement, remain unclear. Interestingly, the *Legionella* protein DrrA, a GEF for Rab1, has been reported to displace Rab1 from GDI, bypassing any need for GDF activity [28,29]. Moreover, ectopic mistargeting of GEFs has been shown to cause mistargeting of their respective Rab proteins, highlighting the importance of GEFs on the membrane delivery and stabilization of Rabs on membranes [28,30-32].

Rab GEFs show a high diversity in primary and tertiary structure, hindering their identification by sequence homology analysis. Consequently, the number of known Rab GEFs is relatively small in comparison to the over 60 identified members of Rab GTPases [33]. Despite their high variation in structure and size, Rab GEFs can be divided into several different families, the two largest being the Vps9 and the DENN domain families [34,35]. Other GEFs do not relate or comprise two or more subunits, such as the multi-domain TRAPP complex which possesses GEF activity towards Ypt1/Rab1 [36]. The general mechanism of GEF-mediated nucleotide exchange of Rab proteins is similar to the one observed for other small GTPases and leads from the binary nucleotide-protein complex via a trimeric nucleotide-GTPase-GEF complex to a binary GTPase-GEF complex [1]. The subsequent binding of the nucleotide, predominantly GTP due to its higher abundance in cells, reverses this series. Both, removal of the Mg^{2+} ion, which is important for nucleotide binding, and the GEF-induced conformational changes within the small GTPase account for the initial nucleotide release leading from the trimeric to the nucleotide-free binary complex [1,37]. In contrast to Rab GEFs, Rab GAPs share a conserved catalytic Tre-2/Bub2/Cdc16 (TBC) homology domain consisting of approximately 200 amino acids [38-40]. Rab GAPs have been shown to promote the hydrolysis of GTP to GDP via a conserved catalytic arginine-glutamine finger [39,41-43]. Interestingly, approximately a quarter of the 42 TBC proteins identified in human and mouse lack the conserved catalytic arginine residue, which makes these proteins unlikely to possess GAP activity towards Rab GTPases [44].

Intensive investigations revealed that the different Rab proteins localize to the cytosolic side of various cellular compartments and function in membrane trafficking throughout the whole secretory pathway (Figure 1.1) [45-47].

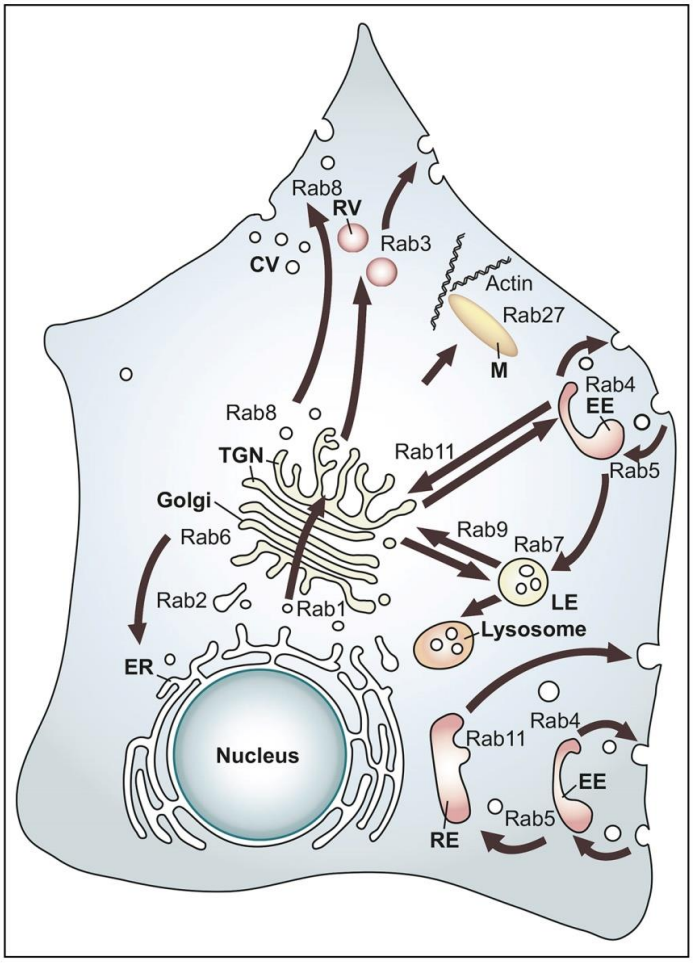

Figure 1.1: Rab GTPases localize to specific cellular compartments and are key players in membrane trafficking. Schematic overview of the cellular localization and function of different Rab proteins in mammalian cells. Figure modified from Stenmark & Olkkonen [48].

Rab GTPases are believed to act in Rab cascades to establish the polarity of the secretory and endocytic pathways (Figure 1.2) [49,50]. This model suggests that a GEF recruits its specific Rab (here denoted RabA) to a specific membrane. The active RabA can then recruit the GEF of the subsequent Rab of the cascade, RabB, which in turn recruits a third GEF to activate RabC. One the one hand, this model is supported by the findings, that most characterized Rab GEFs are cytosolic proteins that can associate with other Rab effectors to activate locally specific Rab proteins [25,51]. While on the other hand, many Rab effectors can simultaneously bind two adjacently acting Rab GTPases, linking their respective localization and function [52-55]. Therefore, Rab effectors may organize the transitions between two Rab proteins within a cascade. Moreover, it was shown that a Rab protein, e.g. RabB, can also recruit the specific GAP of the previously acting Rab, e.g. RabA (Figure 1.2 B) [50]. Thereby RabA would be removed from the respective membrane, sharpening the boundaries between the individual Rab proteins. One example of a Rab cascade is the Ypt1(Rab1)-

Ypt31/31(Rab11)-Sec4(Rab8) cascade which coordinates the secretory pathway in budding yeast [56,57].

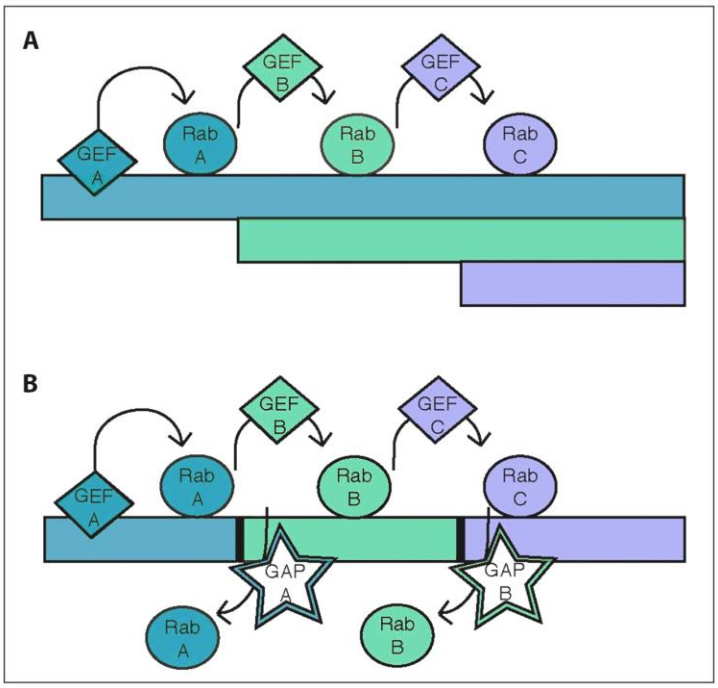

Figure 1.2: Schematic model of Rab GTPase cascades. A) Rab GTPases are believed to act in Rab cascades. First, a GEF recruits its cognate Rab protein (RabA) to a membrane. The active RabA can subsequently recruit the GEF of RabB which in turn recruits GEF C after activation. In this model, all Rab proteins of a cascade can be active simultaneously. B) In this second model, a Rab protein recruits also the GAP of the antecedent Rab, resulting in its deactivation and removal from the membrane. Thereby, the boundaries between the different Rabs of a cascade are sharpened. Figure modified from Pfeffer *et al.* [25].

The first Ypt/Rab protein identified in yeast was the Golgi-resident Ypt1 [58]. Both, Ypt1 and its mammalian homologue Rab1, are essential for the homeostasis of the Golgi complex and function in vesicular transport at the endoplasmic reticulum (ER) - Golgi interface [59-61]. Rab1 has been shown to localize to ER-derived COPII-coated vesicles and is believed to mediate tethering and fusion of these vesicles [62-65]. In fact, numerous Rab1 effector proteins including p115, GM130, Giantin and Golgin84 are Golgi-resident tethering factors [62,66-68]. Moreover, Rab1 has been found to regulate cargo sorting at ER exit sites (ERES) as well as autophagosome formation [69,70]. Initially Rab1 was believed to mediate only the anterograde ER-to-Golgi transport, but was subsequently found to be also essential for retrograde transport [61,71]. The two identified isoforms, Rab1a and Rab1b, share a high degree of sequence similarity (~ 92 %) and seem to have similar but distinct functions [72-75].

The multi-subunit protein complex Transport Protein Particle (TRAPP) has been established as a GEF for Ypt1/Rab1 and potentially Ypt31/32 [36]. While the composition and function of the three distinct TRAPP complexes found in yeast are well understood, the two proposed mammalian TRAPP complexes (mTRAPP) are less characterized [76-78]. Mutation

analysis has assigned the three yeast TRAPP complexes to distinct steps of the secretory pathway, where TRAPP I functions in the ER to *cis*-Golgi transport, TRAPP II in the *trans*-Golgi to plasmamembrane transport and TRAPP III mediates trafficking from the ER to the pre-autophagosomal structure (PAS) [79-82]. In contrast, direct evidence was found for only one mammalian TRAPP complex, mTRAPP II, and a second mTRAPP complex (mTRAPP III) was proposed by proteomic studies [76,78,83]. Similar to their yeast orthologs, different subunits of mTRAPP II were found to interact with COPI and COPII coat components [78,84]. Thus, mTRAPP II is believed to associate to vesicles after budding from the ER and to subsequently activate Rab1, ensuring proper targeting of the vesicles to the Golgi complex [85,86]. Whether the function of mTRAPP II in ER-to-Golgi transport is restricted to its function as a Rab1 GEF or if the complex itself could act as a tether for vesicle tethering and fusion, remains controversial [76,80,86-88].

The ER-resident protein TBC1D20 was identified as a GAP for Rab1b and Rab2a [89-93]. TBC1D20 shares 26 % homology with the yeast Ypt1 GAP Gyp8 and consists of 403 amino acids [90]. As its name suggests, TBC1D20 contains the Tre-2/Bub2/Cdc16 (TBC) homology domain, which is common for all Rab GAPs and promotes hydrolysis of Rab GTPases by a dual arginine/glutamine finger mechanism [38-43]. Unlike other Rab GAPs TBC1D20 contains a C-terminal transmembrane domain mediating its cellular localization [90]. Due to its role as a negative regulator of Rab1b, TBC1D20 overexpression causes disruption of the ER-to-Golgi transport and loss of the Golgi complex [89,91]. Interestingly, inactivation or depletion of TBC1D20 blocks ER exit sites, but did not alter the secretory pathway or the Golgi structure in mammalian cells, suggesting that another, yet unknown GAP may contribute to Rab1 inactivation during ER-to-Golgi trafficking [69,91,94]. Recently, a role of TBC1D20 in regulating autophagy has also emerged [89].

1.1.2 The small GTPase Rheb

Ras homolg enriched in brain (Rheb), a member of the Ras family of small GTPases, is evolutionary highly conserved from yeast to human [95-97]. While no Rheb was found in plants and only one *RHEB* gene has been described in lower eukaryotes such as yeast or *Drosophila*, two *RHEB* genes, *RHEB1* and *RHEB2,* were found in mammals [98-100]. Although the two gene products share 54 % identity and 74 % similarity, their tissue expression profile differs. Despite its name, Rheb1 is ubiquitously expressed, while Rheb2 expression is more limited [97,98,100,101]. Hereafter, Rheb refers to Rheb1.

Rheb consists of 184 amino acids and shares the common architecture of Ras-like GTPases. The N-terminal 169 amino acids contain the GTPase domain, whereas the 15 C-terminal amino acids form the hypervariable region (HVR), including a CAAX

prenylation motif. Similar to other small GTPases, the switch I region of Rheb undergoes conformational changes during the nucleotide cycle. In contrast, the switch II region of Rheb maintains a relatively stable structure, adopting a unique conformation that differs from the long α–helix observed in other Ras GTPases [98,102]. Moreover, the catalytic mechanism of GTP hydrolysis of Rheb differs. On the one hand, the Gln64, which corresponds to Gln61 in Ras, is buried in a hydrophobic core and cannot interact with GTP or the catalytic site. On the other hand, Tyr35 was shown to inhibit the intrinsic GTPase activity, maintaining Rheb in its highly active state [103]. In fact, mutation of Tyr35 to alanine increases the intrinsic GTPase activity by approximately 10-fold and renders this mutant insensitive to GAP activity [103]. Although Rheb shares the C-terminal CAAX motif with other Ras family members, it lacks the polybasic domain in the HVR, which in combination with prenylation of the CAAX motif, targets Ras proteins to the cytoplasma membrane [104,105]. Both Rheb1 and Rheb2 become farnesylated [106,107] and associate with various endomembranes, including lysosomes, mitochondria and peroxisomes [101,106,108-113]. Farnesylation, followed by cleavage of the -AAX motif and subsequent carboxymethylation are essential for membrane targeting and biological function of Rheb [100].

The best characterized function of Rheb is its role as an activator of the mechanistic/mammalian target of Rapamycin (mTOR) complex 1, which acts as a master regulator of cell metabolism, growth and proliferation [114]. mTOR, a highly conserved serine/threonine kinase, can form two structurally and functionally distinct complexes, mTORC1 and mTORC2 [115-117]. Interestingly, Rheb activates only mTORC1 but not mTORC2 [118]. mTORC1 is regulated by various extracellular stimuli and intracellular mechanisms including the energy status, growth factors and amino acids, and integrates these signals to cell metabolism (Figure 1.3). Intensive research of the last decades has identified two distinct mechanisms by which mTORC1 senses the availability of nutrients. The first well-established mechanism is the growth factor signaling. Growth factor stimulation is a multi-step process which leads to the activation of the PI3K-Akt signaling axis, resulting in Akt-mediated phosphorylation of the tuberous sclerosis (TSC) complex. The TSC complex is an oligomeric complex comprising TSC1, TSC2 and TBC1D7. TSC2 possesses GAP function towards Rheb, positioning the TSC complex as a major negative regulator of mTORC1 [113,119-125]. On the one hand, the phosphorylation of the TSC complex inhibits the GAP activity of TSC2 towards Rheb, allowing the small GTPase to become active by a yet unidentified mechanism. On the other hand, phosphorylated TSC dissociates from the lysosomal surface and thus away from its substrate. Rheb-GTP is believed to subsequently activate mTORC1 but the exact mechanism remains elusive [126-129]. In addition to growth factors, the TSC complex is also regulated by various other signals, including hypoxia, genotoxic stress and low energy (Figure 1.3) [122,130-132]. These signals seem to be integrated equally to growth factor sensing onto Rheb via regulation of the TSC complex.

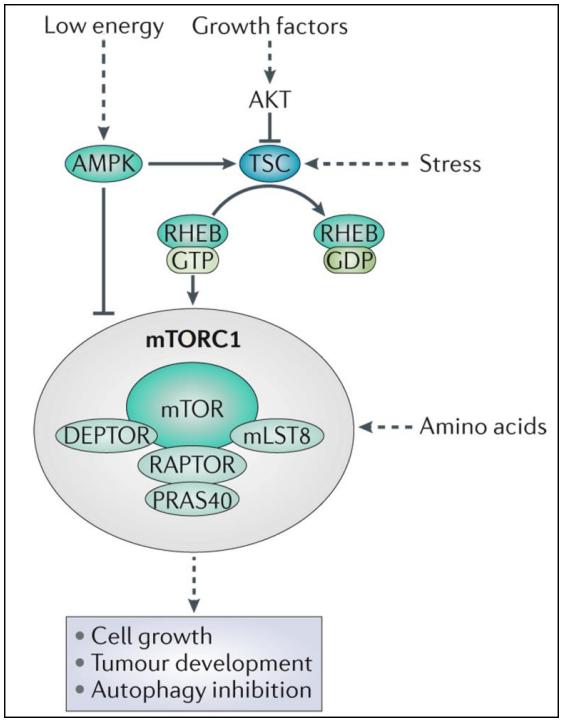

Figure 1.3: Integration of different stimuli on mTORC1 signaling. Growth factor stimulation activates a multi-step signaling pathway which causes AKT-mediated phosphorylation of the TSC complex. Phosphorylation is thought to inhibit the GAP activity of TSC2 towards Rheb and induces the dissociation of the TSC complex from the lysosomal surface and thus away from its substrate. Rheb adapts the GTP-bound state by a yet unknown mechanism and Rheb-GTP subsequently activates mTORC1. Similar to growth factor sensing, mTORC1 is regulated by stress and energy status. In contrast, amino acids are sensed via the Rag GTPases which act on mTORC1 in a Rheb-independent fashion. Activation of mTORC1 promotes cell growth and proliferation, while mTORC1 inactivation initiates autophagy, a catabolic process enabling cells to adapt to starvation. Figure modified from Jewell *et al*. [133]

The second mechanism mediating mTORC1 activation is the availability of amino acid. The presence of amino acids is sensed by the v-ATPase (Figure 1.4). Under low amino acid conditions, the v-ATPase binds the Ragulator complex, inhibiting its GEF activity towards RagA. In parallel, the GATOR1 complex exerts its GAP activity towards RagA, maintaining the heteromeric RagGTPases in an inactive state which is does not allow for recruitment of mTORC1 to the lysosomal surface. Hence, mTORC1 is distributed diffusely in the cytosol. Upon amino acid stimulation, the v-ATPase and Ragulator undergo conformational changes, allowing Ragulator to activate RagA. In parallel, the Folliculin complex promotes the GTP hydrolysis of RagC, resulting in an active Rag GTPase heterodimer. The active RagGTPases, containing RagA-GTP and RagC-GDP, recruit mTORC1 to the lysosomal surface, allowing for Rheb-mediated activation.

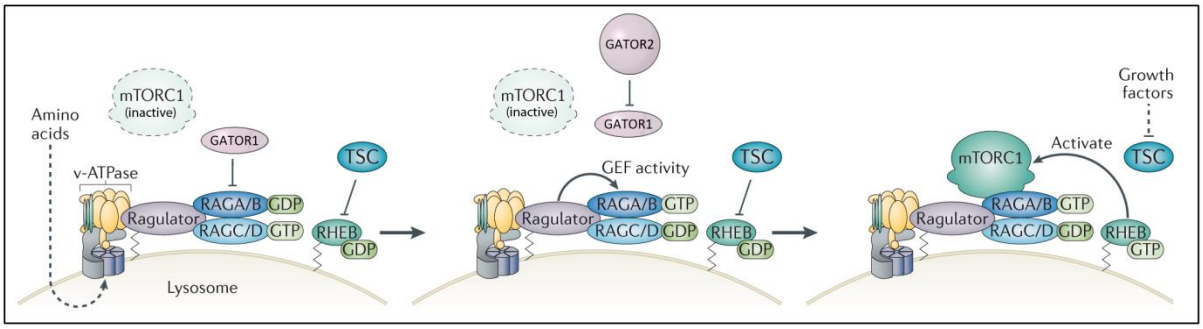

Figure 1.4: Amino acid sensing on the lysosomal surface. In the absence of amino acids the v-ATPase inhibits the Ragulator complex, preventing its GEF activity towards RagA. In addition, the GATOR1 complex exerts its GAP activity on RagA, maintaining the heterodimeric Rag GTPases in an inactive state which does not allow for mTORC1 recruitment to the lysosomal surface. Amino acid stimulation causes conformational changes in the v-ATPase and the Ragulator complex, enabling the Ragulator complex to function as a GEF for RagA. GATOR1 may be inhibited by GATOR2. The active RagGTPases recruit mTORC1 to the lysosomal surface, enabling its activation by Rheb-GTP in the presence of growth factors. Figure modified from Jewell *et al.* [133]

Whether this mechanism senses all 20 amino acids equally or only specific amino acids, such as leucine and arginine, remains controversial. Although leucine and arginine are crucial for mTORC1 activation, they are not sufficient for mTORC1 activation in cells deprived of the remaining 18 amino acids [134,135]. However, some amino acid transporters in the plasma membrane cotransport different amino acids, hindering the precise differentiation between cellular transport and sensing event [136].

The current model of mTORC1 activation is that the presence of amino acids regulates mTORC1 recruitment to the lysosome, whereas the growth factor signaling integrates on Rheb-mediated mTORC1 activation. Thus, both stimuli are required to activate mTORC1 and promote cell growth (Figure 1.5).

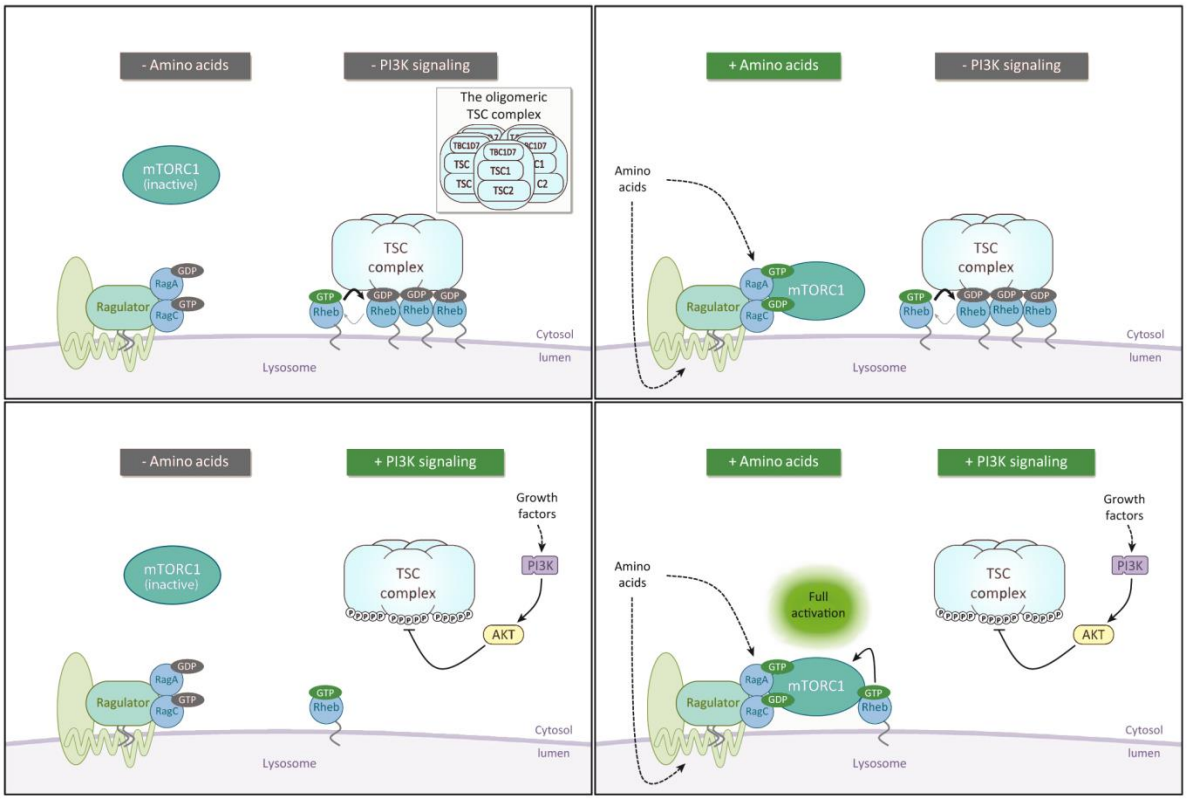

Figure 1.5: Nutrient signal integration at the lysosomal surface. Both, the amino acid availability and the growth factor signaling axes converge on the lysosomal surface to regulate mTORC1 activity. Amino acid signaling integrates on the v-ATPase/Ragulator pathway and enables mTORC1 recruitment to the lysosome, enabling subsequent mTORC1 activation by GTP-bound Rheb. The activity of Rheb is regulated by growth factor signaling, a multi-step signaling process resulting in phosphorylation of the TSC complex via the PI3K/Akt axis. The phosphorylated TSC dissociates from the lysosomal surface, allowing Rheb to become active. Hence, mTORC1 can only be activated by Rheb if both signaling pathways are triggered. Figure modified from Dibble *et al.* [132]

In addition to the TSC complex-dependent regulation of mTORC1 activity, other signals regulating Rheb activity in a TSC-independent fashion have been reported. On the one hand, Rheb seems to be regulated by PRAK-mediated phosphorylation, which was found to decrease the nucleotide binding of Rheb, which may weaken its ability to activate mTORC1 [137]. Zheng *et al*. found that this process is induced by energy depletion and may represent an AMPK-independent mechanism of mTORC1 regulation in response to the energy status. On the other hand, two proteins were reported to bind Rheb and potentially sequester Rheb away from the lysosomal surface, which may lead to a decrease of mTORC1 signaling. Kim *et al*. found that PDE4D, which is responsible for the degradation of cAMP, binds Rheb under low cAMP conditions, whereas high cAMP levels disrupted this interaction [138]. A similar interaction was found by Lee *et al*. for GAPDH and Rheb [139]. Under low glucose conditions GAPDH was reported to bind Rheb independently of its nucleotide state, whereas high levels of Gly-3P, the GAPDH substrate, inhibited the interaction. In fact, this

interaction has been found to decrease mTORC1 activity. Hence, this study identified a mechanism of Rheb/mTORC1 regulation that seems to be independent of AMPK/TSC signaling [139,140].

Thus, Rheb and thereby mTORC1 activity, is regulated by a variety of signaling pathways. Some of these pathways seem to act on the nucleotide state of Rheb, e.g. by recruitment of its GAP, the TSC complex, while other stimuli may utilize binding to Rheb to eliminate Rheb-mediated mTORC1 activation.

1.2 FRET-based biosensors

Due to their role in a plethora of intracellular signaling processes, small GTPases are popular targets for biosensor development. A majority of biosensors are based on Foerster Resonance Energy Transfer (FRET), a non-radiative energy transfer between two fluorophores that have overlapping emission and excitation spectra [141]. In addition to the spectral overlap, this energy transfer depends on the distance and the relative orientation of the two fluorophores. FRET has been widely used in cellular studies to assess protein-protein interactions or protein activity using biosensors.

Several imaging methods can be utilized to monitor FRET. The practically most feasible strategy is ratiometric imaging which utilizes separate fluorescence intensity images of the donor and the acceptor to calculate the ratio of the fluorescence intensities of the two images [141]. When FRET occurs, this ratio is increased. Although this method can be used at any fluorescence microscope, due to photo-bleaching, spectral bleed-through it is prone to artifacts and requires appropriate subtraction of the background. Moreover, proper signal detection may be impaired by probe relocation, especially when monitoring bimolecular probes. The most commonly used fluorescent proteins for ratiometric imaging are CFP and YFP, or the respective enhanced variants such as Cerulean and Venus [142-145].

A more sensitive method to detect FRET is fluorescence lifetime imaging (FLIM) [146]. When a fluorophore is excited, it emits fluorescence in a decaying, typically exponential fashion from the time of activation. This fluorescence lifetime of a donor molecule is shortened when FRET occurs, allowing for quantitative measurements of FRET signal changes (FLIM-FRET). Moreover, the fluorescence lifetime is independent of the fluorophore concentration and the acceptor fluorescence and thus less prone to artifacts caused by changes in the local concentration of donor or acceptor. Although eGFP is often used as a donor molecule, mCitrine or mTurquoise are superior for fluorescence lifetime imaging due to their mono-exponential decay and higher fluorescence lifetime [142,143,147]. A mono-exponential decay facilitates fitting of the obtained decay curves, simplifying the data

analysis and interpretation greatly [147]. Moreover, higher donor lifetimes allow for a broader dynamic range when used in FRET probes.

Based on their architecture FRET-based biosensors can be generally divided into two groups (Figure 1.6). While bimolecular probes consist of two chains, with one fluorophore attached to each chain, unimolecular probes contain both fluorophores within a single chain. Depending on the mode of action, the two fluorophores are brought in close proximity in one conformational state, allowing efficient FRET to occur, while the other state prevents FRET. To sense the activation event many biosensors utilize an affinity tag, which, in the case of small GTPases, is most commonly a specific binding domain of an effector protein. This strategy was initially developed to generate a specific bimolecular sensor for Rac1 activity and was further applied to other small GTPases [148]. The affinity tag recognizes the different conformations of the small GTPase, allowing for discrimination between the two activity states. In the GTP-bound state, the effector binding domain can interact with the small GTPase, bringing the two fluorescent proteins in close proximity and enabling FRET (Figure 1.6). In contrast, nucleotide hydrolysis of GTP to GDP, and thereby the inactivation of the small GTPase, disrupts the interaction and prevents FRET.

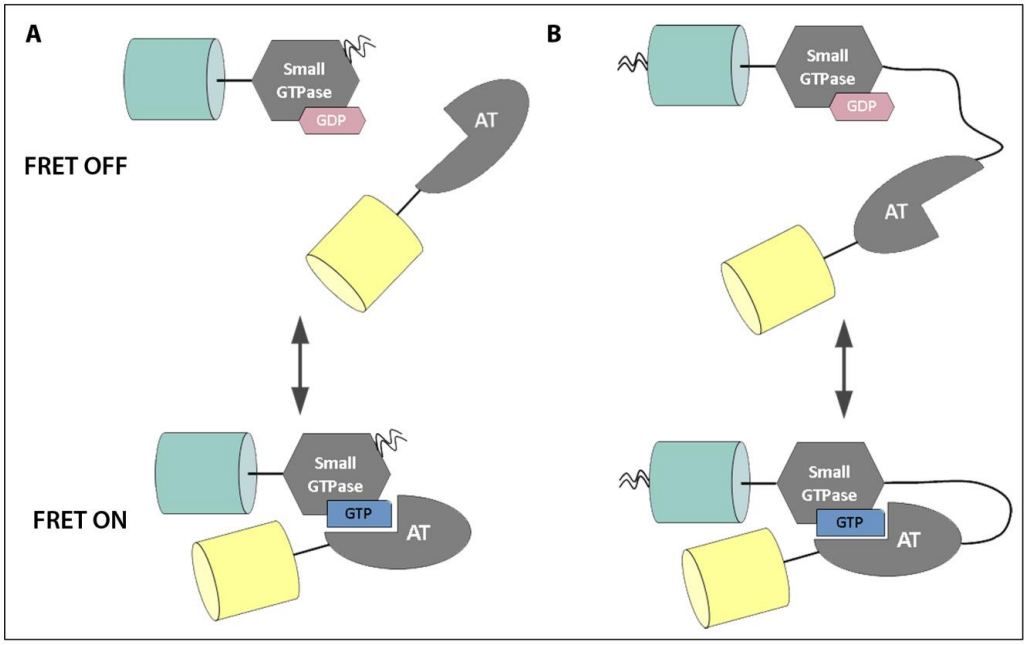

Figure 1.6: Design of FRET-based probes to monitor spatiotemporal small GTPase activity. A) The general design of bimolecular FRET-bases biosensors. These sensors consist of two separate chains, the small GTPase and its specific affinity tag (AT), each fused to a fluorescent protein (e.g. CFP and YFP). These two chains interact only in the GTP-bound state of the small GTPase, bringing the two fluorescent proteins in close proximity and enabling FRET. B) A general design of a FRET-based unimolecular probe to visualize small GTPase activity. The sensor consists of two fluorescent proteins, the small GTPase and its affinity tag, all units linked by spacers.

The most commonly used biosensors to monitor small GTPase activity are Ras and interacting protein chimeric unit (RAICHU) probes. RAICHU probes are FRET-based unimolecular sensors that were initially developed to assess the spatiotemporal Rap1 and HRas activity in cells [149]. The basic architecture of these probes is similar to the calcium sensor Chameleon [150], consisting of two fluorescent proteins, the target protein and its respective affinity tag, linked by spacers (Figure 1.6 B) [149]. For membrane targeting, the probe is fused to the native C-terminal prenylation motif of the respective small GTPase. This sensor design was successfully applied to several small GTPases, including members of the Rap, Rho, Rab, Ran and Ras families [151-157]. The architecture of RAICHU probes for Rho GTPases was slightly altered to reduce the basal FRET-levels by interchanging the small GTPases and the effector unit [152,158]. Most FRET probes conventionally use CFP as a fluorescence donor and YFP as an acceptor, allowing for ratiometric assessment to obtain the probe read-out [159]. Since the FRET efficiency of RAICHU probes correlates with the nucleotide loading, the small GTPase activity can be calculated by the CFP/YFP fluorescence intensity ratio [149,152,154,158].

Although widely used, RAICHU probes exhibit several disadvantages. The major pitfall of this sensor design is the use of an affinity tag. On the one hand, the tag allows for discrimination between the nucleotide states, but on the other hand, the affinity tag competes in binding to the small GTPase with endogenous proteins, such as effectors or GAPs. Moreover, effector binding is believed to stabilize small GTPases on membranes. Therefore, a RAICHU probe may be regulated differentially to the respective endogenous GTPase and the read-out may not reflect the native activity state. Furthermore, the RAICHU sensor design is limited to small GTPases with known effector proteins and cannot be applied to small GTPases for which no effector protein has been identified yet. Another disadvantage is the comparably huge size of the probe, containing the affinity tag, the two fluorescence proteins, the target GTPases and several linkers. In addition, the membrane targeting signal of the small GTPase has to be artificially reintroduced to the probe.

To overcome the disadvantages of traditional probes, a new type of sensors for small GTPase activity was developed recently. These conformational sensors for small GTPase activity (COSGA) are unimolecular probes, consisting of a fluorescent protein, fused to the N-terminus of the small GTPase of interest, and a synthetic dye that is introduced to the protein fold by amino acid side chain labeling [160,161]. Depending on the bound nucleotide and thus, the conformation of the small GTPase, the FRET signal is more or less efficient and can be assessed by fluorescence lifetime imaging. COSGAs have been previously developed and characterized as recombinant proteins and were later on applied for cellular studies using microinjection. Several mutation sites in Rab1b have been identified to tolerate the introduction of the acceptor molecule without interfering with protein folding or function (Figure 1.7 A) [160,161]. Positioning of the acceptor in the small GTPase determined the type of

sensor read-out, e.g. whether the probe reports exclusively the activity state of the small GTPase, or both, activity and effector binding [160,161].

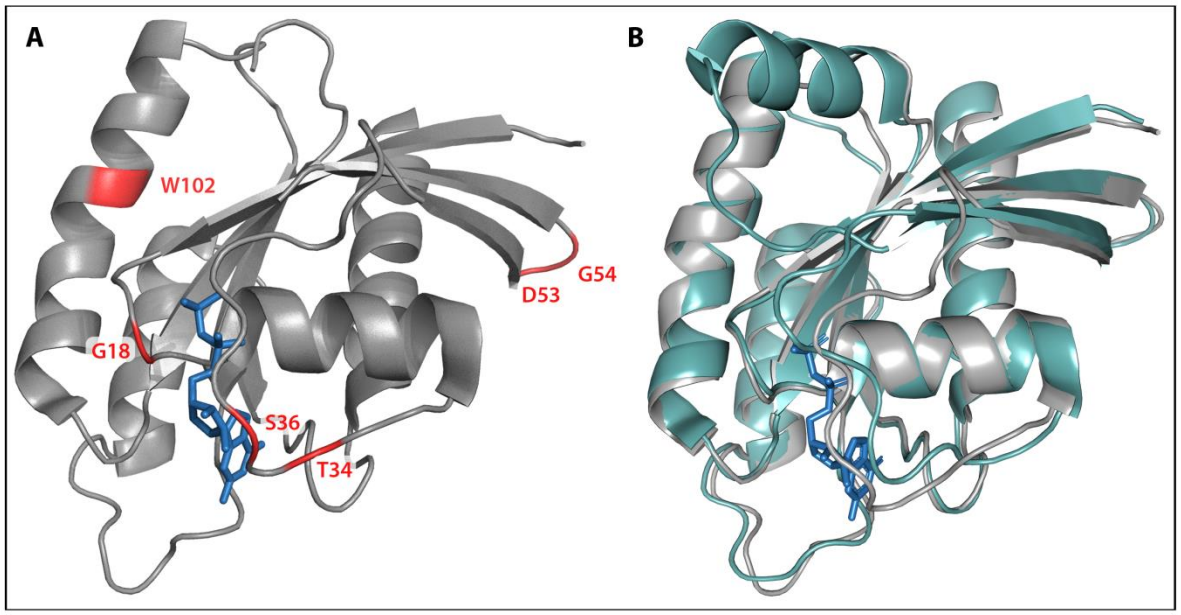

Figure 1.7: Crystal structure of human Rab1 and KRas in complex with GDP. A) The mutation sites in Rab1 allowing for introduction of a synthetic dye via amino acid side chain labeling are highlighted in red. These sites are located either in the switch I region (T34 and S36), in the interswitch region (D53 and G54) or close to the nucleotide binding pocket (G18 and W102). The latter are suitable for the introduction of environment sensitive dyes, while the other positions were utilized to constitute a FRET-based conformational probe. GDP is colored blue. B) Alignment of the crystal structures of human Rab1a (grey) and KRas (dark teal), both in GDP-bound states (blue). PDB: Rab1a 2FOL; KRas 4OBE.

Depending on their localization in the protein fold the mutation sites to introduce the FRET acceptor can be divided into three groups, the switch I region (T34 and S36), the interswitch region (D53 and G54) and positions in close proximity to the nucleotide binding pocket (G18 and W102). The first two groups are suitable to generate FRET-based conformational probes, whereas the last group was successfully used to introduce an environmental sensitive dye reporting the nucleotide state.

Interestingly, the sensor read-out varies depending on the positioning of the acceptor within the protein and also within the same region. While the interswitch mutations, D53 and G54, yield comparable sensor signals, reporting effector binding by an increase in FRET and protein activation by a FRET decrease, the two mutants in the switch I region differ. Positioning of the acceptor at S36 was found to report predominantly effector binding, whereas introduction of the acceptor at T34 yielded a probe that is insensitive to effector binding and reports exclusively nucleotide state [160,161]. Due to the conserved structure that is shared by many small GTPases, the sensor design can be applied to other small GTPases. To demonstrate this versatility, the COSGA sensor approach was subsequently extended to

KRas, which shares high structural similarity with Rab1 (Figure 1.7 B). Similar to Rab1b, different mutation sites in KRas were successfully assessed for GEF-mediated activation and GAP-induced hydrolysis *in vitro*, as well as EGF-induced activation *in vivo*.

Nevertheless, the major disadvantage of COSGA probes is the extremely labor-intensive preparation process. First, the sensor needs to be designed, a process which depends on the empirical evaluation of the probe. The respective position for introducing the acceptor dye has to be mutated to cysteine. Next, the construct requires heterologous expression, e.g. in bacterial expression systems, followed by protein purification and chemical modification. The acceptor is subsequently introduced by cysteine side-chain labeling with iodoacetamide-functionalized dyes. Unwanted, multiple labeling can only be avoided by replacement of non-essential cysteines or, if possible, via kinetic labeling [160,161]. Following introduction of the acceptor fluorophore, the native C-terminus of the small GTPase, which was initially removed to avoid labeling of the cysteine residues in the prenylation motif, needs to be reintroduced by native chemical ligation. Finally, the sensor has to be introduced into cells by microinjection or electroporation to enable cellular studies. Thus, a broad range of biochemical and chemical methods and expertise is required to yield a COSGA sensor.

1.3 Stop codon suppression and bio-orthogonal labeling

Stop codon suppression, also named amber suppression, is a bioorthogonal approach to incorporate an unnatural amino acid (UAA) cotranslationally into a target protein in live cells. This unnatural amino acid carries a unique chemical handle which can then be specifically addressed by an orthogonal reaction. To this end, a nonsense codon, usually the amber stop codon (UAG) is reassigned by extending the endogenous translation system with an orthogonal system. The essential components for amber suppression are an orthogonal $tRNA_{CUA}$ and a cognate aminoacyl-tRNA synthetase, which loads the UAA onto the tRNA (Figure 1.8). It is essential, that the orthogonal pair functions completely independent of the endogenous translation system. Thus, the orthogonal synthetase should aminoacylate only the orthogonal tRNA and should accept exclusively the UAA as a substrate. Moreover, neither the tRNA, not the UAA should be recognized as substrates by endogenous synthetases. If these criteria are fulfilled, the orthogonal pair can function in parallel to and without interfering with the endogenous translation system.

In the absence of a stop codon suppression system, the translation process pauses when the ribosome reaches an amber codon. The release factor enters the ribosome and terminates the translation process by releasing the two ribosomal subunits, the mRNA and the peptide chain. In prokaryotes, the termination process is mediated by the release

factors 1 and 2 (RF1/RF2), which selectively terminate the translation in response to UAG/UAA and UGA/UAA stop codons, respectively [162,163]. The termination process in eukaryotic cells is more complex and involves the two eukaryotic release factors 1 and 3 (eRF1/eRF3) [164-166]. eRF1 is an orthologue of the prokaryotic release factors and terminates the translation in response to all three stop codons. While eRF1 is the key factor for the termination, eRF3 plays only a stimulatory role [164-167]. In contrast, the presence of an UAA and a cognate orthogonal pair allows for UAA incorporation into the target protein in response to the amber codon (Figure 1.8). However, the orthogonal process competes with the endogenous eRF1-mediated termination process. Thus, the expression yield of amber suppressed proteins depends strongly on the efficiency of the UAA incorporation process. Therefore the expression of amber proteins is usually lower than the expression of the respective wild type protein.

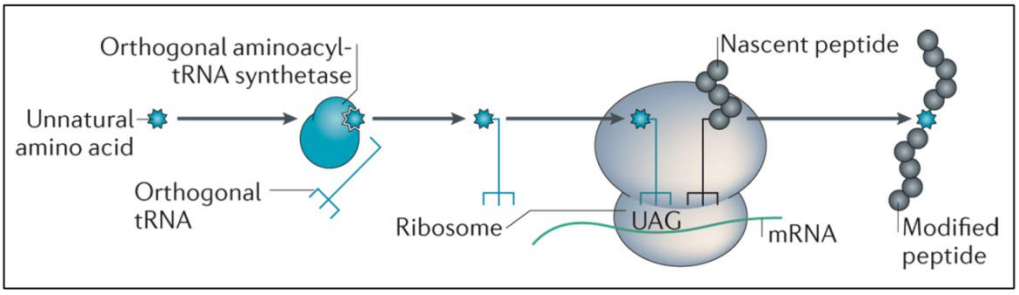

Figure 1.8: Incorporation of an unnatural amino acid into a target peptide in response to an amber stop codon. The unnatural amino acid (UAA) is loaded onto an orthogonal tRNA by an orthogonal aminoacyl-tRNA synthetase. The orthogonal tRNA contains a CUA anticodon, allowing for UAA incorporation into the target protein at the ribosome in response to a UAG codon on the mRNA. Figure modified from Davis & Chin [63].

Orthogonal synthetases are evolved by a two-step process (Figure 1.9) [63,168]. First, a heterologous aminoacyl-tRNA synthetase/tRNA pair is imported from an evolutionary distinct organism into the target host. Then the active site of the synthetase is mutated to allow for recognition of an unnatural amino acid and functional candidates are selected (Figure 1.9 A). Generally, such synthetase candidates still recognize their natural substrate. Thus, libraries of synthetase candidates containing mutations in the active site are generated to remove the natural binding site for endogenous amino acids. These libraries are applied to a two-round selection process to identify mutants that accept exclusively unnatural amino acids as substrates (Figure 1.9 B). First, these libraries are subjected to a positive selection. An essential gene is modified with an amber codon and only synthetases incorporating an amino acid in response to the amber codon can express the gene in full length, allowing for host survival. These clones are applied to a second, negative selection. Here, the host organism is supplied with a toxic gene containing an amber codon. In the

absence of an UAA, this gene should not be translated in full length. Candidate synthetases that accept endogenous amino acids as substrate will incorporate those in response to the amber codon, resulting in the translation of the toxic gene and thereby host death. The scope of an established orthogonal pair can be further expanded by directed evolution [169]. Although most orthogonal synthetases were discovered by import of a synthetase/tRNA pair into a heterologous host, a synthetase/tRNA pair can also be created *de novo* by directed evolution approaches [93].

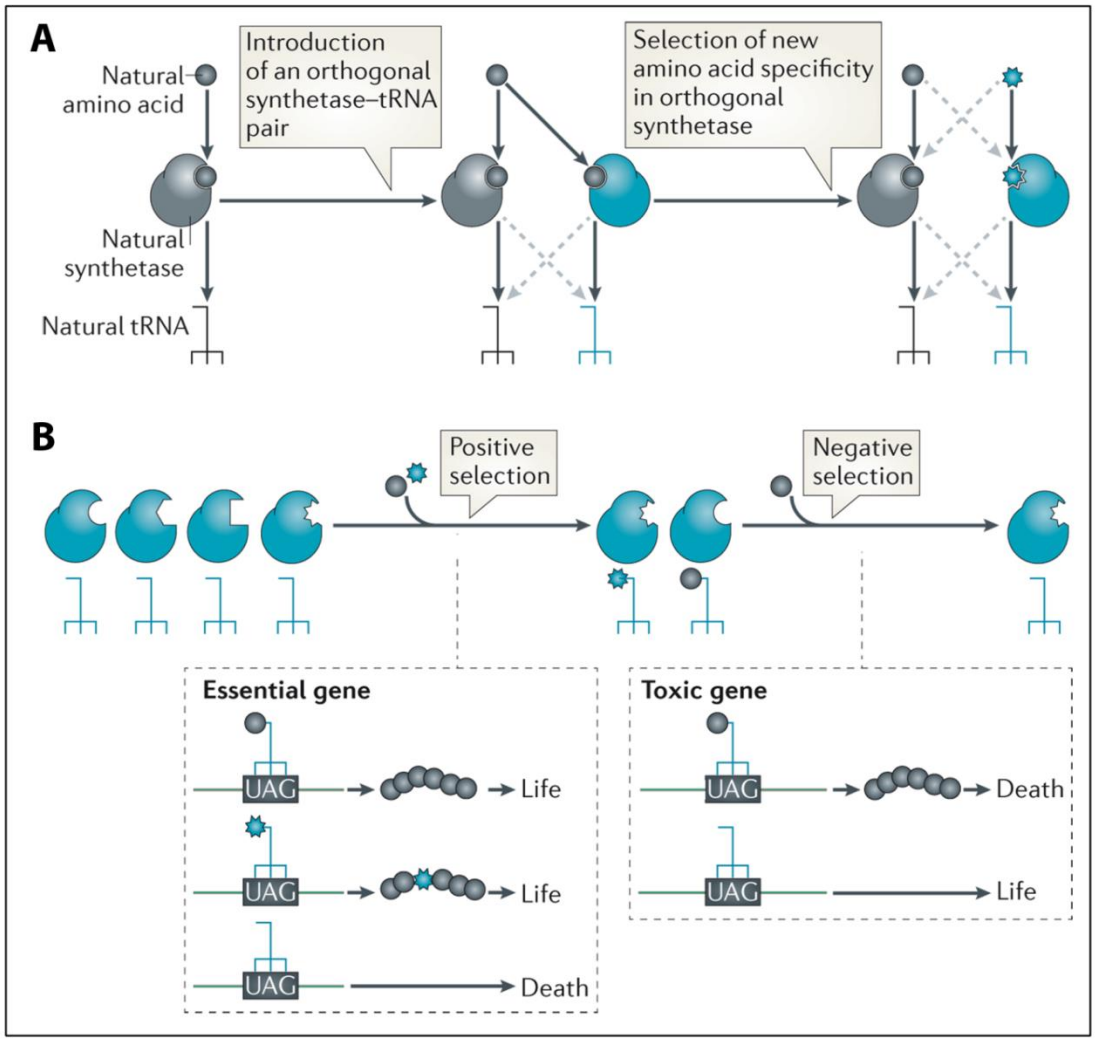

Figure 1.9: Evolution and selection process of an orthogonal pair for stop codon suppression. A) To generate an orthogonal pair, a natural synthetase and the respective tRNA are selected from an evolutionary distinct organism and transferred to the target host. Next, a library of mutants of this synthetase is generated to identify active site mutations allowing for binding of the unnatural amino acid. B) The generated library of active site synthetase mutants is selected in two rounds to achieve orthogonality of the synthetase/$tRNA_{CUA}$ pair. Figure modified from Davis & Chin [63].

While the genetic code is highly conserved between distinct organisms, the sequence, structure and molecular specificity of aminoacyl-tRNA synthetases and tRNA differ. Thus, the orthogonality of amber suppression systems can depend on the host organism (Figure 1.10). Four different orthogonal synthetase/tRNA pairs were developed and are commonly used for various applications. The first pair used to incorporate an unnatural amino acid was the *Methanococcus jannaschii* Tyrosyl-tRNA synthetase (*Mj*TyrRS)/$tRNA_{CUA}$. This pair is bioorthogonal in *Escherichia coli*, but not to synthetases and tRNA in eukaryotes [170]. In contrast, the *E. coli* Tyrosyl-tRNA synthetase (*Ec*TyrRS)/$tRNA_{CUA}$ and the *E. coli* Leucyl-tRNA synthetase (*Ec*LeuRS)/$tRNA_{CUA}$ are orthogonal in yeast and mammalian cells, but not in bacteria [171,172]. The pyrrolysyl-tRNA synthetase (PylRS)/$tRNA_{CUA}$ from *Methanosarcina* species is orthogonal in both, eukaryotes and prokaryotes and has even been used to incorporate unnatural amino acids in *Drosophila melanogaster* and *Caenorhabditis elegans* [169,173-176].

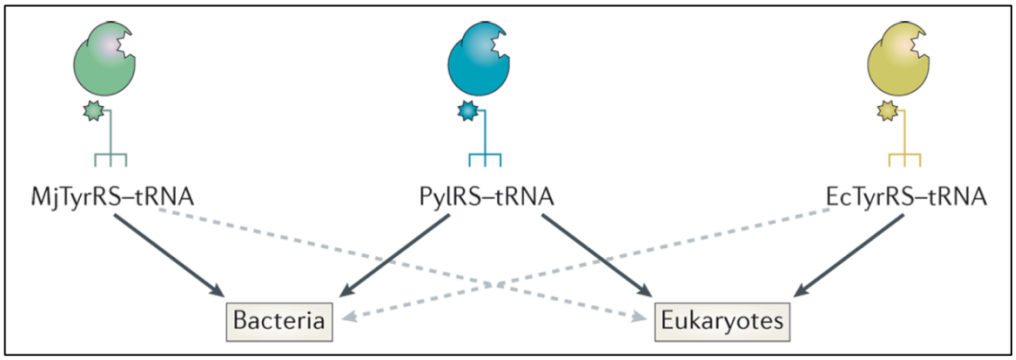

Figure 1.10: Orthogonality of the three different evolved aminoacyl-tRNA synthetase/$tRNA_{CUA}$ pairs allowing for cotranslational incorporation of unnatural amino acids in response to stop codons. While the pyrrolysyl-tRNA synthetase (PylRS)/tRNA pair is orthogonal in bacteria and in eukaryotes, the *Methanococcus jannaschii* Tyrosyl-tRNA synthetase (*Mj*TyrRS)/$tRNA_{CUA}$ pair and the *Escherichia coli* Leucyl-tRNA synthetase (*Ec*LeuRS) /$tRNA_{CUA}$ pair are only orthogonal in bacteria and eukaryotes, respectively. Figure modified from Davis & Chin [63].

The PylRS/$tRNA_{CUA}$ system has two major advantages over the other orthogonal pairs. (1) The PylRS synthetase does not recognize any of the 20 canonical amino acids and therefore does not require an additional mutation of the natural binding site in organisms that do not use pyrrolysine. (2) Due to the orthogonality both in bacteria and eukaryotes, directed evolution and selection processes expanding the scope of recognized UAA can be performed in *E. coli*. This allowed for further evolution of the PylRS/$tRNA_{CUA}$ pair to accept a variety of strained alkenes and alkynes as substrates [177-181].

Genetic code expansion has become a wide-spread technique in the past decades, allowing for a broad range of applications, including photo-crosslinking of proteins [182-184],

installation of post-translational modifications [169,185-197], photo-activation [198-200] and introduction of biophysical probes [201-203] or labels [168,177,178,181,204-208]. In addition to these research applications, amber suppression was also utilized to generate therapeutics, e.g. by protein conjugations (reviewed in [209]).

Introduction of minimal fluorescent tags into a target protein in live cells using UAA mutagenesis has several advantages over the more traditional genetic methods. Traditionally, a protein is fluorescently tagged by genetic fusion of the target protein and a fluorescent protein. Despite constant progress in the field and the generation of numerous variants of GFP, the available spectral ranges, as well as the biophysical properties of the respective fluorophores are limited. To overcome this issue, self-labeling protein tags such as the eDHFR- or SNAP-tag were developed [210]. Even though these tags utilize synthetic fluorophores, which are superior in photostability and which are available in the whole spectral range, the tag size is comparable to that of fluorescent proteins. Moreover, these tags can be introduced exclusively to the target protein's termini. Thus, proteins that require both termini for native folding or function are difficult to address by genetic fusion.

Chemical biological approaches yielded numerous biocompatible strategies to overcome these disadvantages. One approach is the use of short peptide-motifs, e.g. the tetracysteine motif, which can subsequently react with biarsenical-functionalized fluorescent dyes [211-213]. While tetracysteine motifs consist of only four amino acids, their introduction to the target protein is limited to fusion of the protein backbones and thus, the termini of the target protein. An alternative approach is the labeling of amino acid side chains, allowing for introduction of the fluorophore at a distinct position into the protein fold (reviewed in [214]). The most frequent targets of this approach are lysine or cysteine moieties. Nevertheless, due to the biological abundance of these amino acids and the fact that all accessible target moieties can potentially react, the labeling specificity of these reactions is limited. Different bioorthogonal approaches were developed to enhance the labeling specificity, such as the site-specific introduction of an orthogonal group that is unique even in cellular systems, and which can specifically be addressed by a bioorthogonal chemical reaction. Several requirements need to be fulfilled in order to achieve biocompatibility and high specificity in cells. On the one hand, orthogonal reactions should take place under physiological conditions, e.g. in aqueous solution at physiological temperatures and under ambient pressure. Moreover, both reactants should be thermodynamically, metabolically and kinetically stable, and the reaction should yield covalently linked products. Neither the reactants, nor the product or any side product should be toxic to living systems. On the other hand, the orthogonal reaction partners must react exclusively with each other and not with any functional moiety present in cellular systems. Different reactions fulfilling these criteria were successfully used for live cell approaches (reviewed in [204,215]), including the strain-promoted alkyne-azide cycloaddition (SPAAC) and the Diels-Alder cycloaddition between tetrazines and strained alkenes/alkynes

(Figure 1.11). Both reactions have been used to fluorescently label amber suppressed proteins with the respective functionalized dyes [179,207]. Labeling via SPAAC was achieved using a variant of the *E. coli* Tyrosyl-tRNA synthetase (*Ec*TyrRS) in combination with an engineered *Bacillus stereathermophilus* $tRNA^{Tyr}$, allowing for incorporation of a variety of unnatural amino acids, including *p*-azido-L-phenylalanine (AzF) [216]. AzF can subsequently react with bicyclononyne- (BCN) or dibenzocyclooctyl (DBCO)-modified dyes. In contrast, protein labeling by Diels-Alder cycloaddition between tetrazines and strained alkenes/alkynes was performed using the *Methanosarcina mazei* PylRS/$tRNA^{Pyl}$ orthogonal pair. In the past the scope of substrates of this pair was extended continuously, resulting in a broad range of strained alkenes and alkynes that are accepted as substrates [178,179,217,218]. Among these are bicyclo[6.1.0]-nonyne-lysine (BcnK) and Trans-cyclooctene–L-Lysine (TcoK*), which have been recently used to specifically label both extracellular and intracellular proteins [177-179,181,217,219]. However, although both reactions are bioorthogonal and generally applicable in live cells, due to the higher rate constant the Diels-Alder cycloaddition is superior to the SPAAC (10^3-10^4 and 10^{-1} M^{-1} s^{-1}, respectively), allowing for rapid labeling even at low reactant concentrations. Another advantage is the use of tetrazine-functionalized dyes, which are often fluorogenic. Fluorogenic probes exhibit low intrinsic fluorescence emission which is massively increased after coupling to the target protein, facilitating the detection of specifically labeled target protein against the background signals [220-222].

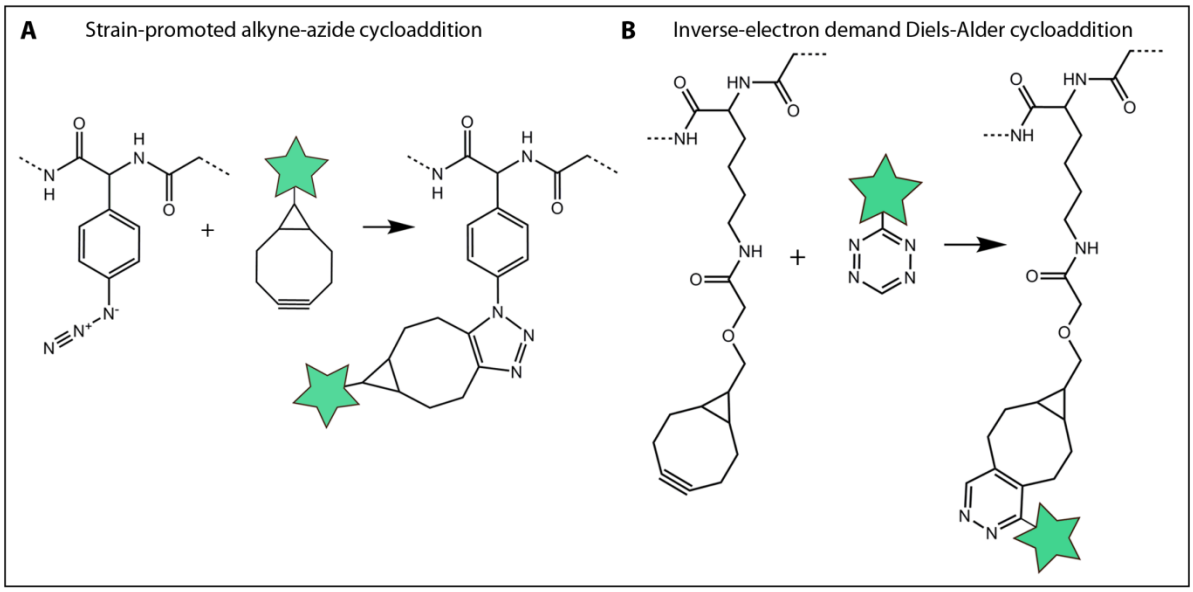

Figure 1.11: Reaction schemes of the labeling of unnatural amino acids incorporated into a protein with functionalized synthetic fluorophores (represented by green stars). A) Strain-promoted alkyne-azide cycloaddition (SPAAC) of the unnatural amino acid (UAA) *p*-azido-L-phenylalanine and a BCN-functionalized fluorophore. B) Inverse-electron demand Diels-Alder cycloaddition of the UAA BCN-L-Lysine incorporated into a protein and an H-tetrazine-functionalized dye.

Intracellular labeling poses a number of requirements on the dye. On the one hand, the functionalized probe requires high cell permeability, while on the other hand, it should not bind unspecifically to cellular components or accumulate in membranes. Most conventional small dyes including cyanine dyes and Alexa Fluor® probes, as well as their derivatives, carry charges and are thus not cell permeable. In contrast, tetramethylrhodamine (TMR) and fluorescein diacetate (FDAC) are highly cell permeable and have been used for several cellular applications in the past [177,181,205,223]. Furthermore, *boron-dipyrromethene* (BODIPY) dyes have been used for various live cell approaches in the past and are thus promising candidates for intracellular labeling of amber suppressed proteins [210,221]. However, the number of available cell permeable dyes and their spectral range are currently rather limited. A new series of TMR-derivates was developed by Atto-TEC [224]. These probes exhibit excellent biophysical properties and cover the whole range of the visible spectra. Nevertheless, it has to be determined whether these Atto dyes are suitable for live cell application approaches and intracellular labeling.

1.4 Objectives

The aim of this work is to develop a new generation of the FRET-based conformational sensors for small GTPase activity (COSGA). These second generation probes will be genetically encoded and thus circumvent the extremely labor-intensive preparation process of the first generation of conformational sensors. This preparation process required expertise in a variety of methodologies, including protein expression and engineering, microinjection for cellular studies. To genetically encode COSGA probes, stop codon suppression mutagenesis, enabling incorporation of an unnatural amino acid into the target protein, and subsequent intracellular fluorescence labeling will be used. The first part of the work presented in this thesis focuses on the establishment of the UAA incorporation into small GTPases and the subsequent intracellular fluorescence labeling in live mammalian cells. While the incorporation of UAAs is nowadays a widely used technology, the subsequent site-specific intracellular fluorescent labeling remains challenging. Therefore, the well-characterized Rab1b conformational probe will serve as a target protein to allow direct comparison of the second generation COSGA probes with the *in vitro* and *in vivo* data obtained from the first generation sensor. Hence, the functionality of the genetically encoded sensors can be confirmed following the same strategies used for the recombinant probes, including effector binding studies and coexpression of GEF and GAP regulatory enzymes.

The second part of the work presented here targets the application of the COSGA approach to the small GTPase Rheb. Rheb is a particularly interesting target for biosensor development due to several reasons. First, it is the only known activator of mTORC1 and is indispensable for mTORC1 activation on lysosomes by virtually all stimuli (reviewed in [225]). Second, the precise mechanism of mTORC1 activation by Rheb remains controversial and it is not known, whether this interaction is direct or mediated by another, yet unknown factor [226-229]. In fact, it has not been clearly shown whether mTORC1 activation under physiological conditions indeed depends on the nucleotide state of Rheb and if Rheb-GTP is sufficient to activate mTORC1 [126,230]. Third, although phosphorylation of the TSC complex, the Rheb GAP, is commonly thought to inhibit the GAP activity of TSC2 on Rheb, the mechanism of this inhibition, as well as the physiological relevance of the phosphorylation sites, have not been dissected yet [230-233]. In addition, no Rheb GEF protein was yet indentified and the exact mechanism by which Rheb is supposed to adopt its active state in absence of the TSC complex on the lysosomal surface remains elusive. In fact, this event was neither monitored nor directly proven and is assumed solely because of the indirectly determined mTORC1 activity. Moreover, several signals and protein interactions seem to regulate Rheb activity independent of its activity state, such as PDE4D or GAPDH binding in the absence of their substrates [138,139]. Thus, the impact of the nucleotide state of Rheb on its function as an mTOR activator is barely understood. And fourth, due to the lack of known Rheb effector proteins, no specific Rheb effector binding is available. As traditional probes for small GTPase activity rely on such domains to differentiate the activity state of the small GTPase, at the present time no Rheb sensor is available. A biosensor reporting Rheb spatiotemporal activity would allow dissecting the role of Rheb activity during nutrient sensing on the lysosomal surface. Moreover, a Rheb probe would enable to shed light on the true regulation of Rheb by upstream signals such as the TSC complex, as well as the link to mTORC1 activation and downstream signals, such as autophagy.

2. Material and Methods

2.1 Material

2.1.1 Chemicals

Table 2.1: Chemicals

Chemicals	Supplier
2-Propanol	J.T. Baker
4% PFA/PBS solution	Morphisto
Acetic acid	Sigma-Aldrich
Acetonitril	
Acrylamid 4 K - Lösung (30%)	Diagonal
Agarose	Invitrogen
Amersham ECL Prime Western Blotting Detection Reagent	GE Healthcare
Ammonium persulfate (APS)	Serva
Ampicillin Sodium Salt	Gerbu
Bovine serium albumin (BSA)	Biomol
Bromophenol Blue	Serva
Dimethylsulfoxide (DMSO)	Serva
Ethanol	Thermo Fisher Scientific
Ethylenediaminetetraacetic adic (EDTA)	Gerbu
Formic acid	
GeneRuler 1kb DNA ladder	ThermoFisher Scientific
Glycerol	Gerbu
Glycine	Carl Roth
HEPES	Carl Roth
Kanamycin	Gerbu
Methanol	Sigma-Aldrich
Phenylmethylsulfonylfluoride (PMSF)	Serva
Prestained protein marker (10-250kDa) '7712S	New England BioLabs
Protease Inhibitor cocktail, EDTA-free	Roche
Roti GelStain	Carl Roth
Skimmed Milk Powder	Carl Roth
Sodium azide	Sigma-Aldrich

Sodium Chloride	Sigma-Aldrich
Sodium dodecyl sulfate (SDS)	Carl Roth
Tris-(hydroxymethyl)-aminomethan (Tris)	Santa Cruz
Triton X-100	Thermo Fisher Scientific
Tween-20	Serva
β-Mercaptoethanol	Serva

Table 2.2: Unnatural amino acids

Unnatural amino acid	Supplier
4-Azido-L-Phenylalanine (AzF)	Chem-Impex International
Endo-Bicyclononyne-Lysine (BcnK)	SiChem
Trans-Cyclooctene-L-Lysine (TcoK*)	Kind gift by E.Lemke

Table 2.3: Tetrazine-functionalized Dyes

Dye	Supplier
6-Methyl-Tetrazine-BDP-FL	Jena Bioscience
6-Methyl-Tetrazine-FDAC	synthesized by X. Chen, AG Wu
Tetrazine-5-FAM	Jena Bioscience
Tetrazine-5-TAMRA	Jena Bioscience
Tetrazine-Atto 520	synthesized by L. Zhao, AG Wu
Tetrazine-Atto 565	synthesized by L. Zhao, AG Wu
Tetrazine-Atto 590	kind gift by Dep. 2
Tetrazine-BDP-FL	Jena Bioscience
Tetrazine-Cy5	Jena Bioscience
6-Methyl-Tetrazine-TAMRA	synthesized by X. Chen, AG Wu

2.1.2 Enzymes and Antibodies

Table 2.4: Enzymes

Enzyme	Supplier
FD XhoI	ThermoFisher Scientific
FD BamHI	ThermoFisher Scientific
FD NheI	ThermoFisher Scientific
DpnI	ThermoFisher Scientific

FastAP Thermosensitive Alkaline Phosphatase	ThermoFisher Scientific
Phusion High-Fidelity PCR Master Mix HF	New England BioLabs
Red-Taq DNA Polymerase 2X MasterMix, 2,0	VWR
T4 DNA Ligase	ThermoFisher Scientific
BigDye Terminator	ThermoFisher Scientific

Table 2.5: Antibodies

Antibody	Supplier
Anti-Actin	Chemicon
Anti-GFP	AnaSpec
Anti-mouse HRP conjugate	Dako
Anti-rabbit HRP conjugate	Millipore

2.1.3 Oligonucleotides

2.1.3.1 Cloning primers

Table 2.6: Cloning primer

Name	Sequence
1056_XhoI_Giantin_fwd	AACCGCTCGAGgaaccgcagcaaagcttttctgaagc
175 Rab1b rv	TTCGGATCCTTAACAGCAACCACCACCCGCC
665_NdeI_Citrine_fw	GGAATTCCATATGGTGAGCAAGGGCGAGG
757_XhoI_KX_fw	CCGCTCGAGGATCCGGCGGTTCCG
758_BamHI_KX_rv	CGGGATCCTTACATAATTACACACTTTGTCTTTGACTTCTTTTTCTT
837_BamHI_Rheb_fl_rv	CGCAAGGATCCTTACATCACCGAGCATGAAGACTTGCCTT
910_XhoI_Olisho_Rab1b_fwd	AACCGCTCGAGGCCGCCTACAGCAGCATCCTGAACCCGGAATAT GACTATCTGTTTAAACTGCTGCTGATCGGCG
914_XhoI_mTurD11_rv	AAGGCCTCGAGggcggcggtcacgaactccagcaggacc
XhoI_D2Rab1b_fw	AAAAACTCGAGGAATATGACTATCTGTTTAAACTGCTGCTGATCG
XhOlisho_Rheb_fw	AATTCTCGAGGCCGCCTACAGCAGCATCCTTCCGCAGTCCAAGTC CCGGAAGATCGCG

2.1.3.2 Single site-directed mutagenesis primers

Table 2.7: Single site-directed mutagenesis primer

Name	Sequence
1213_Rheb_S20N_f	GGGCTACCGGTCTGTGGGGAAAAACTCATTGACG
1215_Rheb_Q64L_f	CTTGTAGACACAGCCGGGCTGGATGAATATTCTATCTTTCCTC
1217_Rheb_G63A_f	CATCTTCAACTTGTAGACACAGCCGCCCAAGATGAATATTCTAT CTTTCC
1218_Rheb_G63V_f	CATCTTCAACTTGTAGACACAGCCGTGCAAGATGAATATTCTAT CTTTCC
1219_Rheb_D60K_f	CATCTTCAACTTGTAAAGACAGCCGGGCAAGATGAATATTCTAT CTTTCC
1220_Rheb_D122N_f	CCTATTATGTTGGTTGGGAATAAGAAAAACCTGCATATGGAAA GGG
730_Rab1b_W102_TAG_fw	TATGCCAACGTGAAACAGTAGCTGCAGGAAATTGATCGTTATG CC
731_Rab1b_G18_TAG_fw	CTGCTGCTGATCGGCGATTCTTAGGTGGGTAAAAGCTGTCTGC TGCTGCG
732_Rab1b_S36_TAG_fw	TTTGCTGATGACACGTATACCGAATAGTATATCAGTACCATTGG CGTCGACTT
733_Rab1b_I41_TAG_fw	CGTATACCGAATCCTATATCAGTACCTAGGGCGTCGACTTCAAA ATCCGTACGATCGAAC
846_Rab1b_T34_TAG_fw	GCGTTTTGCTGATGACACGTATTAGGAATCCTATATCAGTACCA TTGGCG
847_Rab1b_D53TAG_fw	TCGACTTCAAAATCCGTACGATCGAACTGTAGGGTAAAACCAT CAAACTG
848_Rab1b_G54TAG_fw	AATCCGTACGATCGAACTGGATTAGAAAACCATCAAACTGCAG ATCTGGG
890_aRheb D33TAG	CGATTCAATTTGTTGAAGGCCAATTTGTGTAGTCCTACGATCCA ACC
891_aRheb S34TAG	CGATTCAATTTGTTGAAGGCCAATTTGTGGACTAGTACGATCCA ACC
892_aRheb N50TAG	GATCACAGTATAGGGACAAGAATATCATCTTCAACTTGTAGAC ACAGCCG
893_aRheb G51TAG	ATCACAGTAAATTAGCAAGAATATCATCTTCAACTTGTAGACAC AGCCGG
898_aRheb G108TAG	CCATGGCAAATTGTTGGATATGGTGTAGAAAGTACAAATACC
899_Q67L_Rab1b_for	GCAGATCTGGGATACCGCTGGTCTAGAACGTTTCCGTACC
Rab1b D2_rv	GTTATCTAGATCCGGTGGATCCTTATTATTAACCACCACCCGCC GGTTTCACCGGGG

Rab1b_N121I_f	CAACAAACTGCTGGTTGGTATCAAAAGCGATCTGACGACGA
Rab1b_S22N_f	CGATTCTGGTGTGGGTAAAAACTGTCTGCTGCTGCG

2.1.3.3 Sequencing primers

Table 2.8: Sequencing primer

Name	Sequence
108_fwd_n_fluo	CGACCACTACCAGCAGAACACC
372_CMV_fw	CGCAAATGGGCGGTAGGCGTG
905_SV40_rev	GGACAAACCACAACTAGAATGC

2.1.4 Plasmids

Unless indicated otherwise, plasmids were generated within this work.

2.1.4.1 Plasmids for stop codon suppression

Table 2.9: Plasmids for stop codon suppression

Plasmid	Source
(U6-PylT)4 EF1α-BcnKRS	Kind gift by J.Chin
pcDNA_SV40Bst-Yam_CMV(eCFP_P2A_AzF-RS)	
pcDNA-AzpRS (RS-V1)	Kind gift by T.P.Sakmar
pCMV PylRS AF	Kind gift by E. Lemke and C. Schultz
pSVBpUC-Yam	Kind gift by T.P.Sakmar

2.1.4.2 Rab1b plasmids

Table 2.10: Rab1b plasmids

Plasmid	Source
pCitrine_aRab1b fl. D53TAG	
pCitrine_aRab1b fl. G18TAG	
pCitrine_aRab1b fl. G54TAG	
pCitrine_aRab1b fl. I41TAG	
pCitrine_aRab1b fl. S36TAG	
pCitrine_aRab1b fl. T32TAG	
pCitrine_aRab1b fl. T34TAG	

pCitrine_aRab1b fl. W102TAG
pCitrine_Olisho_aRab1b fl. D53TAG
pCitrine_Olisho_aRab1b fl. G54TAG
pCitrine_Olisho_aRab1b fl. S36TAG
pCitrine_Olisho_aRab1b fl. S36TAG N121I
pCitrine_Olisho_aRab1b fl. S36TAG Q67L
pCitrine_Olisho_aRab1b fl. S36TAG S22N
pCitrine_Olisho_aRab1b fl. T34TAG
pCitrine_Olisho_Rab1b fl.
pCitrine_Rab1b fl.
pCitrine_Rab1b fl. N121I
pCitrine_Rab1b fl. Q67L
pCitrine_Rab1b fl. S22N
pCitrine_XPn_aRab1b S36
pCitrine_XPn_Rab1b fl.
pCitrineD11_LE_aRab1b S36

2.1.4.3 Rheb plasmids

Table 2.11: Rheb plasmids

Plasmid	Source
pCitrine_Rheb fl.	
pCitrine_XhOlisho_aRheb fl. D33TAG	
pCitrine_XhOlisho_aRheb fl. G108TAG	
pCitrine_XhOlisho_aRheb fl. G51TAG	
pCitrine_XhOlisho_aRheb fl. N50TAG	
pCitrine_XhOlisho_aRheb fl. S34TAG	
pCitrine_XhOlisho_Rheb fl.	
pmCherry_Rheb fl.	

2.1.4.4 Plasmids for cellular markers and others

Table 2.12: Plasmids for cellular markers and others

Plasmid	Source
pCitrine-C1	Clontech
pEGFP_182TAG	

pEGFP_182TAG_Kx	
pKate2_Giantin 3131-3259	Kind gift by P.I.Bastiaens
pmCherry_OCRL fl.	Kind gift by R.S. Goody
pmCherry-C1	Clontech
pTagBFP_2xFKBPF37V_DrrA 340-533	Ag Wu
pTagBFP_OCRL 539-901	Ag Wu
pTagBFP_TBC1D20 1-362	
pTagBFP-C	Evrogen
pTagBFP-C	Evrogen

2.1.5 Buffers and Solutions

All buffers were prepared using double distilled MilliQ water. Unless indicated otherwise, all percentages are volume/volume.

Table 2.13: Enzyme buffers

Enzyme Buffer	Supplier
10x Fast Digest Buffer	ThermoFisher Scientific
10x T4 DNA Ligase Buffer	ThermoFisher Scientific
10x Tango Buffer	ThermoFisher Scientific
10x FastAP Buffer	ThermoFisher Scientific
5x Sequencing Buffer	ThermoFisher Scientific

Table 2.14: Transfer buffer

Amount	Component
6.04 g	Tris/HCl
30 g	Glycine
1200 mL	H_2O
400 mL	Methanol
ad 2 L	H_2O

Table 2.15: 10x TBS-T buffer

Amount	Component
48.46 g	Tris/HCl
160.12 g	NaCl
1600 mL	H_2O
20 mL	Tween
ad 2 L	H_2O

Table 2.16: Stacking gel buffer

Amount	Component
0.5 M	Tris/HCl pH 6.8
0.4 % (w/v)	SDS

Table 2.17: Separating gel buffer

Amount	Component
1.5 M	Tris/HCl pH 8.8
0.4 % (w/v)	SDS

Table 2.18: 4x SDS Sample Buffer

Amount	Component
130 mM	Tris/HCl pH 6.8
200 mM	DTT
4 % (w/v)	SDS
0.025 % (w/v)	Bromophenol blue
20 %	Glycerin

Table 2.19: RIPA Buffer

Amount	Component
50 mM	Tris/HCl pH 7.8
150 mM	NaCl
0.1 % (w/v)	SDS
0.5 % (w/v)	Sodium deoxycholate
1 %	Triton X-100

Table 2.20: 10x SDS-Page Running Buffer

Amount	Component
250 mM	Tris/HCl
2 M	Glycin
1 % (w/v)	SDS

Table 2.21: 50x TAE Buffer

Amount	Component
242 g	Tris base
57.1 mL	Acidic acid
100 mL	0.5 M EDTA pH 8.0
ad 1 L	H_2O

Table 2.22: 5x DNA Loading Buffer

Amount	Component
30 % (w/v)	Sucrose
20 %	Glycerin
0.2 % (w/v)	Orange G

2.1.6 Kits and Commercials

Table 2.23: Kits and Commercials

Kit	Supplier
E.Z.N.A. Cycle Pure Kit	Omega bio-tek
E.Z.N.A. Gel Extraction Kit	Omega bio-tek
E.Z.N.A. Plasmid Mini Kit	Omega bio-tek
SuperSignal™ West Femto Maximum Sensitivity Substrate	ThermoFisher Scientific
Western Blotting Detection Reagent	GE Healthcare

2.1.7 Bacterial strains

Table 2.24: Bacterial strains

Bacterial strain	Supplier
E.coli XL-1 blue (recA1 endA1 gyrA96 thi-1 hsdR17 supE44 relA1 lac)	Stratagene

2.1.8 Mammalian cell lines

Table 2.25: Mammalian cell lines

Cell line	ATCC no.	Source
CHO	CCL-61™	Kind gift by AG Waldmann
Cos-7	CRL-1651™	Kind gift by AG Bastiaens
HEK 293	CRL-1573™	Kind gift by AG Waldmann
HEK 293T	CRL-3216™	Kind gift by AG Großmann
HeLa	CCL-2™	ATCC
MCF7	HTB-22™	ATCC
U2OS	HTB-96™	Kind gift by AG Hennig

2.1.9 Material

Table 2.26: Frequently used Devices

Device	Supplier
Accu-jet pro	Brand
Alpha Imager HP	Alpha Innotec
BioPhotometer	Eppendorf
Blotting Cassette	GE Healthcare
Centrifuge 5415R	Eppendorf
Centrifuge 5804R	Eppendorf
Countess® II Automated Cell Counter	LifeTechnologies
EPS 301 Power supply	GE HEalthcare
HeraSafe HS12	Hera
IncuCyte Zoom	Essen BioScience
Invo2 Humidified CO_2-supplemented Incubator	Memmert
Lyophilizer	

Microwave	Siemens
MilliQ Water/Millipore Advantage A	Merck Millipore
Mini Trans-Blot®	Bio-Rad
Mini-PROTEAN® Tetra handcast system	Bio-Rad
NanoDrop 2000c	Thermo Fisher Scientific
OptiMax X-ray Flim Processor	PROTEC
PCR Cycler	Analytik Jena
Plasma Surface technology Femto	Diener electronic
PowerPac™ Universal Power Supply	BioRad
QBT Block Heater	Grant Instruments
Shaker ST5	Ingenieurbüro CAT
Typhoon Trio+ Imager	GE Healthcare
VortexGenie2	ScientificIndustries
Waterbath	Memmert

Table 2.27: Cell Culture Medium and Supplements

Medium / Supplement	Supplier
DMEM, high glucose, phenol-red free	ThermoFisher Scientific
Dulbecco's Modified Eagle's Medium, D5796	Sigma-Aldrich
Earle's Balanced Salt Solution, no phenol red	ThermoFisher Scientific
Fetal Bovine Serum	ThermoFisher Scientific
GlutaMAX Supplement	ThermoFisher Scientific
MEM Non-Essential Amino Acids Solution	ThermoFisher Scientific
Minimum Essential Medium Eagle, Hepes-modified (M7278)	Sigma-Aldrich
Opti-MEM	ThermoFisher Scientific
Penicillin-Streptomycin Solution P4333	Sigma-Aldrich
Phosphate buffered saline, P4417	Sigma-Aldrich
Poly-L-Lysine solution, 0.01%, P4832	Sigma-Aldrich
Sodium Pyruvate	ThermoFisher Scientific
Trypsin-EDTA solution, 0.25%, T4049	Sigma-Aldrich
XtremeGene HP DNA Transfection Reagent	Roche
Insulin I9278	Sigma-Aldrich
Trypan blue	Invitrogen

Table 2.28: Frequently used Consumables

Consumable	Supplier
TC-Flasche T75,Standard	Sarstedt
Cell Culture Plate 48-well, tc-treated	Eppendorf
Conical tube 15mL	Sarstedt
Conical tube 50mL	Sarstedt
CryoPure Tube 1.8mL	Sarstedt
Glass Bottom Dish 35mm	MatTek
Safe-Seal Reaktionsgefäße 0,5 mL	Sarstedt
Safe-Seal Reaktionsgefäße 1,5 mL	Sarstedt
Safe-Seal Reaktionsgefäße 2,0 mL	Sarstedt
Sterile serological pipets 10mL	Sarstedt
Sterile serological pipets 25mL	Sarstedt
Sterile serological pipets 5mL	Sarstedt
Falcon TC plate 24 well	ThermoFisher Scientific
TC plate 6 Well, Standard, F	Sarstedt
TC-dish 100, Standard	Sarstedt
x-well slides 4-well on cover glass	Sarstedt
x-well slides 8-well on cover glass	Sarstedt
Pipette tip 10µL	Sarstedt
Pipette tip 200µL	Sarstedt
Pipette tip 1250µL	Sarstedt
Cell scraper	VWR
Countess Cell Counting Chamber Slides	Invitrogen
Whatman cellulose chromatography paper	Sigma-Aldrich
Autoradiography Film	Santa Cruz
Forceps	Carl Roth
0.2 mL PCR tubes	Sarstedt
Multi PCR stripes (8-strip)	Sarstedt

2.1.10 Equipment

Table 2.29: Frequently used Microscopes

Microscopes	Supplier
TCS SP5	Leica Microsystems
SP2	Leica Microsystems
TCS SP8	Leica Microsystems
PrimoVert Inverted Microscope	Zeiss

Table 2.30: Frequently used Software

Software	Publisher
Adobe Photoshop CS4	Adobe
ImageJ 1.51p	W.Rasband (NIH)
IncuCyte Zoom 2016B	Essen BioLabs
JediFLIM	Dr. K. Schuermann (Dep.2, MPI Dortmund)
LasAF Lite Leica Application Suite 2.6.0	Leica Microsystems
MatLab 2015a	MathWorks
Microsoft Office 2010	Microsoft
Modified JediFLIM	B. Scocozza (Dep.2, MPI Dortmund)
OriginPro 9.0G	OriginLab
PyCharm 2017.1.4	JetBrains
PyMol	Schrödinger Suites
SnapGene Viewer 3.1.4	SnapGene
SymPhoTime v5.12	PicoQuant GmbH

2.2 Methods

2.2.1 Biomolecular Methods

2.2.1.1 Template PCR

Single genes or sub genetic fragments were amplified and fused to restriction enzyme recognition sites by Polymerase chain reaction (PCR). Table 2.31 indicates the components and volumes of a standard PCR reaction.

Table 2.31: Standard PCR reaction

Volume	Component
10 µL	2x Phusion High-Fidelity PCR Master Mix HF
0.5 µL	Forward primer (10 pmol/µL)
0.5 µL	Reverse primer (10 pmol/µL)
1.2 µL	DMSO
10-20 ng	Template DNA
ad 20 µL	ddH_2O

All components were thawed on ice, the Phusion High-Fidelity PCR Master Mix HF, both primers, and DMSO were mixed with the PCR template in a 0.2 mL PCR tube and shortly centrifuged before running the program “Template PCR” (Table 2.32) in a PCR cycler. The annealing temperature (*) was selected accordingly to the melting temperature of the used primers, typically 2-4 °C below the lowest melting temperature. All primer pairs were designed to exhibit a maximum of 5 °C difference in melting temperature. Annealing time (**) was set accordingly to the lengths of the gene to be amplified.

Table 2.32: Template PCR program

Temperature	Time	Cycle
98 °C	2 min	-
98 °C	30 sec	30x
50-72 °C *	30 sec	
72 °C	15 sec/1kb**	
75 °C	10 min	-
4 °C	∞	-

Successful amplification of the target gene was verified by DNA gel electrophoresis. The PCR product was purified using a PCR purification kit or via gel extraction, and eluted from the columns in 30 µL elution buffer.

2.2.1.2 Linker Insertion and Modification

Engineering of the linker between the fluorescent protein and the small GTPase was performed by PCR amplification of the respective target gene using a prolonged forward primer encoding an XhoI restriction enzyme recognition site and the respective linker sequence. Linker sequences were manually codon optimized for mammalian cells using the NCBI-GenBank-based Codon Usage Database [234].

2.2.1.3 DNA Gel Electrophoresis

To confirm successful gene amplification and/or restriction enzyme digestion, the PCR product and/or the crude digestion reaction were analyzed by DNA gel electrophoresis. Therefore 1% (w/v) agarose was suspended into 1x TAE buffer and boiled in the microwave until the agarose was fully dissolved. 5 µL Roti-GelStain was added per 100 mL agarose and the solution was mixed intensively. Gels were cast by pouring the solution into a DNA gel electrophoresis device and inserting a comb to generate sample loading pockets. 2-5 µL of the DNA sample was mixed with the respective volume of 5x DNA loading buffer and the whole mixture was loaded onto the DNA gel. Gel electrophoresis was performed for 40 min at 90 V.

2.2.1.4 Restriction Enzyme Digestion

Complementary sticky ends on the PCR product and on the plasmid backbone were generated by restriction enzyme digestion. Table 2.33 and Table 2.34 show standard reactions for digestion of a PCR product and plasmid DNA, respectively. All components were thawed on ice and mixed in a 1.5 mL reaction tube. The digestion was performed for 4-16 h at 37 °C. Successful digestions were controlled by DNA gel electrophoresis.

Table 2.33: Standard reaction for restriction enzyme digest of PCR products

Volume	Component
3.5 µL	10x FD buffer
1 µL	Enzyme 1
1 µL	Enzyme 2
30 µL	Purified PCR product

Table 2.34: Standard reaction for restriction enzyme digest of plasmids

Volume	Component
2 µL	10x FD buffer
1 µL	Enzyme 1
1 µL	Enzyme 2
1 µL	FastAP
0.5-1.0 µg	DNA
ad 20 µL	ddH_20

The digested DNA fragments were purified using a PCR purification kit or via gel extraction. In both cases samples were eluted in 30 µL elution buffer.

2.2.1.5 Ligation

Digested plasmid backbones and the respective PCR products were ligated using T4 DNA Ligase. Table 2.35 shows a standard ligation reaction. All components were thawed on ice, mixed in a 1.5 mL reaction tube, centrifuged shortly and incubated at 16 °C overnight.

Table 2.35: Standard ligation reaction

Volume	Component
1 µL	10x T4 DNA Ligase buffer
1 µL	T4 DNA Ligase
1 µL	Backbone DNA, digested and dephosphorylated
3 µL	Insert DNA, digested
ad 10 µL	ddH_2O

On the following day, the complete ligation reaction was chemically transformed into *E. coli* and positive clones were screened by Colony PCR.

2.2.1.6 Single Site-Directed Mutagenesis

Exchange of up to two amino acids and insertion of single amino acids into a target sequence were performed by single site directed mutagenesis using only one primer. Primers for this purpose were designed with at least 50 bp lengths and more than 20 bp on each side of the mutation site. To ensure selective and strong binding of the primer a 3’ GC

clamp was introduced and primers with melting temperatures higher than 68 °C were generated. Table 2.36 shows a standard single site-directed mutagenesis reaction. All components were thawed on ice, mixed in a 0.2 mL PCR tube and shortly centrifuged. The reaction was performed using the PCR program illustrated in Table 2.37. Annealing temperatures (*) were selected accordingly to the primers used, usually 3-5 °C below the primer melting temperature.

Table 2.36: Standard reaction for single site-directed mutagenesis

Volume	Component
10 µL	2x Phu HF MasterMix
1.5 µL	Primer (100 pmol/µL)
1.2 µL	DMSO
0.4-0.6 µg	Plasmid DNA
ad 20 µL	ddH_2O

Table 2.37: Single site-directed mutagenesis PCR program

Temperature	Time	Cycles
98 °C	30 sec	-
98 °C	30 sec	29x
65-72 °C *	30 sec	
72 °C	30 sec per 1kb	
72 °C	10 min	-
4 °C	∞	-

Following the PCR reaction, 2.3 µL 10x Tango buffer and 1 µL DpnI were added to the reaction mix and incubated at 37 °C for 4-16 h. The whole reaction was subsequently transformed chemically into *E. coli* XL1 blue. Three to five clones were selected, the plasmid DNA was extracted and the sequence of the target gene verified by DNA sequencing

2.2.1.7 DNA Sequencing

Sequencing of plasmid DNA was performed by either sending the samples to external sequencing services (StarSeq GmbH or Eurofins), or performed manually using BigDye Terminator and submitted to the MPI in-house sequencing facility.

For external sequencing services the plasmid of interest was mixed with an appropriate sequencing primer following sample submission guidelines of the respective company.

For in-house submission, the sequencing reaction was performed as displayed in Table 2.38. All components were mixed in a 0.2 mL PCR tube and the sequencing reaction was performed following the protocol shown in Table 2.39.

Table 2.38: Standard DNA sequencing reaction

Volume	Component
2 µL	5x Sequencing buffer
2 µL	BigDye Terminator
1.5 µL	Primer (10 pmol/µL)
0.4-0.6 µg	Plasmid DNA
ad 10 µL	ddH_2O

Table 2.39: DNA sequencing PCR program

Temperature	Time	Cycles
96 °C	4 min	-
96 °C	10 sec	25x
50 °C	5 sec	
60 °C	4 min	
4 °C	∞	-

Following the sequencing reaction, the reaction mix was transferred into a 0.5 mL reaction tube and DNA was precipitated by adding 2 µL 4 M NaAc pH 4.0, 2 µL 100 mM EDTA pH 7.0, 16 µL ddH_2O and 70 µL 100 % EtOH. The mixture was intensively mixed, incubated for 15 min at RT and centrifuged for 30 min at 14 000 rpm and 4 °C. The pellet was washed carefully with 0.5 mL ice cold 70 % EtOH and centrifuged again for 20 min at 14 000 rpm and 4 °C. The supernatant was discarded; the pellets were dried at RT and submitted to the MPI in-house sequencing facility.

2.2.1.8 Transformation into E. coli

Transformation of plasmid DNA into *E. coli* allows amplification of whole plasmids with high efficiency and low error rate. 2-10 ng plasmid DNA or 10 µL crude ligation reaction was mixed with 30-300 µL solution of chemically competent *E. coli* XL-1 blue and incubated for 1 h on ice, followed by a heat shock of 45 sec at 42 °C. 1 mL LB medium was added and the mixture incubated for 1 h at 37 °C and 170 rpm. The bacteria suspension was centrifuged at 8000 x *g* for 3 min, the supernatant discarded and the bacteria pellet resuspended in 50 µL LB medium. The solution was spread on agar plates containing antibiotic for selection of positive clones and the plates were incubated overnight at 37 °C.

2.2.1.9 Bacterial Cultures

Single bacterial colonies were chosen from agar plates after antibiotic selection and transferred into pre-culture tubes containing 4 mL LB medium and the respective selection antibiotic (Ampicillin 125 µg/mL, Kanamycin 50 µg/mL). Bacterial cultures were grown overnight at 37 °C and 170 rpm. Plasmid DNA was extracted using the E.Z.N.A.® Plasmid Mini Kit I following the manufacturer's protocol.

2.2.1.10 Colony PCR

Bacterial clones obtained by antibiotic resistance selection were screened for the plasmid of interest by Colony PCR. Table 2.40 shows the composition of a single standard Colony PCR reaction, for analysis of multiple clones, a master mix solution was calculated based on the number of selected clones. All liquid components were thawed on ice, mixed in a 1.5 mL reaction tube and centrifuged shortly. The master mix was distributed into Multi PCR stripes with 10 µL per tube. Single bacterial colonies were selected and transferred into 10 µL of the reaction mix. The same tips were used to plate the respective colony onto a fresh agar plate and the plates were incubated overnight at 37 °C. The reaction mix was placed in a PCR cycler and the Colony PCR program (Table 2.41) was performed.

Table 2.40: Single Colony PCR reaction mix

Volume	Component
5 µL	2x RedTaq MasterMix
1 µL	Forward primer (10 pmol/µL)
1 µL	Reverse primer (10 pmol/µL)
1x	Bacterial colony
ad 10 µL	ddH_2O

Table 2.41: Colony PCR program

Temperature	Time	Cycles
94 °C	2 min	-
84 °C	1 min	29x
55 °C	2 min	
72 °C	30 sec	
72 °C	10 min	-
4 °C	∞	-

Positive clones were inoculated in pre-cultures for plasmid extraction and DNA sequencing.

2.2.2 Preparation and Storage of Click-Reaction Components

2.2.2.1 Preparation of BcnK Solution

BcnK stock solution aliquots were prepared by dissolving 25 mg BcnK powder in 500 µL 30 % Acetonitrile / 1 % formic acid in water. The suspension was mixed intensively and distributed to ten 1.5 mL reaction tubes with 50 µL per tube (2.5 mg BcnK per tube). The aliquots were snap-frozen in liquid nitrogen, lyophilized and stored at -20 °C. Shortly before an experiment a 250 mM stock solution was prepared by adding 31 µL 0.1 M NaOH to one aliquot and dissolving the BcnK powder by pipetting. 250 mM stock solution aliquots were stored at -20 °C and, if not consumed immediately, thawed maximum up to three times after dissolving.

2.2.2.2 Preparation of AzF Medium

AzF medium was prepared by dissolving 0.12 g AzF powder in plain 500 mL MEM HEPES-modified medium (1 mM final AzF concentration). To enhance dissolving, the solution was sonicated until all AzF aggregates dissolved completely. The medium was sterile-filtered over a 0.2 µM syringe filter and completed by addition of 57 mL FBS, 5.7 mL sodium pyruvate, 5.7 mL NEAA and 5.7 mL GlutaMAX. AzF medium was aliquotted and aliquots were stored at -20 °C.

2.2.2.3 Preparation of Tetrazine-Functionalized Dyes

Tetrazine dyes were dissolved in cell culture grade DMSO and distributed to 1.5 mL reaction tubes with each tube containing 50-100 µg. The aliquots were snap-frozen in liquid nitrogen, lyophilized and stored at -20 °C. 5-10 mM stock solutions were prepared freshly before an experiment by dissolving the dye in cell culture grade DMSO. Aliquots were stored at -20 °C and thawed maximum up to three times.

2.2.3 Cell biological Methods

2.2.3.1 Subculture of Mammalian Cells

Mammalian cell lines were cultured in HEPES-modified Minimum Essential Medium Eagle (MEM) or Dulbecco's modified Eagle's Medium (DMEM), both supplemented with 10 % (v/v) fetal bovine serum (FBS), 1 % (v/v) non-essential amino acids (NEAA), 1 % (v/v) sodium pyruvate and, if required, 1 % (v/v) GlutaMAX, in a humidified incubator at 37 °C and 5 % CO_2, unless indicated otherwise. All mammalian cell lines were passaged two to three times a week by trypsinization and seeding of 1-3 x 10^5 cells in a fresh 10 cm dish. PenStrep was added to the growth medium only for certain experiments, such as reversible cryo-arrest experiments.

2.2.3.2 Cryo-Preservation and Long-Term Storage

Long-term storage of mammalian cells was performed in the gas phase of a liquid nitrogen tank in presence of 10 % DMSO in the growth medium. Therefore, 100 µL DMSO was mixed with 400 µL fully supplemented DMEM in a cryo vial and 500 µL of cell suspension (approximately 1 x 10^6 cells) were added. The cell stocks were stored for one week at -80 °C before being transferred into the vapor phase of a liquid nitrogen tank.

Cryo-preserved cells were thawed in a water bath at 37 °C. To remove DMSO from the growth medium, the cell solution was diluted into 10 mL medium and centrifuged for 5 min at 500 x *g*. The pellet was gently resuspended in 10 mL fresh medium and the cell solution transferred into a dish or flask for further cultivation.

2.2.3.3 Cell Culture Vessel Surface Treatment

Poly-L-Lysine coating

To increase cell adherence to the culture vessel and ensure cell attachment even after multiple medium exchanges, HEK 293 and HEK 293T samples were seeded on culture vessels pre-coated with Poly-L-Lysine. Table 2.42 shows the respective amount of Poly-L-Lysine solution used per well for the different types of growth vessels. Coating was performed by addition of Poly-L-Lysine solution on the bottom of the culture vessel, gentle rocking to distribute the solution evenly and incubation for 15-30 min at RT. The Poly-L-Lysine solution was removed and each well was washed three times in PBS to remove residual solution. The vessels were kept openly in the laminar flow bench to dry the wells before seeding of the cells.

Table 2.42: Coating of growth vessels with Poly-L-Lysine

Vessel Type	Poly-L-Lysine Volume / Well
4-well chamber slide	300 µL
8-well chamber slide	150 µL
24-well plate	200 µL
48-well plate	150 µL
6-well plate	150 µL*

* Only the growth channel was coated on cryo slides.

Glow-discharge surface modification

Samples for cryo experiments were treated by plasma treatment instead of Poly-L-Lysine coating, as this allows for more even and stronger cell adherence. Glow-discharge modification is a plasma irradiation treatment resulting in oxygen incorporation into the irradiated surface. This increases the amount of negative charges of the surface, allowing strong cell adhesion. Plasma surface treatment was performed following the standard procedure using the Femto device from Diener Electronics. Treated cell culture vessels were rinsed three times in PBS before cell seeding. Experiments in plasma surface treated vessels were performed in presence of PenStrep to decrease contamination risk.

2.2.3.4 Transfection

Transfection was performed using two different protocols: the traditional transfection and the fast-forward transfection for transfection of adherent an trypsinized cells, respectively.

Traditional Transfection

Traditional transfection was performed on adherent cells by seeding the cells one day before transfection. A 75-90 % confluent cell culture was rinsed once in 10 mL PBS (HEK 293 and HEK 293T cells were rinsed in 2 mL Trypsin), 1 mL Trypsin was added and the dish was incubated at 37 °C until all cells detached from the vessel bottom. Cell detachment was monitored by light microscopy. After complete cell detachment, 9 mL medium was added and cell aggregates were separated by pipetting. The cell suspension was then transferred into a 50 mL conical tube. 10 µL cell suspension was mixed in a 1.5 mL reaction tube with 10 µL Trypan blue and 10 µL of the mixture transferred on a Countess Cell Counting Chamber Slide. The cell number was counted using the Countess II Cell Counter. Based on the live cell count, the required volume for the cell number per well was calculated and added to each well. The total volume per well was adjusted using growth medium. Table 2.43 indicates the number of cells that were seeded according to the growth area per well for different cell lines.

Table 2.43: Cell numbers per growth area [cm²]

Cell line	Cell Number/cm²
CHO	1.5×10^4
Cos-7	1×10^4
HEK 293	1.875×10^4
HEK 293T	1.875×10^4
HeLa	1.5×10^4
MCF7	1.5×10^4
U2OS	1.5×10^4

Transfection was performed at approximately 60 % cell confluency judged by light microscopy on the morning following seeding of the cells.

Opti-MEM was added into a sterile 1.5 mL reaction tube; the plasmids were diluted into Opti-MEM, and mixed intensively. After addition of the transfection reagent, the mixture was incubated for 15-30 min at RT to allow DNA:reagent complex formation. Meanwhile BcnK was diluted 1:5 in 1 M HEPES buffer pH 7.5 and added to amber suppression samples to a final BcnK concentration of 250 µM, unless indicated otherwise. After complete

incubation time, the transfection mixture was added to each sample. To achieve even complex distribution within each well, the culture vessel was rocked gently. Unless indicated otherwise, all amber suppression samples were incubated in presence of UAA for 1.5 d post-transfection before further treatment. Table 2.44 shows the different culture vessels and the respective transfection conditions.

Table 2.44: Transfection conditions in different culture vessels

Application	Vessel Type	Total Vol./ Well	Growth Area/ Well	Opti-MEM	Total DNA Amount	Xtreme Gene
live cell microscopy	4-well chamber	0.5 mL	1.9 cm^2	80 µL	0.5 µg	0.8 µL
	8-well chamber	0.3 mL	0.8 cm^2	40 µL	0.3 µg	0.4 µL
Lysates	24-well plate	0.5 mL	2.0 cm^2	100 µL	0.5-1.0 µg	1.5 µL
IncuCyte	48-well plate	0.3 mL	0.64 cm^2	40 µL	0.3 µg	0.4 µL
Cryo-arrest	6-well plate	2.0 mL	8.87 cm^2	200 µL	3.0 µg	3.0 µL

Fast forward Transfection

Fast forward transfection was performed on trypsinized cells immediately before cell seeding. First, the respective amount of DNA was incubated with the XtremeGene transfection reagent in OPTI-MEM for 15-30 min at RT. Meanwhile cells of a 75-90 % confluent culture were rinsed in 10 mL PBS, 1 mL Trypsin was added and the dish incubated at 37 °C until cell detachment was completed. 9 mL medium was added and the cell solution was transferred to a 50 mL conical tube. The cell number was counted by mixing 10 µL cell suspension with 10 µL Trypan blue solution, transferring 10 µL of the mixture into a Countess Cell Counter Chamber slide and using the automated cell counting machine Countess II. Based on the live cell number, the required cell number was calculated and the respective volume was transferred into a fresh cell culture vessel for live cell imaging. Growth medium was added to the final working volume of the vessel and the solution was mixed to achieve even distribution of the cells throughout the vessel. The DNA-Reagent complex was added drop wise and the vessel was agitated gently to allow even distribution. The required amount of BcnK was added directly to the cell suspension.

2.2.3.5 Intracellular Chemical Labeling

To remove residual BcnK from the cells and thereby decrease side reactions, the medium was exchanged to BcnK-free DMEM 16-20h before intracellular labeling. Labeling was performed by diluting 5-10 mM stock tzDye to the final concentration of 0.5 µM into DMEM, unless indicated otherwise. The solution was rigorously mixed to avoid local

concentration differences. Cells were rinsed once in the dye-containing medium and incubated for 30-45 min at 37 °C and 5 % CO_2 in the humidified incubator. The dye-containing medium was removed and cells were rinsed at least once in dye-free medium. To remove residual dye from the cells, the samples were washed for several hours before imaging or treatment. Frequent rinsing of the sample can enhance dye removal but, depending on the cell line, may affect cell adherence. For live cell microscopy and IncuCyte experiments, the growth medium was exchanged to phenol red-free medium before imaging or directly after the labeling step, respectively.

2.2.3.6 Chemical Fixation of Cells

Cells were chemically fixed using paraformaldehyde (PFA) fixation. The samples were prepared using the same protocol and culture vessels as for live cell imaging. The medium of respective samples was removed, the cells once rinsed in PBS and incubated in 4 % PFA/PBS for 20 min at RT. The PFA solution was removed; the samples rinsed again in PBS and kept in PBS for imaging.

2.2.4 Biochemical Methods

2.2.4.1 Preparation of Whole Cell Lysates

Whole cell lysates for in-gel fluorescence and Western blot analysis were prepared from mammalian cells cultured in a 24-well plate (Table 2.43 and Table 2.44). Lysis of intracellularly labeled samples was performed 2-8 h post-labeling to allow removal of excess dye. The cells were rinsed once in cold PBS and lysed in 50 µL RIPA-buffer supplemented with 1 mM PMSF and 1x c0mplete EDTA-free protease inhibitor. To enhance lysis, the wells were scratched using a cell scraper. The lysates were transferred to 1.5 mL reaction tubes and centrifuged for 15 min at 4 °C and 14 000 rpm. The supernatants were transferred to fresh tubes and the pellets were discarded. The lysates were stored at -20 °C.

2.2.4.2 SDS-Page Gel Electrophoresis

All SDS polyacrylamide gels were hand cast using the mini-PROTEAN® Tetra handcast system. The acrylamide concentrations in the separation gel was 15 %, for stacking gels 4 % acrylamide was used. Table 2.45 and Table 2.46 show the detailed composition.

Table 2.45: Composition of 15% Separation gel

Separating Gel Concentration	15 %
Total Volume	100 mL
Acrylamide	50 mL
Separating Gel Buffer	25 mL
ddH_2O	22.9 mL
10 % APS	1 mL
TEMED	100 µL

Table 2.46: Composition of 4% Stacking gel

Stacking Gel Concentration	4 %
Total Volume	50 mL
Acrylamide	6.67 mL
Stacking Gel Buffer	12.5 mL
ddH_2O	31.5 mL
10 % (w/v) APS	0.5 mL
TEMED	50 µL

To prepare the stacking and separation gel acrylamide, gel buffer and water were added to two separate 50 mL conical tube and mixed intensively. 10 % (w/v) APS was added and the solution mixed gently. TEMED was added to the separating gel solution, mixed quickly by inverting twice and distributed to the gel casting device and covered with Isopropanol. After complete solidification of the separating gel, the Isopropanol was removed by decanting. TEMED was added to the stacking gel solution, mixed quickly by inverting twice and pipetted on top of the solid separating gels. Gel combs were inserted. Unless used on the same day, the gels were wrapped in wet tissue paper and stored in a plastic bag at 4 °C.

Whole cell lysates were thawed on ice. Unless indicated otherwise, 4x SDS-PAGE loading buffer was added and the samples were boiled at 95 °C for 10 min. Per slot 10 µL prestained protein standard and 10-30 µL lysate were loaded on the SDS-PAGE. The gels were run at 80 V until samples entered the separation gel, followed by 100-120 V for several hours. Proper separation was judged by separation of the prestained protein molecular weight standard.

2.2.4.3 *In-gel Fluorescence Analysis*

The completed SDS polyacrylamide gels were kept in the glass plates and fluorescence was scanned using a Typhoon Trio+ Scanner with the following settings:

Table 2.47: Settings for In-gel Fluorescence detection

Probe	Excitation Line	Sensitivity	Emission Filter	PMT Voltage
FAM	488 nm	Medium	520BP40	600-700 V
TMR	532 nm	Medium	580BP30	600-700 V
Cy5	633 nm	Medium	670BP30	600-700 V
Atto 565	532 nm	Medium	580BP30	600-700 V
Atto 590	532 nm	Medium	580BP30	600-700 V

Samples with low fluorescence intensity, e.g. TcoK incorporation experiments, were scanned with high laser sensitivity and/or increased PMT voltage (up to 750 V).

2.2.4.4 *Western Blot*

To verify the fluorescent bands' identity, the scanned gels were used for western blotting. The samples were transferred from the gel onto a nitrocellulose membrane in transfer buffer in a wet blot module for 40 min at 100 V. All following steps were performed on a tilting shaker at 20 rpm, washing steps at 60 rpm. The membrane was incubated in 5 % (w/v) milk in TBS-T for 1 h to block the residual protein binding sites of the membrane and incubated with rabbit anti-GFP primary antibody over night at 4 °C. The membrane was washed three times for 10 min in TBS-T and incubated with the HRP-conjugated anti-rabbit secondary antibody for 1 h at RT. After washing three times 10 min in TBS-T, the HRP-dependent luminescence reaction was started using standard ECL and/or SuperSignal ECL solution. Luminescence was detected by exposure of X-ray films which were developed in an automated developing machine. Exposure times were varied from few seconds up to 1 h to achieve proper signal detection.

To denature the HRP and thereby inhibit detection of the previously immunostained bands, the membrane was soft-stripped in 0.1 M NaN_3 for 1 h at RT, washed three times for 10 min in TBS-T and reblocked for 45 min in 5 % milk in TBS-T, followed by an overnight incubation with mouse anti-Actin antibody. The membrane was washed three times 20 min in TBS-T and incubated with HRP-conjugated anti-rabbit secondary antibody for 1 h at RT. Following three times 20 min washing steps at RT, the blots were incubated for 1 min with ECL substrate solution, transferred into a transparent plastic bag and fixed into a developing cassette. X-ray films were used to detect luminescence and subsequently developed in a developing machine.

Developed X-ray films were scanned; blots and fluorescence scans of the same gel were cropped, aligned and labeled using Photoshop CS4.

2.2.4.5 Determination of the Intracellular Labeling Efficiency

To determine the yield of the intracellular labeling reaction whole cell lysates of unlabeled and intracellularly TMR-labeled protein expressing cells were generated as described before (Chapter 2.2.4.1). 1 µM tetrazine FAM or tetrazine Cy5 were added to each lysate, the solution mixed intensively and incubated for 15 min at RT before adding SDS-PAGE loading buffer and further sample preparation. The samples were separated on SDS-PAGE and in-gel fluorescence of the different dyes was monitored.

2.2.5 Microscopy

2.2.5.1 Confocal Fluorescence Microscopy

Confocal fluorescence images of live cells were obtained using a Leica SP2, Leica TCS SP5 or SP8 laser scanning microscope using a HCX PL APO (λ blue) 63x oil objective. All microscopes were equipped with an incubation chamber, enabling live cell imaging at 37 °C and 5 % CO_2. Excitation wavelengths and emission detection bands of the respective fluorophores are listed in Table 2.48. FRET partners that have overlapping excitation spectra, e.g. Citrine and TMR, were imaged sequentially to ensure proper separation of the fluorescence signals. Unless indicated otherwise, all samples were imaged under live cell conditions.

Table 2.48: Settings for confocal imaging of different fluorophores

Type	Fluorophore	$\lambda_{excitation}$	$\lambda_{emission}$	Laser Source
Fluorescent protein	mCitrine	514 nm	520-540 nm	Argon/WLL
	eGFP	488 nm	503-530 nm	Argon/WLL
	mTurquoise2	458 nm	468-511 nm	Argon
	mCherry	587 nm	610-750 nm	WLL
	TagBFP	405 nm	520-540 nm	UV Diode
	mKate2	587 nm	640-790 nm	WLL
Organic Dye	BDP FL	496 nm	506-600 nm	WLL
	Fluorescein	496 nm	506-600 nm	WLL
	Atto 565	565 nm	595-700 nm	WLL
	Atto 590	590 nm	605-750 nm	WLL
	Atto 520	514 nm	530-600 nm	WLL
	TMR	552 nm	567-700 nm	WLL

2.2.5.2 Fluorescence Lifetime Imaging

Time domain fluorescence lifetime was performed at a TCS Leica SP5 or SP8 laser scanning microscope, both equipped with PciQuant's compact FLIM and FCS upgrade Kit and White Light Lasers from Koheras. Excitation wavelengths and emission detection bands were set according to the settings for confocal microscopy for the respective fluorophore and the pinhole was kept half open at 300 µm. Before each FLIM image, a sequential confocal image was acquired first. Laser power was adjusted to keep the photon count rate stable, below 10 % of the laser frequency (20 MHz). FLIM images were captured at 200 Hz scan speed and 256x256 or 512x512 format. Depending on the protein of interest, a minimum of 500-1000 counts per pixel or at least 15 000 counts per image were acquired.

2.2.5.3 Reversible Cryo-Arrest

Samples for reversible cryo-arrest were prepared as described before, but cells were seeded on modified glass slides. Reversible cryo-arrest was performed in collaboration with Dr. J. Hübinger (Dep. 2, MPI Dortmund) as previously described using the Leica TCS SP5 or SP8 microscopes [235]. Different stage inlays were tested to avoid frequent issues of sample movement post-freezing.

2.2.6 Image Manipulation and Data Analysis

2.2.6.1 Fluorescence Lifetime Image Analysis

Time-domain FLIM data was analyzed using the customized MatLab script for Global analysis [147]. Based on the obtained photon count images binary masks were generated using ImageJ and applied on the lifetime images. Single cells were selected manually and average lifetimes of whole cells or cellular segments, such as the Golgi apparatus or the Cytosol, were measured. FLIM images were false colored using the ImageJ look up table "*royal*" and data box charts were generated using OriginPro 9.0G.

2.2.6.2 Intensity-based Fluorescence Quantification

Microscopy experiments for image-based Fluorescence quantification were captured at 16-bit depth and with stable microscope settings during sample acquisition. Fluorescence intensities were quantified using ImageJ. In-gel and western blot densitometry analysis were performed similarly using ImageJ. Data illustrations were generated using Microsoft Excel 2010 or OriginPro 9.0G.

2.2.6.3 Analysis of Reversible Cryo-Arrest Data

FLIM data obtained from Cryo-arrest experiments was analyzed using either the MatLab-based Global Analysis script or the newly developed Python-based JediFLIM software by Dr. K. Schürmann (Dep.2, MPI Dortmund). XY-Correction of FLIM data was achieved by a modified version of JediFLIM, kindly developed by B. Scocozza (Dep.2, MPI Dortmund). Vesicle extraction was performed using a modified version of the ImageJ plugin "*Vesicle extraction*", originally written by Dr. M. Massip (Dep.2, MPI Dortmund). This modified version is based on detection of local maxima in intensity images and was developed in the frame of this work.

2.2.7 *In silico* Linker Optimization Strategies

2.2.7.1 In silico Prediction of the Secondary Structure

Secondary structures of the linker regions were predicted using the online PSIPRED Protein Sequence Analysis Workbench [236].

2.2.7.2 Calculation of Linker Lengths

Unstructured linker

To calculate the maximal distance between the FRET partners the distance of the fluorophores to the C-terminus or N-terminus was measured in the crystal structure of mCitrine and Rab1, respectively. Next, the length of the linker was determined using Equation 2.1. mCitrine and Rab1 amino acids that were not resolved in the crystal structures were treated as part of the linker. The sum of the three values represents the maximal distance between the FRET partners, assuming that the linker region does not adapt a secondary structure and that the fusion protein adapts a linear conformation. The distance and orientation between the synthetic dye fluorophore and the protein backbone is not taken into account in this calculation.

Equation 2.1

$$r = \sqrt{C_n} \times b_0 \times \sqrt{(n)}$$

r = distance [Å]
n = number of amino acids
b_0 = 3.8 Å
C_n = 2.3

Helical linker

To determine the maximal distance between the FRET partners assuming a helical linker, the amino acid sequence of the linker region plus 15 amino acids each upstream and downstream of the linker were applied to secondary structure prediction. The number of amino acids forming an alpha helix was divided by 3.6 to determine the number of windings. The result was multiplied with 5.4 Å, which is the length of one winding. The result was added to the distance of the fluorophores to the termini of mCitrine and Rab1b, assessed by crystal structure as described before. Amino acids of mCitrine and Rab1 those were not resolved in the crystal structures as well as amino acids between secondary structures were treated as unstructured and their distance was calculated using Equation 2.1. The sum of all values represents the maximal distance between the FRET partners assuming a helical conformation of the linker region and a linear conformation of the fusion protein.

3. Results

The focus of the study presented in this thesis was to genetically encode the previously developed FRET-based conformational sensors for small GTPase activity (COSGA). These conformational probes consist of a fluorescent protein tag as FRET donor and a synthetic dye introduced to the protein fold as acceptor [160,161]. Positioning of the acceptor position determines whether the sensor reports exclusively the nucleotide state of the small GTPase, or the nucleotide state as well as effector binding. The first generation of COSGA probes has been extensively characterized for Rab1b and KRas GTPases both *in vitro* and *in vivo* [160,161]. The major limitation of COSGA sensors is the labor-intensive preparation process, which requires various methods ranging from protein expression and purification to chemical protein engineering. Moreover, cellular application of these recombinant probes requires microinjection or electroporation. Therefore, this work focused on the development of a second, genetically encoded generation of COSGA probes to facilitate the use of these novel sensors. To this end, amber suppression approach and subsequent intracellular fluorescent labeling are utilized to side-specific introduce the FRET acceptor into the small GTPase fold. The first target protein is Rab1b, allowing comparison of the sensor properties of the first and second generation probes. The principle was subsequently applied to the small GTPase Rheb, which is the only known activator for the mammalian target of rapamycin (mTOR) complex 1 [126-128]. The lack of known Rheb effectors and thereby a specific Rheb binding domain that could be exploited as affinity tags impeded the development of traditional probes to monitor spatiotemporal Rheb activity.

3.1 Genetically Encoding of the Conformational Sensor

Two major steps are essential to genetically encode COSGA probes, (1) the cotranslational incorporation of an unnatural amino acid (UAA) into the target protein in mammalian cells and (2) the subsequent intracellular fluorescence labeling reaction to embed the FRET acceptor into the small GTPase fold. While the first step, to incorporate an UAA, has become a well-established method within the last decades [63,237], the second step, where the UAA is dye-labeled intracellularly, was achieved only in single cases [177,181]. As the labeling of intracellular proteins in mammalian cells remains challenging, the reaction and its major pitfalls were intensively assessed in this work.

3.1.1 Stop Codon Suppression in small GTPases

Stop codon suppression of small GTPases in mammalian cells was performed using two different amber suppression systems. Due to its artificial nature, the UAA incorporation event competes with the termination of the translation process (see Chapter 1.3). In eukaryotic cells, translation is terminated by the eukaryotic release factors 1 and 3 (eRF1/eRF3) [164-167]. When exogenously expressed, the orthogonal aminoacyl-tRNA synthetase (RS) loads the orthogonal $tRNA_{CUA}$ with the UAA, allowing UAA incorporation in response to an amber codon at the ribosome [63,237]. The orthogonal incorporation process competes with the endogenous release factor-mediated termination of the translation, yielding a mixed expression of the amber protein as a full-length protein (UAA incorporation) and a N-terminal fragment (translational termination) [180,238,239]. The incorporation efficiency, and thereby the expression rate of an amber protein, depends on the target protein, the incorporation site, the abundance of the orthogonal $tRNA_{CUA}$ and the used cell line. Two different parameters were evaluated to estimate the UAA incorporation efficiency of a sample: (1) the number of incorporating cells per sample and (2) the ratio of full-length and fragment expression of the small GTPase.

3.1.1.1 Evaluation of UAA Incorporation Efficiency

To establish a general protocol for UAA incorporation in mammalian cells amber GFP182TAG (aGFP) and different amber mutants of mCitrine-Rab1b (hereafter referred to as aRab1b) were utilized. aGFP is a reporter construct consisting of an eGFP cassette modified with an internal TAG stop codon at position 182 [240]. The amber codon prevents the full-length expression and fluorophore maturation in the absence of an UAA, whereas UAA presence and incorporation result in a mature and fluorescent protein. Thereby, the reporter construct allows for precise detection of the UAA incorporation event. In contrast, the fluorescent protein (FP) of the COSGA sensor is fused to the N-terminus of Rab1b, positioning the FP upstream of the amber codon (Figure 3.1 A). On the one hand, this allows for native prenylation of the Rab1b C-terminus, a process essential for membrane targeting [46,47,241], while on the other hand, the mCitrine fluorophore can mature even in the absence of an UAA and without full-length expression of the construct. Therefore, fluorescence emission cannot serve as an indicator for UAA incorporation into aRab1b. Instead, the incorporation efficiency was estimated by phenotypic comparison of the cellular localization of aRab1b and the wild type protein. Rab1b localizes predominantly to the Golgi complex and the cytosol, but not to the nucleus (Figure 3.1 B). The membrane association of aRab1b mutants depends on the presence of the C-terminal prenylation motif

[46,47,241] and thereby on the successful incorporation of the UAA and the full-length expression of the construct (Figure 3.1 A).

To estimate the UAA incorporation rate of single cells the cellular localization of aRab1b constructs was compared with Rab1b wild type (WT) and soluble mCitrine as positive and negative controls, respectively (Figure 3.1 B). Three parameters can serve as indicators for the UAA incorporation into Rab1b, (1) the proper localization of aRab1b to the Golgi apparatus, (2) the amount of aRab1b in the cytosol and (3) the mCitrine fluorescence intensity in the nucleus.

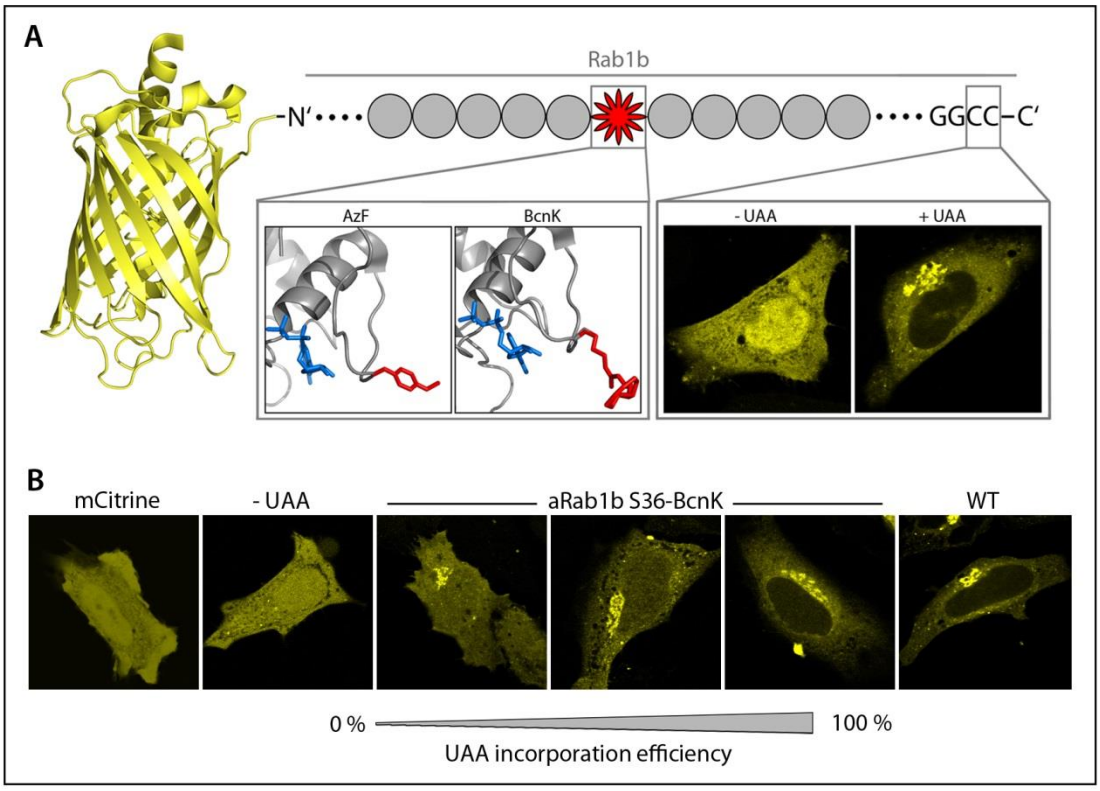

Figure 3.1: Subcellular localization of aRab1b depends on the presence of its C-terminus, and can therefore serve as an indirect for successful UAA incorporation. A) Schematic overview of the sensor architecture; the fluorescent protein mCitrine is fused to the C-terminus of Rab1b; the amber codon (red asterisk) in amber Rab1b allows for the incorporation of an unnatural amino acid, e.g. *p*-azido-L-phenylalanine (AzF) or Bicyclo[6.1.0]-nonyne-L-lysine (BcnK). Full-length expression of the construct allows for prenylation of the C-terminus of Rab1b and thereby membrane targeting of the sensor. B) HeLa cells expressing amber Rab1b (aRab1b) S36 displaying three different incorporation efficiencies; mCitrine and Rab1b wild type (WT) served as negative and positive controls, respectively. aRab1b S36 grown in the absence of UAA (-UAA) lacks the typical Rab1b subcellular localization pattern and resembles the expression of soluble mCitrine.

Expression of aRab1b S36 mutants in HeLa cells revealed various phenotypes, suggesting different incorporation efficiencies (Figure 3.1 B). Low UAA incorporation resulted in weak association of Rab1b to the Golgi complex and high cytosolic and nuclear

fluorescence intensity, resembling the phenotype of aRab1b expressed in the absence of UAA or expression of soluble mCitrine. High UAA incorporation efficiency yielded a subcellular localization pattern comparable to that observed for Rab1b wild type (WT) indicated by association of the construct to the Golgi complex and low fluorescence intensity in the nucleus (Figure 3.1 B).

3.1.1.2 UAA Incorporation into Rab1b

Two different amber suppression systems were tested for the UAA incorporation into Rab1b in mammalian cells. The first system is based on an *E. coli* tyrosine aminoacyl-tRNA synthetase variant and an engineered *Bacillus stereathermophilus* $tRNA^{Tyr}$ (Chapter 1.3 and Figure 1.10). This orthogonal pair allows for the incorporation of *p*-azido-L-phenylalanine (AzF) [171,216,242]. The second system consists of an aminoacyl-tRNA synthetase (RS)/$tRNA_{CUA}$ pair from *Methanosarcina mazei* and naturally encodes for pyrrolysine [243,244]. As the wild type RS/$tRNA^{Pyl}$ pair did not efficiently incorporate cyclooctene lysine derivatives, two mutations based on rational design were introduced to the RS [179,217]. The Y306A and Y384F mutant synthetase ($PylRS^{AF}$, here after referred to PylRS) efficiently incorporated different strained alkenes and alkynes, including Bicyclo[6.1.0]-nonyne-lysine (BcnK) and Trans-cyclooctene–L-Lysine (TcoK*) [178,179,217,218]. The PylRS system can be operated in both, prokaryotes and eukaryotes, whereas the AzF system is restricted to eukaryotic cells (Chapter 1.3).

The incorporation of AzF into the reporter construct aGFP suffered from extremely low efficiency and high cytotoxicity (data not shown). Although the transfection of HeLa cells for the AzF system and different amber Rab1b mutants revealed a small but detectable number of transfected cells, only few cells exhibited the expected Rab1b subcellular localization pattern indicating UAA incorporation (data not shown). In addition to the low incorporation efficiency, the system caused massive cytotoxicity. Intensive optimizations of transfection and cultivation conditions neither enhanced the UAA incorporation efficiency nor decreased the cytotoxicity, raising the question of suitability of the AzF system for the development of genetically encoded COSGA sensors (data not shown).

In contrast, the BcnK/TcoK* system exhibited surprisingly high transfection efficiency (up to 90 %) for several proteins of interest (POIs) with moderate to low cytotoxicity (data not shown). The BcnK incorporation efficiency varied between different amber proteins and different incorporation sites within the same protein, causing high heterogeneity of the fluorescence intensity and the Rab1b localization pattern (data not shown). In contrast, the TcoK* incorporation into aRab1b produced comparable numbers of incorporating cells per sample, but all cells exhibited a low to moderate fluorescent intensity (data not shown). Due to the high efficiency, the comparably low cytotoxicity and the rapid labeling reaction

with tetrazine-functionalized probes, the BcnK/TcoK* system was selected for the establishment of the genetically encoded COSGA sensor.

Figure 3.2 illustrates the newly established general protocol for the UAA incorporation into small GTPases in mammalian cells using the amber suppression technique. The protocol spans three days; the cells were seeded on day 1, transfected the following morning and imaged or lysed on day 3. The UAA was added during transfection on day 2 and kept in the growth medium for the whole time. The expression time in presence of the UAA can be prolonged for an additional one to two days but should be evaluated empirically to avoid cytotoxicity or, depending on the used cell line, over confluency of the culture.

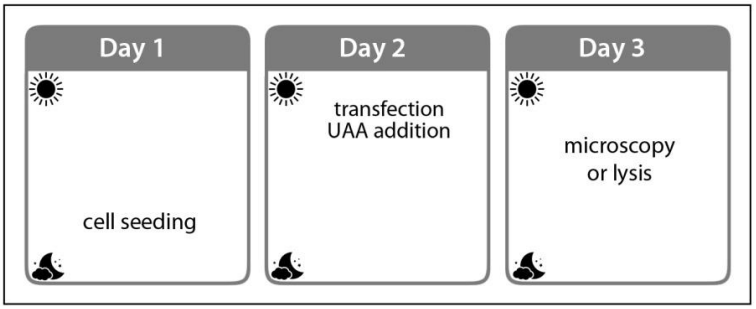

Figure 3.2: Scheme of the established protocol for UAA incorporation into small GTPases in mammalian cells. The cells were seeded on the evening of day 1 and transfected with the orthogonal pair and the amber protein plasmids on the following morning. 250 µM of the UAA was added during transfection. The samples were incubated at least for 24 h post-transfection and imaged or lysed on day 3.

Unless indicates otherwise, BcnK was used as the standard UAA for all experiments and, if not specified differently, all amber proteins were grown in the presence of 250 µM BcnK. In certain cases, BcnK and TcoK* were used in parallel to compare their different properties.

3.1.1.3 Comparison of Different Amber Rab1b Mutants

To compare the UAA-dependent localization pattern of different aRab1b mutants, the constructs were coexpressed with a cellular Golgi marker. The marker consists of a far-red fluorescent protein, mKate2, and the C-terminal membrane anchor of the Golgi-resident transmembrane protein Giantin (amino acids 3131-3259). On the one hand, mKate2-Giantin$_{3131-3259}$, hereafter revered to as GntC, enables the identification of the Golgi-localized fraction of aRab1b, while on the other hand, the marker allows for visualization of homeostasis of the Golgi apparatus. Inactive Rab1 mutants, such as the dominant negative Rab1b S22N or N121I mutants, act as dominant suppressors of endogenous Rab1b function [245-247]. Exogenous expression of inactive Rab1 mutants in cells

causes partial or complete disintegration of the Golgi complex, resulting in redistribution of Golgi-localized proteins to perinuclear fragments and the ER [245,248,249]. If Rab1b function is impaired due to the incorporation of the UAA, a similar or comparable phenotype would be expectable. In contrast, mutations that impair nucleotide hydrolysis, e.g. the constitutively active Rab1b Q67L mutant, localize natively to the Golgi apparatus and do not impair Golgi biogenesis. Figure 3.3 A illustrates the different amber Rab1b mutants coexpressed with the Golgi marker in HeLa cells.

The colocalization between Rab1b and GntC was quantified to identify the Golgi-bound fraction of the different Rab1b mutants (Figure 3.3 B). Rab1b wild type (WT), the empty mCitrineN1 vector (mCitrine) and the aRab1b mutant S36 grown in the absence of BcnK served as phenotype controls for the cellular localization of Rab1b. The non-amber suppressed Rab1b WT/S22N mutant served as a control for the disruption of the Golgi complex.

All examined amber mutants, except for the G18 construct, exhibited the typical subcellular localization pattern of Rab1b, displaying a clearly visible Golgi apparatus and varying fractions of cytosolic and nuclear fluorescence (Figure 3.3 B). This distribution is abolished in the absence of BcnK, resulting in a diffuse cytosolic localization resembling the expression of soluble mCitrine. Cells expressing aRab1b exhibited a well-structured Golgi apparatus as indicated by the marker GntC. mCitrine fluorescence intensity varied between cells expressing different amber mutants, suggesting differences in the expression levels among the mutants. Cells expressing aRab1b S36 showed the highest fluorescence intensity, whereas cells expressing D53 and G54 exhibited only moderate fluorescence intensity. T34, I41 and W102 expression was low, resulting in hardly visible fluorescent signals. The D53 and G54 constructs which contain an amber mutation in the interswitch region, exhibited a larger nuclear fraction than the other mutants, potentially indicating a mixture of mCitrine-Rab1b fragment and full-length protein. No Golgi association was found for the aRab1b G18 construct, suggesting a lack of UAA incorporation.

These results demonstrate that UAA incorporation into different sites of Rab1b was successful and yielded functional proteins that did not interfere with Golgi homeostasis. An exception is the mutation site G18, which seemed to lack stop codon suppression, and thereby full-length expression of the construct, completely. A possible explanation could be that G18 is equivalent to the oncogenic KRas G12D mutation and UAA incorporation at this position might impair the protein's function, causing rapid degradation of the construct [250].

The varying fluorescent intensity of the different amber Rab1b mutants indicates differences in expression levels. In order to establish the FRET-based conformational sensor the aRab1b T34, S36, D53 and G54 constructs were used for further experiments, whereas the G18 and W102 mutants as well as I41 constructs were not further assessed.

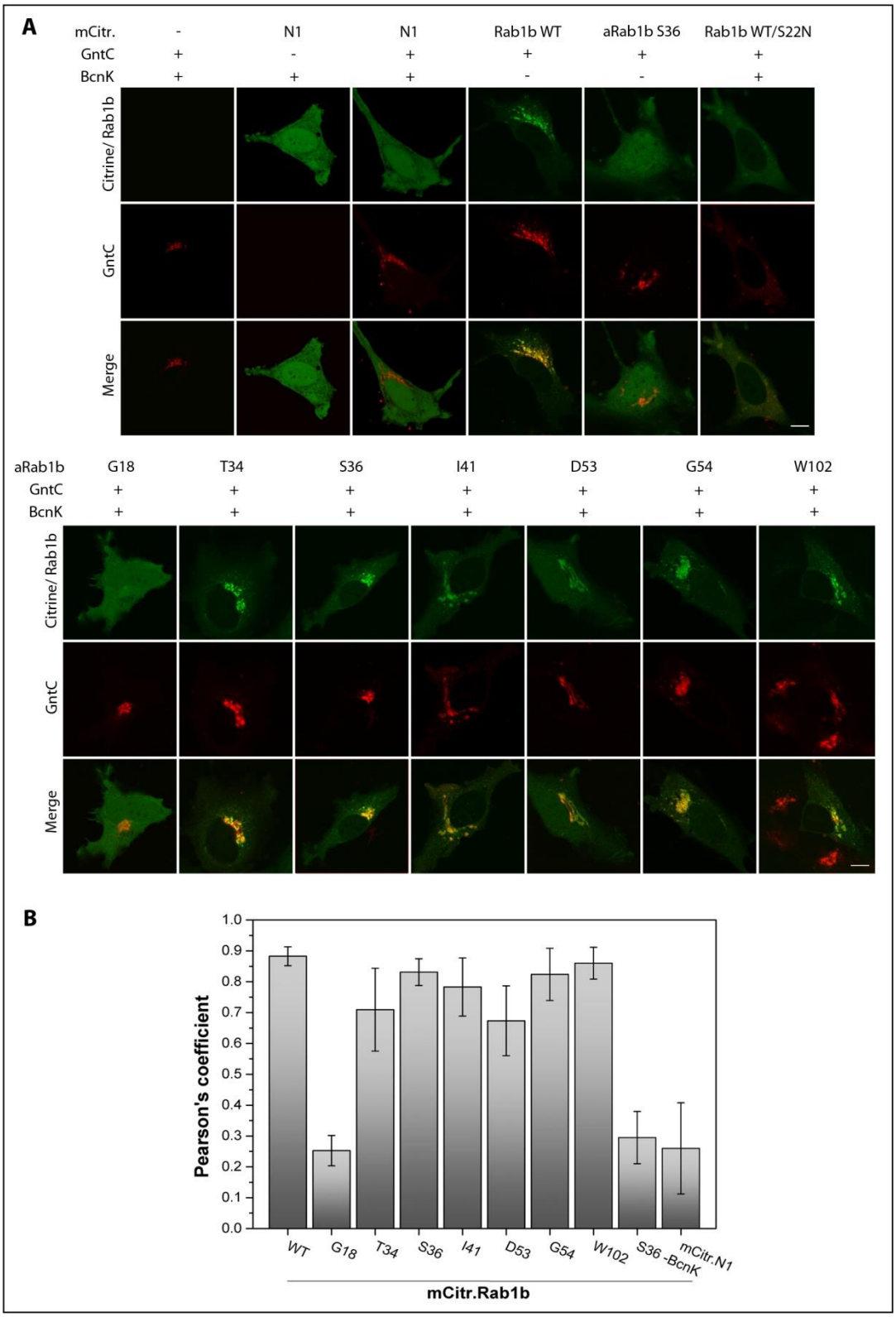

Figure 3.3: Amber Rab1b mutants localize to the Golgi complex in a UAA-dependent fashion.
A) HeLa cells coexpressing different amber mutants of Rab1b and the Golgi marker (GntC).
B) Quantification of the colocalization of the Golgi marker and the different aRab1b mutants. Rab1b WT, mCitrineN1 and aRab1b S36 in the absence of BcnK served as controls. Scale bars: 10 µm.

3.1.1.4 Evaluation of Amber Rab1b Expression Levels

Next, the expression yields of the different amber Rab1b mutants were determined. To this end, aRab1b expression in the presence and the absence of an UAA was analyzed by western blot (Figure 3.4 A). The bands indicating full-length aRab1b expression were extremely faint and their detection required prolonging of the exposure time. Therefore, two different exposure times are illustrated. The prolonged exposure resulted in the detection of an unspecific band around 42 kDa. Although full-length expression of aRab1b mutants was detectable, the obtained expression yields were much lower than observed for the wild type protein. Moreover, the expression levels varied between the mutants. aRab1b S36 showed the highest full-length expression, whereas D53 expression was moderate and G54 and T34 yielded comparable low amounts of full-length constructs. Moreover, the mCitrine-Rab1b fragment was detected in all amber suppression samples and its size varied with the position of the mutation site within Rab1b. Interestingly, the presence or absence of an UAA did not affect its abundance.

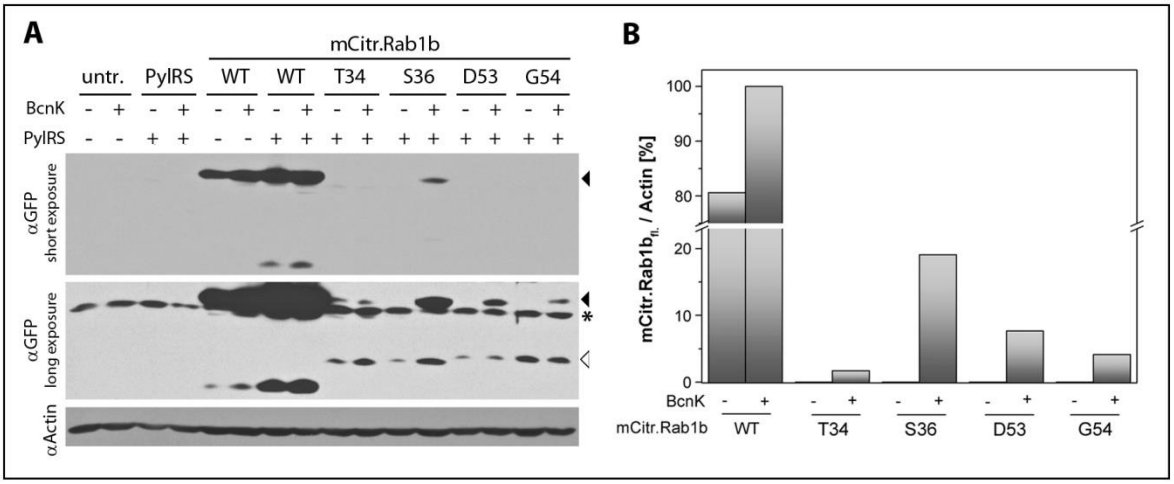

Figure 3.4: Evaluation of the expression yields of different amber Rab1b mutants in HEK 293T cells. A) Western blot analysis of Rab1b WT and four aRab1b mutants in the presence and absence of BcnK (αGFP). Two different exposure times are displayed. Full-length expression of the mCitrine-Rab1b construct (49 kDa) is indicated by a black arrow head; mCitrine-Rab1b fragment expression (approx. 30 kDa) is marked by a white arrow head; the asterisk indicates an unspecific band (~42 kDa). Untransfected cells and PylRS expressing cells served as negative controls; immunoblotting of Actin (αActin) served as a loading control. B) Densitometric quantification of the expression yield of the different amber mutants and Rab1b WT in the presence and absence of BcnK normalized on Actin.

The same experiment was performed using TcoK* (data not shown). TcoK* was incorporated in a similar fashion observed for the incorporation of BcnK into aRab1b mutants, but the observed expression yields were generally lower (data not shown).

3.1.1.5 UAA Incorporation into Rheb

In parallel to amber suppression of Rab1b, the newly established protocol for the UAA incorporation into small GTPases was applied to different amber mutants of mCitrine-Rheb (hereafter referred to as aRheb).

The mutation sites in Rheb were selected by two strategies. On the one hand, the previously described sites for introduction of the FRET acceptor into Rab1b were applied to Rheb by structural alignment of the two proteins (Figure 3.5). This approach yielded the mutation sites D33, S34, N50 and G51. On the other hand, a RMSF modulation, a measure of the average atomic mobility of backbone atoms, was performed by collaborators, suggesting the additional mutation site G108 as a candidate (data not shown).

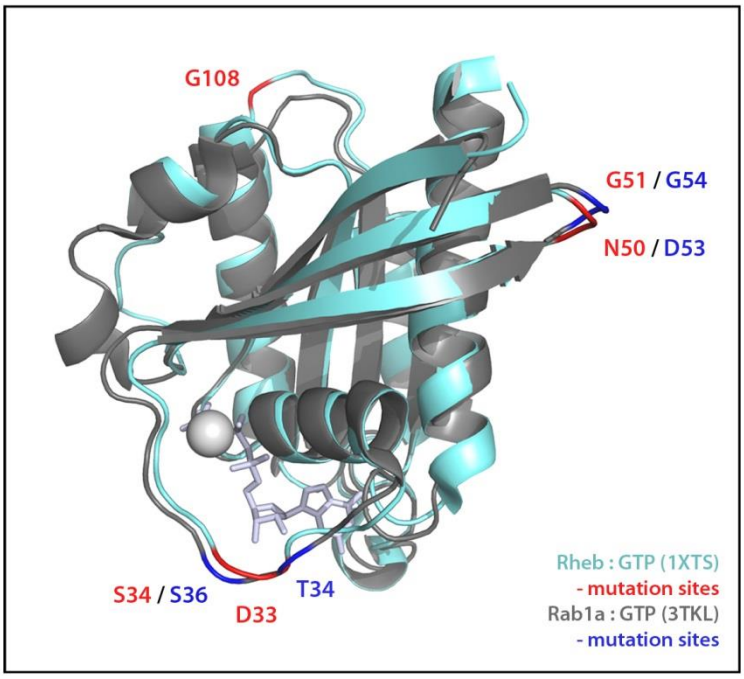

Figure 3.5: Structural alignment of Rab1a and Rheb small GTPases. GTP-bound Rab1a (PDB: 3TKL) is illustrated in grey, the previously characterized mutation sites for introduction of the FRET acceptor fluorophore are highlighted in blue. The active state of the small GTPase Rheb (PDB: 1XTS) is depicted in cyan. The structural equivalents of the mutation sites of Rab1b in Rheb are highlighted in red. The additional mutation site, G108, was identified by RMSF modulation.

In contrast to Rab1b, the small GTPase Rheb does not localize predominantly to one cellular compartment [101,106,108,111,113,251,252]. Consequently the phenotype of Rheb expression is not as clearly defined as for Rab1b. The largest fraction of mCitine-Rheb localized in a diffuse cytosolic pattern with faintly visible endomembrane systems and dense fluorescence signals in the perinuclear area (Figure 3.6 A). A smaller fraction of Rheb localized to the nucleus. The difference in fluorescence intensity of the nucleus and the cytoplasm was similar between Rheb WT and the amber mutants when expressed in

presence of BcnK, but was abolished in its absence (Figure 3.6 A). Some aRheb mutants, e.g. D33 and G108, exhibited irregular punctate structures, suggesting unspecific accumulation of the constructs. Although all aRheb expressing cells showed fluorescence differences between nucleus and cytosol, perinuclear densities as displayed by Rheb WT expressing cells were hardly detectable. Moreover, most cells expressing aRheb constructs displayed elevated nuclear fluorescence levels than observed for the expression of Rheb WT, suggesting abundance of non-suppressed mCitrine-aRheb fragment (Figure 3.6 A). Incorporation of TcoK* into Rheb yielded comparable results to incorporation of BcnK but suffered of low efficiency.

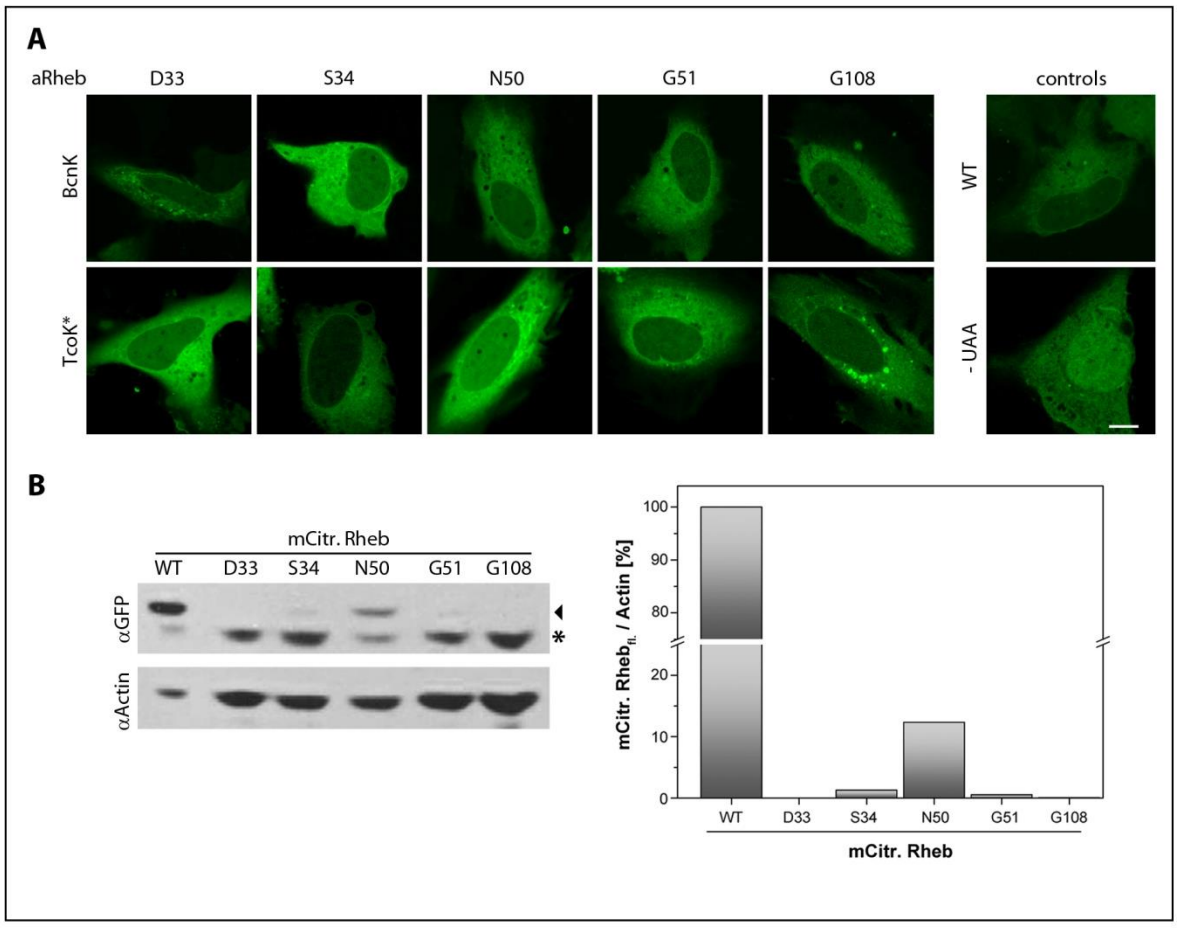

Figure 3.6: Stop codon suppression of amber Rheb. A) Five different incorporation sites were tested for BcnK and TcoK* incorporation in HeLa cells. Rheb WT and aRheb S34 in the absence of UAA served as controls. B) Western blot of HEK 293T cells expressing Rheb WT and different aRheb mutants in the presence of BcnK (αGFP); immunoblotting of Actin served as a loading control (αActin). Full-length Rheb expression (48.2 kDa) is indicated by an arrow head. The asterisk indicates an unspecific band. The loading of Rheb WT was reduced to avoid over-exposure. Expression yields were quantified to allow for the direct comparison of the mutants and the wild type constructs. Scale bar: 10 µm.

To determine the expression yield, western blot analysis of aRheb expression in the presence of an UAA was performed (Figure 3.6 B). The densitometric quantification of the bands representing full-length expressed Rheb construct revealed 12 % expression yield for the highest expressed mutant, aRheb N50, in comparison to the natural translation control Rheb WT. In contrast, full-length expression of aRheb S34 and G51 was hardly detectable and no full-length expression was obtained for aRheb D33 and G108.

The determined expression yields of aRheb were lower than those observed for the expression of aRab1b (Figure 3.4 B), suggesting that the UAA incorporation process into Rheb is not as efficient as UAA incorporation into aRab1b. Moreover, the observed diffuse fluorescent pattern of aRheb mutants may indicate a mixed expression of aRheb in full length and as a non-suppressed fragment.

3.1.2 Establishment of the intracellular chemical labeling

The intracellular labeling of amber suppressed proteins in mammalian cells has remained challenging despite the progress in the field in the last years. Consequently, a major part of this study focused on the establishment of a robust and reproducible protocol allowing for intracellular labeling of various proteins with high specificity and yield in mammalian cells.

3.1.2.1 Fluorescent probes for intracellular labeling

The intracellular labeling of proteins with synthetic fluorophores poses several requirements on the functionalized dye. While on the one hand, the probe needs to be highly cell permeable, on the other hand, it should not bind to cellular components or accumulate in membrane systems unspecifically. Furthermore, the probe needs to be fully removable from the cell and should not cause cytotoxicity even at higher concentrations. Numerous H-tetrazine (tz) and methyl-tetrazine (mtz) functionalized dyes in the green and red spectral range were screened for these parameters (data not shown). Fluorescein diacetate (FDAC) and BODIPY FL (BDP) in the green spectral range, as well as tetramethylrhodamine (TMR), Atto 590 and to a lesser extend Atto 565 in the red spectral range, were identified as optimal candidates for intracellular labeling applications (data not shown). These four probes exhibited high cell permeability and were fully removable from the cell lumen, allowing for the precise detection of specific labeling with good signal-to-noise ratios. In addition to the cell permeability and the removal capacity, the choice of dye for intracellular labeling may also depend on the cellular localization of the target protein. If the protein of interest localizes to the nucleus, it might not react with e.g. BDP, as this

probe seemed to remain exclusively in the cytosol (data not shown). Moreover, the application of interest may affect the choice of dye as some dyes, including Atto 565 and Atto 590, attached to the glass surface of the culture vessel (data not shown). This unspecific accumulation might hinder analysis by e.g. Total Internal Reflection (TIRF) microscopy.

Thus, the choice of dye is a critical factor to achieve specific labeling of intracellular proteins with high yields.

3.1.2.2 Intracellular labeling of Rab1b in HeLa cells

To identify the optimal conditions for intracellular labeling of aRab1b, a range of different incubation times and dye concentrations for the labeling step were assessed (Figure 3.7 A).

Although the typical Rab1b subcellular localization pattern, indicating UAA incorporation into aRab1b, was observed in all samples, no colocalization of the TMR and the mCitrine fluorescence signals was detected. Higher dye concentrations and/or longer incubation times only increased the fluorescence background signals, but did not yield any specific labeling. To circumvent potential sterical hindrance due to protein-protein interactions, the screen was repeated using aRab1b D53, an interswitch mutant. However, similar to the labeling of S36 only unspecific TMR background signals were observed for the labeling of aRab1b D53 (data not shown).

Furthermore, BcnK was exchanged to TcoK*, which led only to an increase of unspecific puncta-like structures in the cell lumen (Figure 3.7 B).

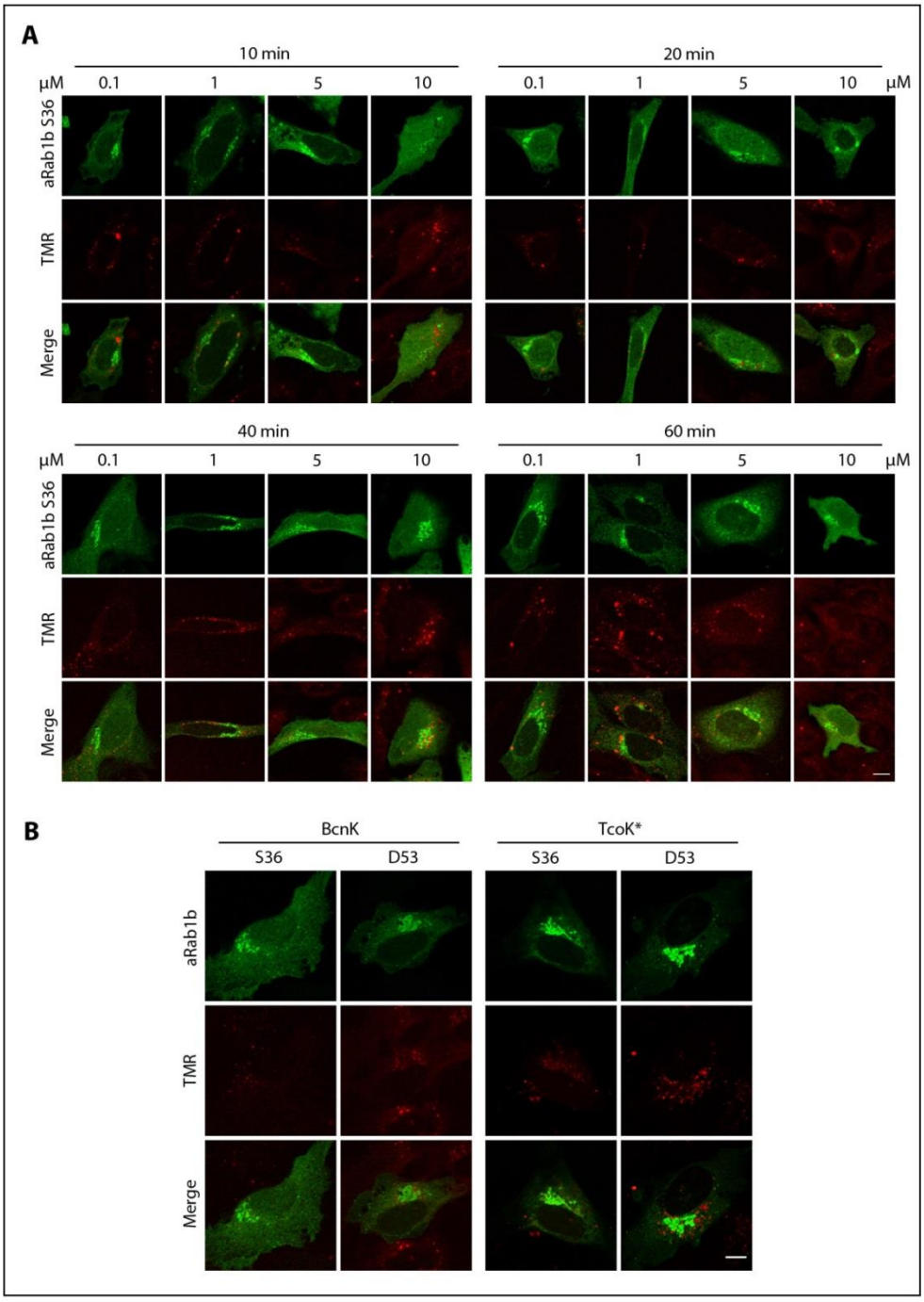

Figure 3.7: Intracellular labeling of amber Rab1b with TMR in HeLa cells. A) Overview of the titration of TMR concentration and incubation time for the labeling of aRab1b S36. B) HeLa cells expressing aRab1b S36 and D53, each suppressed with BcnK or TcoK*, labeled with TMR. Scale bars: 10 µm.

As the incubation of aRab1b S36 or D53 with Atto 565 or Atto 590 did also not yield any specific labeling, we speculated whether the biophysical properties of red dyes might impede the intracellular labeling reaction. Therefore two green probes, BODIPY FL (BDP) and fluorescein diacetate (FDAC) were selected as alternative candidates for the

intracellular labeling of aRab1b. Green dyes are generally smaller in size and less hydrophobic than red fluorophores, which may reduce the observed unspecific accumulation in endomembranes. To test green fluorophores, the fluorescent protein of the sensor construct was exchanged to either mCherry or mTurquoise2, which can both serve as FRET partners for green fluorophores. Figure 3.8 illustrates the results of the intracellular labeling of aRab1b S36 and D53 with BDP, each fused to mCherry or mTurquoise2.

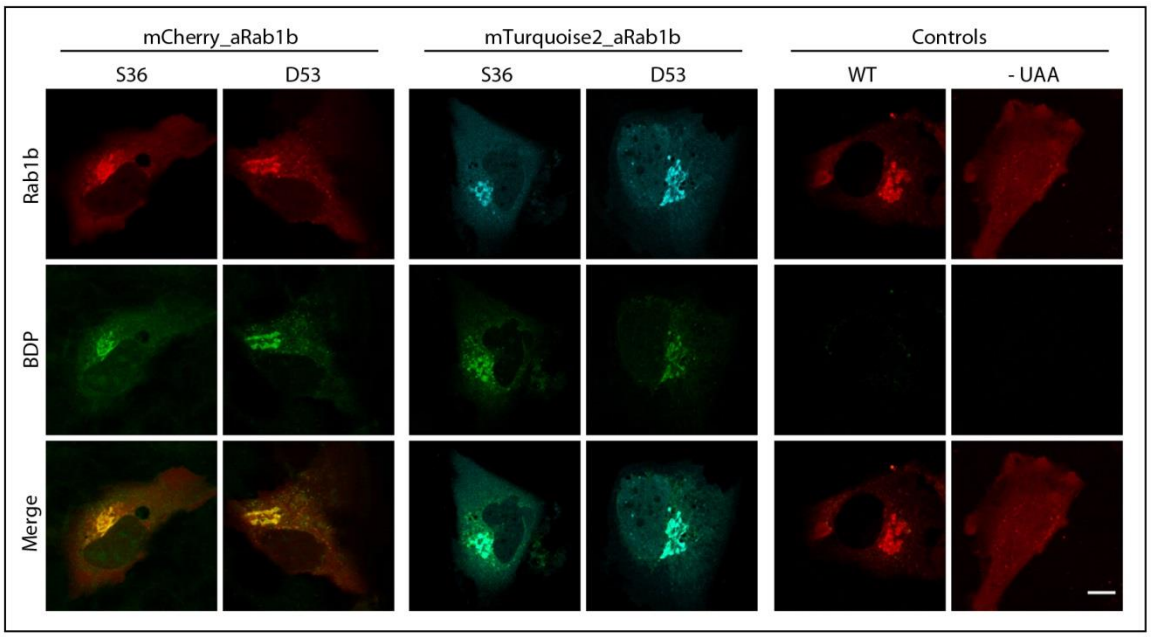

Figure 3.8: Intraccellular labeling of aRab1b with green dyes. HeLa cells expressing aRab1b S36 and D53 in the presence of BcnK were labeled with BODIPY FL (BDP). Rab1b wild type and aRab1b S36 (-UAA) served as positive and negative controls, respectively. Scale bar: 10 µm.

The localization of aRab1b to the Golgi complex confirming BcnK incorporation was detected for both amber mutants and was independent of the fluorescent protein tag. Moreover, the incubation with BDP resulted in highly specific labeling of aRab1b, indicated by the colocalization of the fluorescent signals. This specific labeling was comparable between the two different amber mutants and the respective mCherry and mTurquoise2 constructs. In contrast, no labeling was observed for the two negative controls Rab1b WT and aRab1b (-UAA). Exchange of BDP to FDAC yielded comparable results (data not shown).

Unfortunately, the observed specific labeling signals were rather weak and bleached rapidly during confocal imaging. In fact, the same labeling protocol yielded a diverse labeling efficiency and high heterogeneity of the labeling, ranging from visible specific labeling to only dye background signals. Numerous protocol optimizations did neither enhance the labeling homogeneity nor improve its intensity or the reproducibility.

In summary, these results demonstrate specific intracellular labeling of aRab1b with FDAC and BDP in HeLa cells. The observed labeling was highly specific and UAA-dependent, but exhibited low fluorescence intensity and high photo-bleaching. In contrast, labeling of the same aRab1b mutants under identical conditions with three different red probes did not result in any detectable labeling. Besides the difference of the biophysical properties of green and red fluorophores, the reasons for this discrepancy remain unclear.

3.1.2.3 Intracellular labeling in different mammalian cell lines

To assess whether mammalian cell lines differ in their suitability for intracellular labeling applications, several cell lines with cancer and non-cancer-related background were tested for the intracellular labeling with red fluorescent probes. The reporter gene aGFP182 was modified with a C-terminal linker and a CAAX box (hereafter referred to as aGFP-Kx), targeting the construct to the cytosolic side of the plasma membrane. The cytoplasma membrane targeting circumvents unspecific dye accumulations in the cell lumen, allowing for the precise detection of specific labeling (Figure 3.9 A). In parallel to aGFP-Kx, labeling of aRab1b S36, the highest expressing Rab1b amber mutant, was assessed (Figure 3.9 B). Fluorescence emission and membrane association was observed for both target proteins in all examined cell lines, indicating successful stop codon suppression. HEK 293T cells exhibited specific labeling with high fluorescence intensity for both target proteins, whereas only moderate to low labeling intensities were observed in COS-7 and CHO cells. Interestingly, U2OS cells displayed a weak but specific labeling of the Golgi compartment but no labeling of the cytoplasma membrane. Neither aRab1b, nor aGFP-Kx labeling was detected in HeLa and MCF7 cells. In fact, these two cell lines exhibited non-specific accumulations of the dye, which were hardly observed in HEK 293T cells.

Based on the detected plasma membrane labeling, the assessed cell lines can be divided into two groups. The first group comprises HeLa, MCF7 and U2OS, which did not exhibit any specific labeling, while the second group, CHO, COS-7 and HEK 293T, displayed specific labeling of the plasma membrane. In fact, the first group consists only of cell lines with a cancer-related background, whereas the cell lines of the second group do not originate from cancer tissues. However, specific labeling of aRab1b was also observed in U2OS cells, suggesting that intracellular labeling may also be possible in cancer-derived cell lines. Since COS-7 and HEK 293T cells exhibited the strongest labeling and the lowest TMR background signals, further experiments were performed exclusively in these two cell lines.

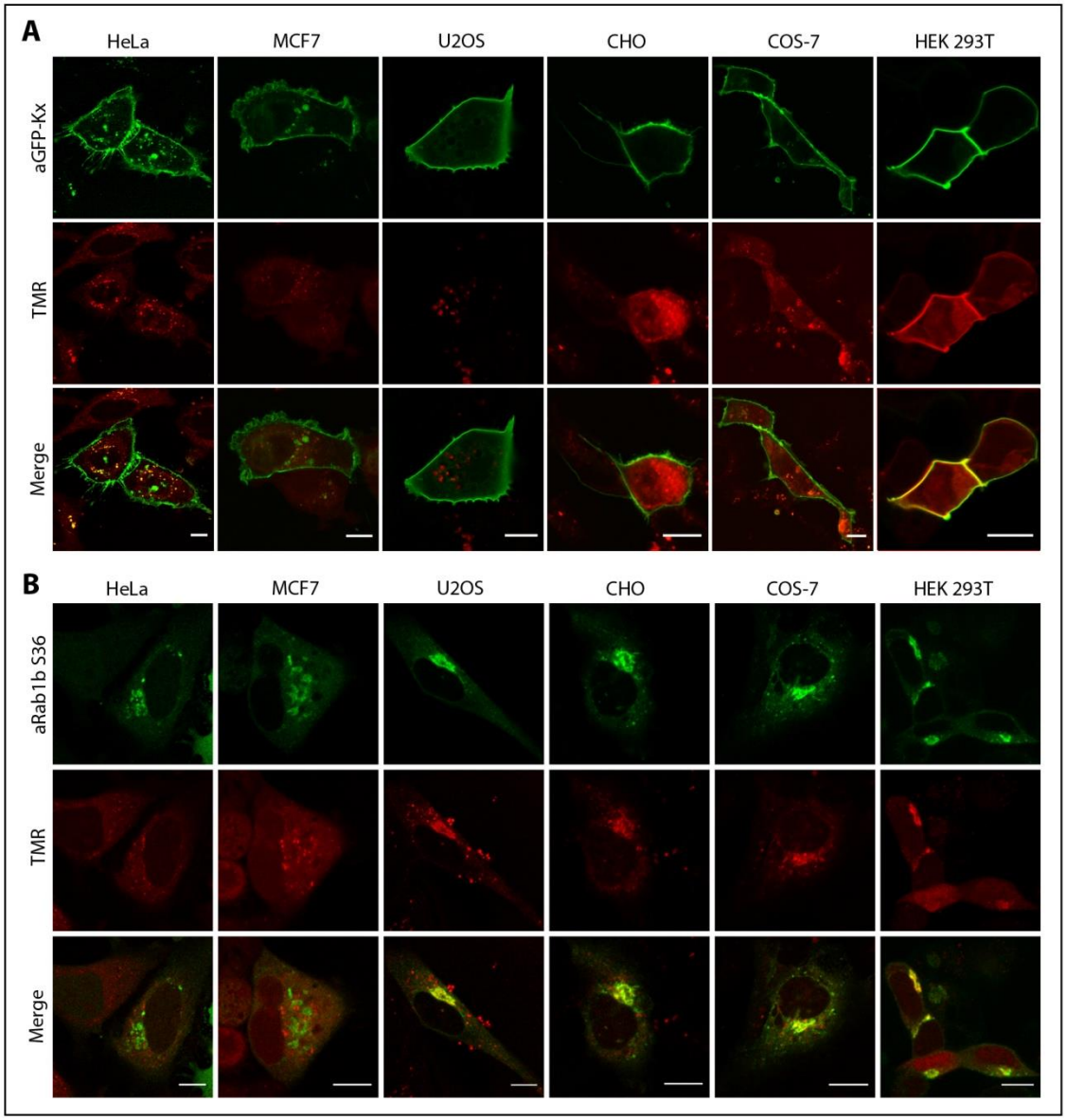

Figure 3.9: Intracellular labeling in different mammalian cell lines. A) Labeling of the reporter construct aGFP-Kx with TMR Specific plasma membrane labeling was observed only in CHO, COS-7 and HEK 293T cells. B) Labeling of amber Rab1b S36 with TMR in different cell lines. U2OS, CHO, COS-7 and HEK 293T cells displayed highly specific labeling of the Golgi complex, whereas only TMR background signals were detected in HeLa and MCF7 cells. Scale bars: 10 µm.

3.1.2.4 Red dyes for intracellular labeling

To determine an optimal FRET pair, labeling in HEK 293T cells was assessed using three different red dyes, TMR, Atto 565 and Atto 590 (Figure 3.10 A). Specific labeling with a high signal-to-noise ratio was obtained with for all three probes, but the labeling homogeneity differed. The incubation with TMR resulted in the most efficient labeling and the highest sample homogeneity, whereas labeling with Atto 590 yielded a similar homogeneity but lower labeling intensity. In contrast, samples labeled with Atto 565 exhibited only a small fraction of specifically labeled cells. In all three cases the intensity of the specific labeling correlated with the mCitrine fluorescence signals, resulting in a strongly labeled Golgi region and lower TMR fluorescence intensity in the cytoplasm (Figure 3.10 A). Fluorescence lifetime analysis revealed a lifetime reduction of $\Delta\tau_{+TMR}$ = 290 ± 75 ps for the TMR-labeled sample in comparison to the unlabeled control (Figure 3.10 B). In contrast, labeling with Atto 565 or 590 decreased the donor lifetime by only $\Delta\tau_{+Atto}$ = 90 ± 40 ps. The decrease in fluorescence lifetime correlated spatially with the labeling intensity, displaying low lifetimes in the Golgi region and higher lifetimes in the cytoplasm (Figure 3.10 A). Although this spatial distribution was similar in all labeled cells, the average fluorescence lifetime differed between the three dyes used. On the one hand, this difference may be due to the spectral properties of the dyes, allowing for distinct FRET efficiency when paired with mCitrine. On the other hand, this difference may be due to potential variations in labeling efficiency. A low labeling efficiency results in a minor fraction of donor-acceptor pairs and leaves a large amount of aRab1b unlabeled, which represents donor only fraction in fluorescence lifetime imaging. As both fractions are acquired equally, the obtained lifetime of a sample represents the average of these fractions. Hence, high labeling efficiency causes a major reduction in fluorescence lifetime, whereas the lifetime of samples exhibiting low labeling efficiency is closer towards the donor only lifetime ($\tau_{mCitrine}$ = ~3.0 ns).

In addition to HEK 293T cells, labeling of aRab1b S36 with TMR, Atto 565 and Atto 590 was performed in COS-7 cells (data not shown). Similar to the findings in HEK 293T cells, specific aRab1b labeling was observed for all three dyes, but the observed signal-to-noise ratio and the decrease of fluorescence lifetime upon labeling was generally lower in COS-7 cells (data not shown).

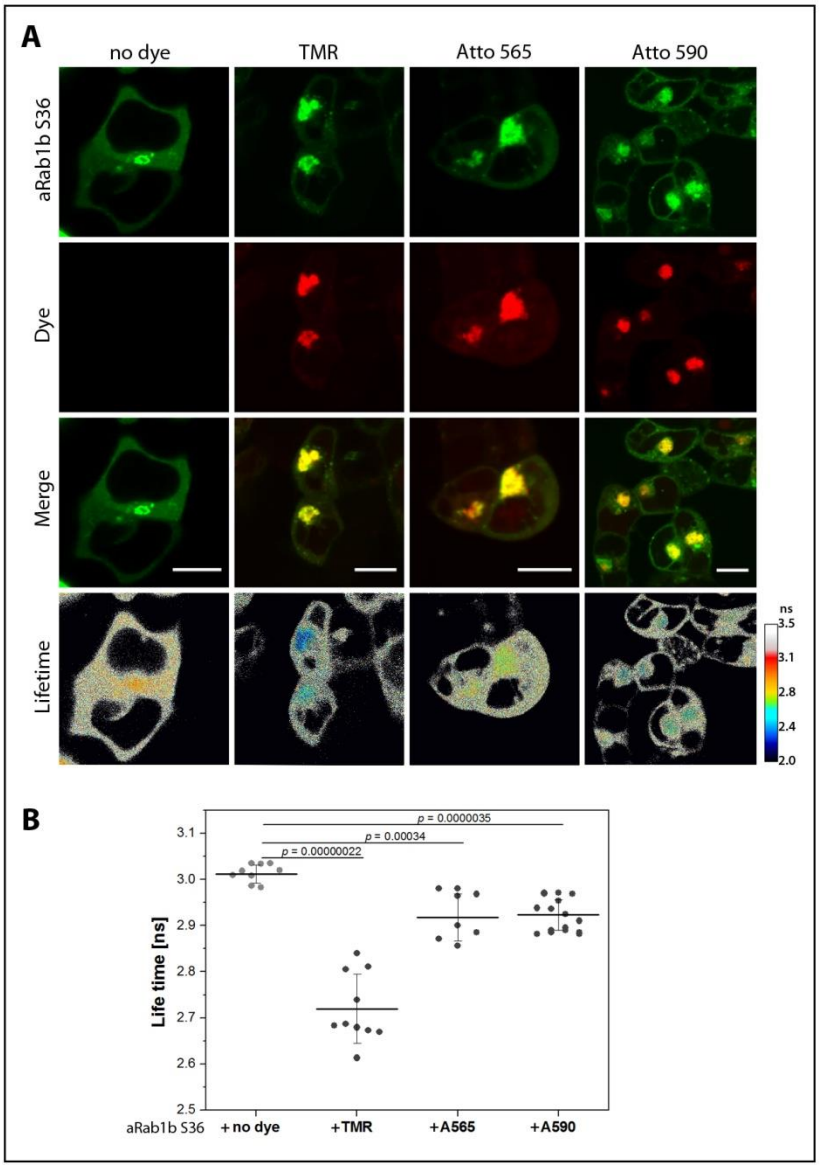

Figure 3.10: Intracellular labeling of aRab1b S36 in HEK 293T cells using three different red dyes. A) Fluorescence lifetime analysis of HEK 293T cells expressing aRab1b S36 labeled with TMR, Atto 565 and Atto 590. B) Single cell fluorescence lifetime analysis of the same experiment. Scale bars: 10 µm.

In conclusion, these findings identified TMR as the most potent dye for the intracellular labeling of amber Rab1b. Labeling of aRab1b with TMR was homogenous, highly specific and yielded a reproducible decrease of mCitrine fluorescence lifetime in comparison to unlabeled control samples, indicating the presence of the acceptor on the unimolecular sensor. Moreover, the labeling did not affect the cellular localization of aRab1b, Golgi biogenesis or the cell phenotype evidentially in HEK 293T cells. Labeled HEK 293T cells exhibited no apparent stress indications such as vacuole formation, blebbing or rounding as observed for the labeling of intracellular proteins in COS-7 cells (data not shown). Therefore, TMR was used primarily in further experiments.

3.1.2.5 Optimization of the intracellular labeling

Using different cell lines raised the question of the cell culture medium and the nutrient requirements to ensure maintenance of robust and viable cells for efficient amber suppression and intracellular labeling. The standard medium used for initial experiments was a low glucose/low vitamin medium. The comparison of two equally treated amber suppression samples, one cultivated in low glucose medium, the other one in high glucose medium, revealed lower cytotoxicity in samples grown in nutrient rich medium. The nutrient rich medium comprises 4-fold more glucose and essential nutrients in comparison to the low glucose medium, allowing for rapid proliferation. However, the enhanced proliferation emerged as a pitfall, as the established protocol for UAA incorporation and intracellular labeling spans over four days, resulting in over-confluent samples on the day of imaging. Therefore the number of initially seeded cells was gradually reduced to identify the optimal cell number yielding 80-90 % cell confluency on the day of imaging. These samples were transfected at 50-60 % confluency, instead of 70-80 %, but did not exhibit increased cytotoxicity. The concentration of BcnK in the growth medium did not affect the labeling efficiency. Nevertheless, an attempt to identify the cause of the puncta structures revealed their dependency on the presence of UAA in the culture medium (Figure 3.11). While untransfected cells incubated with BDP did not display any punctate structures, cells grown in the presence of BcnK exhibited a high abundance of punctate structures following labeling with BDP. Therefore we speculated that removal of the excess of residual BcnK before labeling may reduce the number of puncta and potentially augment the specific labeling, as the effective dye concentration would not be reduced by side reactions. Although BcnK has been previously reported to be removed from cells within one hour [181], this time frame was not sufficient for the intracellular labeling of aRab1b and aRheb. Prolongation of the BcnK removal time to 16 h pre-labeling resulted in highly specific labeling with a high signal-to-noise ratio and a negligible amount of punctate structures in HEK 293T cells (Figure 3.10 A). In fact, the BcnK removal time was found to depend strongly on the number of incorporating cells per sample and on the cell line (data not shown). As protein expression levels vary between different cell lines and as the BcnK consumption depends on the number of consuming cells and the stop codon suppression efficiency of these cells, the BcnK removal time should be empirically determined for each application to ensure complete removal or consumption of BcnK before the intracellular labeling step.

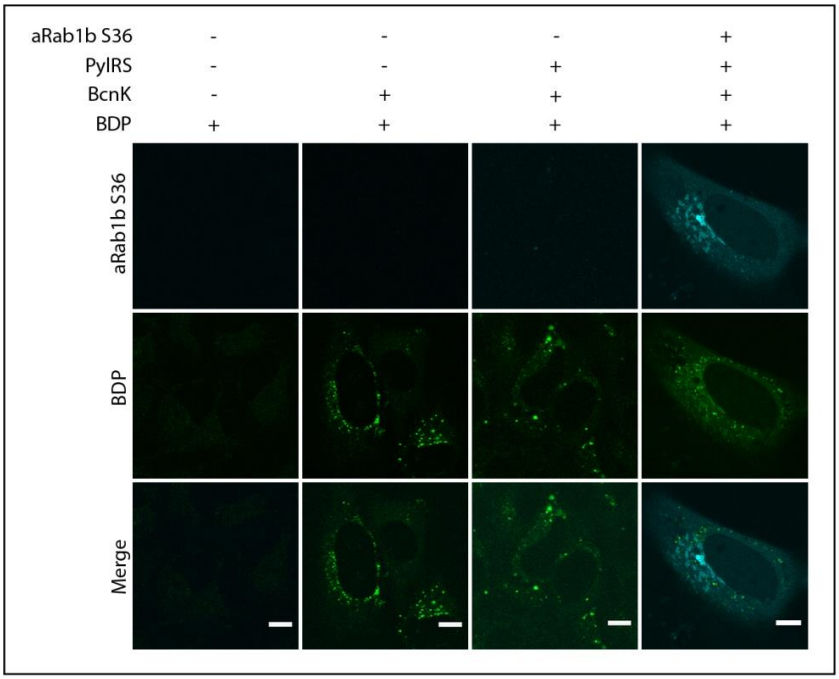

Figure 3.11: Excess UAA during intracellular labeling causes high abundance of punctate structures. Untransfected HeLa cells cultured in the presence and absence of BcnK and cells expressing the orthogonal pair (PylRS), as well as the orthogonal pair and aRab1b, were labeled with BODIPY FL (BDP). Scale bars: 10 µm.

Due to the high reaction rate of the inverse electron-demand Diels-Alder reaction, dye concentrations in the nanomolar range are sufficient for intracellular labeling [168,178,179,181,204,253]. We found that increasing the dye concentration up to 1 µM increased the labeling efficiency noticeable. However, higher dye concentrations required longer wash-out time post-labeling to achieve good signal-to-noise ratios. Furthermore, prolonging of the incubation time from 15-20 min to 1 h increased the labeling efficiency dramatically (data not shown). Longer incubation of up to 3 h did not further enhance the specific labeling but increased the background signal massively (data not shown).

Based on these findings the previously established protocol for UAA incorporation into small GTPases (Figure 3.2) was extended, allowing for robust and specific labeling of intracellular proteins with high reaction yields (Figure 3.12).

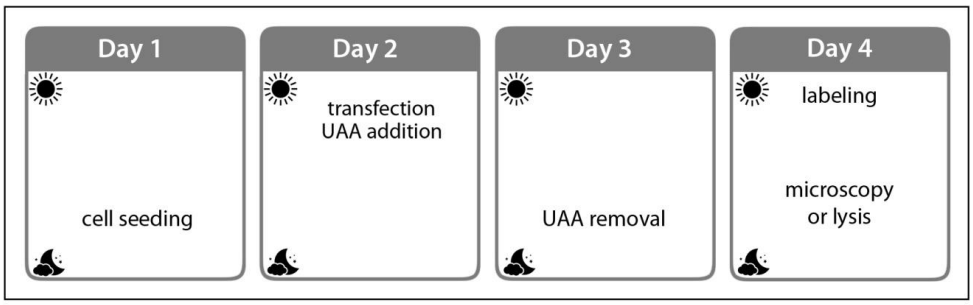

Figure 3.12: Scheme of the established protocol for intracellular labeling of small GTPases in live mammalian cells. The adherent mammalian cells were seeded on the first day and transfected in the following morning (~ 16 h post-seeding). 250 µM of the UAA was added to the growth medium during the transfection and kept in the medium over night. The UAA was removed from the samples the following day to achieve complete removal of residual UAA from the cell lumen before labeling (> 12-16 h). Intracellular labeling was performed in the morning on day 4; cells were washed for 2-8 h and analyzed.

3.1.3 Labeling of amber Rab1b

Furthermore, the observed intracellular labeling of amber Rab1b was assessed to confirm the covalent binding of the acceptor to the sensor construct and to determine whether the observed change in fluorescence lifetime indeed depends on the presence of the acceptor. Moreover, the intracellular labeling reaction was characterized intensively to ensure the bioorthogonality of the reaction.

3.1.3.1 Intracellular labeling of Rab1b is bioorthogonal

To confirm that the intracellular labeling reaction is indeed bioorthogonal, HEK 293T cells expressing Rab1b WT with and without the components of the amber suppression system, or different aRab1b mutants, were labeled with TMR (Figure 3.13 A). Specific labeling of the Golgi apparatus was clearly visible in both samples transfected for an aRab1b mutant, but no TMR fluorescence signal was detected in cells expressing Rab1b WT. The presence of the components of the amber suppression system in Rab1b WT samples increased the TMR background signals mildly but did not yield any labeling as observed for the amber mutants. These findings were consistent with the mCitrine fluorescence lifetime analysis of the samples (Figure 3.13 B). Rab1b WT samples exhibited fluorescence lifetimes comparable to donor only lifetime ($\tau_{Rab1b\ WT}$ = 2.97-3.01 ns), whereas both amber mutants displayed significantly lower lifetimes (τ_{S36} = 2.71 ± 0.07 ns and τ_{D53} = 2.82 ± 0.11 ns).

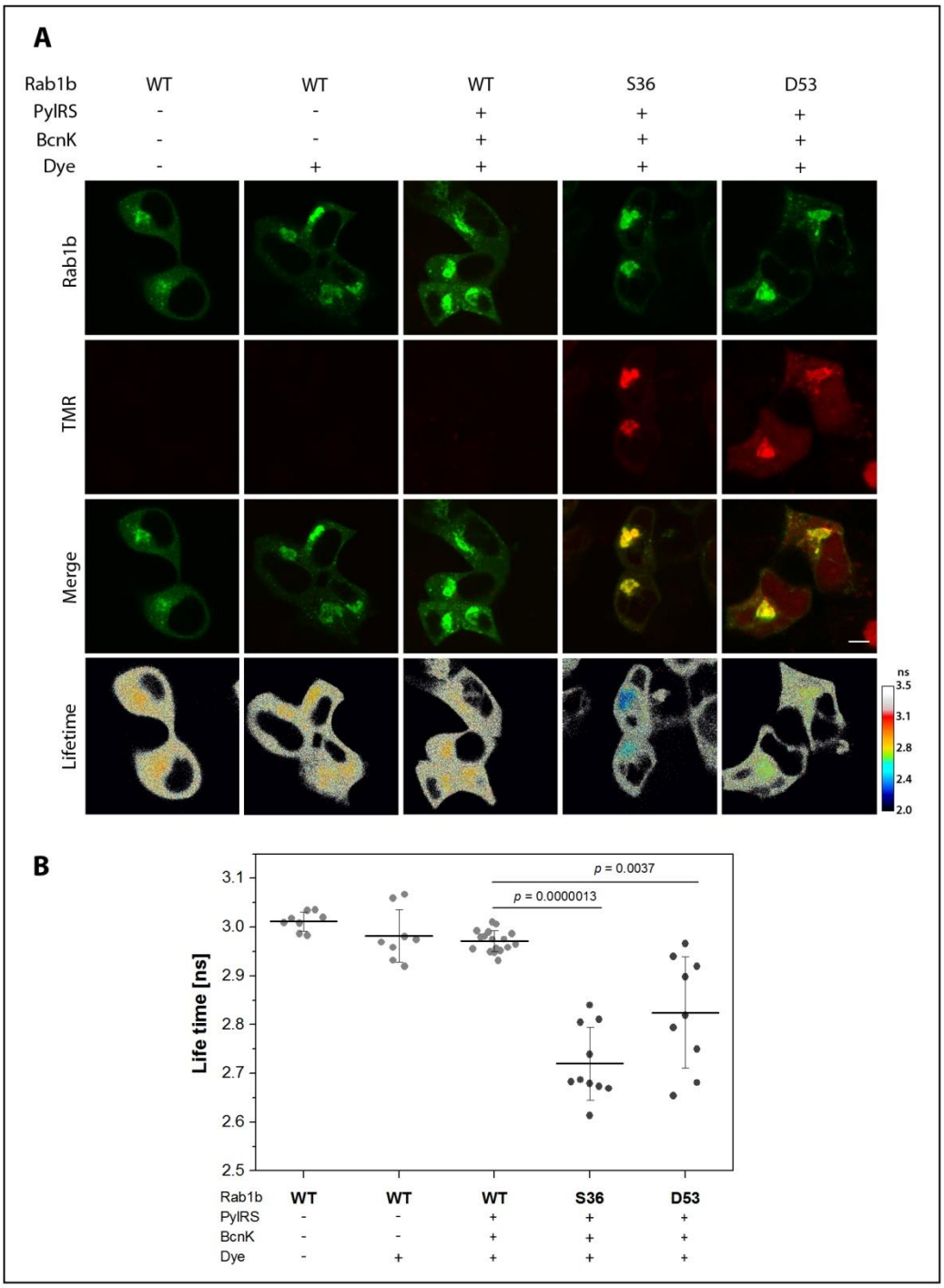

Figure 3.13: The intracellular labeling of amber Rab1b is bioorthogonal. A) HEK 293T cells expressing Rab1b WT and amber Rab1b mutants in the absence and presence of the components of the amber suppression system and TMR. B) Single cell lifetime analysis of the respective samples. Scale bar: 10 µm.

Next, labeling of aRab1b was assessed by denaturing in-gel fluorescence analysis to verify covalent binding of the dye to the amber construct and to further confirm the specificity and the UAA-dependency of the reaction (Figure 3.14). To this end, HEK 293T

cells expressing Rab1b WT or different amber mutants were cultured in the presence and absence of either BcnK or TcoK*. Two fluorescent bands were detected in all aRab1b samples in the presence, but not in the absence of an UAA (Figure 3.14, indicated by arrow heads). The lower band, at the heights of 46 kDa molecular weight marker band, represents the full-length expressed and TMR-labeled mCitrine-aRab1b (49.9 kDa, black arrow head), whereas the upper band was identified as the PylRS (50.8 kDa, white arrow head, see Figure 3.18). The fluorescence intensities of labeled full-length constructs varied between the different amber mutants, suggesting differences in expression levels or the labeling efficiency. The most intense bands were detected for aRab1b S36 and D53, whereas T34 and G54 exhibited weaker fluorescence intensities. This order of the mutants is in agreement with the previously determined expression levels of the different aRab1b mutants (Figure 3.4). Although TcoK* containing samples exhibited generally fainter bands, the same order among the mutants was observed. The lower signals observed for labeling of TcoK*-containing aRab1b may be due to the lower incorporation efficiency that was previously determined (data not shown), but could also be caused by a less efficient labeling reaction.

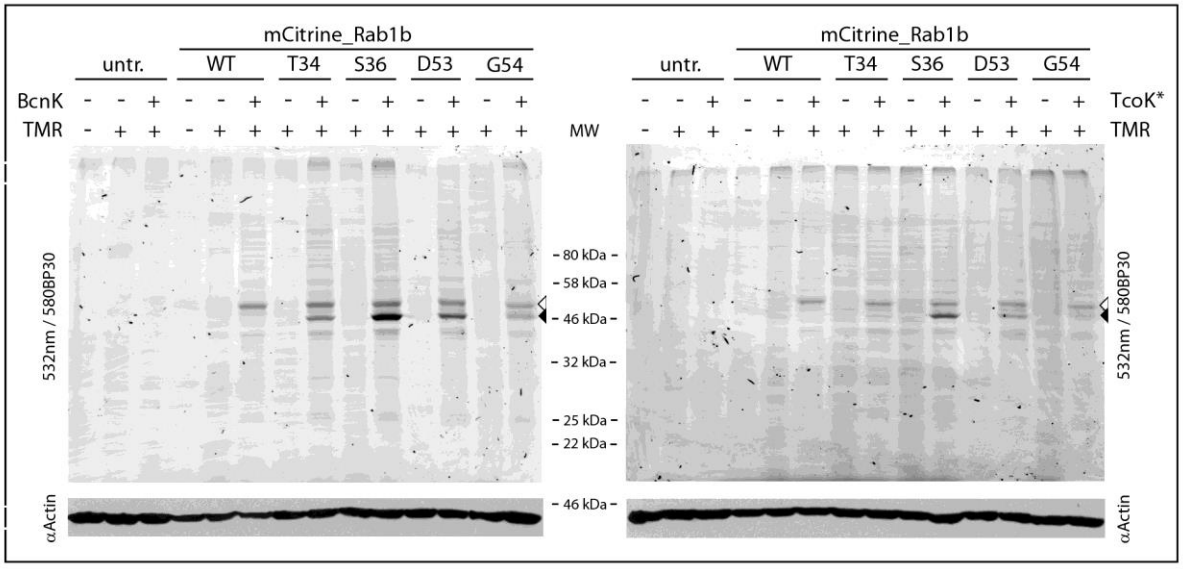

Figure 3.14: In-gel analysis of Rab1b WT and amber variants suppressed for BcnK or TcoK*. The back arrow heads indicate the UAA-dependent full-length expression and labeling of the aRab1b constructs (49.9 kDa), whereas the white arrow heads mark the PylRS (50.8 kDa), which was frequently observed during in-gel fluorescence analysis. Immunoblotting of Actin (αActin) served as a loading control.

3.1.3.2 Comparison of different UAA for intracellular labeling

Furthermore, the intracellular labeling of BcnK and TcoK* was compared by fluorescence lifetime analysis to determine which UAA is more suitable for the genetically encoding of the conformational probes for small GTPase activity (Figure 3.15).

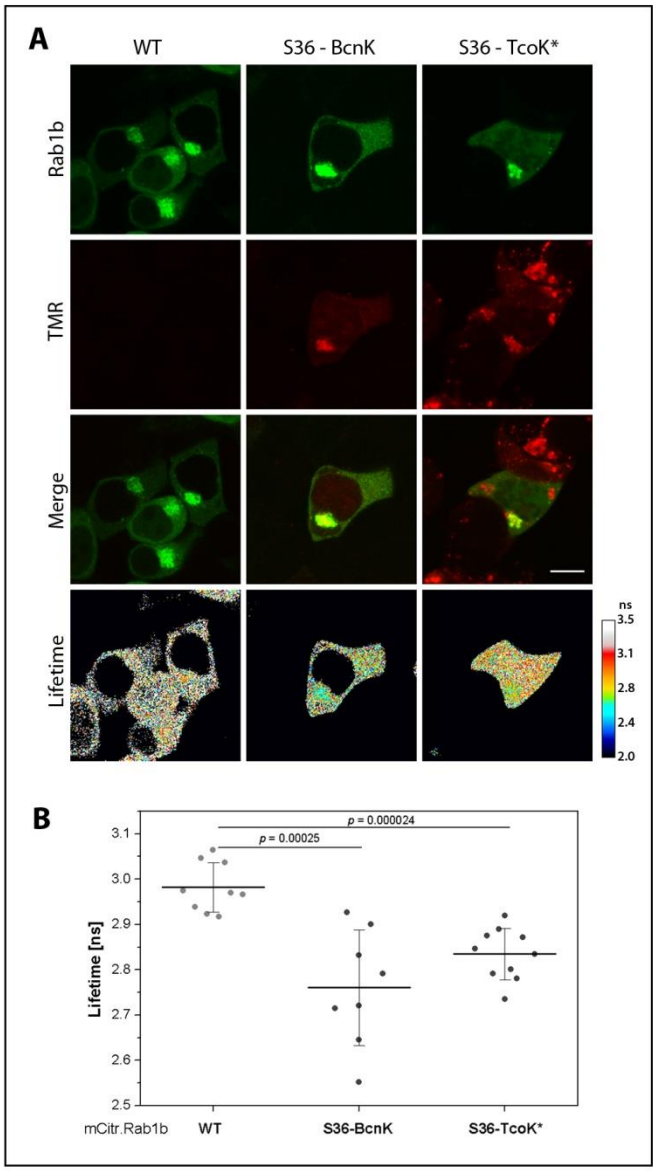

Figure 3.15: Comparison of two different UAA for the intracellular labeling of aRab1b.
A) TMR-labeled HEK 293T cells expressing Rab1b WT and aRab1b S36 in the presence of BcnK or TcoK*. B) Single cell analysis of the fluorescence lifetime of these samples. Rab1b WT served as a donor only control. Scale bar: 10 µm.

The subcellular localization observed in both UAA samples indicated successful incorporation of BcnK and TcoK* into aRab1b S36 (Figure 3.15 A). Moreover, both UAA

allowed for specific labeling of the amber constructs. In contrast to the labeling of BcnK containing amber proteins, punctate structures and unspecific dye accumulations were frequently observed in TcoK* containing samples. The fluorescence lifetime analysis showed a significant difference between labeled samples and the unlabeled control Rab1b WT (Figure 3.15 B). While the labeling of aRab1b S36-BcnK resulted in an average lifetime of τ_{BcnK} = 2.76 ± 12 ns, the lifetime of TcoK*-labeled samples was in average higher (τ_{TcoK*} = 2.83 ± 0.06 ns).

These findings are in agreement with the previous results demonstrating a discrepancy of the UAA incorporation efficiency and the labeling between the two UAA (Chapters 3.1.1.1 and 3.1.3.1). Generally, TcoK* incorporation into aRab1b and the subsequent labeling seemed to be less efficient than observed for BcnK. Moreover, TcoK* samples displayed large amounts of unspecific dye background signals after labeling, which may be due to the higher hydrophobicity of TcoK*.

3.1.3.3 The intracellular labeling of aRab1b is time- and dose-dependent

To verify the direct dependency of the decrease of the donor fluorescence lifetime on the presence of the acceptor, the labeling reaction was monitored over time in live cells. To this end, Rab1b WT and aRab1b S36 expressing HEK 293T cells were analyzed by confocal and fluorescence lifetime microscopy before and after the addition of 1 µM TMR (Figure 3.16).

In both samples the dye entered the cell lumen within two minutes and distributed evenly throughout the cell lumen in Rab1b WT expressing cells. In contrast, specific labeling of the Golgi-bound fraction of aRab1b S36 was clearly visible against the background fluorescence within five minutes (Figure 3.16 A, indicated by arrow heads). The fluorescence lifetime of aRab1b S36 expressing cells decreased continuously within 5 minutes post-dye addition and stabilized after 40 minutes at a total difference of $\Delta\tau$ = 400 ± 30 ps in comparison to the Rab1b WT control (Figure 3.16 B). In contrast, the fluorescence lifetime of Rab1b WT expressing cells remained almost constant, even in the presence of 1 µM TMR.

To determine the effects of the labeling efficiency on the sample lifetime, the same experiment was performed using different TMR concentrations (Figure 3.16 C). A dose-dependent decrease of the fluorescence lifetime on the used TMR concentration was observed (Figure 3.16 C).

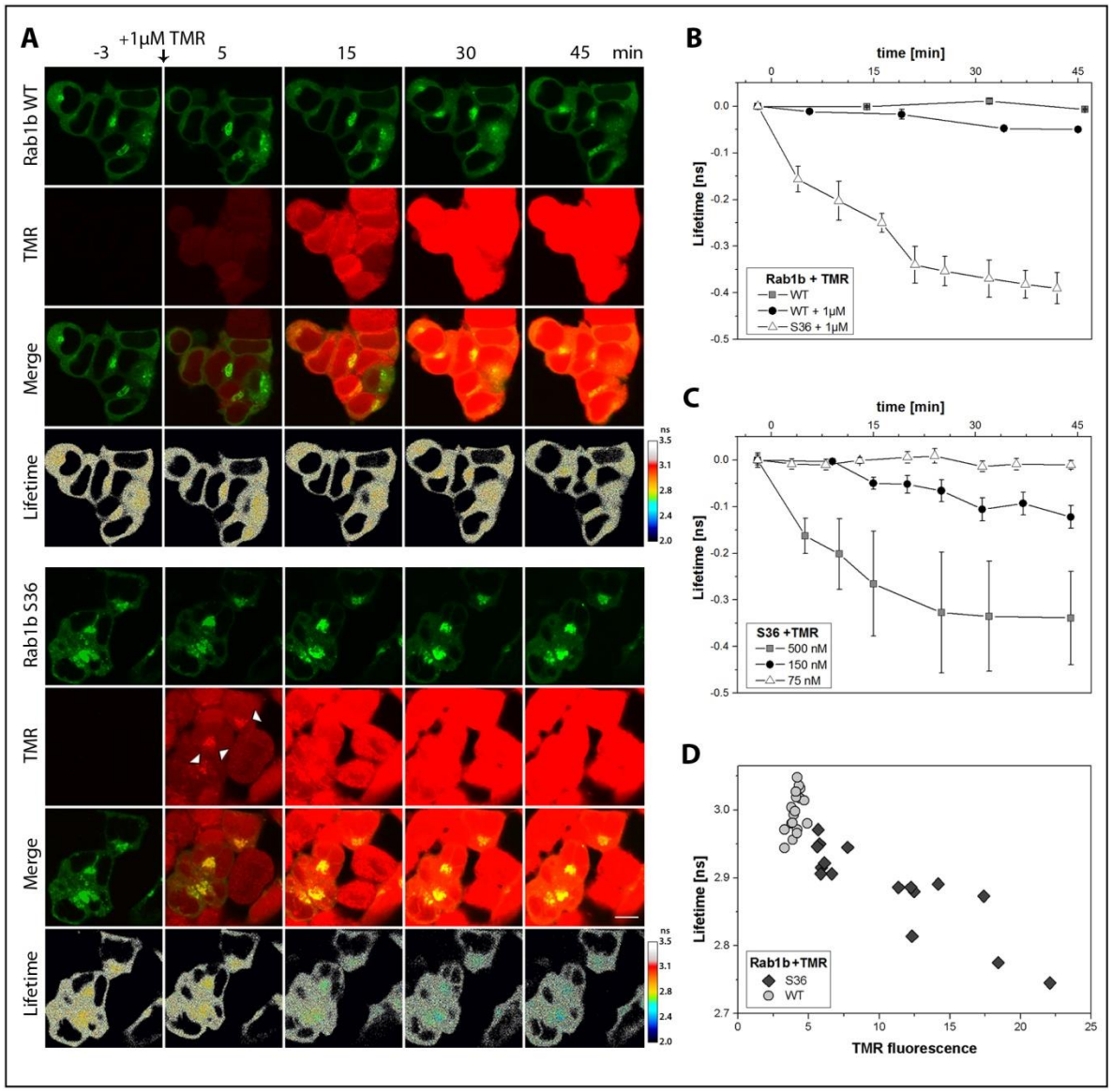

Figure 3.16: The intracellular labeling of Rab1b is time- and dose-dependent. A) HEK 293T cells expressing Rab1b WT or amber Rab1b S36 were monitored by confocal and fluorescence lifetime microscopy before and after the addition of 1 µM TMR. White arrow heads indicate the specific labeling of the Golgi apparatus which was detectable within 5 min post dye addition. B) The average of single cell lifetime analysis of unlabeled Rab1b WT as well as Rab1b WT and S36 incubated with 1 µM TMR. C) Single cell lifetime analysis of aRab1b S36 expressing cells incubated with different concentrations of TMR. D) Scatter plot of TMR-labeled HEK 293T cells expressing either Rab1b WT or aRab1b S36. The TMR fluorescence was quantified after intense washing and plotted against the fluorescence lifetime of the respective cell. Each data point represents a single cell. Scale bars: 10 µm.

These time-resolved lifetime measurements of aRab1b S36 labeling demonstrate a clear dependency of the change in fluorescence lifetime on the specific labeling. Moreover, the intracellular labeling reaction was titratable using different concentrations of TMR, indicating a dose-dependency of the labeling reaction on the abundance of the dye. The observed change in lifetime correlated with the respective dye concentration, confirming

the influence of the labeling yield on the fluorescence lifetime of the sensor construct. In contrast, presence of even 1 µM dye in Rab1b WT control samples did not affect the sample lifetime, verifying that even high abundance of the dye did not alter the fluorescence lifetime in the absence of amber protein. The labeling reaction seemed to be completed within 30-40 minutes in the presence of 500 nM TMR, whereas lower dye concentrations seemed to prevent completion of the labeling reaction within the same time period. Hence, the availability of the dye may be the rate-limiting factor for intracellular labeling. To achieve saturation of the labeling reaction and thereby the highest possible yield of labeled amber protein, the intracellular labeling was performed using 500 nM TMR and at least 45 minutes incubation for all further experiments.

3.1.3.4 Determination of the labeling yield

Another important factor for the establishment of the genetically encoded conformational sensor is the yield of the labeling reaction, which directly affects the fluorescence lifetime of a sample and thereby the accuracy and the dynamic range of the sensor. To determine the reaction yield, and thus, the efficiency of the intracellular reaction, HEK 293T cells expressing aRab1b S36 were labeled with TMR and lysed after intense washing. The lysates were divided in a half and a second, spectrally isolated dye was added to one aliquot. This second dye can react only with the previously unlabeled fraction of amber protein and can thereby serve as a direct indicator for the size of this fraction. Thus, fluorescence quantification of both fluorophores by in-gel fluorescence imaging allows for an indirect determination of the labeling yield (Figure 3.17 A). Subsequent western blot analysis was performed to identify the amount of full-length Rab1b, enabling the normalization the dye fluorescence on the amount of amber Rab1b per sample (Figure 3.17 B). While the labeling reaction in cells might be impaired by various factors, such as protein-protein interactions or activation state of the target protein, the labeling site should be fully accessible after cell lysis and protein denaturation. Thus, labeling of intracellularly unlabeled lysates should allow for a complete labeling reaction and served as a positive control. The experiment was performed using two different cell-impermeable fluorescent dyes for the second, in-lysate labeling, FAM and Cy5. Two single-labeled lysates, one labeled only with TMR in live cells and one labeled only post-lysis with FAM/Cy5, served as controls for the total intracellular labeling and the complete post-lysis labeling, respectively.

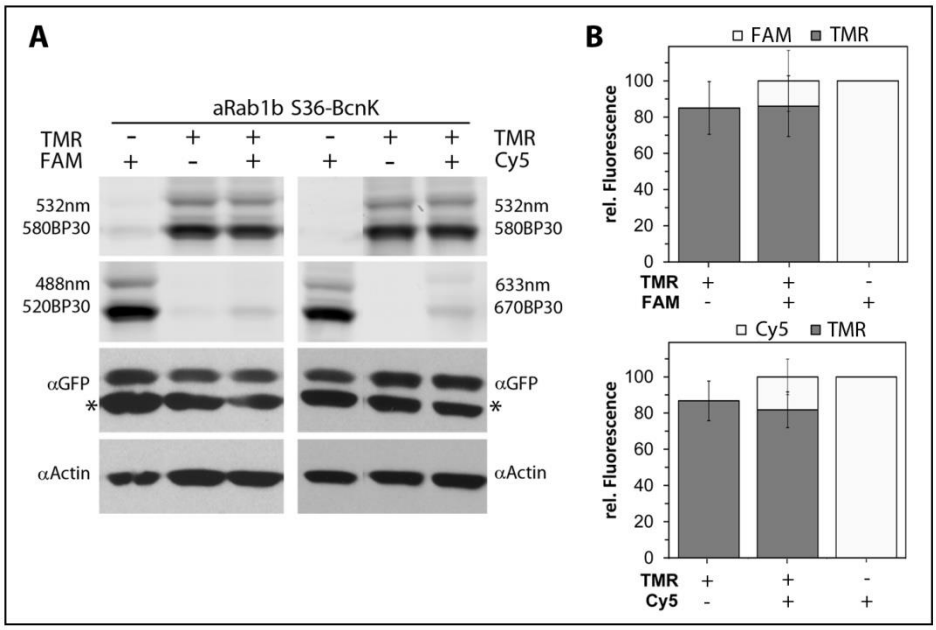

Figure 3.17: Evaluation of the intracellular labeling yield of the reaction of aRab1b S36-BcnK with TMR. A) In-gel fluorescence and western blot analysis (αGFP) of HEK 293T cells labeled with TMR pre-lysis and/or labeled post-lysis with FAM (left panel) or Cy5 (right panel). Asterisks indicate unspecific bands; Immunoblotting of Actin (αActin) served as a loading control. B) Quantification of the fluorescence intensity of the fluorescent signals of each fluorophore, normalized on the respective amount of full-length aRab1b S36 per sample. The upper graph illustrates the results of the post-lysis labeling with FAM and the lower panel the post-lysis labeling with Cy5.

The in-gel fluorescence analysis revealed the two previously described bands for full-length and labeled aRab1b S36 (49.9 kDa) and the PylRS (50.9 kDa), independent of the used dye (Figure 3.17 A). Intracellular labeling with TMR resulted in strong fluorescent bands in all labeled samples, while the labeling post-lysis with FAM or Cy5 exhibited high labeling in the previously unlabeled samples, but only faint secondary labeling in the intracellularly TMR-labeled samples. The quantification of the fluorescent band intensity, normalized on the respective amount of full-length aRab1b, revealed labeling yields of 85.0 ± 14.5 % for sole TMR-labeling in live cells and 86.1 ± 16.8 % for TMR-labeling in live cells followed by post-lysis FAM labeling. The samples labeled with Cy5 as a secondary dye displayed yields comparable to the labeling with FAM (81.83 ± 9.90 % and 86.76 ± 10.96 %, respectively).

These data demonstrate that the intracellular labeling of aRab1b S36 with TMR in live cells allows for high reaction yields using the protocol established in this work. The reaction yields were robust and reproducible, but depended strongly on the quality of the dye solution. Multiple freeze-thaw cycle of the dye stock solution were found to reduce the labeling yield up to 50% after the third cycle (data not shown).

3.1.4 Intracellular labeling of amber Rheb

In parallel to the establishment of the intracellular labeling of aRab1b, the same strategy was followed to achieve specific labeling of amber suppressed Rheb. Comparable to aRab1b labeling (Figure 3.7), the labeling of aRheb in HeLa cells with red probes did not result in any detectable specific labeling (data not shown). Furthermore, labeling with green dyes, e.g. FDAC or BDP, did also not succeed, neither for BcnK nor for TcoK* incorporation (data not shown). Moreover, the six mammalian cell lines that were tested for aRab1b labeling were also examined for the labeling of aRheb S34 and N50, the structural equivalents to aRab1b S36 and D53, respectively. Specific labeling of aRheb with TMR was not observed in any of the six cell lines, including HEK 293T cells, which is surprising considering the previously observed BcnK-dependent full-length expression of aRheb N50 detected by Western blot (Figure 3.6 B). To further assess whether any full-length expressed aRheb is labeled, in-gel fluorescence analysis was performed for the different amber Rheb mutants (Figure 3.18).

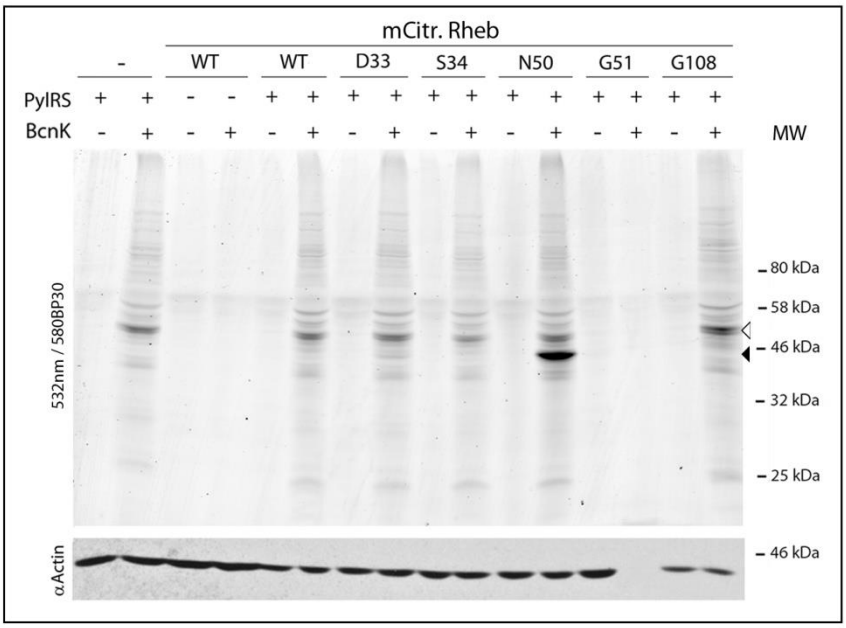

Figure 3.18: Intracellular labeling of different amber Rheb mutants with TMR. In-gel fluorescence analysis of TMR-labeled HEK 293T cells expressing Rheb WT and different amber variants in the presence and absence of BcnK. Fluorescent bands were detected for the PylRS (50.9 kDa, white arrow head) and full-length amber Rheb (48.2 kDa, black arrow head). Immunoblotting of Actin (αActin) served as a loading control.

Similar to in-gel analysis of the aRab1b mutants, two major UAA-dependent fluorescent bands were detected. The upper band representing the PylRS (50.8 kDa, indicated by the white arrow head) and a marginally lower band, indicating full-length expressed and

TMR-labeled aRheb (48.2 kDa, black arrow head). The labeling intensity varied for the different aRheb mutants; the strongest band was detected for labeling of aRheb N50 and only faint fluorescent bands indicating labeling of D33 and S34. No respective band was observed for the G108 labeling; G51 incubation with TMR caused massive cell detachment, resulting in complete cell loss before the lysis. The order of the mutants is in agreement with the previous findings for UAA-incorporation into aRheb (Figure 3.6 B), which demonstrated a yield of full-length expressed aRheb N50 of 12 % of the natural translation control, Rheb WT. In contrast, UAA incorporation into other Rheb mutants was hardly detectable.

To further assess these findings on the single cell level, HEK 293T cells expressing aRheb N50 were screened by confocal microscopy for specific TMR labeling. Only a small number of cells exhibited low but still detectable dye fluorescence against the background signals. These cells were analyzed by fluorescence lifetime microscopy to confirm the specificity of the labeling (Figure 3.19 A and B).

As previously described, the lack of clearly visible subcellular localization pattern of Rheb impedes the precise determination of the UAA incorporation efficiency of aRheb by microscopy. Direct comparison of the localization patterns of Rheb WT and aRheb N50 in HEK 293T cells revealed only minor differences. While the wild type protein localized almost exclusively in the cell lumen and displayed only a small nuclear Rheb fraction, the difference between the cytosolic and nuclear fluorescence was less distinct in aRheb expressing cells (Figure 3.19 A). Moreover, Rheb WT expression showed diffuse membranous patterns and high fluorescence densities in the perinuclear area, which were not observed in cells expressing aRheb, suggesting either functional impairment caused by the mutation or a low UAA incorporation efficiency. Low UAA incorporation efficiency would cause a mixed expression of mCitrine-Rheb fragment and full-length expression construct. Depending on its abundance, the fragment could mask the specific localization of the full-length expressed and prenylated aRheb mutants, further impeding the verification of the UAA incorporation process by the subcellular localization of the full-length construct. In fact, the fluorescence intensity of the detected TMR-labeling signals was rather low and did not evidently correlate with aRheb abundance, which raises the question of the specificity of the observed TMR signals. In addition, high fluorescence of the dye was observed in the nucleus, indicating unspecific side reactions.

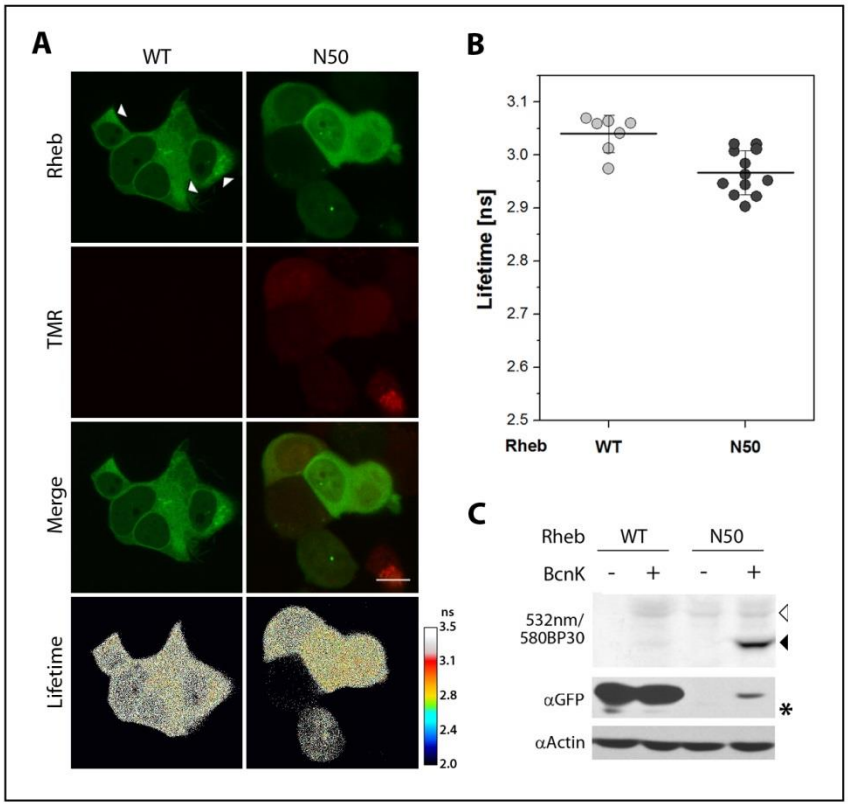

Figure 3.19: Intracellular labeling of aRheb N50 with TMR in HEK 293T cells. A) Confocal and fluorescence lifetime microscopy of aRheb N50 and Rheb WT. Arrow heads indicate the perinuclear fluorescence densities observed for Rheb WT but not for the amber mutant. B) Single cell lifetime analysis of the respective experiment. C) In-gel and western blot analysis of TMR-labeled HEK 293T (αGFP) cells expressing Rheb WT and aRheb N50 in presence and absence of BcnK. The black arrow head indicates full-length expressed and TMR-labeled aRheb (48.2 kDa); the white arrow head indicates the PylRS (50.9 kDa); the asterisk marks an unspecific band. Immunoblotting of Actin (αActin) served as a loading control. Scale bar: 10 µm.

mCitrine fluorescence lifetime analysis showed an average decrease of $\Delta\tau$ = 73.4 ± 41 ps for aRheb N50 in comparison to the unlabeled Rheb WT sample (Figure 3.19 B). This lifetime reduction is only a minor change in comparison to the observed decrease in lifetime of aRab1b after labeling ($\Delta\tau$ = 300 - 400 ps). Although the lifetime difference is rather marginal, it indicates the presence of the acceptor on the amber construct and thus, the specific labeling of at least a small fraction of aRheb. Furthermore, western blot and in-gel fluorescence analysis of aRheb N50 demonstrated full-length expression and specific TMR-labeling of the construct (Figure 3.19 C, black arrow head).

To confirm that the decrease of lifetime is due to the specific labeling of the construct, the labeling reaction was followed over time by fluorescence confocal and lifetime microscopy (Figure 3.20).

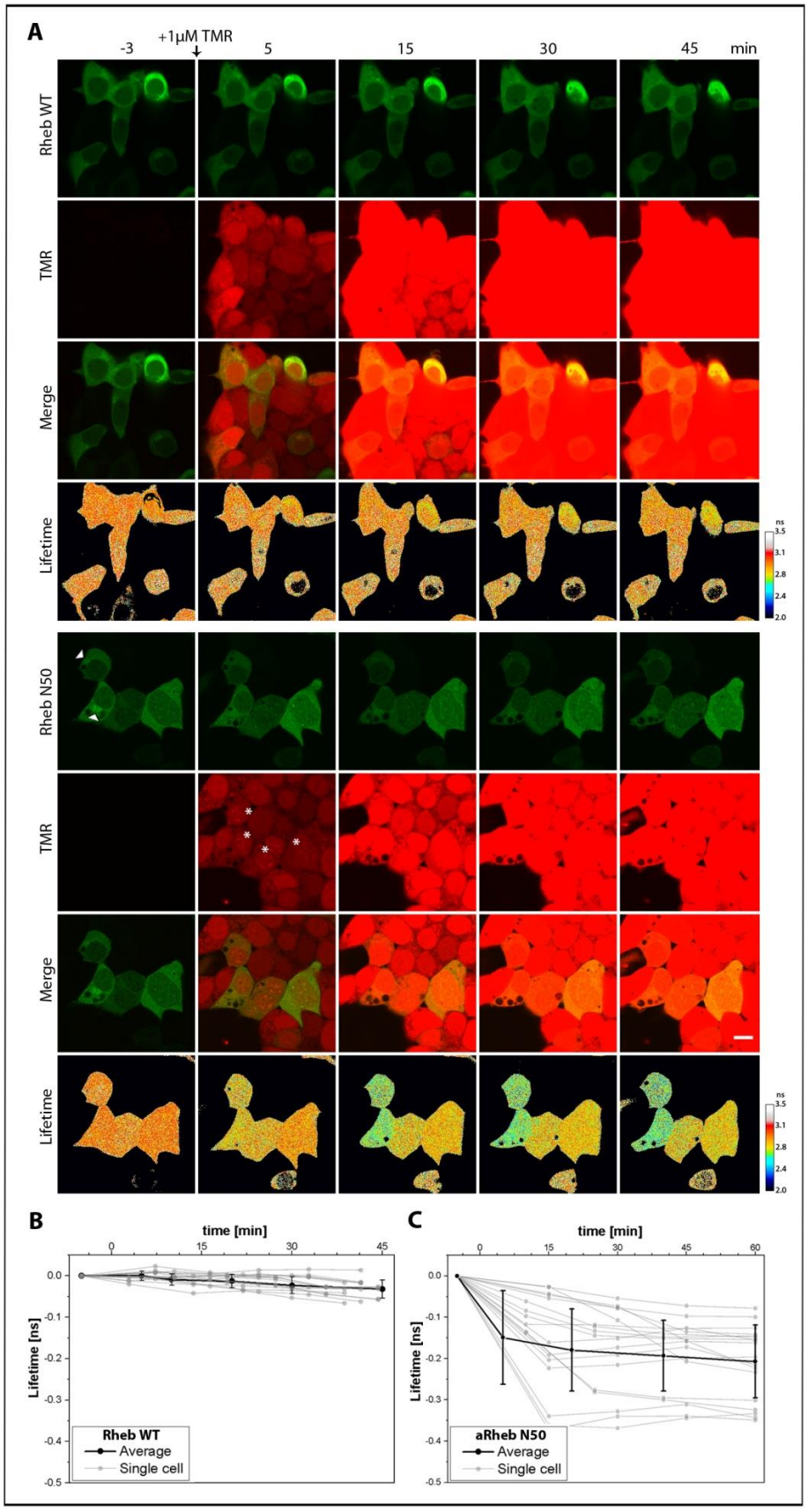
A
-3
+1µM TMR
5
15
30
45
min
Rheb WT
TMR
Merge
Lifetime
ns
3.5
3.1
2.8
2.4
2.0
Rheb N50
TMR
Merge
Lifetime
ns
3.5
3.1
2.8
2.4
2.0
B
time [min]
0
15
30
45
Lifetime [ns]
0.0
-0.1
-0.2
-0.3
-0.4
-0.5
Rheb WT
Average
Single cell
C
time [min]
0
15
30
45
60
Lifetime [ns]
0.0
-0.1
-0.2
-0.3
-0.4
-0.5
aRheb N50
Average
Single cell

Figure 3.20: Time-resolved monitoring of the intracellular labeling reaction of aRheb N50 and TMR in HEK 293T. A) Confocal and lifetime analysis of HEK 203T cells expressing Rheb WT and aRheb N50 pre- and post- addition of 1 µM TMR. White arrow heads indicate the perinuclear fluorescence densities in cells expressing aRheb N50. The asterisks indicate unspecific nuclear TMR-labeling. B, C) Single cell analysis of the change in lifetime of HEK 293T cells expressing Rheb WT (B) or aRheb N50 (C) pre- and post- addition of 1 µM TMR. Grey lines indicate single cells; the black line the sample average. Scale bar: 10 µm.

Only few cells expressing aRheb N50 exhibited the perinuclear Rheb fraction as observed in Rheb WT expressing cells, indicating the native localization of the construct (Figure 3.20 A, indicated by arrow heads). The majority of cells displayed a more diffuse localization throughout the cytoplasm and partially the nucleus. In both samples the dye entered the cells rapidly but, in contrast to the labeling of aRab1b, no specific labeling of aRheb was visible against the background signal. However, transfected cells, but not neighboring untransfected cells or Rheb WT expressing control cells, exhibited a nuclear TMR staining resembling nucleoli structures (Figure 3.20 A, marked by asterisks). Single cell fluorescence lifetime analysis revealed a change in the lifetime of aRheb N50 expressing cells post-dye addition, whereas the lifetime of the Rheb WT sample remained constant. The detected change in the lifetime of the aRheb N50 samples represented the heterogeneity of observed phenotypes; cells exhibiting a diffuse cytosolic Rheb pattern showed an average decrease in lifetime of $\Delta\tau$ = 100-150 ps, whereas the lifetime of cells with perinuclear densities decreased up to $\Delta\tau$ = 350 ps depending on the size of this fraction (Figure 3.20 C). In both cases no further decrease of the lifetime was observed after 30 minutes, indicating completion of the labeling reaction. In comparison, labeling of aRab1b S36 expressing cells with 1 µM TMR caused an average change in lifetime of $\Delta\tau$ = 350-400 ps within 45 minutes.

In summary, these findings demonstrate the specific labeling of aRheb N50 with TMR using the recently established protocol in HEK 293T cells. Nevertheless, the aRheb N50 labeling exhibited high heterogeneity both in the TMR labeling signals and in the lifetime reduction during labeling. Monitoring the labeling reaction over time identified a direct dependency of the lifetimes of single cells on the cellular localization of the aRheb construct, suggesting low incorporation efficiency as the major pitfall for amber suppression and labeling of aRheb N50. In contrast to aRab1b labeling, strong nuclear staining was observed for aRheb labeling, indicating unspecific side reactions similar to the previously reported nuclear labeling observed for the labeling of cytoplasmic BcnK-suppressed amber proteins [218]. Further optimization of both, the UAA incorporation efficiency and the labeling yield may allow for higher expression yields of full-length aRheb and thereby higher homogeneity of the sample, allowing for precise monitoring of Rheb spatiotemporal activity in live cells.

3.2 Characterization of the Genetically Encoded Sensors

3.2.1 Rab1b Conformational Sensor

The recombinant Rab1b conformational probes have been shown to report nucleotide exchange, effector binding or both events, depending on the position of the acceptor within the small GTPase [160,161]. Moreover, the probe read-out also depends on the labeling site. Labeling of mutation sites within the switch I region resulted in an increase of the sensor lifetime upon activation or effector binding, whereas introduction of the acceptor into the interswitch region caused a decrease in lifetime upon activation. Except for T34, a mutation site located in the switch I region, all previously characterized Rab1b mutants allowed for the detection of effector binding and activation events simultaneously. Nevertheless, due to the low expression and fluorescence brightness the amber variant of Rab1b T34 was not suitable for fluorescence lifetime analysis and was therefore not further assessed within this study. Unless indicated otherwise aRab1b S36 was used in all further experiments.

3.2.1.1 Sensing effector binding

To confirm the functionality of the genetically encoded conformational sensor, Rab1b effector binding was assessed. Introduction of the acceptor at the position S36 in Rab1b has been demonstrated to efficiently report effector binding events both *in vitro* and *in vivo* [160,161]. In this study a truncated version of the inositol-5-phosphatase OCRL1, a Rab effector protein, was used to confirm the signal change of the conformational sensor upon effector binding [160,161]. OCRL1 is a multi-domain membrane-bound protein that has been shown to interact in a nucleotide state dependent manner with different Rab proteins, including Rab1b [54,254-257]. Therefore, the C-terminus of OCRL1, which contains the Rab binding domain [255,256], was fused to the fluorescent protein TagBFP (TagBFP-OCRL1$_{539\text{-}901}$, hereafter referred to as OCRL) and was coexpressed with aRab1b S36 (Figure 3.21). Expression of Rab1b WT in the absence and the presence of OCRL and the expression of aRab1b S36 in the presence of soluble TagBFP served as negative controls.

In both samples the OCRL localization correlated with the Rab1b localization, resulting in a cytosolic and a Golgi-bound fraction (Figure 3.21 A). Neither the Rab1b localization nor the intracellular labeling reaction seemed to be affected by the presence of OCRL.

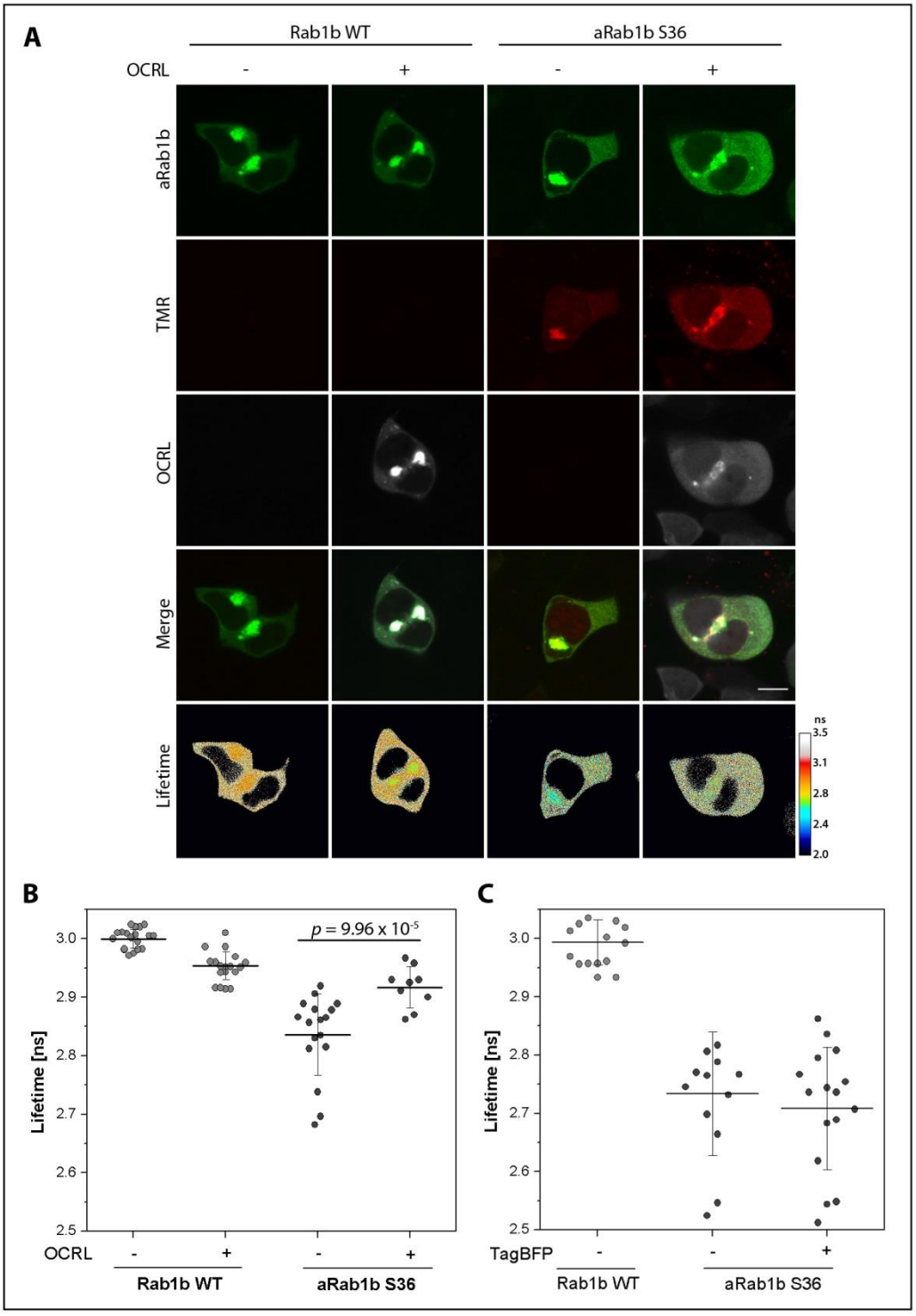

Figure 3.21: The genetically encoded conformational Rab1b sensor reports effector binding. A) HEK 293T cells expressing Rab1b WT and aRab1b S36 in the presence and absence of TagBFP-OCRL539-901 (OCRL). B) Single cell fluorescence lifetime analysis of HEK 293T cells expressing Rab1b WT or aRab1b S36 in the absence and presence of OCRL. C) Fluorescence lifetime analysis of HEK 293T cells expressing Rab1b WT and aRab1b S36 in the absence and presence of TagBFP. Scale bar: 10 µm.

The presence of OCRL increased the average fluorescence lifetime of aRab1b S36 significantly by $\Delta\tau_{S36+OCRL}$ = +120 ps, whereas the coexpression of OCRL and Rab1b WT resulted in a minor decrease in lifetime ($\Delta\tau_{WT\pm OCRL}$ = -60 ps, Figure 3.21 B). The lifetime increase of aRab1b correlated spatially with the OCRL localization, resulting in a change in lifetime especially for the Golgi-bound aRab1b (Figure 3.21 A). In contrast, expression of the soluble TagBFP fluorescent protein did not affect the lifetime of aRab1b S36 noticeably ($\Delta\tau_{S36\pm TagBFP}$ = 35 ps), excluding potential fluorophore cross-talk or side effects due to the presence of the third fluorophore.

These findings demonstrate that the labeled aRab1b S36 protein functions as a sensor for effector binding events. The sensor read-out and its dynamic range are in agreement with the previous studies demonstrating that the recombinant Rab1b S36C sensor displayed an increase of the fluorescence lifetime of eGFP upon binding to effectors [160,161].

3.2.1.2 Linker optimizations

To optimize the dynamical range of the sensor, the linker between the fluorescent protein and the small GTPase was engineered. This linker is a short peptide sequence encoded by the expression plasmid, allowing for rapid and simple optimizations of the linker properties by cloning. Two parameters influencing the sensor's dynamic range were assessed. The first parameter is the linker length, which defines mainly the distance between the two fluorophores. The second parameter is the linker flexibility, which can affect the orientation of the fluorophores towards each other. A highly flexible linker allows for a high number of different conformational states, whereas a more rigid linker locks the two FRET partners in distinct orientation states. Each conformational state of the sensor possesses its own fluorescence lifetime, thus, the acquired fluorescence lifetime represents an average of the different conformational states during signal acquisition. To reduce the number of conformational states, the linker rigidity was increased already in the beginning of this study. To this end, the native linker sequence, deriving from the insertion of the Rab1b gene into the pCitrineC1 backbone, was exchanged to a nine amino acid peptide sequence (Figure 3.22 A). This sequence has been reported to form an alpha helix[258,259] and *in silico* analysis indicated that the mCitrine C-terminus participates in the helix formation, extending the alpha helix towards the beta barrel of mCitrine (data not shown)[236]. Only five amino acids predicted to be unstructured are located on each side of the linker helix, both, towards the end of the mCitrine beta barrel and the first beta sheet in Rab1. When expressed in mammalian cells, this construct localized natively to the Golgi compartment and was comparable to the aRab1b construct with the more flexible linker (data not

shown). Unless indicated otherwise, all amber Rab1b and Rheb constructs used within this work contain the helical nine amino acid linker.

In addition to the helical linker, two shorter linker sequences, a two amino acid linker and a proline rich rigid linker, were assessed (Figure 3.22 B and C). The first one aims for an increase of the FRET efficiency and the dynamic range of the sensor by bringing the two fluorophores in closer proximity. Depending on the helicity of the linker, a maximal distance of 8.4-9.4 nm between the fluorophores was calculated for the helical nine amino acid linker constructs (Chapter 2.2.7). To bring the two fluorophores closer to the optimal distance R_0, the linker length was shortened to two amino acids and the last C-terminal eleven amino acids of mCitrine were removed. Previous studies showed that the C-terminal depletion of up to eleven amino acids of GFP did neither affect the protein fold, nor the fluorophore maturation or the biophysical properties [150,260-262]. These truncated fluorescent proteins allowed improving the dynamic range of orientation-dependent FRET-based sensors significantly [150,160,161,261].

The maximal distance calculated for the Rab1b construct containing the shortened linker is 6.0 nm, which is close to the R_0 value for the mCitrine-TMR FRET pair (est. 5.57 nm [263]). The expression of this construct in HEK 293T cells revealed a cytosolic and partially nuclear localization, but no association to the Golgi apparatus (Figure 3.22 B). In addition, no labeling was observed for the short linker construct, whereas the control, aRab1b S36, showed strong and specific labeling. Moreover, the Golgi marker GntnC localized in a diffuse pattern throughout the cell lumen, indicating perturbance of the Golgi homeostasis and thus, potential malfunction of the Rab1b short linker construct.

The second linker is a proline-rich linker (XPn). Proline is a unique amino acid which has a restricted backbone conformation due to the cyclization of its backbone [264]. Linkers consisting of multiple repetitions of proline and another amino acid, preferentially alanine, lysine or glutamine, have been shown to possess high stiffness due to the formation of proline helices [253,265-267]. The Rab1b_XPn linker construct localized to the Golgi compartment and displayed a labeling specificity comparable to the control sample, but with lower labeling intensity (Figure 3.22). In fact, the number of incorporating cells per sample was reduced in comparison to the helical linker control sample. mCitrine fluorescence lifetime analysis revealed an average lifetime of $\tau_{XPn\_S36} = 2.91 \pm 0.04$ ns, resulting in $\Delta\tau = 100$ ps difference between the two linker constructs ($\tau_{helical\_S36} = 2.82 \pm 0.08$ ns). However, whether this difference is due to the altered orientation of the fluorophores or their distance towards each other remains unclear. Further characterization of this constructs may give more insights into the influence of the linker rigidity on the dynamic range of the conformational sensor.

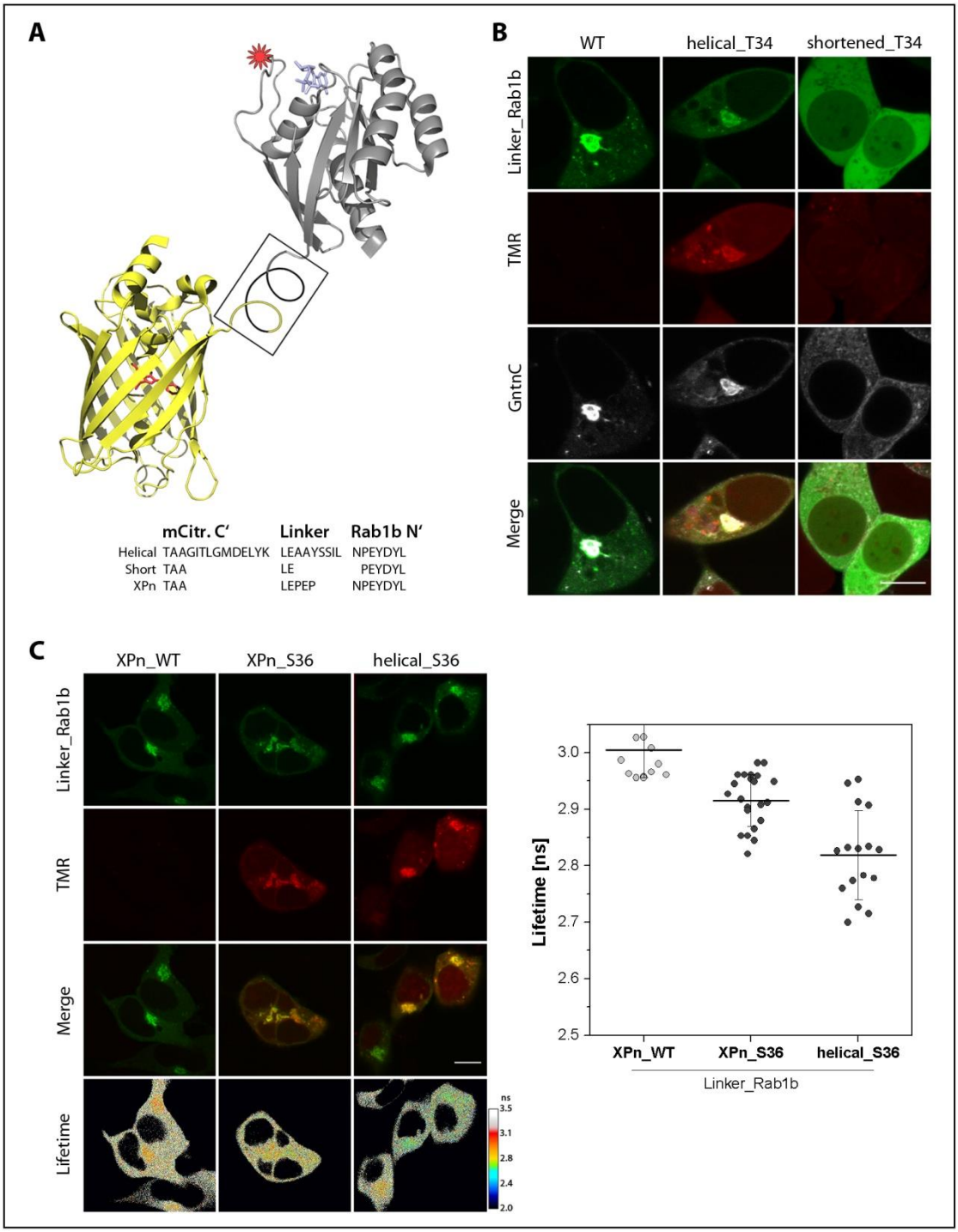

Figure 3.22: Optimizations of the proteinogenic linker between the fluorescent protein and Rab1b small GTPase. A) Scheme of the conformational sensor's architecture. The black box marks the linker region between the fluorescent protein and Rab1b; the respective linker sequences are illustrated below. B) HEK 293T cells expressing Rab1b WT and different linker variants of aRab1b T34. GntnC served as a marker for the Golgi compartment. C) Confocal microscopy and mCitrine lifetime analysis of HEK 293T cells expressing Rab1b WT and different linker variants of aRab1b S36. Scale bars: 10 µm.

3.2.1.3 Viability of sensor expressing cells

During the establishment and the optimization of the intracellular protocol aRab1b expressing samples exhibited lower fluorescence intensity and a more diffuse localization pattern when imaged one day post-labeling. To determine the potential time range for imaging of an amber sample, treatment and other applications, time-course experiments were performed. To this end, the fluorescence emission and the total cell confluency of Rab1b WT and sensor expressing cells were monitored for 48 h following the intracellular labeling with TMR (Figure 3.23).

mCitrine fluorescence was detectable for both samples despite the lower expression levels of the amber mutant in comparison to Rab1b WT (Figure 3.23 A). Although the number of fluorescent cells was higher in the aRab1b S36 sample, the observed fluorescence intensity was generally lower. Moreover, mCitrine fluorescence decreased over time in the aRab1b sensor sample but not for Rab1b WT. Quantification of the average fluorescent area per sample revealed that the fluorescence started to decay 6 h post-labeling and reached the level of background signals at 40 h post-labeling (Figure 3.23 A). In contrast, the Rab1b WT fluorescence remained constant over the whole measurement. As indicated by the microscopy images this fluorescence decrease of the Rab1b sensor was not due to a sudden loss of transfected cell, but due to a constant reduction of fluorescence intensity over time, especially within the first 12 h after labeling. One explanation for this decay may be the cellular Rab1b turn-over, which results in a continuous decrease of the protein over time. Due to the lack of UAA in the growth medium, expression of aRab1b S36 is prevented after the removal of the UAA prior to labeling, whereas Rab1b WT expression does not depend on the presence of the UAA and thus may compensate for the protein degradation by turn over. On the other hand, cells transfected for aRab1b did not notably divide during this experiment and were partially overgrown by neighboring untransfected cells. Repetitions of this experiment demonstrated that the decrease in fluorescent area can be delayed by using lower initial cell numbers, which prevents the overgrowths of untransfected cells and thereby the loss of fluorescent cells (Figure 3.23 B). However, the reduction of aRab1b S36 fluorescent area over time was monitored in all amber Rab1b samples, independent of the presence of TMR or its concentration.

Whether this fluorescence decay was also present in other amber proteins, e.g. amber Rheb mutants, remains unclear. However, depending on the cellular turn-over rate of a protein it is likely that all amber proteins may suffer from this pitfall. Consequently, all samples, independent of the protein of interest, the cell line or the dye used for labeling were imaged or lysed within 2-8 h post-labeling.

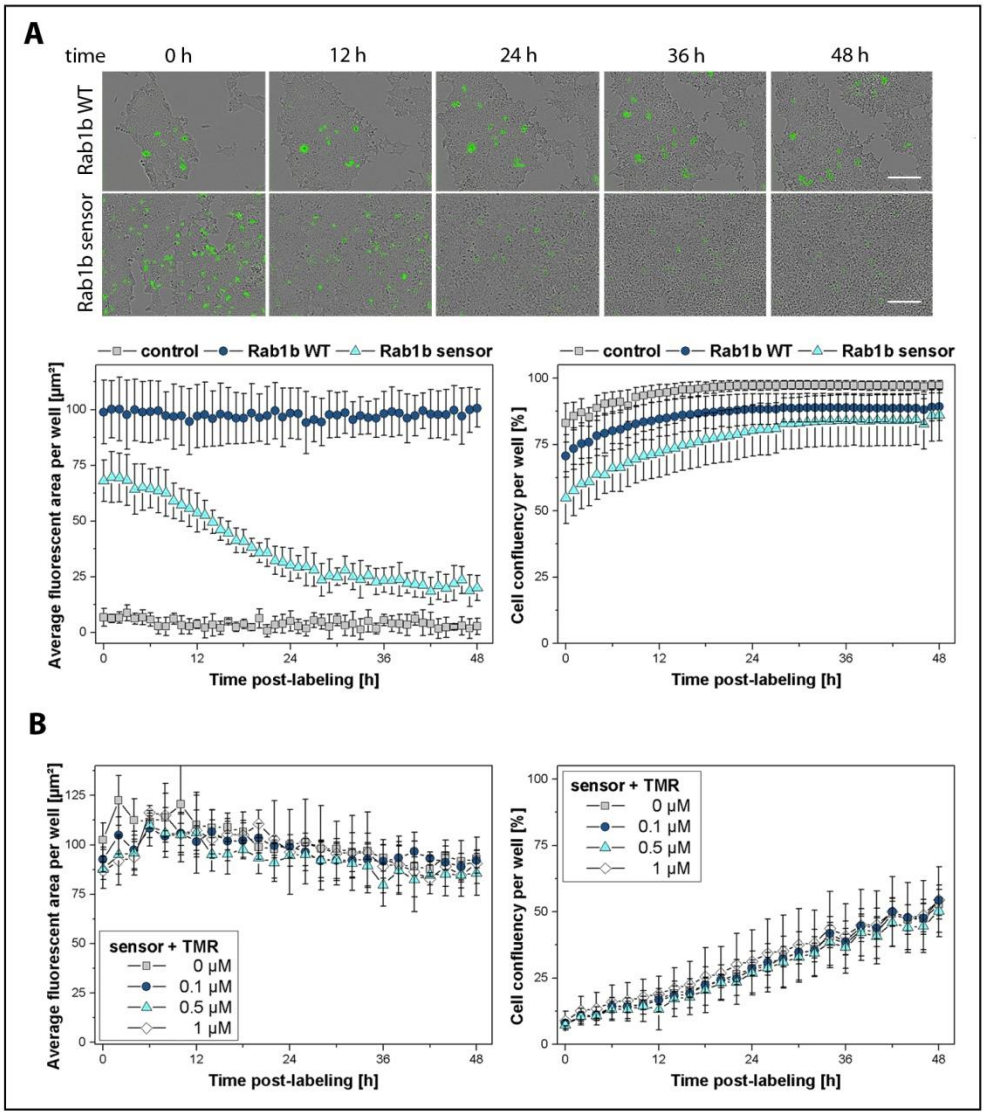

Figure 3.23: Viability and proliferation assay of TMR-labeled HEK 293T cells expressing TMR-labeled aRab1b S36. A) Bright field and fluorescence microscopy of HEK 293T cells expressing Rab1b WT and aRab1b S36 over 48 h post-labeling with TMR. The fluorescent area and cell confluency per sample were quantified to illustrate viability and proliferation. Data points represent the mean of three technical replicates over time. Error bars illustrate the SD. B) Fluorescent area and cell confluency of cells expressing aRab1b S36 labeled with different concentration of TMR. Lower initial cell numbers were used for this experiment to avoid loss of transfected cells due to overgrowth of neighboring cells. Scale bars: 200 µm.

3.2.1.4 Determination of the sensor's dynamic range

Different strategies can be utilized to ascertain the dynamic range of a sensor, e.g. (1) using mutations that affect the protein's activity or that lock the protein in a respective activity state, (2) regulation by coexpression of activating or inactivating proteins or (3) exploiting the cognate signaling pathway and thereby activating the target protein by a known stimulus. Because of the lack of stimuli for Rab1b activation due to its role in ER-to-Golgi vesicular transport, the last option is not applicable for the conformational Rab1b sensor. Therefore, the two first strategies were followed, using Rab1b mutants that affect the nucleotide state and regulating the sensor by coexpression of GEF and GAP proteins.

Regulation of the nucleotide state by GEF and GAP

To determine the lifetime of the active Rab1b sensor, the *Legionella* protein DrrA was exploited. During infection *Legionella* injects a number of proteins into the host cell of which many have been shown to modulate the function of Rab GTPases (reviewed in [268]). Among these proteins is DrrA, which has been reported to act as a Rab1 GEF. DrrA consists of three domains and the central domain possesses the catalytic GEF activity towards Rab1 [29,269]. Therefore, coexpression of DrrA should result in predominantly GTP-loaded Rab1b protein, allowing for the determination of the Rab1b sensor's 'ON' signal. To this end, Rab1b WT and aRab1b S36 were coexpressed with $DrrA_{340-533}$ fused to TagBFP (TagBFP-$DrrA_{340-533}$, hereafter referred to as DrrA, Figure 3.24).

The DrrA presence caused a reduced Golgi association and relocalization of Rab1b to the cytosol and partially the nucleus (Figure 3.24 A). In Rab1b WT expressing cells this phenotype correlated with the abundance of DrrA. Low DrrA expression allowed for partial Rab1b localization to the Golgi compartment, while high expression levels induced predominantly cytosolic Rab1b localization. Coexpression of DrrA and amber Rab1b S36 resulted in a variety of phenotypes, ranging from cytosolic to partially Golgi-associated aRab1b and did not depend on the DrrA expression level. Furthermore, DrrA presence increased signs of cytotoxicity in the amber suppression samples noticeably, whereas Rab1b WT and DrrA coexpressing cells were viable and healthy. Moreover, cells expressing aRab1b S36 and DrrA displayed a drastic reduction of TMR-labeling, which in fact correlated with DrrA abundance (Figure 3.24 A). Quantification of TagBFP (indicating DrrA expression level) and TMR (indicating specific labeling) fluorescence intensities within single cells revealed a strong dependency of the TMR amount of a cell on the abundance of DrrA (Figure 3.24 C). mCitrine fluorescence lifetime analysis showed an increase in lifetime of aRab1b S36 in the presence of DrrA in comparison to its absence ($\Delta\tau_{S36\pm DrrA}$ = +77 ps, Figure

3.24 B). In contrast, coexpression of DrrA and Rab1b WT sample caused a minor fluorescence lifetime reduction ($\Delta\tau_{WT\pm DrrA}$ -20 ps).

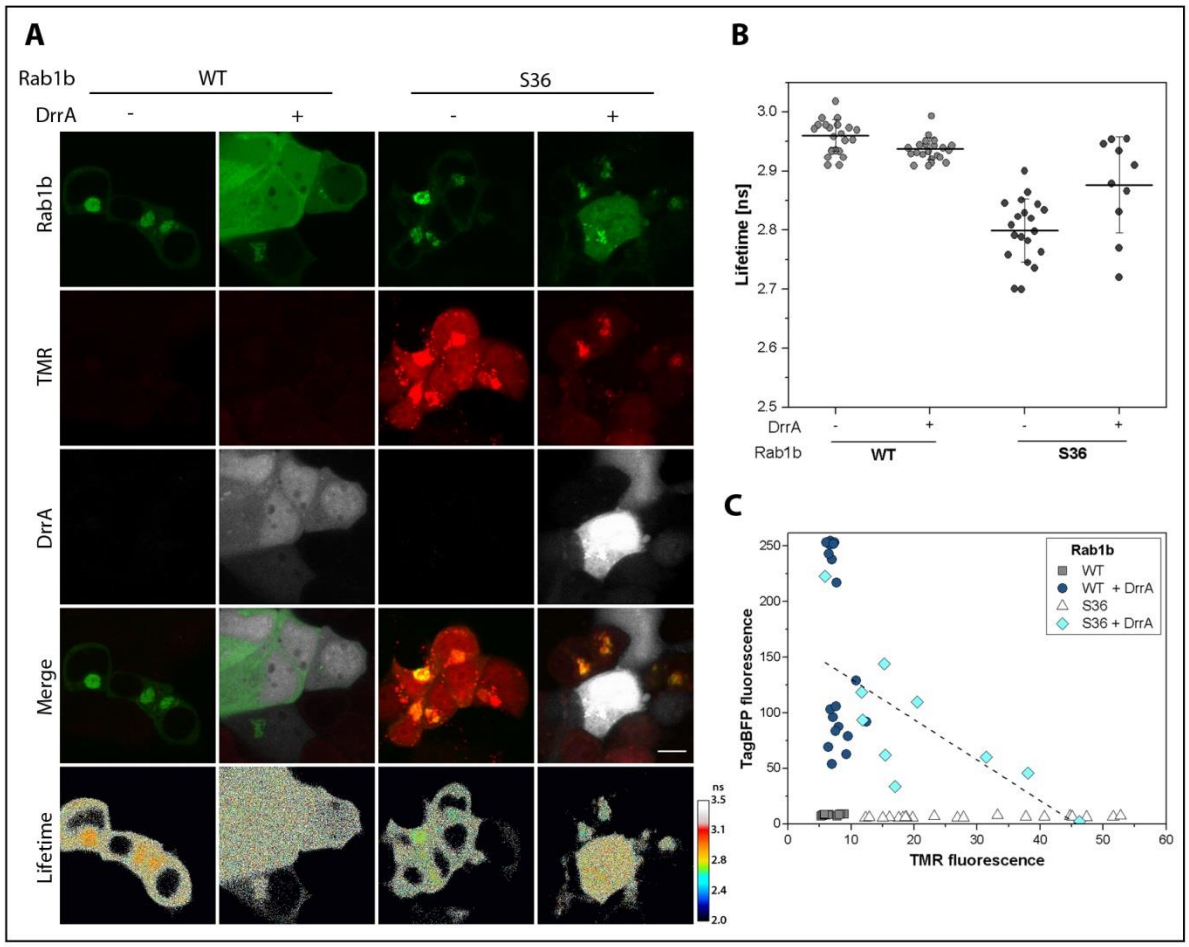

Figure 3.24: Directing the Rab1b sensor's nucleotide state by coexpression of the Rab1 GEF DrrA.
A) HEK 293T cells expressing Rab1b WT and the amber mutant S36 in the absence and presence of TagBFP-DrrA340-533 (DrrA). B) Single cell lifetime analysis of the respective experiment. C) Quantification of the TagBFP and TMR fluorescence intensity of HEK 293T cells expressing Rab1b WT and aRab1b S36 in the absence and presence of DrrA. Each data point represents a single cell; the dashed line represents the linear fit of the aRab1b S36+DrrA. Scale bar: 10 µm

As the activation of the Rab1b S36 sensor is reported by an increase of the fluorescence lifetime, an augmented fluorescence lifetime of mCitrine-aRab1b S36 is expected in the presence of DrrA. However, in this case, it cannot be excluded that the detected increase in sensor lifetime is indeed due to the DrrA-mediated activation and not caused by an impaired intracellular labeling reaction. Impairments in the labeling reaction and thereby a lower labeling yield would artificially decrease the donor-acceptor population, resulting in an increase of the average sample lifetime. The observed dependency of the TMR fluorescence on the TagBFP fluorescence intensity supports this possibility. Another

possibility is that the DrrA coexpression causes degradation of the sensor construct. If fully intact, single mCitrine displays an even distribution throughout the cell, which cannot be reliably distinguished from the cytosolic Rab1b localization caused by DrrA coexpression. This possibility is supported by the complete lack of labeling in respective cells and the sample lifetime that is comparable to the donor only lifetime. Nevertheless, a full-length expression of the construct but a lack of labeling would also yield similar lifetimes and cannot be differentiated from protein degradation.

Furthermore, coexpression of Rab1 GAP TBC1D20 was performed. TBC1D20 functions as a Rab1b and Rab2a GAP protein, regulating the ER-to-Golgi vesicular transport and maintaining the homeostasis of the Golgi complex [90,91,93]. Overexpression of the catalytically active TBC1D20 has been reported to maintain Rab1b in its inactive, GDP-loaded state, causing disruption of the ER-to-Golgi trafficking and the loss of the Golgi structure [89,91]. To determine the sensor's 'OFF' state, a truncated version of TBC1D20, fused to TagBFP, was coexpressed with aRab1b S36. $TBC1D20_{1\text{-}362}$ contains the catalytic RabGAP domain, but lacks the C-terminal transmembrane domain and thereby the protein's localization signal [90]. Hereafter, TagBFP-$TBC1D20_{1\text{-}362}$ is referred to as TBC1D20.

The presence of TBC1D20 caused a predominantly cytosolic and partially nuclear localization of Rab1b WT and prevented the localization of Rab1b to the Golgi apparatus. In contrast, aRab1b S36 localized mainly to the cytosol (Figure 3.25 A). Rab1b WT and TBC1D20 coexpressing cells were markedly rounded in comparison to TBC1D20-negative samples. As observed for DrrA coexpression, specific labeling of aRab1b S36 was not detectable in the presence of TBC1D20, although aRab1b S36 expressing cells displayed low TMR fluorescence. These signals were above the background signals of untransfected neighboring cells, but the TMR fluorescence intensity did not correlate with the localization of aRab1b. Moreover, TBC1D20 and aRab1b S36 coexpression yielded extremely dim fluorescent cells which were hardly detectable. mCitrine fluorescence lifetime analysis revealed an average lifetime of $\tau_{S36+TBC1D20}$ = 2.85 ± 0.10 ns of aRab1b S36 in the presence of TBC1D20 and τ_{S36} = 2.75 ± 0.09 ns in its absence.

Due to its GAP activity towards Rab1, coexpression of TBC1D20 maintains Rab1b predominantly in its GDP-loaded state [89,91]. Inactivation of the Rab1b sensor has previously been shown to decrease the lifetime of the eGFP-Rab1b recombinant sensor by approximately 10 % [160,161]. Thus, the observed increase in mCitrine lifetime is not in agreement with the previous findings. However, similar to DrrA coexpression, it cannot be excluded that the lifetime increment was due to the lack of specific labeling, resulting in a larger donor only fraction and thereby a higher average lifetime.

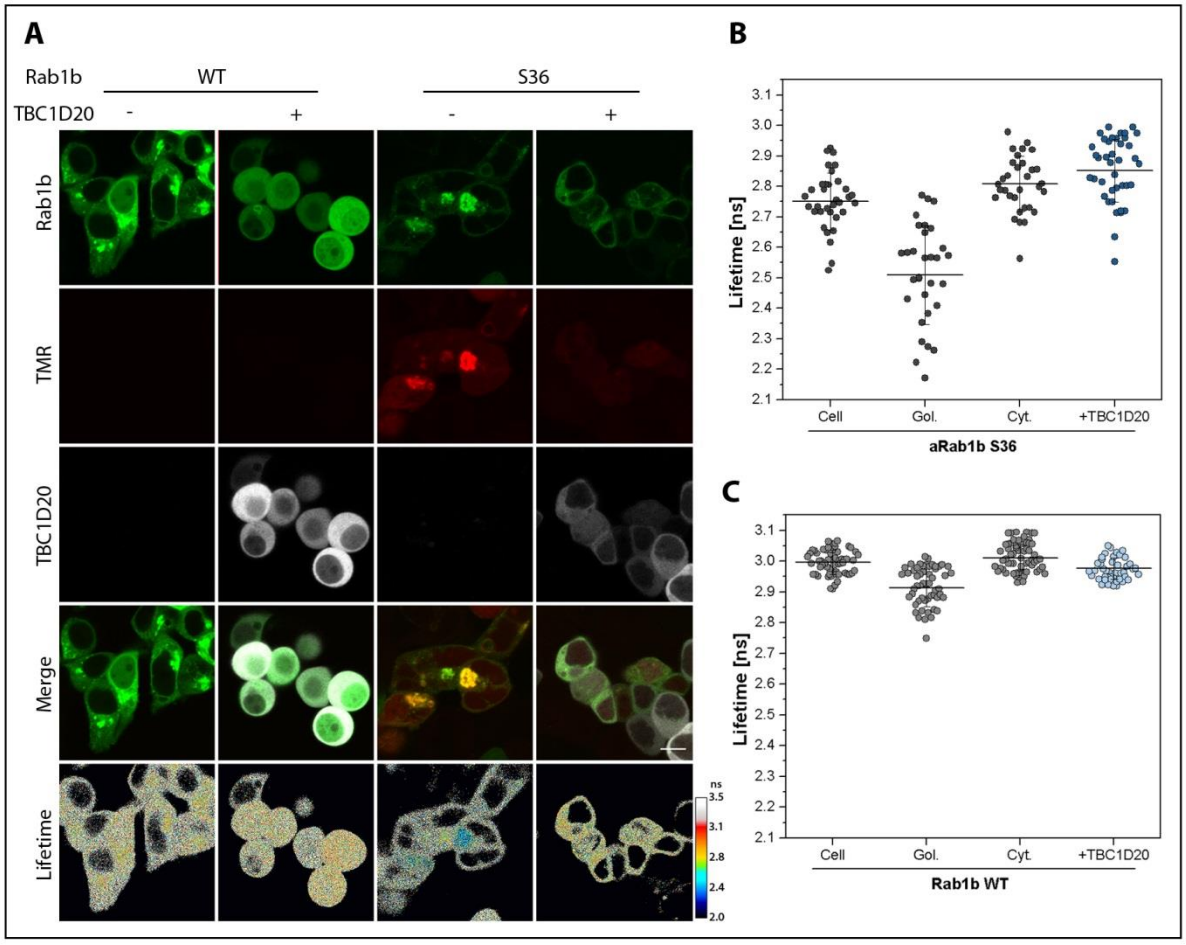

Figure 3.25: Determining the Rab1b sensor's 'OFF' state by the coexpression the Rab1 GAP TBC1D20. A) HEK 293T cells expressing Rab1b WT or aRab1b S36 in the presence and absence of TBC1D20. B) and C) Single cell fluorescence lifetime analysis of aRab1b S36 (B) and Rab1b WT (C) in the absence and presence of TBC1D20. Cells expressing only Rab1b were segmented for analysis (Cell = whole cell, Gol. = Golgi, Cyt. = Cytoplasm). Scale bar: 10 µm.

In summary this data demonstrates that coexpression of regulatory proteins can affect the intracellular labeling reaction of an amber protein, potentially causing artificial changes in the fluorescence lifetime of a sample. In fact, coexpression of the Rab1 binding domain of the effector OCRL did not affect aRab1b labeling which raises the possibility that aRab1b must be fully functional and requires free cycling between the two different nucleotide states to allow for complete labeling.

Amber Rab1b nucleotide state mutants

To avoid exogenous expression of regulatory proteins, three nucleotide state affecting mutations of Rab1b, S22N (SN), Q67L (QL) and N121I (NI), were assessed to determine the different activation states of the sensor. The Q67L mutation of Rab1 lowers the intrinsic nucleotide hydrolysis and impairs the GTPase-GAP interaction, leading to a dominant active protein which exhibits 2-3 fold higher GTP-loading than the wild type protein *in vivo* [21,63,249]. The Rab1b S22N mutant has a lower affinity for GTP than GDP, resulting in a predominantly GDP-loaded protein, whereas N121I exhibits low affinity for both nucleotides [245,246,249]. The two inactive mutants act as dominant suppressors of endogenous Rab1b function and their exogenous expression causes a partial or complete disruption of the Golgi complex [245-249].

First, the BcnK incorporation and TMR-labeling was assessed for the active and inactive mutants of aRab1b S36 (Figure 3.26). Similar to aRab1b S36 wild type (S36/WT) the dominant active mutant aRab1b S36/QL (S36/QL) localized to the Golgi apparatus and exhibited comparable TMR-labeling with high specificity (Figure 3.26 A and C). Expression of the two dominant negative mutants aRab1b S36/SN and S36/NI resulted in low fluorescence signals and an even distribution within the cytosplasm and nucleus. No specific labeling with TMR was detectable for the two inactive amber mutants (Figure 3.26 A and C). Single cell mCitrine fluorescence lifetime analysis of the samples revealed an average lifetime of $\tau_{S36/QL}$ = 2.82 ± 0.05 ns for S36/QL which is slightly lower than the lifetime of S36/WT (τ_{S36} = 2.85 ± 0.06 ns, Figure 3.26 B). In contrast, the S36/SN and S36/NI samples exhibited drastically higher lifetimes ($\tau_{S36/SN}$ = 2.96 ± 0.03 and $\tau_{S36/NI}$ = 2.97 ± 0.03) that were comparable to the unlabeled Rab1b WT/WT control ($\tau_{WT/WT}$ = 2.99 ± 0.03). In combination with the observed lack of acceptor fluorescence, this increase in lifetime suggests a complete lack of TMR-labeling. To further assess, whether the lack of labeling is due to failure of BcnK incorporation into the inactive amber mutants, in-gel fluorescence and western blot analysis were performed (Figure 3.26 C). Full-length expression and specific labeling were detected for aRab1b S36/WT and /QL mutant, whereas the /SN and /NI variants lacked any full-length expression detected by western blot. Interestingly, the more sensitive in-gel fluorescence analysis revealed very faint bands, indicating low abundant but full-length expressed and labeled /SN and /NI mutants (Figure 3.26 C, black arrow head).

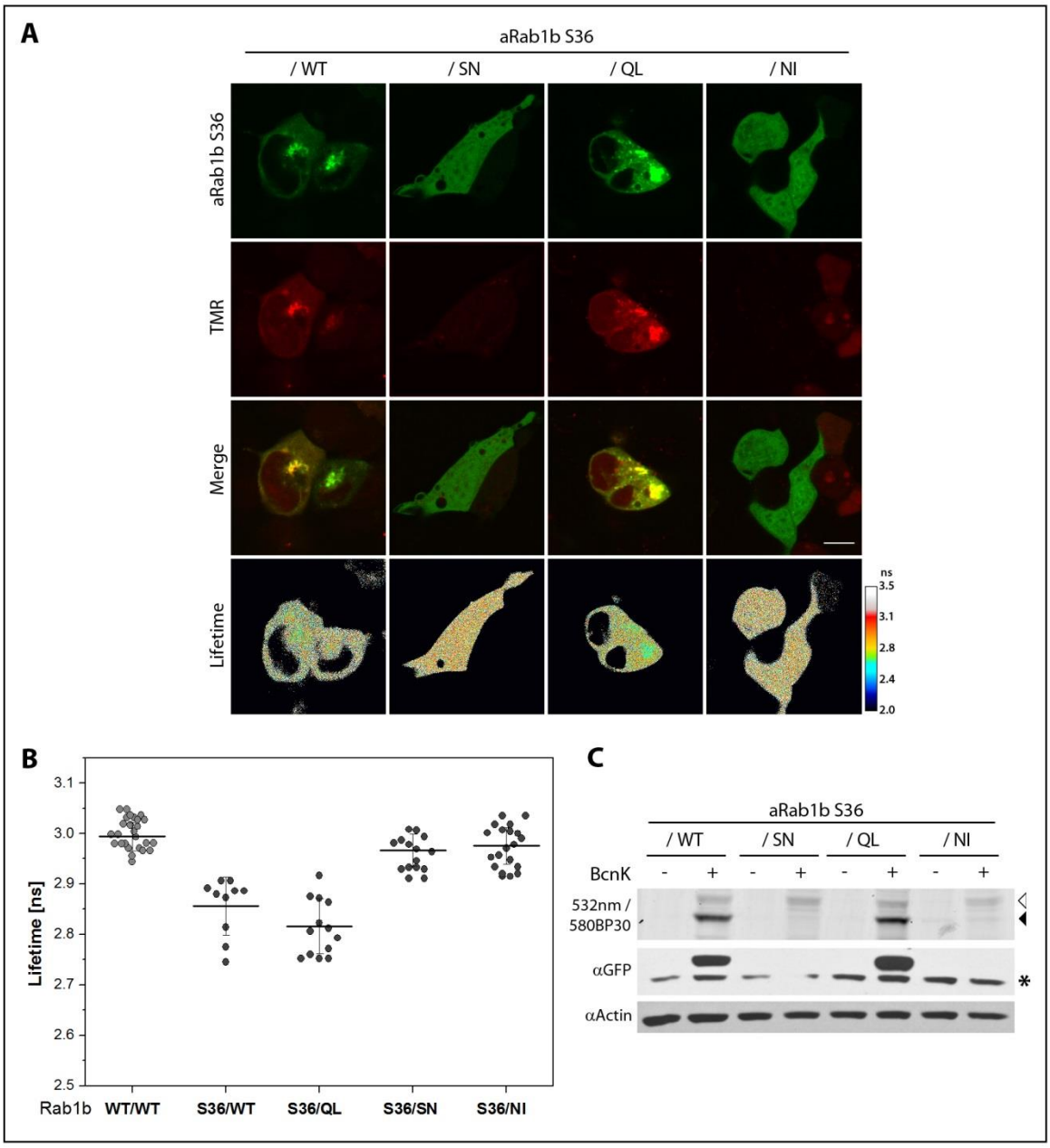

Figure 3.26: Determining the dynamic range of the conformational sensor using dominant active and inactive mutants of Rab1b. A) HEK 293T cells expressing Rab1b WT and three different amber Rab1b S36 nucleotide state mutants, S22N (SN), Q67L (QL) and N121I (NI). B) Single cell fluorescence lifetime analysis of the different amber nucleotide state mutants and aRab1b S36/WT. Rab1b WT (WT/WT) served as the donor only control. C) In-gel fluorescence and western blot analysis of the different mutants. The white arrow head marks the PylRS, the black arrow head labeled aRab1b, the asterisk indicated an unspecific band. Immunoblotting of Actin served as a loading control (αActin). Scale bar: 10 µm.

Characterization of the sensor's 'ON' state

Following verification of the BcnK-dependent full-length expression and the labeling of the dominant active mutant aRab1b S36/QL, the sensor signal was analyzed in a higher spatial resolution in live cells. To this end, lifetime images of S36/WT and S36/QL expressing cells were segmented into three regions of interest (ROI): whole cell (Cell), cytoplasm (Cyt.) and Golgi apparatus (Gol.) and the average lifetime was determined for each region (Figure 3.27).

Segmentation of Rab1b expressing cells revealed different lifetimes for cytosolic and Golgi-bound Rab1b fractions in all samples (Figure 3.27 B). The Golgi region exhibited a lower lifetime than the cytoplasm. While this difference amounted to $\Delta\tau_{WT\ Gol\text{-}Cyt.}$ = 90 ps in Rab1b WT/WT and WT/QL samples, the gap between Golgi complex and cytoplasm was larger in TMR-labeled aRab1b S36 samples ($\Delta\tau_{S36\ Gol\text{-}Cyt.}$ = 250 ps). Interestingly, although S36/QL mutant expressing cells displayed a minor increase of the fluorescence lifetime in comparison to S36/WT ($\Delta\tau_{Cell\ (S36/WT\text{-}S36/QL)}$ = 32 ps), the lifetime of the Golgi-bound aRab1b fraction was higher ($\Delta\tau_{Gol.(S36/WT\text{-}S36/QL)}$ = 170 ps). Thus, the lifetime difference between Golgi and cytoplasm ($\Delta\tau_{S36/QL\ Gol\text{-}Cyt.}$ = 90 ps) is 2.5-fold less than observed for S36/WT and is comparable to the difference observed in Rab1b WT cells.

Although the average sample lifetimes of S36/WT and /QL differed by only $\Delta\tau$ = 40 ps, the labeling of the two constructs was further assessed to exclude varying labeling efficiency as a cause for the detected lifetime increment. The amount of TMR fluorescence of S36/WT and /QL expressing cells was quantified and plotted against the lifetime of the respective cell (Figure 3.27 C). Both samples, aRab1b S36/WT and S36/QL, displayed a similar dependency of the lifetime on the abundance of the acceptor. Moreover, the linear fitting of the two data sets was comparable, indicating similar labeling and lifetime distribution of the two constructs. Furthermore, in-gel fluorescence and western blot analysis of the amber wild type protein and the QL mutant revealed similar expression levels and labeling intensity, excluding a reduced labeling efficiency as an artificial cause for the observed fluorescence lifetime differences of the two samples (Figure 3.27 D).

In summary, the dominant active QL mutant of amber Rab1b S36 was expressed in full-length and labeled comparably to the amber wild type protein. Moreover, the predominantly active QL mutant displayed an increase in fluorescence lifetime of the Golgi-bound aRab1b fraction, which is consistent with previous studies using the recombinant COSGA sensor [160,161]. Nevertheless, the lifetime increment observed for the Golgi region of the genetically encoded sensor, about 6.5 %, is slightly less than reported for the active recombinant sensor (10 %).

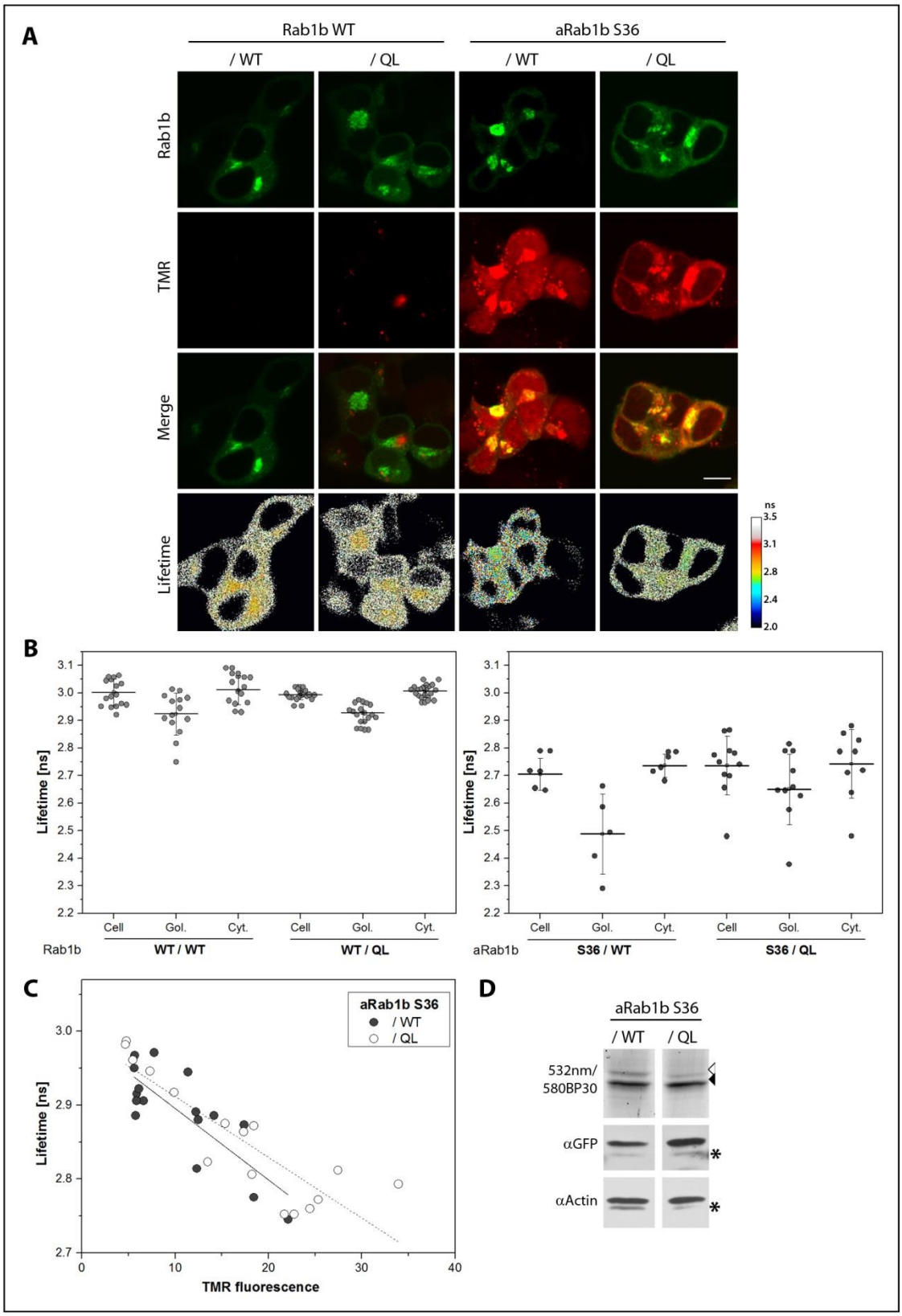
A
Rab1b WT
aRab1b S36
/ WT
/ QL
/ WT
/ QL
Rab1b
TMR
Merge
Lifetime
ns
3.5
3.1
2.8
2.4
2.0
B
Lifetime [ns]
Cell
Gol.
Cyt.
Rab1b
WT / WT
WT / QL
aRab1b
S36 / WT
S36 / QL
C
aRab1b S36
/ WT
/ QL
Lifetime [ns]
TMR fluorescence
D
aRab1b S36
/ WT
/ QL
532nm/
580BP30
αGFP
αActin

Figure 3.27: Characterization of the sensor's 'ON' state using the dominant active Q67L mutant. A) HEK 293T cells expressing Rab1b WT and aRab1b S36, both as wild type protein and Q67L variant. B) Single cell fluorescence lifetime analysis of Rab1b WT and aRab1b S36 and their respective QL mutants. The lifetime was quantified for whole cells (Cell), Golgi apparatus (Gol.) and cytoplasm (Cyt.). C) Comparison of the dependency of the lifetime on the abundance of the acceptor for aRab1b S36 WT and /QL. The black lines shows the linear fit for S36/WT, the dashed line for S36/QL. D) Comparison of the aRab1b S36/WT and /QL expression and labeling by in-gel fluorescence and western blot analysis. The white arrow head marks the PylRS, the black arrow head indicates labeled aRab1b and the asterisk an unspecific band. Scale bar: 10 µm.

Determining the sensor's 'OFF' state

As previously determined by western blot analysis, the inactive amber Rab1b mutants S22N and N121I lacked BcnK incorporation and thus full-length expression of the construct (Figure 3.26). Furthermore, the reliable detection of BcnK incorporation by fluorescence microscopy was impaired by the cytosolic localization of the inactive mutants which cannot be distinguished from the expression of the non-suppressed mCitrine-Rab1b fragment. However, if full-length expressed, inactive Rab1b mutants cause a dispersion of the Golgi apparatus, allowing for an indirect detection of BcnK incorporation. To identify any full-length expression of SN or NI amber mutants, the Golgi marker GntC was coexpressed with both inactive mutants of aRab1b S36 or D53 and the samples were screened for fragmentation of the Golgi complex (Figure 3.28). Rab1b WT/SN and /NI mutants served as phenotype controls.

The compact and defined Golgi structure detected in WT/WT sample was not observed in any cell expressing Rab1b WT/SN or /NI mutant. Even low expression of these constructs resulted in complete dispersion of the Golgi apparatus as indicated by the diffuse localization of GntC (Figure 3.28 A). Comparison of the inactive amber mutants with the control samples revealed several differences. Despite the cytosolic and partially nuclear localization of aRab1b S36 and D53 /SN and /NI mutants, the Golgi structure remained intact and tightly packed, similar to the wild type protein control samples. Additionally, cells expressing amber /SN and /NI mutants seemed less rounded than the respective controls. The same results were found in HeLa and Cos7 cells, and are consistent with the lack of full-length expression of the dominant negative aRab1b mutants as detected by western blot.

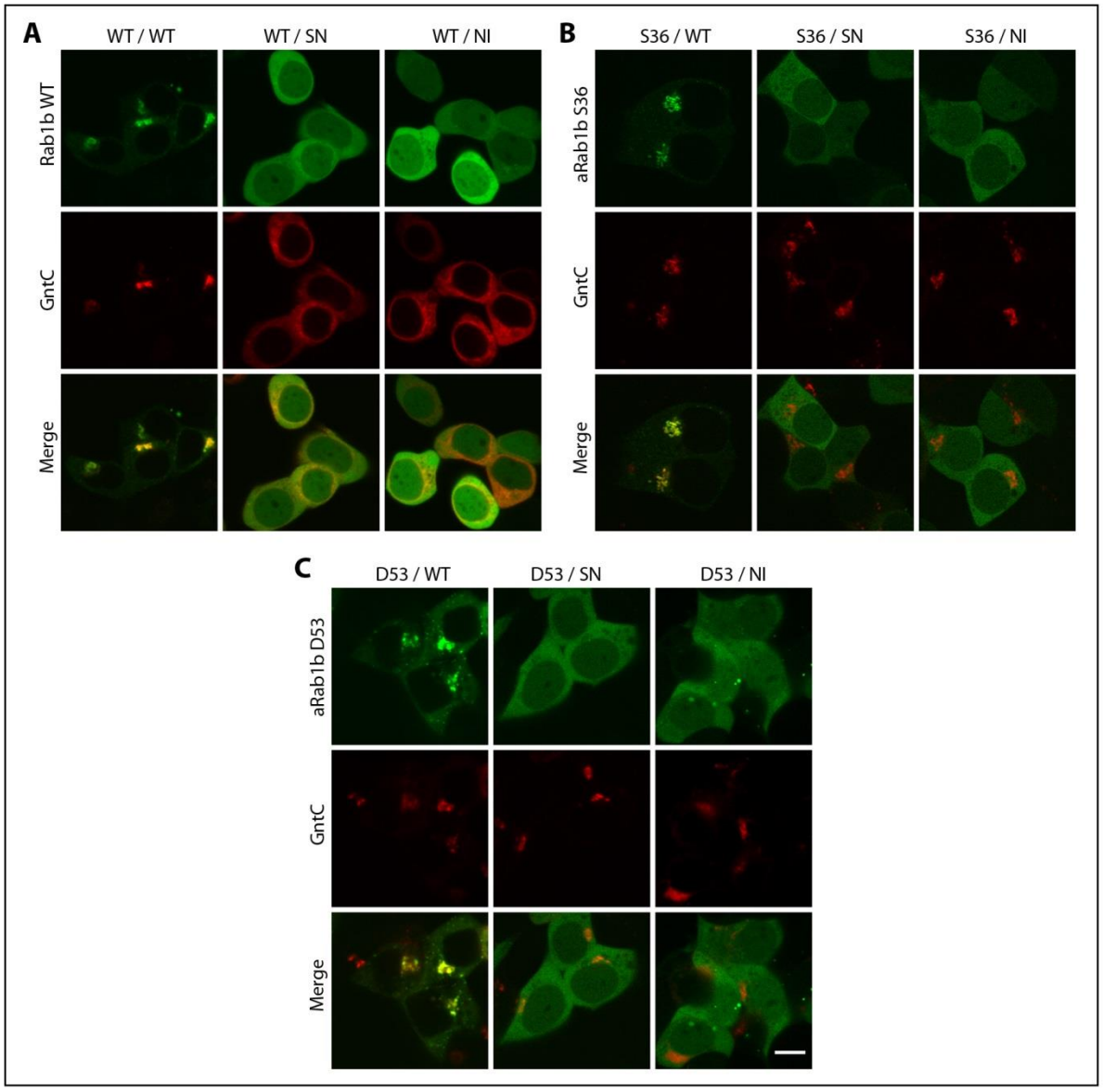

Figure 3.28: Phenotypic screen to identify full-length expressed dominant negative Rab1b amber variants. GntC served as a Golgi marker. The expression of the dominant negative mutants S22N (SN) and N121I (NI) was assessed for Rab1b WT (A), aRab1b S36 (B) and aRab1b D53 (C). Scale bar: 10 µm.

An alternative strategy to determine the lifetime of the predominantly GDP-loaded sensor is the deletion of the C-terminal double cysteine motif of Rab1b (CΔ2), which prevents its prenylation and thereby the membrane association of the sensor. Consequently, the construct remains cytosolic and does not underlie regulation by GEF proteins [30]. Figure 3.29 A illustrates HEK 293T cells expressing aRab1b S36 and the truncated protein S36/CΔ2 before and after labeling with TMR.

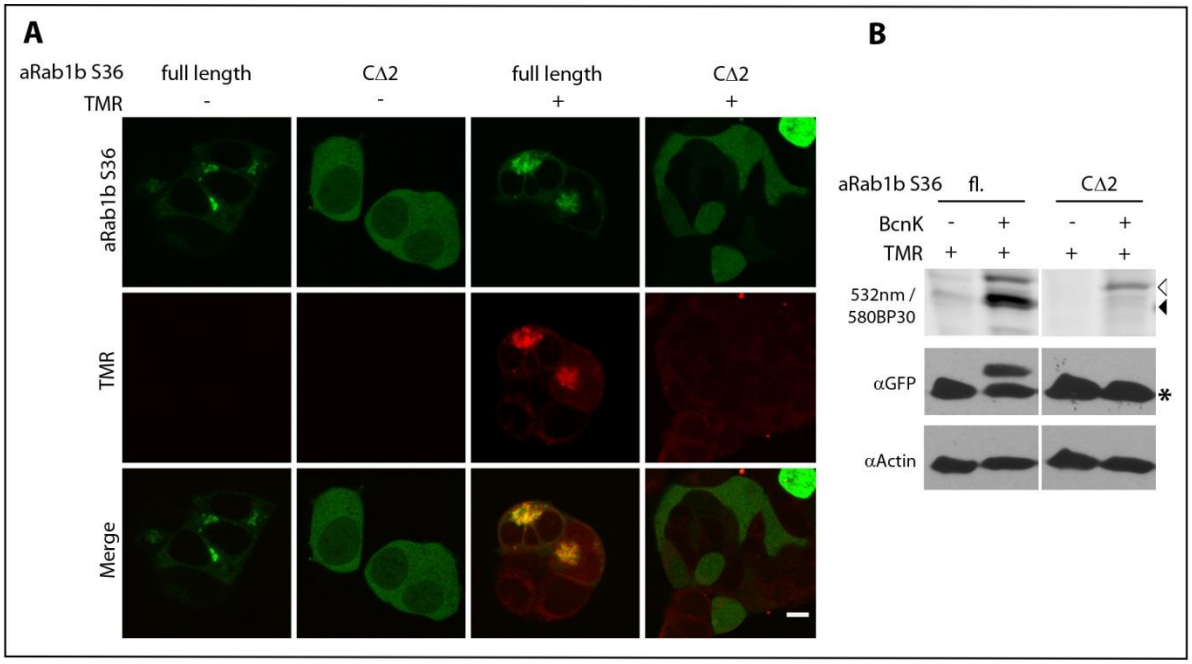

Figure 3.29: UAA incorporation and labeling of full-length and C-terminal truncated aRab1b S36 (CΔ2). A) TMR-labeled and unlabeled HEK 293T cells expressing aRab1b S36 full-length and CΔ2 variant. B) In-gel fluorescence and western blot analysis of aRab1b S36 full-length (fl.) and C-terminal truncated (CΔ2). Fluorescent bands indicating the PylRS and aRab1b are marked with white and black arrow heads, respectively. The asterisk indicates an unspecific band. Scale bar: 10 µm.

As expected, the C-terminal deletion prevented the Golgi localization of the construct and resulted in an even cytosolic and partially nuclear distribution of the sensor. aRab1b S36 displayed clearly visible TMR-labeling, whereas no labeling was detectable for the CΔ2 mutant. In fact, the labeling step seemed to affect the localization of the truncated construct (Figure 3.29 A). While unlabeled cells displayed clear fluorescence intensity differences between nucleus and cytosol, cells transfected under the same conditions, but labeled with TMR, revealed even fluorescence throughout the cell lumen and nucleus. Furthermore, in-gel fluorescence and western blot analysis demonstrated a lack of full-length expression and specific labeling of the truncated protein S36/CΔ2 (Figure 3.29 B). Similar to the inactive mutants, this lack of full-length expression may be due to failure in BcnK incorporation. Another possibility is that the labeling step may affect the fate of the amber protein, e.g. causing rapid degradation of the construct.

In conclusion these results demonstrate that the sensor's 'OFF' state was not assessable by coexpression of TBC1D20 Rab1b GAP, utilizing inactive Rab1b mutants or C-terminal truncation. Furthermore, the findings show that introduction of mutation sites into an amber protein may affect stop codon suppression or the proteins fate, potentially resulting in reduction or complete degradation of the construct. On the other hand,

interfering with the protein function, e.g. by coexpression of regulatory proteins, may cause deficiencies in the labeling reaction.

3.2.1.5 Monitoring Rab1b vesicular transport by reversible cryo-arrest

Since Rab1b is involved in ER-to-Golgi membrane trafficking, the conformational Rab1b sensor was investigated in vesicular transport. Initial UAA incorporation experiments already showed that amber suppressed and labeled Rab1b participated in vesicular transport by formation of vesicles comparably to the wild type protein. These vesicles were traceable by confocal microscopy, but determination of the lifetimes of single vesicle was hindered by the comparably long acquisition periods during fluorescence lifetime imaging and the relatively fast vesicle movement. Therefore a new strategy, the reversible cryo-arrest of live cells, was applied to lock live cells in a temporary state by freezing, allowing for even prolonged measurements without biological interferences in the sample during acquisition [235].

The Rab1b sensor participates in vesicular transport

First, labeled aRab1b S36 was monitored before and after freezing by fluorescence microscopy to confirm that the fluorescence emission of TMR is not affected by the change in temperature or the drastic increase in DMSO concentration during freezing (Figure 3.30). Cryo-arrest of the samples at -45 °C revealed a large number of Rab1b-positive vesicles which were not visible at 37 °C, but clearly distinguishable from the cytosolic fraction after freezing. Rab1b is known to participate in ER-to-Golgi transport, mediating vesicle tethering and fusion of COP-coated vesicles [59]. These vesicles exhibit a rapid traveling speed under physiological conditions, impairing their detection by common fluorescence lifetime microscopy in live cells.

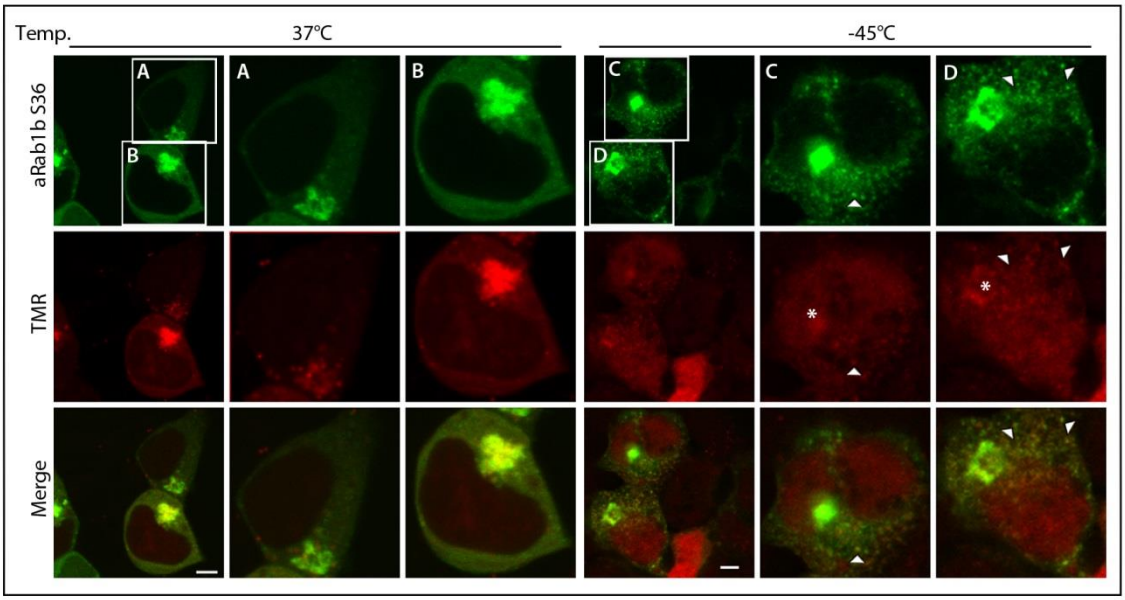

Figure 3.30: Monitoring Rab1b vesicular transport by reversible cryo-arrest. Confocal microscopy images and close-ups of HEK 293T cells expressing TMR-labeled Rab1b S36 at 37 °C and -45 °C. Arrow heads indicate labeled Rab1b vesicles; labeling of the Golgi apparatus is indicated by asterisks. Scale bars: 5 µm.

Despite the low temperatures and the increased DMSO concentration during cryo-arrest, TMR remained fluorescent. However, TMR fluorescence signals showed a diffuse pattern throughout the cell post-freezing, lowering the signal-to-noise ratio in comparison to 37 °C. These TMR background signals may be caused by an excess of dye that was solubilized by the increase in DMSO concentration during freezing. Nevertheless, specific labeling of the Golgi apparatus, as well as labeling of single vesicles was detectable against the background fluorescence. Thus, the amber suppressed and labeled Rab1b protein indeed seems to function in vesicular trafficking.

Rab1b sensor read-out pre- and post-freezing

Precise determination of the fluorescent lifetime of subcellular Rab1b sensor fractions during cryo-arrest was impaired by movement of the sample during fluorescence lifetime image acquisition. Mechanic improvements of the cryo-arrest set up did neither solve nor improve this issue. Therefore the acquired lifetime data was *in silico* corrected by XY-alignment of the fluorescence intensity frames and application of the correction vectors onto the respective fluorescence lifetime frame set, before fitting of the average lifetime per pixel. This correction method provided sharp fluorescence intensity and lifetime images which displayed single Rab1b vesicles and well defined Golgi structures after freezing (Figure 3.31 A). mCitrine fluorescence lifetime analysis of whole cells, Golgi and cytoplasmic segments of the Rab1b sensor pre- and post- freezing revealed the previously described

lifetime distribution between the three segments (Figure 3.31 B and C). The fluorescence lifetime of the Rab1b sensor was comparable at 37 °C and -45 °C ($\Delta\tau_{-45\,°C\,(Gol\text{-}Cyt)}$ = 260 ps and $\Delta\tau_{37\,°C\,(Gol\text{-}Cyt)}$ = 280 ps). In contrast, Rab1b WT expressing cells displayed lifetime differences between the Golgi region and the cytosol before and after freezing ($\Delta\tau_{Gol\,(-45\,°C\text{-}37\,°C)}$ = -140 ps and $\Delta\tau_{Cyt\,(-45\,°C\,–\,37\,°C)}$ = 60 ps).

These data demonstrate that TMR was not only fluorescent at -45 °C and in the presence of 50 % DMSO, but also functioned as a FRET acceptor. Moreover, the fluorescence lifetime analysis indicated comparable FRET efficiency between mCitrine and TMR before and after freezing. In fact, plotting of the lifetime of Golgi-bound Rab1b against the lifetime of the cytoplasmic fraction of the respective cell revealed no differences in the Golgi/Cytoplasm ratio of the Rab1b sensor at the two different temperatures (Figure 3.31 D). Interestingly, mCitrine and TMR fluorescence was massively increased at -45 °C in comparison to 37 °C. The acquisition of fluorescence lifetime images required about 100-fold less laser power to achieve the same photon count rate at -45 °C in comparison to 37 °C (data not shown).

Figure 3.31: Determination of Rab1b sensor lifetimes on single vesicles by reversible cryo-arrest. A) Intensity image of a HEK 293T cell expressing the Rab1b sensor illustrating sample movement during fluorescence lifetime image acquisition during cryo-arrest at -45 °C. Arrow heads mark single vesicles which are blurred before and well defined after the *in silico* correction. B) HEK 293T cells expressing the Rab1b sensor at 37 °C and at -45 °C. C) Segmented single cell fluorescence lifetime analysis of Rab1b sensor and Rab1b WT at 37 °C and at -45 °C. D) Ratio and linear fitting of the Golgi and cytoplasmic lifetimes of single cells expressing Rab1b sensor or WT protein at 37 °C and -45 °C. Scale bars: 5 µm.

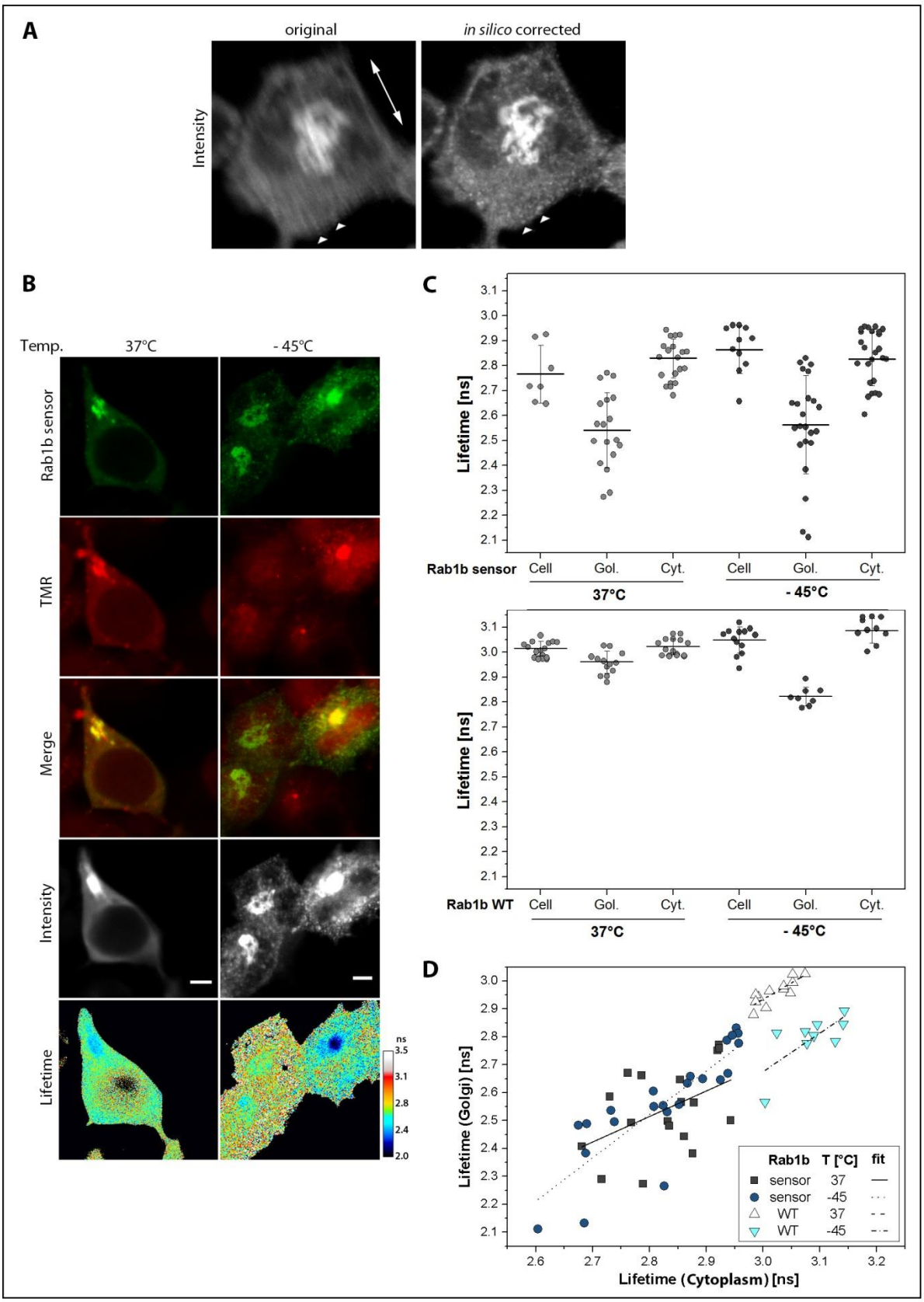
A
original
in silico corrected
Intensity
B
Temp.
37°C
- 45°C
Rab1b sensor
TMR
Merge
Intensity
Lifetime
ns
3.5
3.1
2.8
2.4
2.0
C
Lifetime [ns]
Rab1b sensor
Cell
Gol.
Cyt.
37°C
- 45°C
Rab1b WT
D
Lifetime (Golgi) [ns]
Lifetime (Cytoplasm) [ns]
Rab1b
T [°C]
fit
sensor
37
-45
WT

Lifetime analysis of single Rab1b vesicles

To determine the sensor signal on single vesicles Rab1b intensity images were masked on local intensity maxima representing the observed vesicle structures. The binary mask was transferred onto the respective XY-corrected lifetime image and mean lifetime values were calculated for each vesicle (Figure 3.32 A). mCitrine lifetime analysis of the extracted Rab1b vesicles revealed a broad range of mean fluorescence lifetimes for the Rab1b sensor on vesicles in different cells ($\tau_{Ves.\,(Sensor)}$ = 2.54 - 2.71 ns). Despite the difference in average, the lifetime distribution of mean vesicle values correlated with the lifetime of the Golgi region and the cytoplasm within the same cell (Figure 3.32 B). Moreover, the four analyzed Rab1b sensor expressing cells showed a similar range of single vesicle mean lifetimes, which was comparable to that observed for Rab1b WT vesicles. (σ_τ = 0.12 - 0.17 ns, Figure 3.32 B). Nevertheless, the mean vesicle lifetimes of vesicle-bound Rab1b sensor were significantly different from Rab1b WT vesicles (Figure 3.32 C).

In summary, these results demonstrate that the genetically encoded Rab1b conformational sensor participates in the vesicular trafficking, allowing for the detection of single Rab1b vesicle lifetimes. A range of mean vesicle values was observed in different cells expressing the Rab1b sensor. This range was comparable within different samples and similar to the lifetimes observed for Rab1b WT vesicles, but single vesicle lifetimes of the Rab1b sensor differed significantly. However, further investigation is required to correlate the detected signals with the spatiotemporal Rab1b activity. One possibility may be the coexpression of the Golgi-localized tether protein p115, which is a Rab1b effector. Colocalization of p115 and Rab1b sensor on vesicles may enable the determination of the effector bound sensor fraction. Another possibility is the identification of ER exit sites (ERES), highly specialized ER areas from where COPII vesicles are budding [270,271]. Rab1b is known to localize to ERES, regulating cargo sorting and targeting the budded vesicles to the Golgi complex, where is subsequently functions in tethering and fusion of the vesicles [62-65]. As it is not clearly known at which distinct point during ER-to-Golgi trafficking Rab1b becomes activated, the conformational sensor could give further insights into the mechanism of ER-to-Golgi vesicular transport.

Figure 3.32: Extraction of the Rab1b sensor lifetime on single vesicles in live cells. A) Identification of vesicles by intensity based binary masking of the lifetime image. The identified vesicles were extracted and a mean lifetime value was determined for each vesicle. B) Lifetime histograms of measured vesicles in different cells expressing Rab1b sensor or Rab1b WT control. The black line and the dashed line mark the average lifetime of the cytoplasm and the Golgi region of the corresponding cell, respectively. C) Mean vesicle lifetime values for one cell expressing Rab1b WT and four cells expressing the Rab1b sensor. All Rab1b sensor vesicle populations were significantly different from the WT vesicle population ($p < 6.0 \times 10^{-14}$). Scale bars: 5 µm.

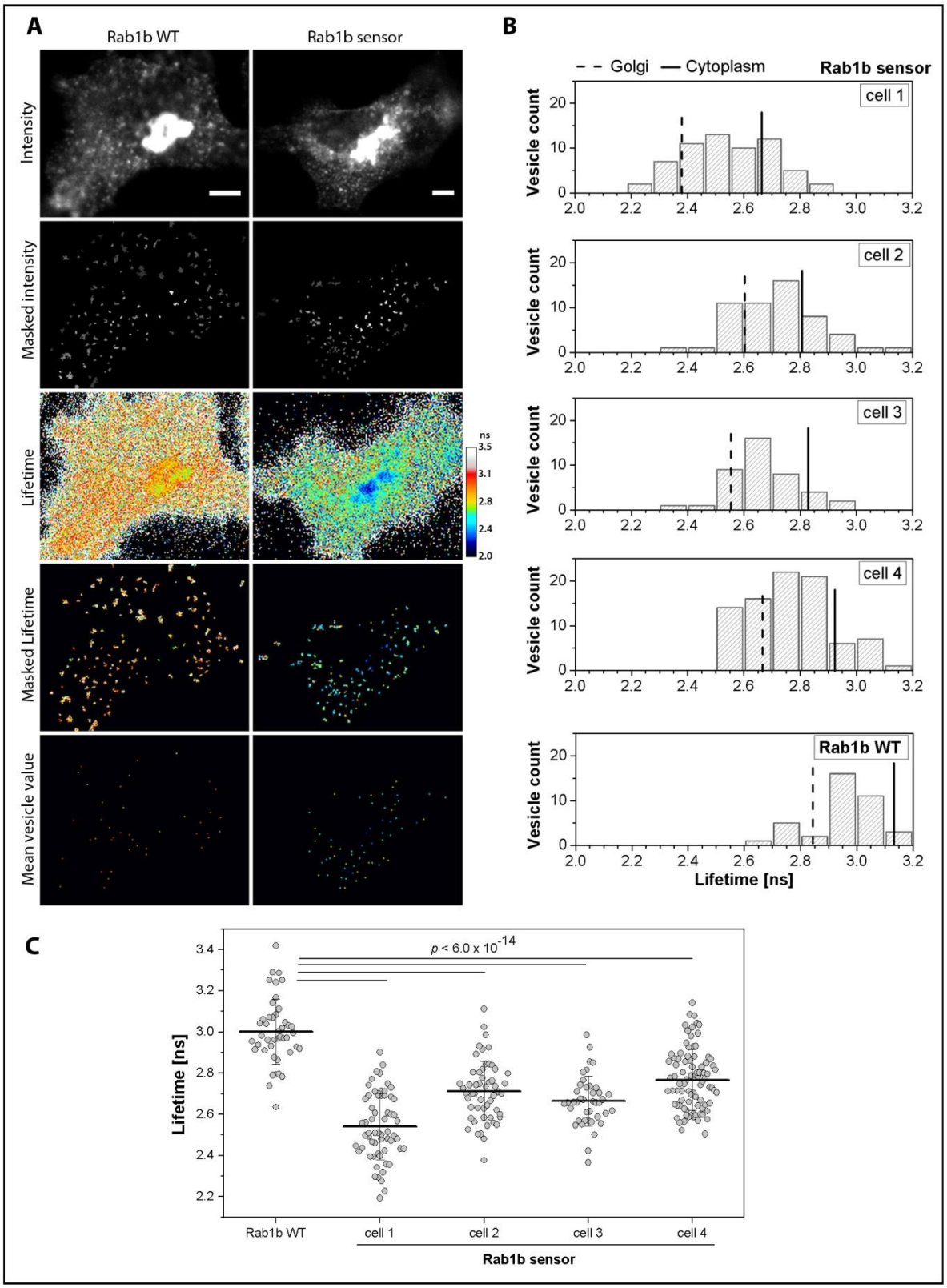
A
Rab1b WT
Rab1b sensor
Intensity
Masked intensity
Lifetime
Masked Lifetime
Mean vesicle value
ns
3.5
3.1
2.8
2.4
2.0
B
Golgi
Cytoplasm
Rab1b sensor
cell 1
cell 2
cell 3
cell 4
Rab1b WT
Vesicle count
Lifetime [ns]
C
p < 6.0 x 10-14
Lifetime [ns]
Rab1b WT
cell 1
cell 2
cell 3
cell 4
Rab1b sensor

3.2.2 Rheb Conformational Sensor

In parallel to the characterization of the conformational Rab1b sensor, preliminary experiments were performed to assess whether the TMR-labeled aRheb N50 protein also functions as a Rheb sensor. To this end, HEK 293T cells expressing aRheb N50 were serum-starved overnight to induce inactivation of the lysosomal Rheb fraction. Cells were labeled in serum-free medium, washed intensively and screened for specific TMR labeling. In fact, few cells displayed TMR signals above background levels and the fluorescence intensity correlated only partially with the localization and abundance of aRheb N50. Fluorescence lifetime analysis of those cells revealed a lifetime decrease of $\Delta\tau$ = 270 ps in comparison to the Rheb WT control sample. These cells were analyzed first in starved condition, then treated with insulin and analyzed again 15 minutes post-treatment (Figure 3.33). Insulin stimulation activates the PI3K/AKT signaling pathway and results in a rapid and enduring activation of the lysosomal Rheb fraction[124].

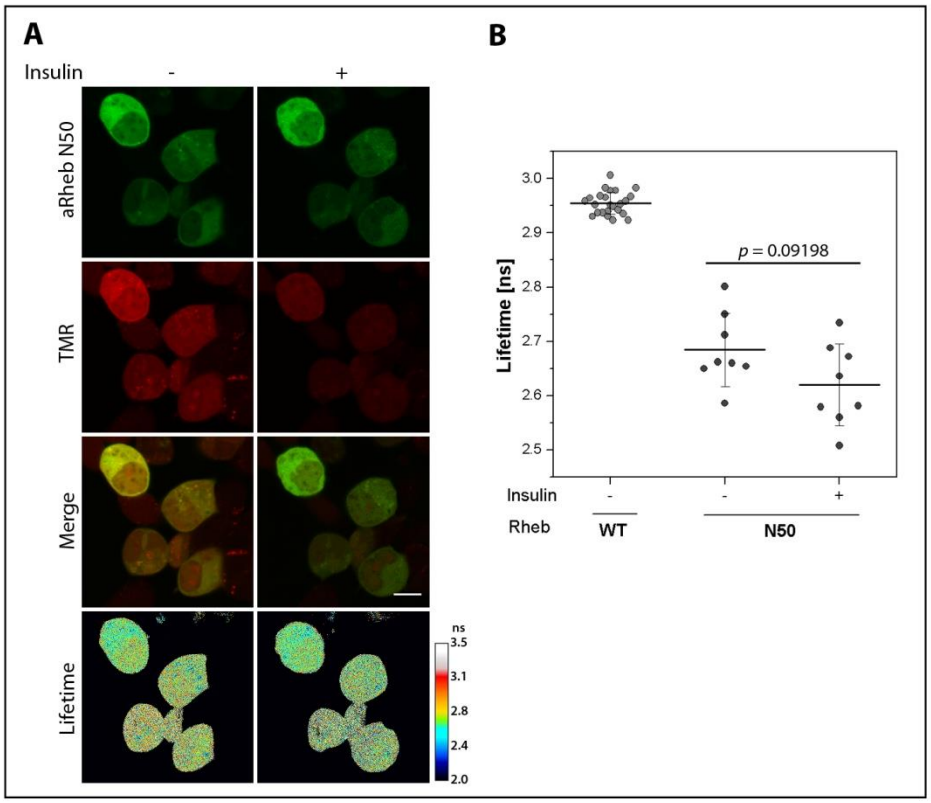

Figure 3.33: Insulin stimulation of HEK 293T cells expressing the Rheb sensor. A) HEK 293T cells were serum-starved overnight (> 16 h) and the same cells were analyzed before and after treatment with insulin. B) Single cell lifetime analysis of A). Scale bar: 10 µm.

mCitrine lifetime analysis revealed an average change of lifetime of $\Delta\tau$ = -65 ps following insulin stimulation, indicating a response of the sensor signal to the activation of the signaling pathway. Positioning of the acceptor in the interswitch region of aRheb is expected to report protein activation as a decrease in sensor lifetime, which is in agreement with these findings. Thus, these preliminary data showed that the labeled amber Rheb construct indeed reports Rheb activity upon stimulation with insulin. However, further investigation is required to confirm that the observed alteration of fluorescence lifetime of the Rheb sensor is indeed due to the insulin-induced activation.

4. Discussion and Perspectives

4.1 UAA incorporation into small GTPases

This study demonstrates the successful and specific UAA incorporation into Rab1b and Rheb GTPases. Both proteins were subsequently labeled specifically in live mammalian cells and the labeled constructs allowed for spatiotemporal detection of the protein activity. The observed UAA incorporation was fully orthogonal, despite the frequent abundance of amber stop codons within eukaryotic cells. Six different incorporation sites of Rab1b tolerated the UAA incorporation and yielded functional proteins. In contrast, UAA incorporation and full-length expression was achieved for only one of the five mutation sites of Rheb GTPase. The expression yields of the amber mutants of both GTPases were rather low, maximum 12-20 % of the respective wild type protein (Chapters 3.1.1.4 and 3.1.1.5). Low protein expression is a major pitfall of the stop codon suppression approach and has been subject to various studies [239,272-274]. The limited expression is largely due to two reasons, (1) the availability of the orthogonal $tRNA_{CUA}$ (PylT) and (2) the competition between the UAA incorporation event and the termination of the translation process at the ribosome [273-275]. The first possibility has been successfully addressed by amplification of the PylT expression cassette and optimizations of the promoter region [180,198]. In contrast, the competition between the UAA incorporation and the translational termination remained more challenging. If the translation machinery reaches a stop codon, the ribosome pauses, a release factor enters the ribosome and releases the translated peptide by separation of the two ribosomal subunits [164]. In the presence of an orthogonal pair, the orthogonal tRNA can enter the ribosome, allowing for the incorporation of the UAA in response to a stop codon [171]. Nevertheless, the endogenous release factor-mediated termination process can still operate and thereby competes with the orthogonal UAA incorporation process. Depending on the efficiency of each process, the amber protein is expressed as a mixture of fragment (translational termination) and full-length protein (UAA incorporation). In prokaryotes the termination process is mediated by the release factors 1 and 2 (RF1/RF2), which selectively terminate translation in response to UAG/UAA and UGA/UAA stop codons, respectively [162,163]. Several studies successfully augmented the UAA incorporation efficiency in bacteria by disruption of RF1 function [162,238,239,272,273,276,277]. In contrast, translational termination in eukaryotic cells is more complex, involving the eukaryotic release factors 1 and 3 (eRF1/eRF3)[164-166]. eRF1, an orthologue of the two prokaryotic release factors, recognizes all three stop codons. While eRF1 is the key protein in the translation termination process, eRF3 possesses only a stimulatory role [164-167]. A recent study targeted

eRF1 function to enhance UAA incorporation process, while maintaining low read-through of opal and ochre stop codons [180]. The resulting engineered eRF1 allowed for 17-20-fold higher expression levels of UAA containing proteins using the PylRS/PylT amber suppression system in mammalian cells. Besides the significantly higher yields, which were comparable to the respective natural translation controls, the engineered eRF1 also enabled efficient multiple stop codon suppression within the same protein [180].

Furthermore, the incorporation efficiency has been shown to depend on the local sequence context of the amber codon in bacteria [274,278]. Pott *et al*. investigated the effects of two random codons, one upstream and one downstream of the amber codon, on the incorporation efficiency and found a strong preference of the UAA incorporation efficiency on the local sequence context [274]. Moreover, the dependency on the local sequence context was versatile between different proteins and allowed for expression yields of 70-110 % of the respective natural translation control [274]. In fact, the local sequence context seems to also affect the endogenous termination of the translation in yeast and human [164,279,280]. Studies identified the nucleotide immediate downstream of the stop codon, at +1 position, as a key factor for the translation termination efficiency. Thereby the stop codon partially holds characteristics of a quadruplet codon, where the fourth base determines the efficiency of a process [164,279,280]. Thus, a dependency of the UAA incorporation process on the local sequence context is also like to exist in mammalian cells.

Another relatively new approach to enhance the UAA incorporation is the construction of orthogonal ribosomes that do not function with eRF1 [273,275]. This engineered ribosome selectively binds modified mRNA encoding amber proteins and also allowed for utilizing quadruplet codons, enabling encoding of multiple different UAA within one protein [253,275].

However, most of these approaches were developed in parallel to the work presented in this thesis and therefore were not assessed here. Further investigations will show whether these strategies may also improve UAA incorporation into small GTPases, especially in the case of Rheb GTPase.

4.2 Intracellular labeling of small GTPases

Following the UAA incorporation into the small GTPases Rab1b and Rheb, both proteins were subsequently labeled intracellularly in live cells. Highly specific and covalent labeling was confirmed for the full-length expressed amber Rheb mutant, as well as for four amber Rab1b mutants. The intracellular labeling reaction with different fluorophores and the effects of the protein labeling on its function and on the cell health were intensively characterized in this work, providing vast insights into major pitfalls and challenges of the

approach. Among those are the findings that intracellular labeling depends not only on the target protein and the choice of dye, but also on the cell line and potentially the protein's activity state. Intracellular labeling of Rab1b was highly specific, bioorthogonal and resulted in up to 90 % reaction yield (Chapter 3.1.3.4). These observed high yields of the labeling reaction opposes the previous assumption that utilizing the PylRS AF/PylT orthogonal pair in the absence of the engineered eRF1 allows only for 'sparse labeling' of intracellular proteins [181]. Nikic *et al.* have reported the specific labeling of an extracellular loop region of IGFR using the PylRS AF/PylT pair to incorporate strained alkynes and alkenes [178,281]. The extracellular labeling was performed using 1.5 µM tetrazine-functionalized dye for 10 min at 37 °C, a much shorter incubation time than required for efficient intracellular labeling of aRab1b observed during this study. Nevertheless, the 3-fold higher dye concentration may accelerate the reaction sufficiently to compensate for the short labeling period. Moreover, labeling of extracellular proteins does not require the dye to enter the cell lumen, a process which may decrease the efficient dye concentration due to potential hydrophobic interactions with endomembranes. Uttamapinant *et al*. have recently demonstrated highly specific labeling of several intracellular proteins using BcnK and TcoK* incorporation in HEK 293T and COS-7 cells [181]. In that study, intracellular labeling was performed using 0.4 µM tetrazine-FDAC and 20 min incubation time, which is comparable to the labeling conditions initially used in this work. Nevertheless, complete labeling of aRab1b required more than 30 min in presence of 0.5 µM dye, as monitored for the labeling reaction over time by fluorescence lifetime imaging (Chapter 3.1.3.3). One possible explanation for the prolonged labeling time might be the high expression levels of the amber protein [281]. However, the highest expressing amber Rab1b mutant, aRab1b S36, was expressed only about 20 % of the wild type protein (Chapter 3.1.1.4). In contrast, Uttamapinant *et al*. utilized the engineered eRF1 release factor allowing for expression levels of amber proteins comparable to the respective wild type protein [180,181]. Consequently, the expression levels of the two amber proteins used within that study were much higher than expression yields of aRab1b in this work. A second possibility for the prolonged labeling times for intracellular labeling of aRab1b may be the choice of dye. Uttamapinant *et al*. used fluorescein diacetate (FDAC) for intracellular labeling, whereas Rab1b and Rheb amber proteins were labeled with TMR or other red fluorophores. FDAC has been shown to enter the cell rapidly and spread evenly throughout the cell (Chapter 3.1.2.1). Cell permeability of TMR was comparably fast, but TMR distributed exclusively within the cytosol and exhibited a partially membranous localization pattern within the cell, suggesting unspecific membrane association of the dye. In addition to cell permeability, the unspecific accumulation of dyes in the endomembrane system has been a limiting factor for intracellular labeling approaches [178,281]. In order to be highly cell permeable, fluorescent probes require a certain hydrophobicity, which in turn may cause the unspecific membrane binding after cell entry.

Nevertheless, the choice of dye for the establishment of the genetically encoded conformational sensor for small GTPase activity was not only limited by their cell permeability and suitability for intracellular labeling, but also to the demand to serve as a FRET acceptor for a fluorescent protein.

It has to be noted that the observed high labeling yields of Rab1b may be partially due to its intrinsic cycling between membrane-associated and membrane-independent state. In fact, Rab1b is not only targeted to one compartment, but localized to the Golgi apparatus, to ERES and to COP-coated vesicles during vesicular transport (Chapter 3.1.3.4). Thus, the presence of aRab1b at different membrane systems may enhance the labeling reaction by promoting the encounter between amber protein and tetrazine-dye. Linked to the change in localization, Rab1b also cycles between the active and inactive state, enabling interaction with effectors and other proteins. The rapid nature of this cycle may allow for the observed high efficiency of the labeling reaction, as not only one conformational state of the protein is exposed to the dye. In addition, interactions of Rab1b with other proteins may be limited to the time frame a vesicle requires from budding to tethering and may thereby not affect the labeling reaction e.g. by sterical hindrance. In contrast, Rheb is a less flexible GTPase concerning cycling and subcellular localization under normal growth conditions. Rheb resides on a number of endomembranes including the ER, Golgi, Mitochondria, peroxisomes and lysosomes [101,106,108,111,113,251,252]. The lysosome-located Rheb fraction was intensively investigated in the last decades due to its role as an activator of the mTOR complex 1 in nutrient sensing (reviewed in [282]). In presence of amino acids and growth factors, the lysosomal Rheb fraction is thought to be GTP-bound, allowing activation of mTORC1 [113,124,125]. The absence of amino acids causes a RagGTPase-mediated recruitment of the TSC complex, the Rheb GAP, to the lysosomal surface [119-123]. The TSC complex consists of TSC1, TSC2 and TBC1D7 and is also regulated by the growth factor-dependent PI3K-AKT pathway [113,120,124,283]. In order to avoid sterical hindrance of the labeling reaction by continuous interaction of Rheb and mTORC1 on the lysosomal surface, intracellular labeling was performed in serum-starved condition (Chapter 3.1.4), causing Rheb dissociation from the lysosomes [124,125]. However, the effects of the localization of Rheb and its nucleotide state on the labeling reaction were not further investigated.

While intracellular labeling of Rab1b was highly specific and did not yield any visible side reactions, aRheb expressing cells labeled with TMR displayed high TMR fluorescence intensities in the nucleus (Chapter 3.1.4). Side reactions of the intracellular labeling in the nucleus are a well-known issue that has been successfully addressed by fusion of the PylRS AF to a nuclear export signal (NES) [218]. In addition to lower PylRS AF accumulation in the nucleus, the NES modification also increased the UAA incorporation rate significantly [218]. Although the yields of intracellular labeling of aRheb were not determined, the change in mCitrine fluorescence lifetime upon incubation of aRheb with TMR was comparable to

intracellular labeling of aRab1b, indicating similar reaction yields ($\Delta\tau$ = 300 – 400 ps, Chapter 3.1.4). However, unlike aRab1b, aRheb labeling was highly heterogeneous and only a small fraction of aRheb expressing cells displayed the large lifetime changes indicating complete labeling. These cells also exhibited perinuclear fluorescence densities, suggesting successful BcnK incorporation and proper localization of the construct. Nevertheless, the localization pattern of aRheb was not as clearly defined as observed for the wild type protein, suggesting low UAA incorporation rate.

In conclusion, our data, together with the few previously reported cases of UAA-based labeling of intracellular proteins, leads to a better understanding of the major pitfalls and challenges of this approach. Vast insights into the effects of diverse parameters on the intracellular fluorescence labeling were achieved, including a screen for potential fluorophores for intracellular labeling, labeling of different target proteins and in different cell lines. Moreover, the intracellular labeling reaction was time-resolved monitored by fluorescence lifetime imaging, demonstrating that the reaction is not only time but also highly dose-dependent. Labeling and microscopic analysis were performed in live cells and cells expressing TMR-labeled aRab1b or aRheb have been shown to remain viable and healthy even over longer time periods (Chapter 3.2.1.3).

4.3 Characterization of the genetically encoded Rab1b sensor

Following successful establishment of the UAA incorporation and labeling protocol for small GTPases, functionality of the Rab1b sensor was confirmed by effector binding studies. Moreover, the sensor's dynamic range was investigated by coexpression of regulatory enzymes, nucleotide state affecting mutants and deletion of the C-terminal prenylation motif.

Previous studies showed that introduction of the acceptor at position S36 in Rab1b yields a probe reporting predominantly effector binding both *in vitro* and *in vivo* [160,161]. In fact, coexpression of the Rab binding domain of the Rab1 effector protein OCRL1 resulted in a significant change of sensor lifetime. The observed lifetime increase in presence of OCRL (~ 5 %) demonstrates that the labeled Rab1b protein reports effector binding events in a comparable manner to the recombinant probe [160,161]. Despite the intracellular labeling step, which did not yield 100 % labeled protein (Chapter 3.1.3.4), the dynamic range of the genetically Rab1b sensor was similar to the recombinant conformational sensor (~ 5 % and ~ 6 % signal change, respectively) [160,161]. Incomplete labeling may leave a distinct fraction of aRab1b construct unlabeled, increasing the donor only fraction in fluorescence lifetime

imaging and thereby the samples average lifetime. Depending on the size of the donor only fraction, the sensor's dynamic range could be narrowed.

Although the observed change in signal in presence of OCRL was stable and reproducible, it remains unclear whether the change in FRET is due to conformational changes within the small GTPase or due to binding of the effector. The preceded study establishing the recombinant, first generation of COSGA sensors found, that probes with acceptors introduced at position S36, D53 and G54, but not at T34, report effector binding in the same manner. Thus, a common sensing mechanism for effector binding is likely. One possibility is that effector binding limits the space available for the N-terminal fluorophore. This notion is supported by the observation, that larger effectors caused a larger change in sensor signal, but does not explain why the FRET signal of the T34 probe is not altered by effector binding [160,161].

While OCRL coexpression did not affect the specific labeling of aRab1b, coexpression of the Rab1 GEF protein DrrA impaired the labeling reaction massively. Presence of the catalytic Rab1 GEF domain of DrrA caused Rab1b to localize predominantly in the cytosol and partially in the nucleus. This phenotype was similar for Rab1b sensor and wild type protein, but no specific labeling of aRab1b was detectable (Figure 3.24 A). In the same sample cells expressing aRab1b but not DrrA displayed strong and specific TMR-labeling, suggesting the presence of DrrA as cause for the impaired labeling reaction. In fact, TMR fluorescence intensity (indicating specific labeling) correlated with TagBFP fluorescence intensity (indicating DrrA expression levels), revealing a direct dependency of the two parameters (Figure 3.24 C). This correlation raises the possibility, that the incorporated UAA may not be accessible for labeling due to interaction of aRab1b and DrrA. In fact, the incorporation site S36 is located in the switch I region, one of three regions involved in the interaction interface of Rab1 and DrrA [126,284]. Nevertheless, the interaction of small GTPases with their cognate GEF proteins is rather transient and generally terminated by the nucleotide exchange of GDP to GTP. Thereby the interaction should not affect specific labeling of aRab1b. On the other hand, although both proteins are exogenously overexpressed, aRab1b is most likely less abundant due to the amber suppression approach. Thus, the bulk of DrrA protein might shift the equilibrium towards complex formation, reducing the availability of free aRab1b for the labeling reaction. To circumvent this, DrrA mutants with lowered GEF activity could be used. These mutants show reduced complex formation with Rab1b which may enable aRab1b to become labeled [126]. Another approach may be to incorporate BcnK at position D53 in Rab1b instead of S36. In contrast to S36, D53 is not involved in the interaction interface with DrrA and should hence be accessible for labeling [126].

Coexpression of the Rab1 GAP TBC1D20 revealed a similar lack of aRab1b labeling, but the phenotype differed from DrrA coexpression (Figure 3.25). While aRab1b/DrrA expressing cells displayed high mCitrine fluorescence intensities, aRab1b and TBC1D20 positive cells exhibited only faint fluorescence, indicating low levels of mCitrine-aRab1b fusion protein. Due to the competition of translational termination and incorporation event, the population of amber protein can be divided into two fractions. The first fraction, and in case of aRab1b the major fraction, is the amber protein expressed in full-length. The second fraction is the non-amber suppressed mCitrine-aRab1b fragment. The observed mCitrine fluorescence comprises both fractions, but since full-length expressed aRab1b is the major fraction, its abundance may proportionally constitute for the fluorescence intensity. Hypothetically, if the amber protein expressed in full length and as a fragment are degraded differentially, mCitrine fluorescence intensity would decrease massively, leaving the mCitrine-aRab1b fragment as the predominant source for fluorescence emission. Moreover, degradation of only full-length aRab1b fraction would eliminate the labeled fraction and, due to reduction of the donor acceptor population, the sample's fluorescence lifetime would be shifted to donor only signal. All three parameters of the above scenario are in agreement with the observations made for aRab1b and TBC1D20 coexpression, suggesting possible degradation of the full-length amber construct (Figure 3.25 C). However, it is striking, that presence of TBC1D20 did not affect fluorescence intensity of mCitrine-Rab1b WT expressing cells, indicating that presence of the GAP does not alter Rab1b WT abundance. This raises the possibility of amber suppression and/or intracellular labeling as cause for degradation of aRab1b. One possibility to dissect whether aRab1b is degraded due to the labeling of the GDP-bound state or due to presence of the GAP could be coexpression of the catalytically inactive mutant TBC1D20 R105A [89-91]. This mutant binds Rab1b, but cannot catalyze nucleotide hydrolysis.

Another approach to coexpress regulatory enzymes while enabling complete labeling of the amber construct may be to utilize an inducible expression system, such as the tetracycline-controlled transcriptional activation [170,172]. In combination with the established protocol for amber suppression and intracellular labeling an inducible system may allow for induction of exogenous GEF or GAP expression post-labeling. Consequently, the amber protein would first be labeled and then be regulated by its cognate enzyme. However, due to the reduction in aRab1b abundance within -labeling and the required additional expression time for the GEF or GAP protein this strategy might be challenging.

As a second strategy to determine the dynamic range of the genetically encoded conformational sensor, three nucleotide mutants of aRab1b were assessed. Amber suppression and fluorescent labeling was successful for the dominant active Q67L (QL)

mutant, whereas both steps failed for the two constitutively inactive aRab1b mutants (Figure 3.26).

The dominant active amber suppressed Rab1b S36 mutant QL was expressed and labeled comparably to the wild type amber protein, allowing comparison of the constructs. In contrast to the inactive Rab1b mutants, the active QL mutant allows for functional ER-to-Golgi transport and does not impair Golgi homeostasis. The segmentation of sensor expressing cells revealed a fluorescence lifetime difference for the sensor QL mutant and the wild type amber protein. Interestingly, the greatest change in sensor signal was detected for the Golgi region, which displayed a significant increase. In contrast, lifetimes of the cytosolic aRab1b fraction and the whole cell lifetime were comparable to the wild type amber protein. The fluorescence lifetime alteration in the Golgi region is in agreement with previous studies reporting that microinjection of an active mutant of the recombinant sensor Rab1b T34C results in elevated sensor lifetime predominantly in the Golgi region [160,161]. However, the preceded studies used the T34C probe, which does not sense effector binding and reports exclusively nucleotide state. In contrast, introduction of the acceptor at position S36 in Rab1b, which was mainly used in this work, reports majorly effector binding events and has only a minor read-out for nucleotide state. In fact, the elevated sensor lifetime of aRab1b S36/QL in the Golgi region ($\Delta\tau_{QL(Golgi)}$ = 170 ps) was similar to the increase observed for coexpression of the Rab1 effector OCRL ($\Delta\tau_{+OCRL(Cell)}$ = 120 ps). It is thus possible, that the detected increase in sensor lifetime is due to binding of endogenous Rab1 effectors, e.g. p115 or Giantin which are localized in the Golgi complex [62,66-68,285]. The Rab1 QL mutant has a lower intrinsic hydrolysis rate and is predominantly GTP-loaded in cells, allowing for interactions with effector proteins[63,248,286].

In contrast to the active aRab1b QL mutant, determining the sensor's 'OFF' state using the constitutively inactive aRab1b mutants S22N (SN) and N121I (NI) was not successful. In-gel fluorescence analysis of cells expressing aRab1b S36/SN and /NI mutants revealed faint bands at the size of full-length expressed aRab1b, but western blot analysis failed to confirm the bands' identity (Figure 3.26 C). Although faint, the detected fluorescent bands hint at low but successful stop codon suppression and specific labeling of both amber constructs. The low intensity of the bands in combination with the faint mCitrine fluorescence of aRab1b S36/SN and /NI expressing cells observed by fluorescence microscopy indicate low abundance of the amber construct. While low abundance of the target constructs may have different reasons, in this case, a degradation of the full-length constructs similar to the observations made for TBC1D20 coexpression, is likely. Differential degradation of the full-length expressed and labeled aRab1b fraction would reduce mCitrine fluorescence intensity, and eliminate the labeled aRab1b fraction. An alternative for the lack of full-length amber protein might be failure of BcnK incorporation into the target proteins. However, the two mutation sites yielding constitutively inactive Rab1b proteins are located

both upstream and downstream of the amber codon. While mutation of S22 to asparagine may affect BcnK incorporation, e.g. by altering the conformation of the partially translated fusion protein, the N121I mutation is translated identically as the wild type protein when reaching the amber codon at position S36. Consequently, differential UAA incorporation might be a possible reason for the lack of aRab1b S36/SN expression, but not for the lack of full-length expressed aRab1b S36/NI, whereas selective protein degradation would affect both constructs. The extended phenotypic screen for full-length expression of inactive mutants of aRab1b S36 and D53 in three different mammalian cell lines demonstrated that this pitfall is independent of the cell line (data not shown).

Interestingly, UAA incorporation was observed for both, SN and NI mutants, in combination with a different linker between aRab1b and the FP. In this setup, the two amber mutants mTuquoise2Δ11-aRab1b S36 and D53 caused Golgi fragmentation when expressed in HeLa cells (data not shown). There are two differences between the above constructs and the constructs described before (Figure 3.26 and Figure 3.28), (1) the type of fluorescent protein (FP) and (2) the linker connecting the FP and aRab1b. The linker used in mTurquoise2-tagged constructs was modified by truncation of the fluorescent protein's flexible C-terminus, resulting in a shorter and less flexible linker that brings the two proteins in closer proximity. Thus, the linker may be less accessible to proteolytic cleavage, potentially preventing degradation of the full-length amber protein. Consequently, these constructs are not only full-length expressed, but can also act as dominant suppressors for Rab1 function, causing Golgi fragmentation. However, it remains unclear whether aRab1b constructs containing C-terminal truncated mCitrine are full-length expressed and TMR-labeled or whether the shortened linker indeed prevents degradation.

The third strategy to determine the sensor's 'OFF' state, the deletion of the C-terminal double cysteine motif of aRab1b, did also not yield a specifically labeled construct (Figure 3.29). In fact, the observed differences in aRab1b localization pre- and post-labeling may indicate a change of protein fate due to the labeling step. Similar to coexpression of TBC1D20 and expression of inactive aRab1b mutants, the full-length amber construct may be degraded while the mCitrine-aRab1b fragment remained in the cell. If this process is due to the labeling reaction, the localization of aRab1b would differ before and after labeling as observed for the CΔ2. This finding, together with the observations made for TBC1D20 coexpression and expression of constitutively inactive aRab1b mutants, raises the possibility that the labeling of the inactive state of aRab1b may cause the construct's degradation. However, further investigations, such as Western blot analysis of aRab1b CΔ2 pre- and post-labeling may confirm whether inactivation of labeled aRab1b or labeling of inactive aRab1b proteins causes degradation. Another possibility might be monitoring the labeling

reaction of aRab1b CΔ2 by confocal and fluorescence lifetime microscopy over time, as previously performed for aRab1b and aRheb labeling.

As an alternative strategy to dissect different Rab1b sensor signals without interfering with its function, Rab1b trafficking was investigated by reversible cryo-arrest approach. Despite the lower temperature and the elevated DMSO concentration during the freezing process, specific labeling of vesicles-bound aRab1b was detected against the background signals. Since Rab1b is known to participate in vesicular transport at the ER-Golgi interface [59-61], these vesicle structures may represent COPII-coated vesicles. However, the vesicle identity was not further determined, but will be targeted by future work, e.g. by immunostaining of COPII coat subunits.

Analysis of the sensor lifetime pre- and post-freezing revealed similar signals for Golgi and cytosolic fraction at 37 °C and -45 °C. Although the fluorescence lifetime of mCitrine-Rab1b WT differed marginally between the two conditions, both signals were comparable for the Rab1b sensor. Interestingly, the Rab1b sensor fraction on vesicles varied in mean vesicle lifetimes between cells, but the vesicle fraction of a single cell correlated with the lifetimes of Golgi region and independent within the same cell. It is thus possible, that the variations of mean vesicle lifetimes between cells are due to differences in sensor expression levels or labeling efficiency. Nevertheless, the mean vesicle lifetimes extracted from Rab1b sensor expressing cells were significantly different to lifetimes of Rab1b WT vesicles. The observed range of mean vesicle lifetimes ($\tau_{vesicles}$ = 2.2 – 2.9 ns) is almost three fold broader than the dynamic range observed for effector binding reported by aRab1b S36 ($\Delta\tau$ = ~170 ps). It may thus be possible, that other, so far unknown factors, affect the sensor's read-out. Moreover, the dramatic changes in temperature and environment may affect the sensor's dynamic range. Further investigations are required to dissect the sensor read-out and to identify e.g. effector bound sensor fractions. Future experiments will include coexpression of the Rab1b effector p115 as well as specific markers for ER exit sites (ERES). p115, the mammalian homologue of the yeast protein Uso1, is a Rab1 effector protein and is thought to mediate COPII vesicle tethering and fusion at the ER-Golgi interface [62]. Cryo-arrest of cell expressing p115 and the Rab1b sensor will allow for identification of the effector bound sensor fraction on vesicles. To confirm versatility of the sensor signal between live cell and cryo-arrest conditions, the OCRL RBD coexpressed with the sensor during cryo-arrest will serve as a control. In addition, identification of ERES, highly specialized ER areas that are responsible for cargo sorting and formation of COPII vesicles, will enable to determine the nucleotide state of Rab1b sensor on budding vesicles. This approach will allow dissecting the role of Rab1b activity during ER-to-Golgi vesicular transport.

4.4 Characterization of the genetically encoded Rheb sensor

In parallel to the characterization of the genetically encoded Rab1b conformational sensor, preliminary experiments were performed to demonstrate whether the labeled aRheb N50 amber protein indeed reports Rheb activity. To this end, cells were serum starvation overnight, labeled and analyzed pre- and post-treatment with insulin. Insulin stimulation activates the PI3K-AKT signaling pathway, resulting in phosphorylation of the TSC complex [113,124,282]. The phosphorylated TSC complex dissociates from the lysosomal surface, allowing Rheb to adopt GTP-bound state and thus to become active by a yet unknown mechanism [113,282]. In fact, insulin stimulation of serum-starved aRheb N50 expressing cells caused a rapid decrease in fluorescence lifetime of specifically labeled cells. The observed lifetime reduction is in agreement with previous results on COSGA sensors that have the acceptor fluorophore introduced in the interswitch region, reporting GTPase activation by a decrease in sensor lifetime. However, it has to be noted that introduction of the FRET acceptor at position D53 in recombinant Rab1b protein, the structural equivalent to aRheb N50, yielded a probe reporting effector binding both *in vitro* and *in vivo* by a significant increase in sensor lifetime ($\Delta\tau$ =~ +10 %) [160,161]. In contrast, GEF-mediated protein activation of Rab1b D53C *in vitro* was reported by a non significant reduction in sensor lifetime ($\Delta\tau$ =~ -3 %). Interestingly, the here observed lifetime decrease of aRheb N50 equals a 3 % change in sensor lifetime and is thus similar to the previously reported sensor signal reporting GEF-mediated activation of the recombinant Rab1b D53C probe. Nevertheless, the Rheb sensor signal was analyzed for the whole cell and not on higher spatial resolution, e.g. only for the perinuclear fraction. Extraction of the lysosomal Rheb fraction may allow for a more precise read-out of Rheb activity in response to growth factor stimulation. Moreover, additional removal of essential amino acids may increase the fraction of inactivated lysosomal Rheb via Rag GTPase signaling and may thereby lead to a larger signal change upon stimulation [113,124,287-289].

Future work will further investigate whether the Rheb conformational probe in fact specifically reports Rheb activation and to which extend effector binding may contribute to the signal. Determining whether the sensor reports binding of effector proteins is quite challenging, due to the lack of known effector proteins for Rheb. Further investigations may involve coexpression of Phospholipase D1 (PLD1), which was proposed as a Rheb effector protein [229]. If PLD1 is indeed a Rheb effector, the Rheb N50 probe should report the binding event by a significant signal change. Furthermore, the sensor signal will be integrated with traditional methods to monitor Rheb-mTORC1 activity such as S6K1 activity and phosphorylation of 4E-BP1. Although the amber mutation site was not reported to affect

Rheb function [98], this approach may also reveal whether the incorporated UAA or the subsequent labeling impairs Rheb function. Moreover, nucleotide mutants, such as the active Rheb Q64L mutant, may enable eliminating the sensor signal's origin [174]. Using mutants which exhibit e.g. an altered nucleotide state or lower sensitivity for GAP activity will influence the sensor read-out and thus, allow eliminating different events which may contribute to the sensor signal. Moreover, engineering of the sensor's CAAX box to generate an exclusively cytosolic sensor, or to redirect the sensor to another compartment, could give further insights into the signal's dependency on the endogenous regulation factors. In addition, transfection and cultivation conditions of aRheb samples may increase BcnK incorporation efficiency. Higher stop codon suppression efficiency in turn elevates intracellular labeling intensity, enlarging the donor-acceptor fraction which may increase the dynamic range of the sensor.

4.5 Conclusion and Perspectives

In conclusion, this study demonstrates the development of a new type of genetically encoded conformational probe for small GTPase activity by amber suppression and intracellular labeling approach. First, the sensors were genetically encoded by amber suppression and intracellular labeling, allowing monitoring of Rab1b effector binding in live cells. In the second part of this work, the sensor principle was applied to the small GTPase Rheb, demonstrating the versatility of this approach. To date this is the first sensor spatiotemporally reporting Rheb activity in live cells.

Comparison of the two genetically encoded conformational sensors presented in this work revealed the impact of a cognate stimulus enabling to directly address the GTPase activity state. Growth factor deprivation and subsequent insulin treatment, a signal leading to activation of the lysosomal Rheb fraction, served as a simple and rapid method to confirm functionality of the Rheb sensor in live cells. In contrast, determining the dynamic range of the conformational Rab1b sensor suffered from a number of pitfalls. Due to its function during vesicular transport, Rab1b activity is hardly addressable by external stimuli. Thus, three different strategies were applied to determine an 'OFF' state signal for the Rab1b sensor, including coexpression of the respective GAP, nucleotide state mutants and deletion of the C-terminal double cysteine motif. Unfortunately, none of these strategies yielded success. Further investigations are required to determine the conformational Rab1b sensor's 'OFF' state. However, interfering with Rab1b function affects Golgi biogenesis massively, causing a dramatic change in cellular physiology. In contrast, identification of the Rab1b sensor's "ON" state using the active QL mutant was successful. In fact, the observed increase in sensor lifetime was predominantly in the Golgi region and was similar to the

sensor read-out obtained for effector coexpression. It is thus possible, that the sensor reports predominantly effector binding events, which would be in agreement with the previous *in vitro* characterization of the respective recombinant probe [160,161].

Although the findings of this study are restricted to the development of the genetically encoded conformational sensor and did not asses Rab1b biology further, the combination of the conformational probe and the novel reversible cryo arrest of living cells allows for precise tracking of Rab1b activity during vesicular transport. The here obtained results will pave the way for elaborate studies allowing dissection of Rab1b activity during ER-to-Golgi transport using the genetically conformational Rab1b sensor.

Unless specifically determined, the activity state of small GTPases is traditionally assumed by colocalization with their cognate GEF and GAP proteins. Although no GEF is known for Rheb yet, this strategy is frequently applied to the lysosomal Rheb fraction, which is supposed to be inactivated if its GAP, the TSC complex, localizes to the lysosomal surface [113,124]. Another indicator for the nucleotide state of the small GTPase could be their cellular localization, being active in membrane-bound state and inactive in cytosolic, GDI-bound state. However, whether these paradigms are ubiquitously applicable to any small GTPase remains elusive. Specific biosensors for small GTPase activity, including the probes developed in this work, enable direct and spatiotemporal detection of the protein's activity state in live cells.

Future experiments will explore the role of Rab1b activity at the ER-Golgi interface using the conformational sensor. Rab1b localizes to different cellular compartments, including the Golgi and COP-coated vesicles at the ER-Golgi interface. Moreover, Rab1b was also found to colocalize with specific ERES markers and seems to play a role in cargo sorting during COPII budding [69,91,290]. In contrast, the known Rab1 GEF and GAP were found to localize to the Golgi complex and the ER, respectively [80,90]. The ER-localized Tre2/Bub2/Cdc16 domain containing protein TBC1D20 has been shown to promote GTP hydrolysis of Rab1b and Rab2a [89,90,93]. While overexpression of TBC1D20 maintained Rab1b in its inactive state, causing a block of ER-to-Golgi transport and Golgi fragmentation [89,91], depletion of TBC1D20 did not affect anterograde transport [90]. It was thus proposed, that an alternative, yet unknown GAP may be responsible for negative Rab1 regulation at the Golgi complex [90]. Moreover, little is known about the Rab1 GEF, the mammalian multi-subunit protein complex Transport Protein Particle (mTRAPP). Three distinct multi-domain TRAPP complexes possessing GEF activity for Ypt1 were found in yeast. Each complex functions in a different trafficking pathway, including anterograde transport and trafficking from the ER to pre autophagosomal structures (PAS) [79,81,82]. In contrast, composition and function of the mammalian TRAPP complex (mTRAPP) remain largely elusive (reviewed in [76]). Based on genetic interaction maps, two mammalian TRAPP complexes, mTRAPP II and III, were

proposed, but no evidence was found for a potential mTRAPP I complex [78]. Localization and knock down studies of specific subunits suggested a role of mTRAPP II in ER-to-Golgi transport, whereas trafficking at the late Golgi is independent of mTRAPP II [80,85]. Moreover, due to the interaction of mTRAPP II and III subunits with COPI and COPII coat components, a role for TRAPP complexes as tethers for vesicle tethering and fusion has been proposed [78,80,84]. Whether the function of mTRAPP complexes in ER-to-Golgi transport is restricted on its function as a Rab1 GEF, or if the complex alone could act as a tether, remains controversial. Thus, both regulatory enzymes of Rab1 are involved in ER-to-Golgi anterograde transport, but their colocalization with Rab1 is not sufficient to explain Rab1 activity in membrane trafficking.

The lysosomal fraction of the small GTPase Rheb has been shown to play a key role in nutrient sensing and mTORC1 activation upon growth factor stimulation. Although in this study insulin treatment was used as a proof of principle to confirm Rheb sensor functionality, it is the first direct evidence of Rheb activation during the growth factor sensing process. Rheb activity was traditionally monitored by indirect read-out of phosphorylation of mTORC1 substrates such as S6K1 or 4E-BP1, because Rheb-mediated mTORC1 activation is nucleotide-state dependent [126-129,173]. Another study utilized fluorescent protein tagged mTORC1 and Rheb to monitor their interaction by fluorescence lifetime analysis [291]. However, in both cases the exact activity state of Rheb remained elusive. Different signaling pathways were proposed for signal integration at the lysosomal surface. Two main signaling axes have evolved, the PI3K-AKT-pathway which acts through TSC complex localization and activity to activate mTORC1 via Rheb, and the RagGTPase mediated TSC recruitment to sense amino acids. However, a plethora of other signals collectively restrict mTORC1 mediated cell growth, such as hypoxia [130,132,292], low energy [137,175] and genotoxic stress [131]. Several stimuli regulate mTORC1 in a TSC-dependent fashion, while other signals, such as energy depletion, have been shown to act directly on Rheb by phosphorylation of Rheb S130 [137]. Thus, Rheb is indispensible for mTORC1 activation by virtually all stimuli, although the exact mechanism remains unclear.

In addition to mTORC1-dependent function, Rheb was reported to play regulatory roles in mTORC1-independent fashion. Rheb were found to bind GAPDH and that interaction is depending on the enzyme's substrate abundance [139,140]. Interestingly, the interaction of Rheb and GAPDH was not altered by the nucleotide state and did not depend on TSC activity. This study suggested a mechanism by which GAPDH sequesters Rheb away from mTORC1 under low glucose conditions, whereas glucose-rich conditions disrupted Rheb-GAPDH interaction, allowing for Rheb-mediated mTORC1 activation and eventually cell growth. A similar substrate-dependent binding mechanism was reported for PDE4D and Rheb, but whether this interaction alters mTORC1 activity was not determined [138]. Hence,

the small GTPase Rheb possesses a variety of cellular signaling functions. While Rheb-mediated mTORC1-activation seems to depend on the Rheb nucleotide-state [126,128,129], other stimuli may not alter Rheb nucleotide binding. The newly developed conformational sensor for Rheb activity will enable to directly monitor spatiotemporally Rheb signaling allowing for precise detection of the Rheb nucleotide state in response to specific stimuli. In combination with traditional methods to monitor mTORC1 activity, the Rheb sensor will provide insights into the signal integration at the Rheb-mTORC1 hub.

In the past, development of a Rheb sensor was impaired by the lack of known Rheb effectors. Specific binding domains of small GTPase effector proteins are traditionally used as affinity tags to generate intramolecular FRET probes, allowing for spatiotemporal tracking of protein activity in cells. However, the FRET signal of such probes depends on the interaction of the affinity tag with the active small GTPase. Thus, protein activation is reported indirectly by the binding of the effector domain. Another disadvantage of these probes is the incorporated specific effector binding, which competes in binding to the small GTPase with endogenous proteins. In contrast, the sensors for small GTPase activity presented here directly report conformational changes instead of a subsequent binding event. Moreover, the conformational probes are independent of an affinity tag and can hence also be applied on small GTPases without known effectors. Furthermore, these sensors underlie native regulation by endogenous proteins, e.g. GEF or GAP, and, due to the lack of an intramolecular affinity tag, interaction with endogenous proteins is not affected. However, although the labor-intensive preparation process of the first generation of conformational sensors for small GTPase activity was circumvented by the use of amber suppression technique and intracellular labeling approach, the sensor establishment remains challenging. UAA methodology has been massively enhanced in the past few years and became more wide-spread, allowing for broad applications. In contrast, intracellular labeling remained largely challenging, which limits its application. Nevertheless, the rapid progress in the UAA field may also promote intracellular fluorescence labeling approaches, e.g. by development of new UAA and tetrazine-functionalized dyes for intracellular labeling [219,293]. The growing number of applications and studies using this sophisticated methodology, such as the here presented work, will enhance general user knowledge, facilitating development of new methods. Ultimately, this process may also promote the use of the genetically encoded conformational probes for small GTPase activity developed in this study.

References

1 Vetter, I. R. & Wittinghofer, A. The guanine nucleotide-binding switch in three dimensions. *Science* (2001).

2 Takai, Y., Sasaki, T. & Matozaki, T. Small GTP-binding proteins. *Physiological reviews* (2001).

3 Wennerberg, K., Rossman, K. L. & Der, C. J. The Ras superfamily at a glance. *Journal of cell science* (2005).

4 Bourne, H. R., Sanders, D. A. & McCormick, F. The GTPase superfamily: conserved structure and molecular mechanism. *Nature* (1991).

5 Chavrier, P. *et al.* Hypervariable C-terminal domain of rab proteins acts as a targeting signal. *Nature* (1991).

6 Brennwald, P. & Novick, P. Interactions of three domains distinguishing the Ras-related GTP-binding proteins Ypt1 and Sec4. *Nature* (1993).

7 Willumsen, B. M., Christensen, A., Hubbert, N. L., Papageorge, A. G. & Lowy, D. R. The p21 ras C-terminus is required for transformation and membrane association. *Nature* (1984).

8 Hancock, J. F., Magee, A. I., Childs, J. E. & Marshall, C. J. All ras proteins are polyisoprenylated but only some are palmitoylated. *Cell* (1989).

9 Farnsworth, C. C., Seabra, M. C., Ericsson, L. H., Gelb, M. H. & Glomset, J. A. Rab geranylgeranyl transferase catalyzes the geranylgeranylation of adjacent cysteines in the small GTPases Rab1A, Rab3A, and Rab5A. *Proceedings of the National Academy of Sciences of the United States of America* (1994).

10 Prior, I. A. & Hancock, J. F. Compartmentalization of Ras proteins. *Journal of cell science* (2001).

11 Itzen, A. & Goody, R. S. GTPases involved in vesicular trafficking: structures and mechanisms. *Seminars in cell & developmental biology* (2011).

12 Sasaki, T. *et al.* Purification and characterization from bovine brain cytosol of a protein that inhibits the dissociation of GDP from and the subsequent binding of GTP to smg p25A, a ras p21-like GTP-binding protein. *The Journal of biological chemistry* (1990).

13 Pylypenko, O. *et al.* Structure of doubly prenylated Ypt1:GDI complex and the mechanism of GDI-mediated Rab recycling. *The EMBO journal* (2006).

14 Touchot, N., Chardin, P. & Tavitian, A. Four additional members of the ras gene superfamily isolated by an oligonucleotide strategy: molecular cloning of YPT-related cDNAs from a rat

brain library. *Proceedings of the National Academy of Sciences of the United States of America* (1987).

15 Chavrier, P., Vingron, M., Sander, C., Simons, K. & Zerial, M. Molecular cloning of YPT1/SEC4-related cDNAs from an epithelial cell line. *Molecular and cellular biology* (1990).

16 Colicelli, J. Human RAS superfamily proteins and related GTPases. *Science's STKE : signal transduction knowledge environment* (2004).

17 Nguyen, U. T. *et al.* Analysis of the eukaryotic prenylome by isoprenoid affinity tagging. *Nat Chem Biol* (2009).

18 Pereira-Leal, J. B. & Seabra, M. C. The mammalian Rab family of small GTPases: definition of family and subfamily sequence motifs suggests a mechanism for functional specificity in the Ras superfamily. *Journal of molecular biology* (2000).

19 Alexandrov, K. *et al.* Characterization of the ternary complex between Rab7, REP-1 and Rab geranylgeranyl transferase. *European journal of biochemistry / FEBS* (1999).

20 Alexandrov, K., Horiuchi, H., Steele-Mortimer, O., Seabra, M. C. & Zerial, M. Rab escort protein-1 is a multifunctional protein that accompanies newly prenylated rab proteins to their target membranes. *The EMBO journal* (1994).

21 Wilson, A. L., Sheridan, K. M., Erdman, R. A. & Maltese, W. A. Prenylation of a Rab1B mutant with altered GTPase activity is impaired in cell-free systems but not in intact mammalian cells. *The Biochemical journal* (1996).

22 Wu, Y. W. *et al.* Membrane targeting mechanism of Rab GTPases elucidated by semisynthetic protein probes. *Nat Chem Biol* (2010).

23 Wu, Y. W., Tan, K. T., Waldmann, H., Goody, R. S. & Alexandrov, K. Interaction analysis of prenylated Rab GTPase with Rab escort protein and GDP dissociation inhibitor explains the need for both regulators. *Proceedings of the National Academy of Sciences of the United States of America* (2007).

24 Alory, C. & Balch, W. E. Molecular evolution of the Rab-escort-protein/guanine-nucleotide-dissociation-inhibitor superfamily. *Molecular biology of the cell* (2003).

25 Pfeffer, S. R. Rab GTPases: master regulators that establish the secretory and endocytic pathways. *Molecular biology of the cell* (2017).

26 Dirac-Svejstrup, A. B., Sumizawa, T. & Pfeffer, S. R. Identification of a GDI displacement factor that releases endosomal Rab GTPases from Rab-GDI. *The EMBO journal* (1997).

27 Sivars, U., Aivazian, D. & Pfeffer, S. R. Yip3 catalyses the dissociation of endosomal Rab-GDI complexes. *Nature* (2003).

28 Schoebel, S., Oesterlin, L. K., Blankenfeldt, W., Goody, R. S. & Itzen, A. RabGDI displacement by DrrA from Legionella is a consequence of its guanine nucleotide exchange activity. *Molecular cell* (2009).

29 Murata, T. *et al.* The Legionella pneumophila effector protein DrrA is a Rab1 guanine nucleotide-exchange factor. *Nature cell biology* (2006).

30 Blumer, J. *et al.* RabGEFs are a major determinant for specific Rab membrane targeting. *The Journal of cell biology* (2013).

31 Gerondopoulos, A., Langemeyer, L., Liang, J. R., Linford, A. & Barr, F. A. BLOC-3 mutated in Hermansky-Pudlak syndrome is a Rab32/38 guanine nucleotide exchange factor. *Current biology : CB* (2012).

32 Cabrera, M. & Ungermann, C. Guanine nucleotide exchange factors (GEFs) have a critical but not exclusive role in organelle localization of Rab GTPases. *The Journal of biological chemistry* (2013).

33 Koch, D. *et al.* A pull-down procedure for the identification of unknown GEFs for small GTPases. *Small GTPases* (2016).

34 Carney, D. S., Davies, B. A. & Horazdovsky, B. F. Vps9 domain-containing proteins: activators of Rab5 GTPases from yeast to neurons. *Trends Cell Biol* (2006).

35 Marat, A. L., Dokainish, H. & McPherson, P. S. DENN domain proteins: regulators of Rab GTPases. *The Journal of biological chemistry* (2011).

36 Jones, S., Richardson, C. J., Litt, R. J. & Segev, N. Identification of regulators for Ypt1 GTPase nucleotide cycling. *Molecular biology of the cell* (1998).

37 Bos, J. L., Rehmann, H. & Wittinghofer, A. GEFs and GAPs: critical elements in the control of small G proteins. *Cell* (2007).

38 Albert, S. & Gallwitz, D. Two new members of a family of Ypt/Rab GTPase activating proteins. Promiscuity of substrate recognition. *The Journal of biological chemistry* (1999).

39 Albert, S., Will, E. & Gallwitz, D. Identification of the catalytic domains and their functionally critical arginine residues of two yeast GTPase-activating proteins specific for Ypt/Rab transport GTPases. *The EMBO journal* (1999).

40 Strom, M., Vollmer, P., Tan, T. J. & Gallwitz, D. A yeast GTPase-activating protein that interacts specifically with a member of the Ypt/Rab family. *Nature* (1993).

41 Ahmadian, M. R., Stege, P., Scheffzek, K. & Wittinghofer, A. Confirmation of the arginine-finger hypothesis for the GAP-stimulated GTP-hydrolysis reaction of Ras. *Nature structural biology* (1997).

42 Pan, X., Eathiraj, S., Munson, M. & Lambright, D. G. TBC-domain GAPs for Rab GTPases accelerate GTP hydrolysis by a dual-finger mechanism. *Nature* (2006).

43 Rak, A. *et al.* Crystal structure of the GAP domain of Gyp1p: first insights into interaction with Ypt/Rab proteins. *The EMBO journal* (2000).

44 Fukuda, M. TBC proteins: GAPs for mammalian small GTPase Rab? *Bioscience reports* (2011).

45 Zerial, M. & McBride, H. Rab proteins as membrane organizers. *Nature reviews. Molecular cell biology* (2001).

46 Nuoffer, C. & Balch, W. E. GTPases: multifunctional molecular switches regulating vesicular traffic. *Annual review of biochemistry* (1994).

47 Pfeffer, S. R., Dirac-Svejstrup, A. B. & Soldati, T. Rab GDP dissociation inhibitor: putting rab GTPases in the right place. *The Journal of biological chemistry* (1995).

48 Stenmark, H. & Olkkonen, V. M. The Rab GTPase family. *Genome biology* (2001).

49 Ortiz, D., Medkova, M., Walch-Solimena, C. & Novick, P. Ypt32 recruits the Sec4p guanine nucleotide exchange factor, Sec2p, to secretory vesicles; evidence for a Rab cascade in yeast. *The Journal of cell biology* (2002).

50 Rivera-Molina, F. E. & Novick, P. J. A Rab GAP cascade defines the boundary between two Rab GTPases on the secretory pathway. *Proceedings of the National Academy of Sciences of the United States of America* (2009).

51 Yoshimura, S., Egerer, J., Fuchs, E., Haas, A. K. & Barr, F. A. Functional dissection of Rab GTPases involved in primary cilium formation. *The Journal of cell biology* (2007).

52 de Renzis, S., Sonnichsen, B. & Zerial, M. Divalent Rab effectors regulate the sub-compartmental organization and sorting of early endosomes. *Nature cell biology* (2002).

53 Vitale, G. *et al.* Distinct Rab-binding domains mediate the interaction of Rabaptin-5 with GTP-bound Rab4 and Rab5. *The EMBO journal* (1998).

54 Fukuda, M., Kanno, E., Ishibashi, K. & Itoh, T. Large scale screening for novel rab effectors reveals unexpected broad Rab binding specificity. *Molecular & cellular proteomics : MCP* (2008).

55 Rai, A., Goody, R. S. & Muller, M. P. Multivalency in Rab effector interactions. *Small GTPases* (2017).

56 Mizuno-Yamasaki, E., Rivera-Molina, F. & Novick, P. GTPase networks in membrane traffic. *Annual review of biochemistry* (2012).

57 Lipatova, Z., Hain, A. U., Nazarko, V. Y. & Segev, N. Ypt/Rab GTPases: principles learned from yeast. *Critical reviews in biochemistry and molecular biology* (2015).

58 Novick, P., Field, C. & Schekman, R. Identification of 23 complementation groups required for post-translational events in the yeast secretory pathway. *Cell* (1980).

59 Plutner, H. *et al.* Rab1b regulates vesicular transport between the endoplasmic reticulum and successive Golgi compartments. *The Journal of cell biology* (1991).

60 Saraste, J., Lahtinen, U. & Goud, B. Localization of the small GTP-binding protein rab1p to early compartments of the secretory pathway. *Journal of cell science* (1995).

61 Tisdale, E. J., Bourne, J. R., Khosravi-Far, R., Der, C. J. & Balch, W. E. GTP-binding mutants of rab1 and rab2 are potent inhibitors of vesicular transport from the endoplasmic reticulum to the Golgi complex. *The Journal of cell biology* (1992).

62 Allan, B. B., Moyer, B. D. & Balch, W. E. Rab1 recruitment of p115 into a cis-SNARE complex: programming budding COPII vesicles for fusion. *Science* (2000).

63 Alvarez, C., Fujita, H., Hubbard, A. & Sztul, E. ER to Golgi transport: Requirement for p115 at a pre-Golgi VTC stage. *The Journal of cell biology* (1999).

64 Bannykh, S. I., Rowe, T. & Balch, W. E. The organization of endoplasmic reticulum export complexes. *The Journal of cell biology* (1996).

65 Cao, X., Ballew, N. & Barlowe, C. Initial docking of ER-derived vesicles requires Uso1p and Ypt1p but is independent of SNARE proteins. *The EMBO journal* (1998).

66 Moyer, B. D., Allan, B. B. & Balch, W. E. Rab1 interaction with a GM130 effector complex regulates COPII vesicle cis--Golgi tethering. *Traffic* (2001).

67 Rosing, M., Ossendorf, E., Rak, A. & Barnekow, A. Giantin interacts with both the small GTPase Rab6 and Rab1. *Experimental cell research* (2007).

68 Satoh, A., Wang, Y., Malsam, J., Beard, M. B. & Warren, G. Golgin-84 is a rab1 binding partner involved in Golgi structure. *Traffic* (2003).

69 Peter, F., Nuoffer, C., Pind, S. N. & Balch, W. E. Guanine nucleotide dissociation inhibitor is essential for Rab1 function in budding from the endoplasmic reticulum and transport through the Golgi stack. *The Journal of cell biology* (1994).

70 Zoppino, F. C., Militello, R. D., Slavin, I., Alvarez, C. & Colombo, M. I. Autophagosome formation depends on the small GTPase Rab1 and functional ER exit sites. *Traffic* (2010).

71 Kamena, F., Diefenbacher, M., Kilchert, C., Schwarz, H. & Spang, A. Ypt1p is essential for retrograde Golgi-ER transport and for Golgi maintenance in S. cerevisiae. *Journal of cell science* (2008).

72 Sannerud, R. *et al.* Rab1 defines a novel pathway connecting the pre-Golgi intermediate compartment with the cell periphery. *Molecular biology of the cell* (2006).

73 Saraste, J. Spatial and Functional Aspects of ER-Golgi Rabs and Tethers. *Frontiers in cell and developmental biology* (2016).

74 Marie, M., Dale, H. A., Sannerud, R. & Saraste, J. The function of the intermediate compartment in pre-Golgi trafficking involves its stable connection with the centrosome. *Molecular biology of the cell* (2009).

75 Monetta, P., Slavin, I., Romero, N. & Alvarez, C. Rab1b interacts with GBF1 and modulates both ARF1 dynamics and COPI association. *Molecular biology of the cell* (2007).

76 Kim, J. J., Lipatova, Z. & Segev, N. TRAPP Complexes in Secretion and Autophagy. *Frontiers in cell and developmental biology* (2016).

77 Scrivens, P. J. *et al.* C4orf41 and TTC-15 are mammalian TRAPP components with a role at an early stage in ER-to-Golgi trafficking. *Molecular biology of the cell* (2011).

78 Bassik, M. C. *et al.* A systematic mammalian genetic interaction map reveals pathways underlying ricin susceptibility. *Cell* (2013).

79 Sacher, M. *et al.* TRAPP I implicated in the specificity of tethering in ER-to-Golgi transport. *Molecular cell* (2001).

80 Barrowman, J., Bhandari, D., Reinisch, K. & Ferro-Novick, S. TRAPP complexes in membrane traffic: convergence through a common Rab. *Nature reviews. Molecular cell biology* (2010).

81 Meiling-Wesse, K. *et al.* Trs85 (Gsg1), a component of the TRAPP complexes, is required for the organization of the preautophagosomal structure during selective autophagy via the Cvt pathway. *The Journal of biological chemistry* (2005).

82 Nazarko, T. Y., Huang, J., Nicaud, J. M., Klionsky, D. J. & Sibirny, A. A. Trs85 is required for macroautophagy, pexophagy and cytoplasm to vacuole targeting in Yarrowia lipolytica and Saccharomyces cerevisiae. *Autophagy* (2005).

83 Behrends, C., Sowa, M. E., Gygi, S. P. & Harper, J. W. Network organization of the human autophagy system. *Nature* (2010).

84 Zong, M. *et al.* TRAPPC9 mediates the interaction between p150 and COPII vesicles at the target membrane. *PloS one* (2012).

85 Yamasaki, A. *et al.* mTrs130 is a component of a mammalian TRAPPII complex, a Rab1 GEF that binds to COPI-coated vesicles. *Molecular biology of the cell* (2009).

86 Yu, S. *et al.* mBet3p is required for homotypic COPII vesicle tethering in mammalian cells. *The Journal of cell biology* (2006).

87 Szul, T. & Sztul, E. COPII and COPI traffic at the ER-Golgi interface. *Physiology (Bethesda)* (2011).

88 Cai, Y. *et al.* The structural basis for activation of the Rab Ypt1p by the TRAPP membrane-tethering complexes. *Cell* (2008).

89 Sidjanin, D. J., Park, A. K., Ronchetti, A., Martins, J. & Jackson, W. T. TBC1D20 mediates autophagy as a key regulator of autophagosome maturation. *Autophagy* (2016).

90 Sklan, E. H. *et al.* TBC1D20 is a Rab1 GTPase-activating protein that mediates hepatitis C virus replication. *The Journal of biological chemistry* (2007).

91 Haas, A. K. *et al.* Analysis of GTPase-activating proteins: Rab1 and Rab43 are key Rabs required to maintain a functional Golgi complex in human cells. *Journal of cell science* (2007).

92 Liegel, R. P. *et al.* Loss-of-function mutations in TBC1D20 cause cataracts and male infertility in blind sterile mice and Warburg micro syndrome in humans. *American journal of human genetics* (2013).

93 De Antoni, A., Schmitzova, J., Trepte, H. H., Gallwitz, D. & Albert, S. Significance of GTP hydrolysis in Ypt1p-regulated endoplasmic reticulum to Golgi transport revealed by the analysis of two novel Ypt1-GAPs. *The Journal of biological chemistry* (2002).

94 Morsomme, P. & Riezman, H. The Rab GTPase Ypt1p and tethering factors couple protein sorting at the ER to vesicle targeting to the Golgi apparatus. *Developmental cell* (2002).

95 Urano, J., Tabancay, A. P., Yang, W. & Tamanoi, F. The Saccharomyces cerevisiae Rheb G-protein is involved in regulating canavanine resistance and arginine uptake. *The Journal of biological chemistry* (2000).

96 Gromov, P. S., Madsen, P., Tomerup, N. & Celis, J. E. A novel approach for expression cloning of small GTPases: identification, tissue distribution and chromosome mapping of the human homolog of rheb. *FEBS letters* (1995).

97 Yamagata, K. *et al.* rheb, a growth factor- and synaptic activity-regulated gene, encodes a novel Ras-related protein. *The Journal of biological chemistry* (1994).

98 Heard, J. J., Fong, V., Bathaie, S. Z. & Tamanoi, F. Recent progress in the study of the Rheb family GTPases. *Cellular signalling* (2014).

99 Aspuria, P. J. & Tamanoi, F. The Rheb family of GTP-binding proteins. *Cellular signalling* (2004).

100 Clark, G. J. *et al.* The Ras-related protein Rheb is farnesylated and antagonizes Ras signaling and transformation. *The Journal of biological chemistry* (1997).

101 Saito, K., Araki, Y., Kontani, K., Nishina, H. & Katada, T. Novel role of the small GTPase Rheb: its implication in endocytic pathway independent of the activation of mammalian target of rapamycin. *J Biochem* (2005).

102 Yu, Y. *et al.* Structural basis for the unique biological function of small GTPase RHEB. *The Journal of biological chemistry* (2005).

103 Mazhab-Jafari, M. T. *et al.* An autoinhibited noncanonical mechanism of GTP hydrolysis by Rheb maintains mTORC1 homeostasis. *Structure* (2012).

104 Hancock, J. F., Paterson, H. & Marshall, C. J. A polybasic domain or palmitoylation is required in addition to the CAAX motif to localize p21ras to the plasma membrane. *Cell* (1990).

105 Apolloni, A., Prior, I. A., Lindsay, M., Parton, R. G. & Hancock, J. F. H-ras but not K-ras traffics to the plasma membrane through the exocytic pathway. *Molecular and cellular biology* (2000).

106 Takahashi, K., Nakagawa, M., Young, S. G. & Yamanaka, S. Differential membrane localization of ERas and Rheb, two Ras-related proteins involved in the phosphatidylinositol 3-kinase/mTOR pathway. *The Journal of biological chemistry* (2005).

107 Hanker, A. B. *et al.* Differential requirement of CAAX-mediated posttranslational processing for Rheb localization and signaling. *Oncogene* (2010).

108 Zhang, J. *et al.* A tuberous sclerosis complex signalling node at the peroxisome regulates mTORC1 and autophagy in response to ROS. *Nature cell biology* (2013).

109 Ma, D., Bai, X., Guo, S. & Jiang, Y. The switch I region of Rheb is critical for its interaction with FKBP38. *The Journal of biological chemistry* (2008).

110 Buerger, C., DeVries, B. & Stambolic, V. Localization of Rheb to the endomembrane is critical for its signaling function. *Biochem Biophys Res Commun* (2006).

111 Sancak, Y. *et al.* The Rag GTPases bind raptor and mediate amino acid signaling to mTORC1. *Science* (2008).

112 Sancak, Y. *et al.* Ragulator-Rag complex targets mTORC1 to the lysosomal surface and is necessary for its activation by amino acids. *Cell* (2010).

113 Menon, S. *et al.* Spatial control of the TSC complex integrates insulin and nutrient regulation of mTORC1 at the lysosome. *Cell* (2014).

114 Inoki, K., Ouyang, H., Li, Y. & Guan, K. L. Signaling by target of rapamycin proteins in cell growth control. *Microbiology and molecular biology reviews : MMBR* (2005).

115 Kim, D. H. *et al.* mTOR interacts with raptor to form a nutrient-sensitive complex that signals to the cell growth machinery. *Cell* (2002).

116 Loewith, R. *et al.* Two TOR complexes, only one of which is rapamycin sensitive, have distinct roles in cell growth control. *Molecular cell* (2002).

117 Sarbassov, D. D. *et al.* Rictor, a novel binding partner of mTOR, defines a rapamycin-insensitive and raptor-independent pathway that regulates the cytoskeleton. *Current biology : CB* (2004).

118 Yang, Q., Inoki, K., Kim, E. & Guan, K. L. TSC1/TSC2 and Rheb have different effects on TORC1 and TORC2 activity. *Proceedings of the National Academy of Sciences of the United States of America* (2006).

119 Castro, A. F., Rebhun, J. F., Clark, G. J. & Quilliam, L. A. Rheb binds tuberous sclerosis complex 2 (TSC2) and promotes S6 kinase activation in a rapamycin- and farnesylation-dependent manner. *The Journal of biological chemistry* (2003).

120 Dibble, C. C. *et al.* TBC1D7 is a third subunit of the TSC1-TSC2 complex upstream of mTORC1. *Molecular cell* (2012).

121 Garami, A. *et al.* Insulin activation of Rheb, a mediator of mTOR/S6K/4E-BP signaling, is inhibited by TSC1 and 2. *Molecular cell* (2003).

122 Inoki, K., Li, Y., Xu, T. & Guan, K. L. Rheb GTPase is a direct target of TSC2 GAP activity and regulates mTOR signaling. *Genes & development* (2003).

123 Tee, A. R., Manning, B. D., Roux, P. P., Cantley, L. C. & Blenis, J. Tuberous sclerosis complex gene products, Tuberin and Hamartin, control mTOR signaling by acting as a GTPase-activating protein complex toward Rheb. *Current biology : CB* (2003).

124 Demetriades, C., Doumpas, N. & Teleman, A. A. Regulation of TORC1 in response to amino acid starvation via lysosomal recruitment of TSC2. *Cell* (2014).

125 Carroll, B. *et al.* Control of TSC2-Rheb signaling axis by arginine regulates mTORC1 activity. *eLife* (2016).

126 Long, X., Lin, Y., Ortiz-Vega, S., Yonezawa, K. & Avruch, J. Rheb binds and regulates the mTOR kinase. *Current biology : CB* (2005).

127 Long, X., Ortiz-Vega, S., Lin, Y. & Avruch, J. Rheb binding to mammalian target of rapamycin (mTOR) is regulated by amino acid sufficiency. *The Journal of biological chemistry* (2005).

128 Sancak, Y. *et al.* PRAS40 is an insulin-regulated inhibitor of the mTORC1 protein kinase. *Molecular cell* (2007).

129 Sato, T., Nakashima, A., Guo, L. & Tamanoi, F. Specific activation of mTORC1 by Rheb G-protein in vitro involves enhanced recruitment of its substrate protein. *The Journal of biological chemistry* (2009).

130 Brugarolas, J. *et al.* Regulation of mTOR function in response to hypoxia by REDD1 and the TSC1/TSC2 tumor suppressor complex. *Genes & development* (2004).

131 Budanov, A. V. & Karin, M. p53 target genes sestrin1 and sestrin2 connect genotoxic stress and mTOR signaling. *Cell* (2008).

132 Reiling, J. H. & Hafen, E. The hypoxia-induced paralogs Scylla and Charybdis inhibit growth by down-regulating S6K activity upstream of TSC in Drosophila. *Genes & development* (2004).

133 Jewell, J. L., Russell, R. C. & Guan, K. L. Amino acid signalling upstream of mTOR. *Nature reviews. Molecular cell biology* (2013).

134 Hara, K. *et al.* Amino acid sufficiency and mTOR regulate p70 S6 kinase and eIF-4E BP1 through a common effector mechanism. *The Journal of biological chemistry* (1998).

135 Wang, X., Campbell, L. E., Miller, C. M. & Proud, C. G. Amino acid availability regulates p70 S6 kinase and multiple translation factors. *The Biochemical journal* (1998).

136 Nicklin, P. *et al.* Bidirectional transport of amino acids regulates mTOR and autophagy. *Cell* (2009).

137 Zheng, M. *et al.* Inactivation of Rheb by PRAK-mediated phosphorylation is essential for energy-depletion-induced suppression of mTORC1. *Nature cell biology* (2011).

138 Kim, H. W. *et al.* Cyclic AMP controls mTOR through regulation of the dynamic interaction between Rheb and phosphodiesterase 4D. *Molecular and cellular biology* (2010).

139 Lee, M. N. *et al.* Glycolytic flux signals to mTOR through glyceraldehyde-3-phosphate dehydrogenase-mediated regulation of Rheb. *Molecular and cellular biology* (2009).

140 Buller, C. L., Heilig, C. W. & Brosius, F. C., 3rd. GLUT1 enhances mTOR activity independently of TSC2 and AMPK. *American journal of physiology. Renal physiology* (2011).

141 Ueda, Y., Kwok, S. & Hayashi, Y. Application of FRET probes in the analysis of neuronal plasticity. *Frontiers in neural circuits* (2013).

142 Goedhart, J. *et al.* Structure-guided evolution of cyan fluorescent proteins towards a quantum yield of 93%. *Nature communications* (2012).

143 Griesbeck, O., Baird, G. S., Campbell, R. E., Zacharias, D. A. & Tsien, R. Y. Reducing the environmental sensitivity of yellow fluorescent protein. Mechanism and applications. *The Journal of biological chemistry* (2001).

144 Rizzo, M. A., Springer, G. H., Granada, B. & Piston, D. W. An improved cyan fluorescent protein variant useful for FRET. *Nature biotechnology* (2004).

145 Nagai, T. *et al.* A variant of yellow fluorescent protein with fast and efficient maturation for cell-biological applications. *Nature biotechnology* (2002).

146 Yasuda, R. Imaging spatiotemporal dynamics of neuronal signaling using fluorescence resonance energy transfer and fluorescence lifetime imaging microscopy. *Current opinion in neurobiology* (2006).

147 Walther, K. A., Papke, B., Sinn, M. B., Michel, K. & Kinkhabwala, A. Precise measurement of protein interacting fractions with fluorescence lifetime imaging microscopy. *Molecular bioSystems* (2011).

148 Kraynov, V. S. *et al.* Localized Rac activation dynamics visualized in living cells. *Science* (2000).

149 Mochizuki, N. *et al.* Spatio-temporal images of growth-factor-induced activation of Ras and Rap1. *Nature* (2001).

150 Miyawaki, A. *et al.* Fluorescent indicators for Ca2+ based on green fluorescent proteins and calmodulin. *Nature* (1997).

151 Kamiyama, D. & Chiba, A. Endogenous activation patterns of Cdc42 GTPase within Drosophila embryos. *Science* (2009).

152 Yoshizaki, H. *et al.* Activity of Rho-family GTPases during cell division as visualized with FRET-based probes. *The Journal of cell biology* (2003).

153 Pertz, O., Hodgson, L., Klemke, R. L. & Hahn, K. M. Spatiotemporal dynamics of RhoA activity in migrating cells. *Nature* (2006).

154 Takaya, A. *et al.* R-Ras regulates exocytosis by Rgl2/Rlf-mediated activation of RalA on endosomes. *Molecular biology of the cell* (2007).

155 Kitano, M., Nakaya, M., Nakamura, T., Nagata, S. & Matsuda, M. Imaging of Rab5 activity identifies essential regulators for phagosome maturation. *Nature* (2008).

156 Kalab, P., Weis, K. & Heald, R. Visualization of a Ran-GTP gradient in interphase and mitotic Xenopus egg extracts. *Science* (2002).

157 Kawase, K. *et al.* GTP hydrolysis by the Rho family GTPase TC10 promotes exocytic vesicle fusion. *Developmental cell* (2006).

158 Itoh, R. E. *et al.* Activation of rac and cdc42 video imaged by fluorescent resonance energy transfer-based single-molecule probes in the membrane of living cells. *Molecular and cellular biology* (2002).

159 Nakamura, T., Aoki, K. & Matsuda, M. Monitoring spatio-temporal regulation of Ras and Rho GTPase with GFP-based FRET probes. *Methods* (2005).

160 Voß, S. *Fluorescent sensors for the small GTPase switch* Dr. rer. nat. thesis, TU Dortmund, (2017).

161 Voss, S., Kruger, D. M., Koch, O. & Wu, Y. W. Spatiotemporal imaging of small GTPases activity in live cells. *Proceedings of the National Academy of Sciences of the United States of America* (2016).

162 Petry, S. *et al.* Crystal structures of the ribosome in complex with release factors RF1 and RF2 bound to a cognate stop codon. *Cell* (2005).

163 Scolnick, E., Tompkins, R., Caskey, T. & Nirenberg, M. Release factors differing in specificity for terminator codons. *Proceedings of the National Academy of Sciences of the United States of America* (1968).

164 Bertram, G., Innes, S., Minella, O., Richardson, J. & Stansfield, I. Endless possibilities: translation termination and stop codon recognition. *Microbiology* (2001).

165 Dever, T. E. & Green, R. The elongation, termination, and recycling phases of translation in eukaryotes. *Cold Spring Harb Perspect Biol* (2012).

166 Jackson, R. J., Hellen, C. U. & Pestova, T. V. Termination and post-termination events in eukaryotic translation. *Adv Protein Chem Struct Biol* (2012).

167 Inge-Vechtomov, S., Zhouravleva, G. & Philippe, M. Eukaryotic release factors (eRFs) history. *Biol Cell* (2003).

168 Lang, K. & Chin, J. W. Cellular incorporation of unnatural amino acids and bioorthogonal labeling of proteins. *Chemical reviews* (2014).

169 Neumann, H., Peak-Chew, S. Y. & Chin, J. W. Genetically encoding N(epsilon)-acetyllysine in recombinant proteins. *Nat Chem Biol* (2008).

170 Yousaf, N. & Gould, D. The Tetracycline Responsive System. *Methods in molecular biology* (2017).

171 Chin, J. W. *et al.* An expanded eukaryotic genetic code. *Science* (2003).

172 Das, A. T., Tenenbaum, L. & Berkhout, B. Tet-On Systems For Doxycycline-inducible Gene Expression. *Current gene therapy* (2016).

173 Tee, A. R., Blenis, J. & Proud, C. G. Analysis of mTOR signaling by the small G-proteins, Rheb and RhebL1. *FEBS letters* (2005).

174 Li, Y., Inoki, K. & Guan, K. L. Biochemical and functional characterizations of small GTPase Rheb and TSC2 GAP activity. *Molecular and cellular biology* (2004).

175 Inoki, K., Zhu, T. & Guan, K. L. TSC2 mediates cellular energy response to control cell growth and survival. *Cell* (2003).

176 Bianco, A., Townsley, F. M., Greiss, S., Lang, K. & Chin, J. W. Expanding the genetic code of Drosophila melanogaster. *Nat Chem Biol* (2012).

177 Lang, K. *et al.* Genetic Encoding of bicyclononynes and trans-cyclooctenes for site-specific protein labeling in vitro and in live mammalian cells via rapid fluorogenic Diels-Alder reactions. *Journal of the American Chemical Society* (2012).

178 Nikic, I. *et al.* Minimal tags for rapid dual-color live-cell labeling and super-resolution microscopy. *Angewandte Chemie* (2014).

179 Plass, T. *et al.* Amino acids for Diels-Alder reactions in living cells. *Angewandte Chemie* (2012).

180 Schmied, W. H., Elsasser, S. J., Uttamapinant, C. & Chin, J. W. Efficient multisite unnatural amino acid incorporation in mammalian cells via optimized pyrrolysyl tRNA synthetase/tRNA expression and engineered eRF1. *Journal of the American Chemical Society* (2014).

181 Uttamapinant, C. *et al.* Genetic code expansion enables live-cell and super-resolution imaging of site-specifically labeled cellular proteins. *Journal of the American Chemical Society* (2015).

182 Chin, J. W., Martin, A. B., King, D. S., Wang, L. & Schultz, P. G. Addition of a photocrosslinking amino acid to the genetic code of Escherichiacoli. *Proceedings of the National Academy of Sciences of the United States of America* (2002).

183 Chin, J. W. & Schultz, P. G. In vivo photocrosslinking with unnatural amino Acid mutagenesis. *Chembiochem : a European journal of chemical biology* (2002).

184 Ai, H. W., Shen, W., Sagi, A., Chen, P. R. & Schultz, P. G. Probing protein-protein interactions with a genetically encoded photo-crosslinking amino acid. *Chembiochem : a European journal of chemical biology* (2011).

185 Neumann, H., Hazen, J. L., Weinstein, J., Mehl, R. A. & Chin, J. W. Genetically encoding protein oxidative damage. *Journal of the American Chemical Society* (2008).

186 Liu, C. C. & Schultz, P. G. Recombinant expression of selectively sulfated proteins in Escherichia coli. *Nature biotechnology* (2006).

187 Serwa, R. *et al.* Chemoselective Staudinger-phosphite reaction of azides for the phosphorylation of proteins. *Angewandte Chemie* (2009).

188 Xie, J., Supekova, L. & Schultz, P. G. A genetically encoded metabolically stable analogue of phosphotyrosine in Escherichia coli. *ACS chemical biology* (2007).

189 Park, H. S. *et al.* Expanding the genetic code of Escherichia coli with phosphoserine. *Science* (2011).

190 Ai, H. W., Lee, J. W. & Schultz, P. G. A method to site-specifically introduce methyllysine into proteins in E. coli. *Chem Commun (Camb)* (2010).

191 Groff, D., Chen, P. R., Peters, F. B. & Schultz, P. G. A genetically encoded epsilon-N-methyl lysine in mammalian cells. *Chembiochem : a European journal of chemical biology* (2010).

192 Wang, Y. S. *et al.* A genetically encoded photocaged Nepsilon-methyl-L-lysine. *Molecular bioSystems* (2010).

193 Nguyen, D. P., Garcia Alai, M. M., Kapadnis, P. B., Neumann, H. & Chin, J. W. Genetically encoding N(epsilon)-methyl-L-lysine in recombinant histones. *Journal of the American Chemical Society* (2009).

194 Nguyen, D. P., Garcia Alai, M. M., Virdee, S. & Chin, J. W. Genetically directing varepsilon-N, N-dimethyl-L-lysine in recombinant histones. *Chemistry & biology* (2010).

195 Virdee, S. *et al.* Traceless and site-specific ubiquitination of recombinant proteins. *Journal of the American Chemical Society* (2011).

196 Virdee, S., Ye, Y., Nguyen, D. P., Komander, D. & Chin, J. W. Engineered diubiquitin synthesis reveals Lys29-isopeptide specificity of an OTU deubiquitinase. *Nat Chem Biol* (2010).

197 Li, X., Fekner, T., Ottesen, J. J. & Chan, M. K. A pyrrolysine analogue for site-specific protein ubiquitination. *Angewandte Chemie* (2009).

198 Kang, J. Y., Kawaguchi, D. & Wang, L. Optical Control of a Neuronal Protein Using a Genetically Encoded Unnatural Amino Acid in Neurons. *J Vis Exp* (2016).

199 Gautier, A., Deiters, A. & Chin, J. W. Light-activated kinases enable temporal dissection of signaling networks in living cells. *Journal of the American Chemical Society* (2011).

200 Deiters, A., Groff, D., Ryu, Y., Xie, J. & Schultz, P. G. A genetically encoded photocaged tyrosine. *Angewandte Chemie* (2006).

201 Ye, S., Huber, T., Vogel, R. & Sakmar, T. P. FTIR analysis of GPCR activation using azido probes. *Nat Chem Biol* (2009).

202 Ye, S. *et al.* Tracking G-protein-coupled receptor activation using genetically encoded infrared probes. *Nature* (2010).

203 Daggett, K. A. & Sakmar, T. P. Site-specific in vitro and in vivo incorporation of molecular probes to study G-protein-coupled receptors. *Current opinion in chemical biology* (2011).

204 Lang, K. & Chin, J. W. Bioorthogonal reactions for labeling proteins. *ACS chemical biology* (2014).

205 Liu, D. S. *et al.* Diels-Alder cycloaddition for fluorophore targeting to specific proteins inside living cells. *Journal of the American Chemical Society* (2012).

206 Huber, T., Naganathan, S., Tian, H., Ye, S. & Sakmar, T. P. Unnatural amino acid mutagenesis of GPCRs using amber codon suppression and bioorthogonal labeling. *Methods in enzymology* (2013).

207 Tian, H., Sakmar, T. P. & Huber, T. Site-specific labeling of genetically encoded azido groups for multicolor, single-molecule fluorescence imaging of GPCRs. *Methods in cell biology* (2013).

208 Tian, H. *et al.* Bioorthogonal fluorescent labeling of functional G-protein-coupled receptors. *Chembiochem : a European journal of chemical biology* (2014).

209 Kim, C. H., Axup, J. Y. & Schultz, P. G. Protein conjugation with genetically encoded unnatural amino acids. *Current opinion in chemical biology* (2013).

210 Liu, W. *et al.* A rapid and fluorogenic TMP-AcBOPDIPY probe for covalent labeling of proteins in live cells. *Journal of the American Chemical Society* (2014).

211 Griffin, B. A., Adams, S. R. & Tsien, R. Y. Specific covalent labeling of recombinant protein molecules inside live cells. *Science* (1998).

212 Cao, H. *et al.* A red cy3-based biarsenical fluorescent probe targeted to a complementary binding peptide. *Journal of the American Chemical Society* (2007).

213 Adams, S. R. *et al.* New biarsenical ligands and tetracysteine motifs for protein labeling in vitro and in vivo: synthesis and biological applications. *Journal of the American Chemical Society* (2002).

214 Sletten, E. M. & Bertozzi, C. R. Bioorthogonal chemistry: fishing for selectivity in a sea of functionality. *Angewandte Chemie* (2009).

215 Wu, Y. W. & Goody, R. S. Probing protein function by chemical modification. *Journal of peptide science : an official publication of the European Peptide Society* (2010).

216 Ye, S. *et al.* Site-specific incorporation of keto amino acids into functional G protein-coupled receptors using unnatural amino acid mutagenesis. *The Journal of biological chemistry* (2008).

217 Plass, T., Milles, S., Koehler, C., Schultz, C. & Lemke, E. A. Genetically encoded copper-free click chemistry. *Angewandte Chemie* (2011).

218 Nikic, I. *et al.* Debugging Eukaryotic Genetic Code Expansion for Site-Specific Click-PAINT Super-Resolution Microscopy. *Angewandte Chemie* (2016).

219 Kozma, E. *et al.* Hydrophilic trans-Cyclooctenylated Noncanonical Amino Acids for Fast Intracellular Protein Labeling. *Chembiochem : a European journal of chemical biology* (2016).

220 Carlson, J. C., Meimetis, L. G., Hilderbrand, S. A. & Weissleder, R. BODIPY-tetrazine derivatives as superbright bioorthogonal turn-on probes. *Angewandte Chemie* (2013).

221 Devaraj, N. K., Hilderbrand, S., Upadhyay, R., Mazitschek, R. & Weissleder, R. Bioorthogonal turn-on probes for imaging small molecules inside living cells. *Angewandte Chemie* (2010).

222 Wieczorek, A., Buckup, T. & Wombacher, R. Rigid tetrazine fluorophore conjugates with fluorogenic properties in the inverse electron demand Diels-Alder reaction. *Organic & biomolecular chemistry* (2014).

223 Lang, K. *et al.* Genetically encoded norbornene directs site-specific cellular protein labelling via a rapid bioorthogonal reaction. *Nature chemistry* (2012).

224 AttoTec. *Fluorescent Labels and Dyes*, <https://www.atto-tec.com/> (

225 Lim, C. Y. & Zoncu, R. The lysosome as a command-and-control center for cellular metabolism. *The Journal of cell biology* (2016).

226 Avruch, J. *et al.* Activation of mTORC1 in two steps: Rheb-GTP activation of catalytic function and increased binding of substrates to raptor. *Biochemical Society transactions* (2009).

227 Fang, Y., Vilella-Bach, M., Bachmann, R., Flanigan, A. & Chen, J. Phosphatidic acid-mediated mitogenic activation of mTOR signaling. *Science* (2001).

228 Fang, Y. *et al.* PLD1 regulates mTOR signaling and mediates Cdc42 activation of S6K1. *Current biology : CB* (2003).

229 Sun, Y. *et al.* Phospholipase D1 is an effector of Rheb in the mTOR pathway. *Proceedings of the National Academy of Sciences of the United States of America* (2008).

230 Huang, J. & Manning, B. D. The TSC1-TSC2 complex: a molecular switchboard controlling cell growth. *The Biochemical journal* (2008).

231 Pan, D., Dong, J., Zhang, Y. & Gao, X. Tuberous sclerosis complex: from Drosophila to human disease. *Trends Cell Biol* (2004).

232 Ballif, B. A. *et al.* Quantitative phosphorylation profiling of the ERK/p90 ribosomal S6 kinase-signaling cassette and its targets, the tuberous sclerosis tumor suppressors. *Proceedings of the National Academy of Sciences of the United States of America* (2005).

233 Wang, X. & Proud, C. G. mTORC1 signaling: what we still don't know. *Journal of molecular cell biology* (2011).

234 NAKAMURA, Y. *Codon Usage Database*, <http://www.kazusa.or.jp/codon/cgi-bin/showcodon.cgi?species=9606> (

235 Masip, M. E. *et al.* Reversible cryo-arrest for imaging molecules in living cells at high spatial resolution. *Nature methods* (2016).

236 Science, U. D. o. C. *PSIPRED v3.3*, <http://bioinf.cs.ucl.ac.uk/psipred/> (

237 Wang, Q., Parrish, A. R. & Wang, L. Expanding the genetic code for biological studies. *Chemistry & biology* (2009).

238 Johnson, D. B. *et al.* Release factor one is nonessential in Escherichia coli. *ACS chemical biology* (2012).

239 Johnson, D. B. *et al.* RF1 knockout allows ribosomal incorporation of unnatural amino acids at multiple sites. *Nat Chem Biol* (2011).

240 Wang, W. *et al.* Genetically encoding unnatural amino acids for cellular and neuronal studies. *Nature neuroscience* (2007).

241 Pfeffer, S. R., Soldati, T., Geissler, H., Rancano, C. & Dirac-Svejstrup, B. Selective membrane recruitment of Rab GTPases. *Cold Spring Harbor symposia on quantitative biology* (1995).

242 Hino, N. *et al.* Protein photo-cross-linking in mammalian cells by site-specific incorporation of a photoreactive amino acid. *Nature methods* (2005).

243 Hao, B. *et al.* A new UAG-encoded residue in the structure of a methanogen methyltransferase. *Science* (2002).

244 Srinivasan, G., James, C. M. & Krzycki, J. A. Pyrrolysine encoded by UAG in Archaea: charging of a UAG-decoding specialized tRNA. *Science* (2002).

245 Pind, S. N. *et al.* Rab1 and Ca2+ are required for the fusion of carrier vesicles mediating endoplasmic reticulum to Golgi transport. *The Journal of cell biology* (1994).

246 Nuoffer, C., Davidson, H. W., Matteson, J., Meinkoth, J. & Balch, W. E. A GDP-bound of rab1 inhibits protein export from the endoplasmic reticulum and transport between Golgi compartments. *The Journal of cell biology* (1994).

247 Castellano, F., Wilson, A. L. & Maltese, W. A. Intracellular transport and maturation of nascent low density lipoprotein receptor is blocked by mutation in the Ras-related GTP-binding protein, RAB1B. *Journal of receptor and signal transduction research* (1995).

248 Wilson, B. S. *et al.* A Rab1 mutant affecting guanine nucleotide exchange promotes disassembly of the Golgi apparatus. *The Journal of cell biology* (1994).

249 Alvarez, C., Garcia-Mata, R., Brandon, E. & Sztul, E. COPI recruitment is modulated by a Rab1b-dependent mechanism. *Molecular biology of the cell* (2003).

250 Scheffzek, K. *et al.* The Ras-RasGAP complex: structural basis for GTPase activation and its loss in oncogenic Ras mutants. *Science* (1997).

251 Melser, S. *et al.* Rheb regulates mitophagy induced by mitochondrial energetic status. *Cell metabolism* (2013).

252 Thomas, J. D. *et al.* Rab1A is an mTORC1 activator and a colorectal oncogene. *Cancer cell* (2014).

253 Wang, K. *et al.* Optimized orthogonal translation of unnatural amino acids enables spontaneous protein double-labelling and FRET. *Nature chemistry* (2014).

254 Erdmann, K. S. *et al.* A role of the Lowe syndrome protein OCRL in early steps of the endocytic pathway. *Developmental cell* (2007).

255 Hou, X. *et al.* A structural basis for Lowe syndrome caused by mutations in the Rab-binding domain of OCRL1. *The EMBO journal* (2011).

256 Hyvola, N. *et al.* Membrane targeting and activation of the Lowe syndrome protein OCRL1 by rab GTPases. *The EMBO journal* (2006).

257 Bonetti, B., Fu, L., Moon, J. & Bedwell, D. M. The efficiency of translation termination is determined by a synergistic interplay between upstream and downstream sequences in Saccharomyces cerevisiae. *Journal of molecular biology* (1995).

258 Sabet, O. *et al.* Ubiquitination switches EphA2 vesicular traffic from a continuous safeguard to a finite signalling mode. *Nature communications* (2015).

259 Sabet, O. *The Spatial Organization of EPH Receptor Tyrosine Kinase Activity* Dr. rer. nat. thesis, TU Dortmund, (2013).

260 Li, X. *et al.* Deletions of the Aequorea victoria green fluorescent protein define the minimal domain required for fluorescence. *The Journal of biological chemistry* (1997).

261 Horikawa, K. *et al.* Spontaneous network activity visualized by ultrasensitive Ca(2+) indicators, yellow Cameleon-Nano. *Nature methods* (2010).

262 Komatsu, N. *et al.* Development of an optimized backbone of FRET biosensors for kinases and GTPases. *Molecular biology of the cell* (2011).

263 *EPYS Every Photon Is Sacred*, <http://epys.df.uba.ar/> (

264 Williamson, M. P. The structure and function of proline-rich regions in proteins. *The Biochemical journal* (1994).

265 Bhandari, D. G., Levine, B. A., Trayer, I. P. & Yeadon, M. E. 1H-NMR study of mobility and conformational constraints within the proline-rich N-terminal of the LC1 alkali light chain of skeletal myosin. Correlation with similar segments in other protein systems. *European journal of biochemistry / FEBS* (1986).

266 Evans, J. S., Levine, B. A., Trayer, I. P., Dorman, C. J. & Higgins, C. F. Sequence-imposed structural constraints in the TonB protein of E. coli. *FEBS letters* (1986).

267 George, R. A. & Heringa, J. An analysis of protein domain linkers: their classification and role in protein folding. *Protein engineering* (2002).

268 Goody, R. S. & Itzen, A. Modulation of small GTPases by Legionella. *Current topics in microbiology and immunology* (2013).

269 Machner, M. P. & Isberg, R. R. Targeting of host Rab GTPase function by the intravacuolar pathogen Legionella pneumophila. *Developmental cell* (2006).

270 Hammond, A. T. & Glick, B. S. Dynamics of transitional endoplasmic reticulum sites in vertebrate cells. *Molecular biology of the cell* (2000).

271 Stephens, D. J. De novo formation, fusion and fission of mammalian COPII-coated endoplasmic reticulum exit sites. *EMBO reports* (2003).

272 Wu, I. L. *et al.* Multiple site-selective insertions of noncanonical amino acids into sequence-repetitive polypeptides. *Chembiochem : a European journal of chemical biology* (2013).

273 Wang, K., Neumann, H., Peak-Chew, S. Y. & Chin, J. W. Evolved orthogonal ribosomes enhance the efficiency of synthetic genetic code expansion. *Nature biotechnology* (2007).

274 Pott, M., Schmidt, M. J. & Summerer, D. Evolved sequence contexts for highly efficient amber suppression with noncanonical amino acids. *ACS chemical biology* (2014).

275 Fried, S. D., Schmied, W. H., Uttamapinant, C. & Chin, J. W. Ribosome Subunit Stapling for Orthogonal Translation in E. coli. *Angewandte Chemie* (2015).

276 Lajoie, M. J. *et al.* Genomically recoded organisms expand biological functions. *Science* (2013).

277 Mukai, T. *et al.* Codon reassignment in the Escherichia coli genetic code. *Nucleic acids research* (2010).

278 Major, L. L., Poole, E. S., Dalphin, M. E., Mannering, S. A. & Tate, W. P. Is the in-frame termination signal of the Escherichia coli release factor-2 frameshift site weakened by a particularly poor context? *Nucleic acids research* (1996).

279 McCaughan, K. K., Brown, C. M., Dalphin, M. E., Berry, M. J. & Tate, W. P. Translational termination efficiency in mammals is influenced by the base following the stop codon. *Proceedings of the National Academy of Sciences of the United States of America* (1995).

280 Dumas, A., Lercher, L., Spicer, C. D. & Davis, B. G. Designing logical codon reassignment - Expanding the chemistry in biology. *Chemical science* (2015).

281 Nikic, I., Kang, J. H., Girona, G. E., Aramburu, I. V. & Lemke, E. A. Labeling proteins on live mammalian cells using click chemistry. *Nature protocols* (2015).

282 Yao, Y., Jones, E. & Inoki, K. Lysosomal Regulation of mTORC1 by Amino Acids in Mammalian Cells. *Biomolecules* (2017).

283 Cai, S. L. *et al.* Activity of TSC2 is inhibited by AKT-mediated phosphorylation and membrane partitioning. *The Journal of cell biology* (2006).

284 Muller, M. P. & Goody, R. S. Molecular control of Rab activity by GEFs, GAPs and GDI. *Small GTPases* (2017).

285 Weide, T. *et al.* The Golgi matrix protein GM130: a specific interacting partner of the small GTPase rab1b. *EMBO reports* (2001).

286 Langemeyer, L. *et al.* Diversity and plasticity in Rab GTPase nucleotide release mechanism has consequences for Rab activation and inactivation. *eLife* (2014).

287 Bar-Peled, L. & Sabatini, D. M. Regulation of mTORC1 by amino acids. *Trends Cell Biol* (2014).

288 Kim, J. & Kim, E. Rag GTPase in amino acid signaling. *Amino Acids* (2016).

289 Roccio, M., Bos, J. L. & Zwartkruis, F. J. Regulation of the small GTPase Rheb by amino acids. *Oncogene* (2006).

290 Allaire, P. D. *et al.* The Connecdenn DENN domain: a GEF for Rab35 mediating cargo-specific exit from early endosomes. *Molecular cell* (2010).

291 Yadav, R. B. *et al.* mTOR direct interactions with Rheb-GTPase and raptor: sub-cellular localization using fluorescence lifetime imaging. *BMC cell biology* (2013).

292 Wouters, B. G. & Koritzinsky, M. Hypoxia signalling through mTOR and the unfolded protein response in cancer. *Nature reviews. Cancer* (2008).

293 Knorr, G., Kozma, E., Herner, A., Lemke, E. A. & Kele, P. New Red-Emitting Tetrazine-Phenoxazine Fluorogenic Labels for Live-Cell Intracellular Bioorthogonal Labeling Schemes. *Chemistry* (2016).

Acknowledgements

First, I have to acknowledge my supervisor Dr. Yao-Wen Wu for giving me the opportunity to join his laboratory in which I gained diverse experience of both scientific and personal nature.

I would like to thank Prof. Roger Goody and Prof. Philippe Bastiaens for kindly taking the time of being my thesis advisory committee during the last years and the examiners of this thesis. The scientific feedback and input I have received during my annual TAC meetings were of great value and promoted this project greatly, which I highly appreciated. Moreover, I acknowledge our collaborators for providing essential material, scientific knowledge or practical support.

Further, I am grateful to the IMPRS-CMB for financial support and for giving me the opportunity to participate in numerous scientific and social events, where I met fantastic people from diverse fields of research. Special thank goes to Christa Hornemann for her support and sympathy and for giving me insights into a different way of seeing people.

I would like to thank both, former and current members of the AG Wu, the Chemical Genomics Centre and the Max Planck Institute for Molecular Physiology for sharing part of their life's journey, scientific knowledge and practical expertise with me.

I am very grateful for all the awesome people that I have met during my PhD and who went at least part of the way with me, especially Anna Rudo, Paula Mühlnickel, Shweta Bendre, Lea Kremer, Laura Dietrich and Julia Wernicke. Of course, the mixed international lunch group has to be mentioned here, too. Everything in life requires a counterpart and the highly amusing conversation during lunch were indeed a counterpart for the serious scientific work of the rest of the day.

Θα ήθελα να ευχαριστήσω ολόψυχα τον Δρ. Γεώργιο Κωνσταντινίδη για την τεράστια επιστημονική και προσωπική υποστήριξή του. Και τα δύο θα μου μείνουν αξέχαστα. Η επίτευξη αυτού του στόχου δε θα ήταν δυνατή χωρίς εσένα.

My deepest gratitude goes to my friends outside of Dortmund for their support and help to gather motivation even when there was none left.

Last but not least, I thank my parents and family for their support and the patience they had with me during the last years. I am very grateful for the chance you gave me.

Affidavit (Eidesstattliche Versicherung)

BRAND, Simone	**165219**
Name, Vorname (Surname, first name)	Matrikel-Nr. (Enrolment number)

Belehrung:

Wer vorsätzlich gegen eine die Täuschung über Prüfungsleistungen betreffende Regelung einer Hochschulprüfungsordnung verstößt, handelt ordnungswidrig. Die Ordnungswidrigkeit kann mit einer Geldbuße von bis zu 50.000,00 € geahndet werden. Zuständige Verwaltungsbehörde für die Verfolgung und Ahndung von Ordnungswidrigkeiten ist der Kanzler/die Kanzlerin der Technischen Universität Dortmund. Im Falle eines mehrfachen oder sonstigen schwerwiegenden Täuschungsversuches kann der Prüfling zudem exmatrikuliert werden, § 63 Abs. 5 Hochschulgesetz NRW.

Die Abgabe einer falschen Versicherung an Eides statt ist strafbar.

Wer vorsätzlich eine falsche Versicherung an Eides statt abgibt, kann mit einer Freiheitsstrafe bis zu drei Jahren oder mit Geldstrafe bestraft werden, § 156 StGB. Die fahrlässige Abgabe einer falschen Versicherung an Eides statt kann mit einer Freiheitsstrafe bis zu einem Jahr oder Geldstrafe bestraft werden, § 161 StGB.

Die oben stehende Belehrung habe ich zur Kenntnis genommen:

Official notification:

Any person who intentionally breaches any regulation of university examination regulations relating to deception in examination performance is acting improperly. This offence can be punished with a fine of up to EUR 50,000.00. The competent administrative authority for the pursuit and prosecution of offences of this type is the chancellor of the TU Dortmund University. In the case of multiple or other serious attempts at deception, the candidate can also be unenrolled, Section 63, paragraph 5 of the Universities Act of North Rhine-Westphalia.

The submission of a false affidavit is punishable.

Any person who intentionally submits a false affidavit can be punished with a prison sentence of up to three years or a fine, Section 156 of the Criminal Code. The negligent submission of a false affidavit can be punished with a prison sentence of up to one year or a fine, Section 161 of the Criminal Code.

I have taken note of the above official notification.

Ort, Datum (Place, date)	Unterschrift (Signature)

Titel der Dissertation: **Genetically encoded conformational probes for small GTPase activity**
(Title of the thesis):

Ich versichere hiermit an Eides statt, dass ich die vorliegende Dissertation mit dem Titel selbstständig und ohne unzulässige fremde Hilfe angefertigt habe. Ich habe keine anderen als die angegebenen Quellen und Hilfsmittel benutzt sowie wörtliche und sinngemäße Zitate kenntlich gemacht.
Die Arbeit hat in gegenwärtiger oder in einer anderen Fassung weder der TU Dortmund noch einer anderen Hochschule im Zusammenhang mit einer staatlichen oder akademischen Prüfung vorgelegen.

I hereby swear that I have completed the present dissertation independently and without inadmissible external support. I have not used any sources or tools other than those indicated and have identified literal and analogous quotations.

The thesis in its current version or another version has not been presented to the TU Dortmund University or another university in connection with a state or academic examination.*

*Please be aware that solely the German version of the affidavit ("Eidesstattliche Versicherung") for the PhD thesis is the official and legally binding version.

Ort, Datum (Place, date)	Unterschrift (Signature)